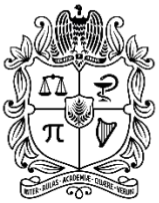

UNIVERSIDAD
NACIONAL
DE COLOMBIA

Evaluation of conductive nanofillers addition in scaffolds for myocardial tissue engineering application

Ana María Muñoz González

Universidad Nacional de Colombia

Facultad de Ingeniería, Departamento de Ingeniería Mecánica y Mecatrónica

Bogotá, Colombia

2024

Evaluation of conductive nanofillers addition in scaffolds for myocardial tissue engineering application

Ana Maria Muñoz Gonzalez

Tesis de investigación presentada como requisito parcial para optar al título de:

Doctorado en Ingeniería - Ciencia y Tecnología de Materiales

Directora:

Ph.D. Aleida Dianey Clavijo Grimaldo

Línea de Investigación:

Nanomateriales e Ingeniería tisular

Grupo de Investigación:

Biomecánica

Universidad Nacional de Colombia

Facultad de Ingeniería, Departamento de Mecánica y Mecatrónica

Bogotá, Colombia

2024

Acknowledgments

First and foremost, I would like to express my deepest gratitude to my thesis advisor, Dianney Clavijo. Throughout this entire journey, she has been there, offering both her technical expertise and personal support.

I also extend my heartfelt thanks to my fiancé, Julian Rubiano, who has walked this path alongside me, often helping to clarify my thoughts.

My appreciation also goes to Andres Gil and SENA, whose assistance was crucial in characterizing many of my samples.

I am grateful to all the laboratory technicians who were always willing to help, especially Cesar Bacca in the mechanical testing.

A special thanks to Sara Leal, who was a bridge in all the work carried out in Germany. I have learned so much from her about characterization techniques and equipment handling. Likewise, I am thankful to Professor Birgit Glasmacher, who graciously accepted me into her research team and facilitated my participation.

My sincere gratitude to my in-laws and relatives, who were like my immediate family, supporting me in both big and small ways throughout this process.

To my family, my sister Maria Fernanda, to whom I dedicate all my learning, and my step-siblings, especially Monica. To Nico, for always being there to help take care of my cats while I was away on research stays.

I am deeply thankful to my close friends, like Angelica Quiroga, who was always there to listen and provide a distraction from my work.

Lastly, to my colleague Angela Quiroga, with whom I shared many moments of both frustration and success in the lab, at the university, and as workmates.

Resumen

Evaluación de la adición de nanorrellenos conductores en andamios para aplicaciones de ingeniería de tejidos miocárdicos

Esta tesis explora el diseño, fabricación y análisis de andamios de nanofibras poliméricas con nanorrellenos electroconductivos para la ingeniería de tejidos cardíacos, centrándose en la reparación del tejido miocárdico mediante la incorporación diferenciada de grafeno y polipirrol (PPy) en matrices de policaprolactona (PCL) a través del electrohilado. El trabajo tiene como objetivo establecer parámetros de fabricación y evaluar las propiedades morfológicas, mecánicas, químicas, eléctricas y de biocompatibilidad de los andamios, con el fin de seleccionar aquellos que ofrezcan un acoplamiento electromecánico teórico óptimo con el tejido miocárdico.

Se distinguen dos estrategias: una centrada en andamios dopados con grafeno, que muestran mejoras en la uniformidad estructural y propiedades mecánicas, y otra en andamios enriquecidos con PPy, conocidos por su significativa conductividad eléctrica. Ambas estrategias presentan ventajas específicas, como la mejora de la hidrofilicidad y la promoción de la adhesión y proliferación celular, cruciales para la regeneración del tejido. A pesar de desafíos como la dispersión uniforme de nanopartículas y la correspondencia de las propiedades mecánicas con las del miocardio nativo, la investigación resalta el potencial de la polimerización in situ de PPy como un método equilibrado para lograr andamios con propiedades eléctricas y biocompatibilidad optimizadas.

Palabras clave: electrohilado, relleno conductor, nanorelleno, policaprolactona, polipirrol, grafeno, andamio, ingeniería de tejidos.

Abstract

Evaluation of conductive nanofillers addition in scaffolds for myocardial tissue engineering application

This thesis explores the design, fabrication, and of polymeric nanofiber scaffolds with electroconductive nanofillers for cardiac tissue engineering, focusing on myocardial tissue repair through differentiated incorporation of graphene and polypyrrole (PPy) into polycaprolactone (PCL) matrices via electrospinning. The work aims to establish fabrication parameters and assess the morphological, mechanical, chemical, electrical and biocompatibility properties of the scaffolds, with the goal of selecting those that offer optimal theorical electromechanical coupling with myocardial tissue.

Two strategies are distinguished: one focused on scaffolds doped with graphene, which show improvements in structural uniformity and mechanical properties, and another on scaffolds enriched with PPy, noted for their significant electrical conductivity. Both strategies present specific advantages, such as enhanced hydrophilicity and the promotion of cell adhesion and proliferation, crucial for tissue regeneration. Despite challenges like the uniform dispersion of nanoparticles and matching the mechanical properties to those of native myocardium, the research highlights the potential of *in situ* polymerization of PPy as a balanced method for achieving scaffolds with optimized electrical properties and biocompatibility.

Keywords: electrospinning, conductive filler, nanofiller, polycaprolactone, polypyrrole, graphene, scaffold, Tissue Engineering.

List of Publications

Manuscript published.

Chapter 2:

Ana M. Muñoz-González, Dianney Clavijo-Grimaldo (2022). Synthesis and Characterization of Graphene-doped Nanofibrous Scaffolds for Tissue Engineering.

Chemical Engineering Transactions, 94, 1423-1428. https://doi.org/10.3303/CET2294237

Manuscript accepted.

Chapter 3:

Ana M. Muñoz-González, Sara Leal-Marin, Dianney Clavijo-Grimaldo, Birgit Glasmacher (2024). Graphene-Enhanced PCL Electrospun Nanofiber Scaffolds for Cardiac Tissue Engineering.

The International Journal of Artificial Organs. SAGE. doi 10.1177/03913988241266088

Manuscripts submitted.

Chapter 4:

Ana M. Muñoz-González, Dianney Clavijo-Grimaldo (2024). Polypyrrole as a Nanofiller: Comparative Effects on the Properties of Polycaprolactone Scaffolds for Potential Myocardial Tissue Applications.

Chemical Engineering Transactions.

Chapter 5:

Ana M. Muñoz-González, Dianney Clavijo-Grimaldo, Sara Leal-Marin, Birgit Glasmacher (2024). Optimizing Electroconductive PPy-PCL Scaffolds for Enhanced Tissue Engineering Performance

Journal of Biomedical Materials Research Part B: Applied Biomaterials. WYLEY.

List of International Conferences

7th INTERNATIONAL CONFERENCE ON INDUSTRIAL BIOTECHNOLOGY

June 5-8, 2022 – Napoli, Italy

Synthesis and Characterization of Graphene-doped Nanofibrous Scaffolds for Tissue Engineering. (Poster)

XI Congreso Internacional de Materiales (XI CIM 2022)

October 26, 27 and 28, 2022 – Santa Marta, Colombia.

Obtención de andamios poliméricos nanofibrosos con adición de polímero conductor para ingeniería tisular (Obtention of nanofibrous polymeric scaffolds with conductive polymer addition for tissue engineering). (Oral)

31st International Materials Research Congress 2023

August 13-18, 2023 – Cancún, Mexico.

Exploring The Conductive Polymers Addition In Electrospun Nanofibrous Scaffolds For Tissue Engineering Application (Oral).

2nd International SIIRI Symposium

January 24-25, 2024 – Hannover, Germany.

Development and Characterization of PCL Electrospun Nanofiber Scaffolds with Graphene Nanofiller for Tissue Engineering (Poster).

List of Scholarships

Beca Asistente Docente – Dirección Académica, Universidad Nacional de Colombia. 2020-2023.

Subjects in charge: Fundamentos de Tecnología e Industrialización de Producto.

Research Grants – Short-Term Grants – DAAD

Research stay in Leibniz Universität Hannover in Institut für Mehrphasenprozesse and NIFE, Niedersächsisches Zentrum für Biomedizintechnik, Implantatforschungund und Entwicklung. October 2023 – January, 2024.

Scholarship for Academic Fee Exemption (Highest Weighted Average GPA) - Faculty of Engineering, Universidad Nacional de Colombia (2021-1).

Table of Contents

List of Figures

List of Tables

Introduction

The purpose of this chapter is to provide an overview of the context in which this research is carried out, to present in more detail the problem that will be addressed throughout this study, and to define precisely the objectives that guided the research work. Through this chapter, we seek to establish a solid foundation that allows readers to understand the relevance and scope of the research, as well as to clearly identify the objectives that are pursued to address the problem posed.

Overview

Over time, we have witnessed impressive technological advancements that have improved the quality of life for people worldwide. As a result, the global population has undergone exponential growth, increasing from approximately 2.5 billion people in 1950 to 8 billion in 2023. Projections by Roser and Ritchie suggest that this trajectory will continue, with the global population expected to reach 9.7 billion by 2050 (Roser & Ritchie, 2023).

Additionally, there has been significant improvement in life expectancy. According to the United Nations Department of Economic and Social Affairs (2022), the life expectancy in the Americas has increased from 58.1 years in 1950 to 74.2 years as of 2021 (United Nations, Department of Economic and Social Affairs, 2022). Global improvements in longevity and general well-being have been facilitated by these technological and medical breakthroughs.

As life expectancy continues to rise, there is an increasing need for solutions to enhance health and well-being. The need for organs and tissues for transplantation is one of the most pressing requirements in this situation. However, despite the increasing demand, there are not enough donors available, resulting in a lengthy wait time for patients looking to improve their quality of life. Transplantation also comes with its own set of challenges, such as the possibility of organ rejection and different ethical and cultural issues (del Maria Javier et al., 2021; Precedence Research, 2022).

Tissue Engineering (TE) offers a viable way to address the increasing demand for treatments given the pressing need. TE is a branch of Regenerative Medicine that builds three-dimensional matrices to support the growth of living, functioning tissues (Furth & Atala, 2014). This field integrates concepts from materials science, engineering, and biology (McClelland et al., 2005). This field integrates concepts from materials science, engineering, and biology (Vunjak-Novakovic, 2017).

The field of TE officially began in the 1980s when Joseph and Charles A. Vacanti developed three-dimensional scaffolds for tissue regeneration (Vacanti, 2006). Later, Joseph P. Vacanti and Robert Langer first used the term "tissue engineering" in 1993 (Langer & Vacanti, 1993). Since then, this discipline has progressed steadily, achieving significant milestones in the synthesis of tissues substitutes, such as skin, cartilage, bone, and muscle.

In this regard, cardiac tissue engineering (CTE) appears to be a potential solution for certain cardio vascular diseases (CVD), which have been the leading cause of death for the past 30 years (WHO, 2022). The prevalence of CVD is expected to reach 46.1% of the population in 2035, with an estimate cost of 1.1 trillion dollars in the United States (Qasim et al., 2019).

One of the most common forms of CVD is the ischemic heart disease, which occurs when the blood supply to the heart decreases due to partial or complete blockage in the coronary arteries, leading to arrhythmias or myocardial infarction. Myocardial ischemia often causes arrhythmias in the sinoatrial (SA) node (considered the natural pacemaker), conduction alterations in the atrioventricular (AV) node, and infarction with the loss of about one million cardiomyocytes in the infarcted area (Ghuran & Camm, 2001; Solazzo et al., 2019).

One attractive alternative is the generation of decellularized and bioartificial hearts (Alcon et al., 2012; Rodrigues et al., 2018). One significant advantage is the preservation of the original structure, which can be repopulated with new tissue. This holds the potential for a new generation of heart transplants. However, these solutions face challenges and limitations. Important considerations are technical complexity, limited feasibility and functionality, the possibility of immune response and rejection, as well as cost and accessibility. While the original structure of the heart is preserved and there is potential for repopulation with new tissue, further research and advancements are needed to overcome these disadvantages and make bioartificial hearts viable and accessible to a larger number of patients.

Other techniques and treatments in Regenerative Medicine are intramyocardial injections into hydrogels and cardiomyoplasty (Fujita & Zimmermann, 2017; Rodrigues et al., 2018). The latter consists of isolated cell administration with regenerative capability. However, limitations arise, with only a few cells differentiating and displaying shortcomings in terms of electromechanical properties. Another solution is the use of a pacemaker to generate electrical signals in the system, but it may occasionally lack synchrony (Mittal, 2005), worsening the issue of arrhythmia. Furthermore, this solution does not seem very effective in the long term, especially for young patients.

Currently, there is a range of cardiac patches and platforms, matrices available for cardiac disease applications, including electrospun scaffolds, hydrogels, and decellularized extracellular matrices (ECMs). These materials can provide structural support and deliver bioactive factors to facilitate

tissue regeneration. Researchers are exploring various strategies to enhance the functionality and integration of these patches, such as incorporating cardiac cells, optimizing their composition, and improving their electrical and mechanical properties (House et al., 2021; Mannhardt et al., 2016; McMahan et al., 2020).

The production of polymeric matrices, whether natural, synthetic, or hybrid, offers immense potential in TE. This approach provides a suitable method for developing unique artificial materials with functional and three-dimensional features that can replicate the extracellular matrix.

Recent research in the field of TE has focused on exploring synthetic polymers, including polyglycerol sebacate (PGS), polyurethane (PU), polycaprolactone (PCL), glycolic acid (PGA), and polylactic-co-glycolic acid (PLGA). These synthetic polymers possess desirable biocompatibility and mechanical properties that closely simulate the desired cellular environment. Notably, PCL, PGA, and PLGA are well-suited for nanofiber production in TE. These polymers exhibit flexibility, low-density, resilience, and wide chemical versatility. Moreover, they are biocompatible, biodegradable, and can be manufactured using electrospinning techniques (Karkan et al., 2019). Electrospinning plays a crucial role in fabricating tissue scaffolds that facilitate cell growth and tissue functionalization(Amaya, 2018; Oprea et al., 2019).

In addition to synthetic polymers, natural polymers such as gelatin (GT), chitosan, collagen, and elastin alginate have garnered attention in TE research. These natural polymers provide a biomimetic environment for cells and offer advantages such as biocompatibility and bioactivity but lack of adequate mechanicals properties (Aziz et al., 2023; Nasr et al., 2020).

One of the most important techniques in TE, which take advantage of the synthetic and natural materials is electrospinning. Electrospinning is a widely used technique in the manufacture of nanofibers and polymeric nanocomposites, where it is possible to obtain fibers with diameters between the nano (2 nm and 100 nm) and micrometers (Chem et al., 2021; Xue et al., 2019). The obtained nanofibers can mimic the natural architecture of the ECM and promote a platform for cell adhesion in a three-dimensional environment.

Electrospinning has facilitated the creation of scaffolds, gaining prominence in TE. Nanometer-sized scaffolds can be designed in 2D and 3D with a porous structure, achieving a high surface/volume ratio, and allowing greater cell interaction. These attributes have collectively contributed to satisfactory results in the restoration of skin tissue, blood vessels, cartilage, and bone, among others (Ding et al., 2019; Jung et al., 2018; Karkan et al., 2019; Park et al., 2018).

In the field of CTE, the development of biomaterials has made significant strides. However, there is still an urgent need for ongoing research and innovation to address present challenges and constraints.

One major challenge is the lack of electrical conductivity in biomaterials used for CTE. To replicate the electrical signaling and communication that naturally takes place in the heart, electrical conductivity is essential. This property is crucial for coordinating the contraction of cardiomyocytes, encourages the transmission of electrical impulses, and affects the viability and maturation of cells. Thus, the fabricating of functional cardiac tissue constructions requires the development of biomaterials with intrinsic electrical conductivity (He et al., 2020; Morsink et al., 2022).

The mechanical characteristics of biomaterials are another crucial factor to consider. The heart is a highly responsive organ that is always under mechanical stress. Therefore, the mechanical properties of the biomaterials utilized in cardiac tissue must closely resemble those of natural cardiac tissue. This encompasses factors such as stiffness, elasticity, and tensile strength. Achieving appropriate mechanical characteristics is essential for sustaining cell viability, promoting cell adhesion, and enabling appropriate tissue integration and function (Bolonduro et al., 2020; Vunjak-Novakovic, 2017; Vunjak-Novakovic et al., 2010).

To solve the drawbacks, especially the electrical conductivity of the tissue, researchers are exploring various strategies. One approach involves incorporating conductive materials, such as polymers or nanoparticles, into the biomaterial matrix to enhance electrical conductivity. Examples include poly(3,4 ethylene dioxythiophene) (PEDOT) , polypyrrole (PPy), and polyaniline (PANI) (Ghovvati et al., 2022; Matysiak et al., 2020; Roshanbinfar et al., 2020). Other materials commonly used to improve the electrical conductivity of tissue are gold nanoparticles (AuNP) and carbon allotropes such as carbon nanotubes (CNT) or graphene (Alegret et al., 2019; Bellet et al., 2021; Gelmi et al., 2015; Gómez et al., 2021; B. Guo & Ma, 2018; S. Kumar & Chatterjee, 2016).

The importance of improving the electrical conductivity (after an infarction) of cardiac tissue focuses on the gradual recovery of the tissue. This intervention helps impede further deterioration of the infarcted heart, promotes cell signaling, and influences the mechanical stretching of cardiomyocytes, achieving synchronous contraction (Blachowicz & Ehrmann, 2020; Gálvez-Montón et al., 2013).

Some authors had used conductive nanofiller to improve the functionality of the engineered cardiac tissue. Liang et al. used PPy blended with silk fibroin electrospun nanofibers; the incorporation of PPy resulted in a reduced fiber diameter, aligning the mechanical properties more closely to the native myocardium. This also provided sufficient electrical conductivity, supporting the contraction of cardiomyocytes (Liang et al., 2021). Additionally, Zarei et al. obtained conductive scaffolds composed of chitosan, collagen, and polyethylene oxide with PPy as nanofiller; after the characterization of fibers with enhanced conductivity and cell adhesion, growth, and proliferation (Zarei et al., 2021). In turn, Wang et al. developed nanofibrous sheets composed by PLA and PANI enhancing conductivity but showing the same diameter; also, PLA/PANI nanofiber exhibited good interaction and viability with cardiomyocytes (L. Wang et al., 2017).

Alternatively, there are some reports of the use of conductive nanofiller in nanofibers and other applications. For example, Maharjan et al. developed an *in situ* polymerization of PPy into a PCL solution; then, the PPy/PCL solution was electrospun, enhancing the mechanical strength, and increased surface roughness, decreased fiber diameter, and better behavior with cells for bone tissue application (Maharjan et al., 2020). Moreover, PPy has been used with polyurethane (PU) and poly-L-lactic acid (PLLA) to obtain a soft conductive, flexible, and handle biomaterial for biomedical applications that supported the proliferation of human skin keratinocytes (S. Cui, Mao, Rouabhia, et al., 2021). Further, PPy has been used in nerve tissue engineering with PLA to improve the conductivity, hydrophilicity, and mechanical properties of the nerve cells (Imani et al., 2021; S. Li et al., 2022).

Regarding the use of graphene or carbon conductive derivatives to improve the electromechanical and biological properties in scaffolds, some investigations have reported improved electrical conduction, Young's modulus, and cardiac cell differentiation, but decreased proliferation due to the limited contact between cells (Ahadian et al., 2016). Chen et al. obtained nanofibrous scaffolds made of polycaprolactone/gelatin (PCL/Gt) loaded with different mass fractions of graphene showing a positive *in vitro* and *in vivo* response in neonatal rat models in a CCK-8 assay and histopathological staining (DAPI, cTNT, and CX43) indicated that cells grew and survived, with no evidence of toxic or inflammatory reaction when graphene mass fraction was less than 0.5% (X. Chen et al., 2019). Other studies support the use of graphene in polymeric matrices for TE obtaining a greater amount of cell growth (PC12 cells) attributable to the unique biological properties of graphene, which leads to greater hydrophilicity and 99% antibacterial properties against gram positive and gram-negative bacteria (Heidari et al., 2017, 2019).

On the other hand, replicating the anisotropic structure of cardiac tissue poses a new challenge, particularly with certain manufacturing techniques, since patterns must be generated for hierarchical control over cell alignment and adhesion, which implies an adequate design of scaffolds (Qasim et al., 2019). Mimicking the structure of the myocardium would improve cardiomyocyte maturation and mechanical properties; as well as its flexibility and the regulation of essential cellular functions (Kharaziha et al., 2014).

Despite the progress in properties achieved by the nanofibers scaffolds made through electrospinning, challenges persist and remain unsolved in CTE. It is necessary to contribute to the development of new materials and electrodynamic techniques such as electrospinning to close the gap between the materials and health sciences for the reconstruction of damaged hearts.

Research statement

The regenerative capacity of the heart muscle is limited, leading to the formation of non-contractile scar tissue in areas of myocardial infarction. This scar tissue is rigid and electrically inactive, forming an unstable electrical substrate that isolates cardiomyocytes, impairs electrical conduction, and contributes to arrhythmias. This ultimately leads to heart failure, characterized by the insufficient pumping capacity of the surviving cardiomyocytes. Depending on the size and location of the infarction, alterations in the conduction system can lead to sudden death from ventricular fibrillation.

Despite current advancements in cardiac regeneration through TE, several biomaterials developed thus far have exhibited limitations. These include the lack of electromechanical coupling between adjacent cells, mismatched physicochemical properties of the materials, inappropriate mechanical properties, limited replication of anisotropic structure, and primarily the absence of electrical conductivity.

Therefore, there is a need to explore and develop new materials that can emulate the mechanical and conductive properties of cardiac tissue, as well as its biological, morphological, and topographic characteristics. In this context, the development of scaffolds using conductive nanofibers manufactured through electrospinning holds promise as an alternative approach to generate new biomaterials for CTE.

Finally, the hypothesis for this project suggests that the addition of a conductive nanofiller is expected to positively influence the final properties of polymeric nanofibers made through electrospinning compared to nanofibers without any conductive nanofiller. To carry out the manufacturing process of the nanofibers, it will be required to conduct experiments to evaluate the proportion of the conductive nanofiller added, as well as the parameters and conditions required for the electrospinning process to manufacture the nanofibers.

The research objectives were designed to address the research question: *"How does the incorporation of conductive nanofillers affect the properties and behavior of polymeric electrospun nanofiber scaffolds for myocardial tissue potential application?".*

Aim and outline of the thesis project

The objectives of the research project are as follows:

General Objective:

To determine the effects of the conductive nanofillers on the polymeric nanofiber scaffold properties to be used in the myocardial tissue.

Specific Objectives:

- To stablish the parameters for the fabrication of the polymer nanofibers scaffolds with conductive nanofillers through electrospinning technique.
- To analyze the morphological, mechanical, chemical, and electrical properties of the developed scaffolds in function of the fabrication parameters.
- To select one of the produced scaffolds which could provide a suitable platform to couple electromechanically to the myocardial tissue.

In the broad and complex field of CTE, a journey begins with an urge to restore the human heart. This thesis presents an adventure of exploration and discovery, with each chapter contributing a piece to the puzzle of cardiac tissue repair. It is a narrative about ingenuity, obstacles, and breakthroughs (see Figure 0 - 1).

In the **Literature Review** chapter, this examination delves into the state of the art regarding the anatomy and function of heart tissue, CTE, and the materials commonly utilized in this field. Additionally, it scrutinizes the challenges that must be addressed within this discipline, offering a comprehensive overview of the current research landscape and the future prospects in CTE.

In the **Chapter The Role of Graphene in Electrospun Multi-Layered Scaffolds for Advancing Tissue Engineering**, we explore how graphene, with its exceptional properties, may transform polymeric nanofibers, especially for heart, muscle, and nerve tissues. We investigate the prospect of using graphene as a nanofiller in multi-layered polymer scaffolds, demonstrating its ability to improve mechanical strength.

The **Chapter Effects of Graphene Nanofiller on Nanofibrous PCL Scaffold Properties for Tissue Engineering**, chapter provides an exhaustive examination of graphene nanoparticles (Gnp) within polycaprolactone (PCL) scaffolds, which is the central focus of the research. With different analytical characterization techniques highlight the major developments in surface uniformity, fiber diameter reduction, and improvements in mechanical and biological properties that are essential for cellular activities in CTE.

The next **Chapter, the Integration of Polypyrrole (PPy) as a nanofiller into polycaprolactone (PCL) fibers**, addresses the challenges and successes in embedding this conductive polymer into PCL scaffolds. Through meticulous experimentation and analysis, we uncover the impact of different forms of PPy on the scaffold properties, highlighting both achievements and hurdles.

To overcome the issues in the last chapter, in the **Chapter From Concept to Application: Optimizing PPy-PCL Scaffolds for Tissue Engineering**, describes the creation of

electroconductive scaffolds using PPy-PCL. Employing *in situ* chemical polymerization of polypyrrole (PPy) and optimizing process parameters, we achieve scaffolds with PCL as template, and the results enhanced conductivity, mechanical strength, and hydrophilicity, proving their suitability for TE applications. The viability and potential of these scaffolds are underscored by extensive cellular testing.

The chapter **Final Insights and Path Forward in Cardiac Tissue Engineering** culminates this thesis by identifying the most promising scaffold for CTE. It synthesizes key findings and evaluates the best scaffold based on comprehensive criteria, setting the stage for future research directions. Recommendations for advancing scaffold technology in cardiac regeneration are discussed, aiming to bridge current research with future innovations.

An **annex** proposes a study design for *in vivo* evaluation of conductive scaffolds' electromechanical coupling in myocardial tissue. Though theoretical, this framework offers a pioneering approach for future research, highlighting the potential of conductive scaffolds in cardiac therapy and engineering. This forward-looking section emphasizes the need for empirical validation to realize the therapeutic potential of these scaffolds in cardiac regeneration.

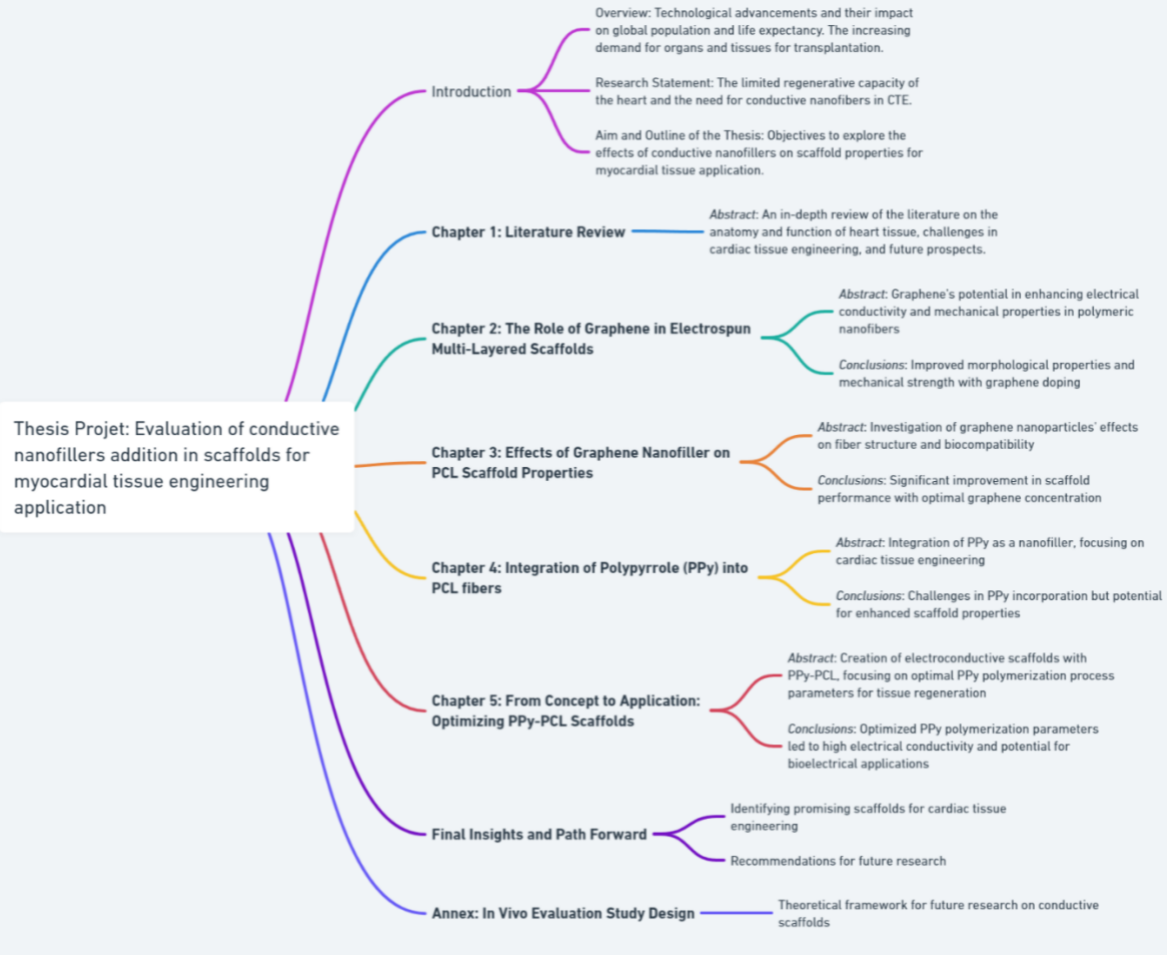

Figure 0 - 1 Summary of the Thesis Project Chapter Structure.

Notes

The thesis is divided into chapters. Chapter 2 is already published, while Chapters 3 and 5 are currently being reviewed. A few changes were made to the manuscript versions to improve readability to meet the requirements of include published papers in the thesis. Renumbering figures and tables, combining all references into one single list for the full thesis, standardizing abbreviations, and units for consistency, and adding minor additions to emphasize certain points pertinent to the thesis theme are among the changes.

1. Literature review

1.1 Abstract

This chapter presents an in-depth review of the literature related to the doctorate project's theme. The review focuses on the anatomy and function of heart tissue, CTE, and commonly used materials. Furthermore, it examines the challenges that must be solved in this the discipline, providing a comprehensive overview of the current state of research and prospects in CTE.

1.2 Introduction

On average, CVD is responsible for 1 in every 5 deaths in the United States. This equates to one death every 34 seconds (Centers for Disease Control and Prevention, 2022). Furthermore, heart disease has been a long-standing problem in the United States having been the nation's leading cause of death in the nation since 1921 (Greenlund et al., 2006). The World Heart Federation estimates that there will be over 23 million deaths related to CVD annually by 2030 (World Heart Federation, 2022). In 2035, 46.1% of the population is projected to be afflicted with some form of CVD, with a cost of 1.1 trillion (Fleischer et al., 2017) and The American Heart Association predicts that over 130 million adults in the United States will have some form of heart disease (Tsao, Connie W; Aday, Aaron W.; Almarzooq, 2022).

CVD and stroke have had a significant economic impact on the United States. According to the American Heart Association, between 2014 and 2015, these conditions cost the country $351.2 billion in healthcare services, medicines, and lost productivity due to death. Unfortunately, researchers expect that these costs will rise to $749 billion by 2035. The National Institutes of Health has also recognized the importance of addressing heart disease and has allocated more than $1.5 billion for research in 2021. It is also worth noting that a significant portion of healthcare spending is dedicated to CVD, with 1 in every 6 healthcare dollars being spent on it. Additionally, hospitalization for a heart attack can be costly with a median cost of $53,384, and bypass surgery can cost between $85,891 and $177,546. Furthermore, people with hypertension tend to spend around $2,000 more per year on healthcare compared to their non-hypertensive peers.

1.3 Cardiac tissue description

The heart is unquestionably one of the most important organs in the human body, moving up to 14,000 liters of blood daily. Given its crucial function and the prevalence of CVDs (CVD), research into conductive scaffolds for cardiac applications is essential. To provide readers a better understanding of the structure and operation of the heart, a vital organ, this section will address a few important heart-related topics. This focus is relevant because the main goal of this research work is the development of conductive scaffolds for cardiac applications.

This magnificent organ is located in the mediastinum and is protected from harm by the pericardium, a membrane that surrounds and shields the heart. This membrane allows the heart to contract properly while maintaining its place, which minimizes friction during movement. Beneath the pericardium is the cardiac wall, composed of the myocardium, and endocardium (inner layer).

Composed of cardiac muscular tissue, the myocardium is the thickest layer. Myocardium is extremely significant since it contains the heart's main functions, including contraction and blood pumping throughout the body. This layer contains around 20 billion quasi-laminar sheets of anisotropic cardiomyocytes per gram of tissue.

Cardiomyocytes are specialized cells that contain intracellular structures called intercalated discs, which connect heart muscle cells and allow communication and coordination between them. These discs contain desmosomes, which function as a junction, and gap junctions that enable the conduction of action potentials between muscle fibers, allowing the entire myocardium to contract as a single unit. Desmosomes, along with the extracellular matrix (ECM), contribute to the native cardiac tissue's elastic modulus of 100-500 kPa (Fleischer et al., 2017; Gelmi et al., 2015) (≈425 kPa) (Dozois et al., 2017) or 50-100 kPa during diastole (You et al., 2011). Its elasticity and resistance help regulate blood flow according to the body's needs. Cardiomyocytes also have a lot of mitochondria, which helps them produce energy for contraction.

One of the heart's most important properties are electrical properties such as electrical conductivity, which are accompanied by its mechanical properties. The heart's capacity to pump blood efficiently is attributed to the presence of cells called pacemaker cells, which are different from cardiomyocytes that produce and transmit electrical impulses that determine the rhythm which allows the heart to contract. Furthermore, these cells comprise the heart's electrical conduction system, which is made up of a network of specialized fibers that provide a conduit for each excitation cycle to propagate through the entire heart in a coordinated manner. The conductivity achieved in native tissue longitudinally is ~0.16 S/cm and transversally $5*10^{-3}$ S/cm (Dozois et al., 2017). However, several

authors have reported a final value of 0.001 S/cm (Baei et al., 2016; Fakhrali et al., 2022; Liau et al., 2012; You et al., 2011).

The sinoatrial node (SA node), a crucial natural pacemaker structure located in the right atrium, initiates the heart's electro-mechanical activity in the heart (MacDonald et al., 2020). This specialized tissue autonomously generates electrical impulses at a physiological rate of 60 to 100 beats per minute in an adult. These impulses remain throughout the entire heart's conduction system, similar to electrical currents in a network, causing successive atrial and ventricular contractions (Kashou & Chhabra, 2020). This highly coordinated procedure ensures that blood is efficiently ejected from the ventricles and into the circulatory system, displaying the sophisticated electromechanical coordination of the heart.

The electrical impulse travels from the sinoatrial node to the atrioventricular node (also called the AV node), located between the atria and ventricles. In the AV node, the impulses are delayed for a moment, allowing the atria to contract a fraction of a second before the ventricles. The blood from the atria flows into the ventricles before they contract (Markowitz & Lerman, 2018). After passing through the AV node, the electrical current continues down through a conduction channel called the bundle of His to the ventricles. The bundle of His splits into the right and left branches to carry the electrical stimulus to the right and left ventricles (Scheetz & Upadhyay, 2022).

CVDs, such as heart failure, are a significant public health issue. These diseases can be caused by the accumulation of plaques in the arteries, limiting blood flow and causing heart attacks. To recover function, the heart can regenerate, but as its regenerative capacity is insufficient, the tissue regenerates with non-contractile fibrotic tissue affecting the mechanical and conductive properties (Q.-Y. Guo et al., 2023; Tenreiro et al., 2021). This is due to the lack of stem cells and the absence of mitosis in cardiac muscle fibers (Tortora & Derrickson, 2006).

In this scenario, conductive scaffolds seem like a novel solution. They can help repair damaged heart tissue and restore electrical conductivity (Y. Li et al., 2022; Shokrollahi et al., 2023). This is especially essential because the heart's normal regeneration is restricted and frequently inadequate.

1.4 Cardiac Tissue Engineering (CTE)

In general terms, TE refers to the development and modulation of different molecules and cells in natural and synthetic constructs for the purpose of replacing and repairing damaged tissue. Meanwhile, the Cardiac Tissue Engineering (CTE) aims to use biomaterials to fabricate myocardium-

like structures or scaffolds to be engrafted into the heart to repaired damage tissue, imitating the structure of the ECM.

ECM is a composite material organized in a network that contains macromolecules such as proteins and carbohydrates that helps to envelop, give structure, and support cells and tissues (Yue, 2014). The ECM is a dynamic structure responsible for other processes such as communication between cells and plays a crucial role in proliferation, adhesion, migration, differentiation, growth, movement, and cell regeneration processes (D. Hao et al., 2020).

Decellularized organs have been a natural source of TE scaffolds, however, the process involves ECM variability from the animal source and risks associated with residues from the decellularized process (Valdoz et al., 2021). To overcome these drawbacks, structures created by means of polymers that mimic the natural structure of ECM have gained strength in recent years (Socci et al., 2023).

Selecting the appropriate fabrication method is decisive in achieving the desired properties for scaffolds used CTE according with the above criteria. While there are several methods to obtain scaffolds, electrospinning is a highly innovative and versatile technique that offers several unique advantages.

1.4.1 Electrospinning as a prominent technique in CTE

Electrospinning is a widely used technique in the manufacture of nanofibers and polymeric nanocomposites (Chem et al., 2021; Nguyen et al., 2023). In this technique, a polymer solution is injected into a high-voltage electric field, where the electrostatic forces are strong enough to overcome the surface tension of the solution. This results in the rapid flow of a narrow jet of the solution, taking on a Taylor-cone shape, towards a collector that can either be grounded or oppositely charged (as shown in *Figure 1 - 1*).

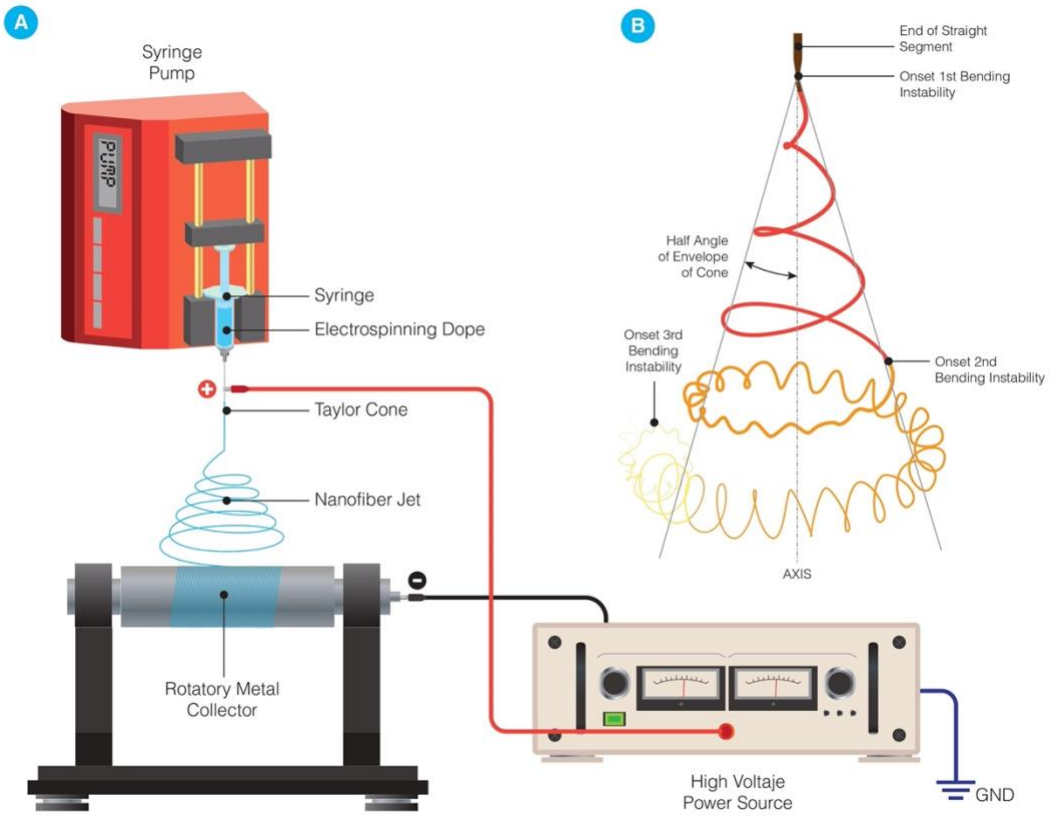

Figure 1 - 1 (A) Representation of the electrospinning process, (B) A diagram illustrating how bending instabilities lead to thinning of the jet emitted from the Taylor cone (author).

The formation of the Taylor cone is explained as follows. This phenomenon undergoes several distinct stages, which are reminiscent of the observations made in the *Figure 1 - 2*. First, the formation of the Taylor cone begins with the emergence of a droplet. At this point, electrostatic forces gradually overpower the surface tension of the liquid, leading to the deformation of the droplet as it emerges from the needle. This deformation process is a crucial step in the creation of the cone.

Once a critical voltage level is surpassed, the process progresses to the formation of a jet. This jet subsequently undergoes continuous deformation and stretching as it progresses along its trajectory from the needle to the collector. During this journey, the jet may assume various morphologies, often including helical and subloop structures. These morphological changes are typically due to instabilities in the process and are influenced by factors such as the electric field, polymer properties, and the ambient conditions. The entire process culminates with the solidification of the material (J. K. Y. Lee et al., 2018).

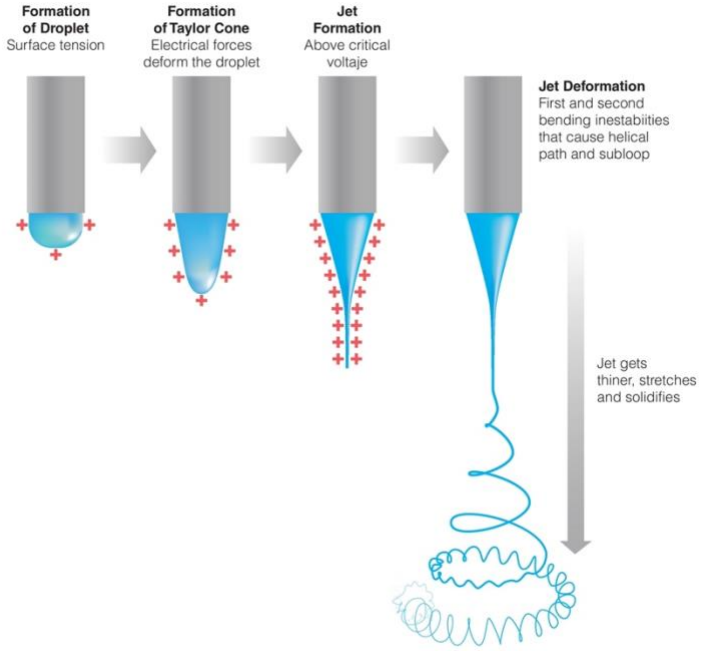

Figure 1 - 2 Stages of the Taylor cone formation process (author). First, the formation droplet; then, the formation of Taylor Cone when de electrical forces deform the droplet. After, jet formation above critical voltage and finally, jet deformation, it gets thinner, stretches, and solidifies.

Variables Affecting the Electrospinning Process and Fiber Formation: polymeric solution.

In the electrospinning process, several variables need to be taken into consideration. Specifically, attention should be paid to the variables pertaining to the polymer solution that is being employed. The following solution-related variables are of particular importance:

Viscosity

The viscosity of the solution plays a crucial role in determining the diameter of the fibers and is influenced by the molecular weight of the polymer and its concentration in the solution (Senthil & Anandhan, 2017). The viscosity generates a force that counteracts the electrostatic repulsion, allowing for jet stretching and thinning (Z.-M. Huang et al., 2003). Reducing the viscosity enables the production of fibers with smaller diameters (Amariei et al., 2017). However, if the viscosity of the solution is too low, there is a risk of electrospraying. This occurs because the applied electric field and surface tension cause the polymer chains to break into fragments before reaching the collector, resulting in bead formation (Haider et al., 2018).

On the other hand, increasing the concentration of the polymeric solution leads to higher viscosity due to the entanglement of polymer chains. This helps to overcome surface tension and produce beadless fibers (Zargham et al., 2012). However, beyond a critical concentration, increasing the solution concentration can result in higher diameters or even the drying of the polymeric solution. This can lead to the blockage of the needle and the appearance of beads in the fibers (Haider et al., 2018; Tiwari & Venkatraman, 2012).

Solution conductivity

In the electrospinning process, the conductivity of the solution can significantly impact the stretching of the jet due to the presence of higher charge carriers. As a result, the formation of the droplet to create the Taylor cone is positively influenced, while the diameter of the fibers is reduced. This is so because the Coulomb force—which exists between the charges on the solution's surface and the external electric field—is essential to the electrospinning process as an entire process (Reneker et al., 2000; Reneker & Yarin, 2008). The formation of the Taylor cone depends on the electrostatic force generated by the surface charges caused by the applied electric field (Hohman et al., 2001). If the polymeric solution is dielectric, there are insufficient charges available to move on the surface, which means that the electrostatic force produced by the applied electric field is insufficient to form a Taylor cone and facilitate the electrospinning process (Haider et al., 2018).

To enhance the conductivity of the solution, sometimes salts are employed as they increase the ion concentration in the solution, thereby raising the charge density. The use of these substances effectively reduces surface tension, promoting greater stretching of the fibers and reducing the forces required to overcome surface tension (Al-Abduljabbar & Farooq, 2023; Topuz et al., 2021; Xue et al., 2019; Yalcinkaya et al., 2015).

Surface tension

Another important factor in the production of fibers through electrospinning is surface tension. Surface tension refers to the force that acts parallel to the surface and perpendicular to a unit length line anywhere on the surface. It causes liquids to tend to minimize their surface area by cohering rather than dispersing, forming droplets (Butt & Kappl, 2018). The surface acts as a film that resists deformation and prevents breakage (Fujihara et al., 2005).

In the electrospinning process, surface tension is influenced by the choice of solvent (Mit-uppatham et al., 2004). If a system involves multiple solvents, each solvent contributes to different surface tensions (Mehta & Pawar, 2018; Son et al., 2004). The formation of uniform fibers is dependent on the surface tension of the solution (Bagbi et al., 2019). High surface tension can lead to the appearance of unstable jets or spray droplets.

In typical chemical solutions, surfactants are commonly used to reduce surface tension. However, in the electrospinning process, the addition of surfactants may introduce impurities into the nanofiber membrane (Ray et al., 2019). Therefore, a more effective approach to obtaining smooth fibers is to incorporate solvents with low surface tension, such as ethanol, dimethylformamide (DMF), or dichloromethane (DMC) (Yang et al., 2004).

Variables Affecting the Electrospinning Process and Fiber Formation: electrospinning process.

In the electrospinning process, several fabrication parameters play a crucial role in the generation of fibers. These parameters are instrumental in controlling and optimizing the manufacturing process. Among the key parameters that require careful monitoring and adjustment are the applied voltage (expressed in kilovolts: KV), the injected flow rate (measured in milliliters per hour: mL/h), and the distance between the needle and the collector (measured in centimeters: cm). These parameters directly influence the characteristics of the resulting fibers, such as diameter, morphology, and alignment. Therefore, precise control and fine-tuning of the applied voltage, injected flow rate, and needle-collector distance are vital for achieving the desired fiber properties in the electrospinning process.

Voltage

Voltage significantly influences the electrospinning process. As the droplet reaches the needle, which is connected to the voltage source transmitting the electric field, the droplet undergoes deformation, transitioning from a round shape to forming the Taylor cone (Ajith et al., 2023). This occurs once a critical voltage value is reached (Reneker et al., 2000). The critical voltage varies depending on the solution and the polymer used, typically falling within the range of 10 to 30 kV (Haider et al., 2018).

In general, higher voltages tend to yield thicker fibers, but distorting the jet, even forming multijets (see *Figure 1 - 3*), and potentially resulting in larger beads. This is because the increased electric charges lead to an elevated exit rate of the polymeric solution and a shortened flight time (Forward & Rutledge, 2012). Conversely, at lower voltages, the solution lacks the necessary momentum for the polymer to reach the collector plate, resulting in reduced elongation of the nanofiber and larger diameter fibers (Haider et al., 2018).

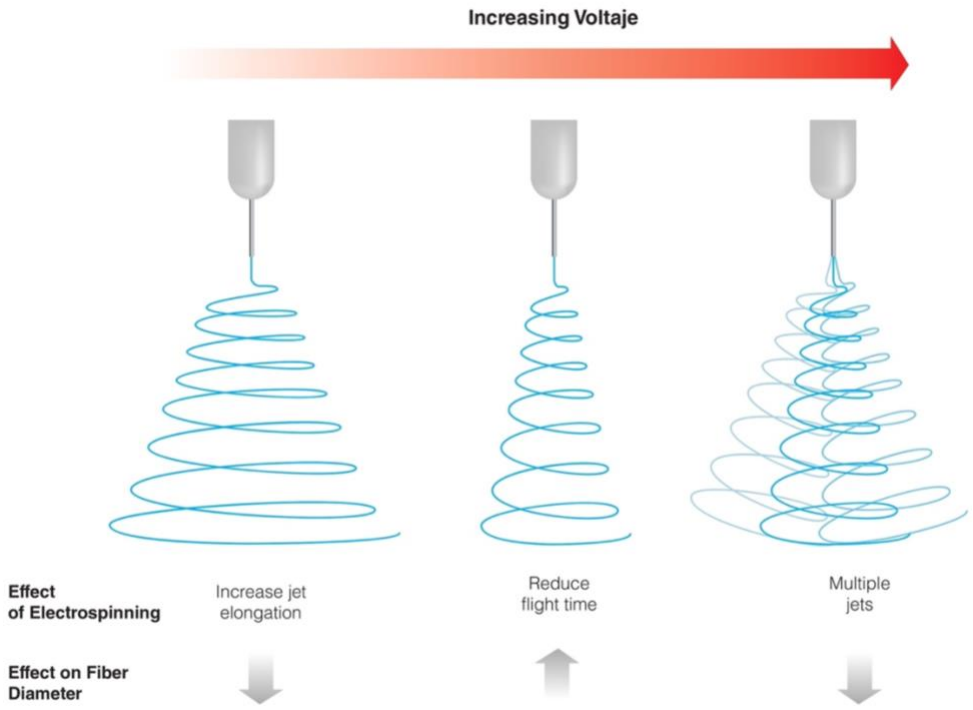

Figure 1 - 3 Jet and multijet formation in the electrospinning process (Author).

Flow rate

The solution flow rate through the needle in the electrospinning process also has a significant impact on the resulting fibers. Higher flow rates cause larger beads to form and thicker fibers to be created (Megelski et al., 2002). On the other hand, fibers without defects may be produced at lower flow rates. However, if the flow rate falls below a critical value, there is an increased solvent evaporation time between the needle and the collector, leading to the formation of beads (Ajith et al., 2023). This is also caused by a decrease in surface charge density (Forward & Rutledge, 2012). The range of flow rates can vary widely and is dependent on the specific solution, typically ranging from 0.1 to 4 mL/h.

Needle-collector distance

Needle-collector distance is another parameter in the electrospinning process that can be manipulated and has an impact on fiber quality and process feasibility. The reported range of distances typically falls between 10 and 30 cm (C. Huang et al., 2012). When using longer distances, it is possible to obtain thinner fibers as the solution can be stretched further from the needle to the collector plate (Deitzel et al., 2001). However, excessively long distances can lead to fiber breakage due to their own weight and the appearance of beads in the resulting membranes. Additionally, at longer distances, the intensity of the electric field becomes weakened (Ajith et al., 2023).

On the other hand, shorter distances provide limited time for solvent evaporation, resulting in fibers that may not be very smooth an uniform as they reach the collector while still damp (Eroğlu, 2022; Refate et al., 2023). Likewise, when using very short distances, the presence of beads significantly increases (Deitzel et al., 2001). It is important to find a balance in the needle-collector distance to achieve optimal fiber morphology and minimize bead formation during the electrospinning process.

Environmental factors that affect the electrospinning process

There are some factors that are very difficult to control in the electrospinning process, one of them being relative humidity and ambient temperature. When there is high humidity in the environment, the resulting fibers may become porous and larger in diameter (De Vrieze et al., 2009). In addition, high relative humidity and temperature could increase de evaporate rate of the volatile solvents, changing the solidification process in the jet (Szewczyk & Stachewicz, 2020).

The versatility of electrospinning enables the creation of scaffolds using a variety of materials, which makes it a highly attractive method for fabricating scaffolds for CTE applications. Various electrospinning assembly setups, such as co-axial electrospinning, melt electrospinning, emulsion electrospinning, and needle-less electrospinning, can generate a broad array of nanoarchitectures, including core-shell, tube-in-tube, porous, hollow, cross-linked, and particle-encapsulated structures (McKeen, 2021).

By utilizing an electrical charge to create nanofibers, electrospinning can produce both 2D and 3D scaffolds with high surface area, aligned morphology, tunable mechanical and chemical properties, and excellent porosity which allows for greater cell interaction. Moreover, electrospinning has been successfully used for the fabrication of scaffolds to restore vascular graft, cartilage, and neural tissue (Jung et al., 2018; Karkan et al., 2019; Park et al., 2018).

Some polymers, such as polycaprolactone (PCL), glycolic acid (PGA), and polylactic-co-glycolic acid (PLGA), are suitable for creating nanofibers in TE because they provide biocompatibility and mechanical properties that simulate the desired cellular environment. Additionally, these materials are flexible, low-density, resilient, and chemically versatile, as well as being biocompatible and biodegradable, and can be manufactured by means of electrospinning.

Scaffolds for CTE depend not only on the manufacturing process but also on the materials used. The selection of materials is crucial in establishing the structural integrity, biocompatibility, and general functionality of the scaffold. The next section will examine the wide range of materials used in scaffold design, their individual characteristics, and how they affect TE application success.

1.4.2 Key Materials in Tissue Engineering

For the scaffolds fabrication in CTE, a wide range of materials are available. The polymeric matrices or scaffolds may be built with natural, synthetic, or hybrid materials and they promise to be a viable alternative to current treatment practices (Boroumand et al., 2021; Jang et al., 2020; Majid et al., 2020). Furthermore, since they efficiently support tissue regeneration, the biomedical nanomaterials used for the scaffolding have been recognized, in recent years, as key players in many tissue-engineering processes (Vunjak-Novakovic, 2017).

Hence, some of the most recent bioengineering research has focused on evaluating different polymers —both synthetic, such as polycaprolactone (PCL), polyvinylpyrrolidone (PVP), polyglycerol sebacate (PGS), polyurethane (PU), glycolic acid (PGA), polylactic-co-glycolic acid (PLGA), and natural, such as gelatin (GT), chitosan (CS), collagen (COL), or elastin alginate (ALG)— in search of new applications in the field of TE (Karkan et al., 2019). Indeed, some of these polymers, especially PCL, PGA, or PLGA, have proven to be suitable for the creation of nanofibers in TE because they guarantee biocompatibility and the mechanical properties necessary for simulating the desired cellular environment. In addition, these materials are flexible, low-density, resilient, chemically versatile, biocompatible, biodegradable and FDA-approved (Margerrison et al., 2021; U.S. FDA Center for Devices and Radiological Health, 2020). Furthermore, this materials are suitable to be manufactured through electrospinning (Oprea et al., 2019).

Polycaprolactone (PCL)

PCL is a linear synthetic and biodegradable polyester that is partially crystalline with a low melting point (60°C) and a glass transition temperature of −60°C. It is fabricated by opening the ε-polycaprolactone ring catalyzed by octanoate to finally obtain the structure shown in the *Figure 1 - 4* (McKeen, 2021; Nair et al., 2017). In addition, its elastic modulus is 190 MPa and its elongation are >500%, these properties can vary according to the porosity and manufacturing method of the polymer.

PCL has been used for scaffolds and long-term implants fabrication because its degraded time is slow, being of 3 or 4 years. Further, PCL degradation by hydrolysis of its ester linkages in physiological conditions can be completed excreted from the body (McKeen, 2021; Sigaroodi et al., 2023).

On the other hand, PCL is hydrophobic and non-conductive polymer, which is not very convenient for cell viability. PCL is often combined with other polymers or fillers to compensate for their limitations. For instance, electrospun nanofibers mats of PCL and poly (glycerol sebacate) (PGS) prepolymer and mildly crosslinked PGS was fabricated using acetic acid as less toxic solvent. In this

case, the results obtained including PGS did not exceed the properties of PCL, for example, the fiber diameters increase from 0.8 ± 0.3 µm to 1.3 ± 0.7 µm, mechanical properties also decrease with the addition of PGS, and degradation time are lowest (Vogt et al., 2019).

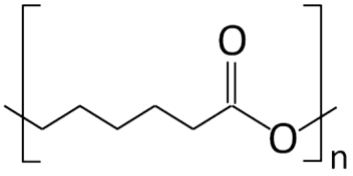

Figure 1 - 4 Polycaprolactone (PCL) structure.

Polyvinylpyrrolidone (PVP)

PVP has been used in different applications and specifically in TE, it has been used in various types of tissues; however, it has not been widely exploited in the CTE, despite its potential properties in this field (Kurakula & Koteswara Rao, 2020). PVP is a water soluble, hygroscopic (absorbs up to 40% of water by its weight), amorphous and synthetic polymer (Kariduraganavar et al., 2014). Unfortunately, PVP lacks tensile strength, which is a disadvantage in CTE applications. To get through it, authors as Pushp et al. development and evaluated PVP/ Poly(vinyl alcohol) (PVA) cardiac patches plasticized with glycerol to bolster patch pliability. With an optimized molar ratio (0.3 % v:v), tensile strength of 5–30 MPa and, percent elongation at break of more than 250%, was achieved. Also, with a PBS contact, patches formed a hydrogel capable for supporting, attach and proliferating neonatal CM with a tensile strength of 1.3-3.0 MPa, same value for the Young's Modulus. They also play an *in vivo* test on rats demonstrating the safety of the PVP/PVA patches (Pushp et al., 2021).

Poly Glycolic acid (PGA)

PGA is biodegradable, linear aliphatic polyester that is characterized by its high crystallinity. This gives PGA a low solubility in water and organic solvents (Abdul Rahman & Bahruji, 2022; Murugan et al., 2022). PGA also boasts a high melting point, ranging from 220 to 230 °C, and a glass transition temperature (Tg) that falls within the range of body temperature, around 35–45°C (X Zhang et al., 2017).

One of the most interesting properties of PGA is its ability to be metabolized and eliminated from the body through the tricarboxylic acid cycle (Abdul Rahman & Bahruji, 2022). With its high tensile modulus and biodegradable nature, PGA is an excellent material for use in scaffolds for CTE because it can equal the flexibility of the heart tissue.

Monofilament sutures, for example, were made using PGA copolymer and trimethyl carbonate (TMC). The results demonstrated suture compatibility with the sternum and PGA/TMC interaction with a mildly hydrophilic structure suitable for use in cardiac procedures (El-Sayed et al., 2021).

Polylactic acid (PLA)

PLA is a good mechanical property that is both biodegradable and biocompatible long-term use polyester having a melting temperature of around 175 °C (Hagen, 2012). However, it does have two main drawbacks: it is hydrophobic due to presence of extra methyl group, and it is relatively brittle (A. Kumar & Kumar, 2019; Sigaroodi et al., 2023).

Flaig et al. produced PLA/PGS 30% fibers with a diameter ranging from 600 to 1300 nm. PGS enhanced hydrophilicity, allowing for more cell-material contact and Matrigel functionalization. The sowed CMs acquire a native tissue form, resulting in fewer fibers and better outcomes. There was no inflammatory reaction following implantation in a mouse model, and neo-vascularization was accomplished (Flaig et al., 2020).

Uniaxial and coaxial electrospinning were employed to fabricate PLA, PLA/Polianiline (PAni), and PLA/PEG/PAni fibers, enhancing electrical conductivity. The addition of PEG improved PLA and PAni packing, while PAni increase the conductivity. PAni/dodecylbenzenesulfonic acid (DBSA) cytotoxicity effects were mitigated by PEG addition and a core-shell configuration. Uniaxial PLA/PAni fibers had diameters ranging from 2359 ± 85 nm to 5200 ± 89 nm, increasing with PAni content. PLA/PEG/PAni and coaxial PLA-PEG-PAni fiber diameters varied from 2129 ± 171 nm to 2378 ± 12 nm and 763 ± 17 nm to 2271 ± 169 nm, respectively. Young's Modulus, decreased with PAni, ranging from 39 ± 5 MPa to 44 ± 5 MPa. Electrical conductivity ranged from 0.23 ± 0.05 μS/cm in PLA/PAni-2.5% to 0.99 ± 0.05 μS/cm in PLA/PAni-10%, slightly increasing to 0.53 ± 0.14 μS/cm with PEG. The core-shell configuration conductivity was approximately 0.5 μS/cm. (Bertuoli et al., 2019).

Polylactic-co-glycolic acid (PLGA)

PLGA is a copolymer of PLA and PGA. It is an FDA-approved polyester with a good biocompatibility and biodegradability. Its uses are favorable for drug delivery due its favorable degradation characteristics (Hirenkumar & Steven, 2012; A. Kumar & Kumar, 2019).

Cristallini et al. discusses the potential use of poly(lactic-co-glycolic acid) (PLGA) in CTE applications. The authors highlight the advantages of using PLGA, such as its ability to control drug release and degradation rate, as well as its non-toxicity and compatibility with different cell types and some of the challenges associated with using PLGA, such as its poor mechanical properties and potential inflammatory response (Cristallini et al., 2019a).

Two distinct electrospun scaffolds made of PLGA alone and PLGA with a platelet-rich plasma (PRP) additive were created by Torabi et al. The diameter of the linked, randomly oriented, and nanofiber bead-less porosity scaffolds was 500 ± 280 nm. Additionally, human induced pluripotent stem cells (iPSC) were seeded on the scaffolds, differentiated into CM, and achieved better outcomes in the PLGA-PRP compared to PLGA, demonstrating that the natural growth factors present in the scaffold had a favorable impact on the outcomes of biocompatibility (Torabi et al., 2021).

A supercritical CO_2 foaming procedure was used to manufacture porous polymeric devices with increased conductive properties in an intriguing work using PLGA and indeed the conductive polymers PEDOT:PSS. The distribution of the polymer was uniform, with 40% porosity and an increase in the expansion factor of 10 orders, and temperature-dependent pore diameters ranging from 97.4 ± 22.0 to 246.6 ± 77.7 nm. Mechanical properties ranged from 0.8 to 13.6 MPa Young's modulus in compression tests, whereas electrical conductivity ranged from $2.2 * 10^{-7}$ to $1.0*10^{-5}$ S/cm (Montes et al., 2023).

Collagen (COL)

COL makes up around 30% of all proteins in mammals, making it the most common and complex protein in both animals and humans. The main element of the ECM in numerous organs, including the heart, is COL. It has several benefits, including good solubility, high tensile strength, controlled stability, biodegradability, low immunogenicity, and positive cell contact. Because to its characteristics and ability to transfer tensile and compressive forces, COL is a suitable biomaterial for use in CTE (Patino et al., 2002; Sell et al., 2009).

Wee et al. used co-electrospinning with separate nozzle control to fabricate bimodal nano and microfibers scaffolds with the aim to enhance focal adhesion signal and porosity to promote cell migration and proliferation. These scaffolds are made up of PLGA microfibers (0.5-1.5 µm diameter) and COL (4-6% in content was the optimal) nanofibers (50-250 nm). Hydrophilicity increased proportionally as COL concentration increased. With the COL addition, these scaffolds outperformed collagen in terms of mechanical characteristics and improved bone marrow-derived mesenchymal stem cell proliferation. Scaffolds containing cells were implanted in a rabbit model for *in vivo* tests, enhancing heart regeneration and long-term stem cell retention. This promotes the secretion of recovery factors, which contribute to tissue regeneration, or the differentiation of cardiac and vascular endothelial cells (Wee et al., 2022).

Gelatin (GT)

GT is a natural polymer that is derived from COL by alkaline or acid hydrolysis. GT has many advantages, including biocompatibility, biodegrability and low toxicity, also it is degraded by body

enzymes without immunogenic response. Further, GT is low-cost and highly hydrophilic polymer that has many applications in CTE such as injectable hydrogels, drug delivery systems and scaffolds. On the other hand, GT lacks thermostability, turning solid or gel depending on the temperature, poor mechanic stability and lack of reproducibility due its origin, which is mainly from porcine skin (Lukin et al., 2022; Nikkhah et al., 2016).

Elamparithi et al. created nanofibrous matrices of GT without the need for a synthetic or natural polymer by electrospinning with acetic acid, a safe solvent for CTE applications. The scaffolds had a Young's modulus of 19.6 ± 3.6 kPa, fiber diameters ranging from 200 to 600 nm. Neonatal rat CMs were cultured in the matrices, resulting in four weeks of synchronous contractions (Elamparithi et al., 2017).

In another study, Nagiah et al. used electrospinning to create three different scaffolds: furfuryl-gelatin (f-gelatin) alone, f-gelatin with polycaprolactone (PCL) 1:1, and coaxial scaffolds with PCL (core) and f-gelatin (sheath). Fiber diameters for f-gelatin, f-gelatin with PCL, and coaxial f-gelatin with PCL were 760 ± 80 nm, 420 ± 110 nm, and 810 ± 60 nm, respectively. The coaxial scaffold had the highest Young's modulus of 164 ± 3.85 kPa and the best adhesion of human-induced pluripotent stem cell (hiPSC)-derived CM. The three scaffolds supported AC16 CM cells with good biocompatibility (Nagiah et al., 2022).

Chitosan (CS)

Chitosan is a biodegradable, non-toxic de-acetylated chitin derivative biopolymer, derived from the outer shells of shellfish, shrimp, lobster, and crabs, as well as fungi cell walls. It is used in CTE due its antifungal, antibacterial, antiviral, and adjustable degradation properties. Among its limitations are its poor mechanical properties and its lack of conductivity (Chakraborty, 2020).

Because of its limitations in properties, few studies have been conducted exclusively on CS without the addition of another polymer or additive. Xu et al., on the other hand, developed an injectable scaffold CS hydrogel to deliver mesenchymal stem cells (MSCs) directly into such infarcted myocardium in rats. According to the findings, CS hydrogel promoted MSC differentiation in CM, increased neovascularization formation, and enhanced cardiac function and hemodynamics after myocardial infarction (B. Xu et al., 2017).

Although chitosan (CS) is typically not ideal for electrospinning, its amalgamation with polyvinyl alcohol (PVA) and a maintained at a consistent 0.1%wt of graphene forms advantageous hydrogen bonds that facilitate nanofiber formation. The experiments revealed that increasing the CS ratio not only improves the electrical conductivity and viscosity of the electrospun solution but also extends stress relaxation times and reduces nanofiber breakage. Moreover, a higher concentration of

chitosan enhances hydrophilicity and results in smaller, spindle-shaped nanofibers with lower surface resistance. This is particularly beneficial for the distribution of graphene within the nanofibers, leading to more efficient and evenly dispersed graphene incorporation, which is crucial for leveraging its advantages in various applications (T. T. Li et al., 2019).

Alginate (ALG)

ALG is a biopolymer found in cell walls of algae and bacteria.
It is a linear copolymer composed of two monomers, -D-mannuronic acid (M) and -L-guluronic acid (L) (G). Because of its unique properties, ALG has a wide range of applications. It is a hydrophilic and anionic polymer capable of forming gels in the presence of divalent cations like calcium (H. Zhang et al., 2021).

Alginate is used as a biomaterial in biomedical engineering for TE and Regenerative Medicine applications. Alginate hydrogels can encapsulate cells and promoting their growth and differentiation into functional tissues. Alginate scaffolds can also help with tissue regeneration and wound healing (M. Xu et al., 2021).

Like other natural polymers, ALG lacks adequate mechanical properties. To enhance the mechanical properties to the scaffold, it is necessary to mix it with other polymers. For instance, Tamimi et al. fabricated ECM solubilized along with ALG and CS enhancing mechanical properties, increasing since 254 kPa to 1110 MPa, despite its 96% porosity. An MTS essay was played to verify the proliferation of human mesenchymal stem cells (hMSC), a histological essay confirmed cardiomyocyte penetration and a higher expression of cardiac marker (cTnT) was shown (Tamimi et al., 2020).

Moreover, to improve not only the mechanical properties but also the electroconductive properties, latest studies have been added conductive particles or carbon derivates elements. For intance, Beltran-Vargas (2022) preparing different ALG/CS scaffolds with and without metallic particles such as gold (AuNp). Hydrophilic scaffolds with more than 90% of porosity, spheroid formation and favorable cardiac markers expression was obtained (Beltran-Vargas et al., 2022).

ALG has been attractive to researchers for being a matrix that houses electroconductive elements as is the case of Serafin et al. who develop a 3D printed hydrogel made of GEL and ALG with carbon nanofibers (CNF) as filler, to strengthen its mechanical properties reaching a Young's modulus of 534.7 kPa and a conductivity of 4.1*10-4 ± 2 × 10−5 S/cm. The obtained scaffold showed to have a good cell attachment (Serafin et al., 2021).

As was mentioned above, numerous functionalized polymers or conductive additives have been utilized recently to increase the scaffold's electrical conductivity. The following is a description of the two most significant conductive materials utilized in CTE.

Electroconductive materials: Graphene

Graphene is a carbon allotrope characterized for single layer of sp^2-bonded carbons arranged in a hexagonal lattice as can be seen in *Figure 1 - 5*. The term 'Graphene' was first proposed in 1986 to denote the single layer of graphite. Following its discovery in 2004, graphene has emerged as a material of significant interest due to its exceptional properties (Mbayachi et al., 2021).

Some properties include a high Young's Modulus, and specific surface area, outstanding electrical and thermal conductivity (Potdar et al., 2020). These properties made graphene suitable in diverse applications across various fields, such as in the fabrication of sensors (Nag et al., 2018), electronics (Avouris & Dimitrakopoulos, 2012), composites (Mohan et al., 2018), and photovoltaic cells (Mahmoudi et al., 2018). Recently, graphene has shown promising potential in drug delivery, bioimaging, antibacterial materials, and TE (Shang et al., 2019), further expanding its range of applications.

Regarding the use of graphene or carbon conductive derivatives to improve the electromechanical and biological properties of scaffolds, some studies report improvements in electrical conduction, Young's modulus, and cardiac cell differentiation, but a decline in cell proliferation due to the limited contact between cells (Ahadian et al., 2016). For instance, Chen et al. created nanofibrous scaffolds made of polycaprolactone/gelatin (PCL/Gt) and loaded with different mass fractions of graphene. These scaffolds showed a positive in-vitro and in-vivo response in neonatal rat models in a CCK-8 assay. Indeed, the histopathological staining (DAPI, cTNT, and CX43) indicated that cells grew and survived, with no evidence of toxic or inflammatory reaction when the graphene mass fraction was less than 0.5% (X. Chen et al., 2019).

Other tissue-engineering studies support the use of graphene in polymeric matrixes, for this results in a greater cell growth (PC12 cells), which, in turn, leads to greater hydrophilicity and 99% antibacterial properties against gram-positive and gram-negative bacteria (Heidari et al., 2017, 2019). These positive effects are attributable to the unique biological properties of graphene.

In a different approach, Jiang et al. created CS with different proportions of Graphene Oxide to handle swelling, porosity, and electric conductivity scaffolds. The electric conductivity was 0.134 S/m. The biological activity was assessed, with H9C2 cardiac cell seeding demonstrating good viability, cell junction and Connexin-43 expression, the latter being involved in cardiac muscle contraction and electrical coupling (Jiang et al., 2019).

Lastly, Karimi et al. fabricate an electrospun conductive and multilayer scaffolds made of two outer layers of ALG and Graphene and an inner PCL layer. The outers layers brings electrical conductivity, viability and junction cells and the inner layer provide a mechanic support. Conductivity rises 7.29 S/m with 1% of graphene addition with maximum tensile strength and Young's modulus of 22.46 and 4.35 MPa (Karimi et al., 2022).

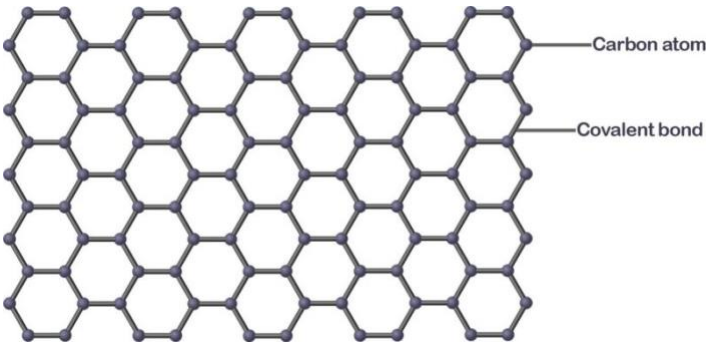

Figure 1 - 5 Graphene layer structure.

Electro-Conductive polymers

In order to tackle the challenges in CTE, especially the electrical conductivity of the tissue, researchers have developed scaffolds composed of conductive polymers such as poly(3,4 ethylene dioxythiophene) (PEDOT), poly(styrene sulfonate) (PSS), polypyrrole (PPy), and polyaniline (PANI) (Ghovvati et al., 2022; Matysiak et al., 2020; Roshanbinfar et al., 2020). Other materials commonly used to improve the electrical conductivity of tissue are gold nanoparticles (AuNP) and carbon allotropes such as carbon nanotubes (CNT) or graphene (Alegret et al., 2019; Bellet et al., 2021; Gelmi et al., 2015; Gómez et al., 2021; B. Guo & Ma, 2018; S. Kumar & Chatterjee, 2016).

Improving the electrical conductivity of cardiac tissue after an infarction is important since, by focusing on the gradual recovery of the tissue, this inhibits further deterioration of the infarcted heart, promotes cell signaling, and influences the mechanical stretching of cardiomyocytes, thus achieving synchronous contraction (Blachowicz & Ehrmann, 2020; Gálvez-Montón et al., 2013).

Polypyrrole (PPy)

Polymers are regarded as insulators owing to their high resistivity, which means that they have poor electrical conductivity. However, some polymers can be turned conductive by altering their chemical composition or using dopants. Developing a polymer that exhibits conductivity qualities traditionally associated with metals is just one example of how materials research is constantly investigating new features in various materials. Although there are other conductive polymers, PPy has been the

subject of the largest investigation (Borges et al., 2023; P. Huang et al., 2023). In this section, we will discuss its potential for CTE.

PPy is a positively charged, heterocyclic conductive polymer containing nitrogen in its oxidized state (S. Cui, Mao, Zhang, et al., 2021). Overoxidation results in a reduction of conductivity and charge of PPy (Y. Wang & Feng, 2022). In contrast to polyaniline (PANI), PPy is easier to manufacture (John & Jayalekshmi, 2023), has higher electrical conductivity, greater environmental stability (Gu et al., 2022), and reduced carcinogenic concerns associated with its degradation products (S. Cui, Mao, Zhang, et al., 2021; Kausar, 2021).

Why can polymers conduct electricity? The presence of free charge carriers, such as electrons or ions, which may move through a material determines its capacity to conduct electricity. While in polymers they can be synthesized by doping the polymer with impurities that can either give or take electrons, electrons are the free charge carriers in metals. By changing their chemical composition to incorporate conjugated π-bonds, which permit electrons to flow freely through the substance, polymers can also be made conductive (Lu et al., 2021; Namsheer & Rout, 2021).

The presence of π-bonds and alternating single and double bonds, which cause the electron density in the molecule to delocalize, is what gives PPy its electrical conductivity (Y. Wang & Feng, 2022). In order to synthesis PPy, pyrrole (Py), a water-soluble monomer, is employed carryng the reactions in. Various dopants can then be added to oxidize PPy, changing its structure from an aromatic benzenoid to a quinoid (John & Jayalekshmi, 2023; Le et al., 2017; Ma et al., 2019). A polaron is created as a result of this reaction, and with additional oxidation, a bipolaron with two charges is created, see *Figure 1 - 6* (Grzeszczuk, 2018; Pang et al., 2021).

Iron chloride (FeCl3), copper chloride (CuCl2), dodecylbenzenesulfonic acid (DBSA), and iron sulfate (Fe2(SO4)3) are some of the most used dopants for PPy. Surfactants including sodium dodecylbenzenesulfonate (NaDBS), naphthalene sulfonic acid (NSA), and SDS are also generally added (Harlin & Ferenets, 2006).

Among the disadvantages of PPy is that it is fragile, which sometimes limits its use, however, it is overcome when combined with other polymers or copolymers. Talebi et al. created a membrane made of PCL/CS/PPy. The electrical conductivity increased from 0.0164±0.008 mS/m to 0.55±0.03 mS/m at 7.5% PPy by blending PCL/CS (7:3) and various PPy compositions. Furthermore, the inclusion of PPy improved the membrane's hydrophilicity, as the water contact angle decreased from 107 2.1° for PCL/chitosan to 101 3.5° at 7.5% PPy. Tensile strength increased from 7.57 MPa for the PCL/chitosan sample to 18.06, 16.02, 15.33, and 13.87 MPa for the 1, 2.5, 5, and 7.5 wt% PPy samples, respectively. Furthermore, the films containing PPy had better antibacterial properties against E. coli and S. aureus (Talebi et al., 2019).

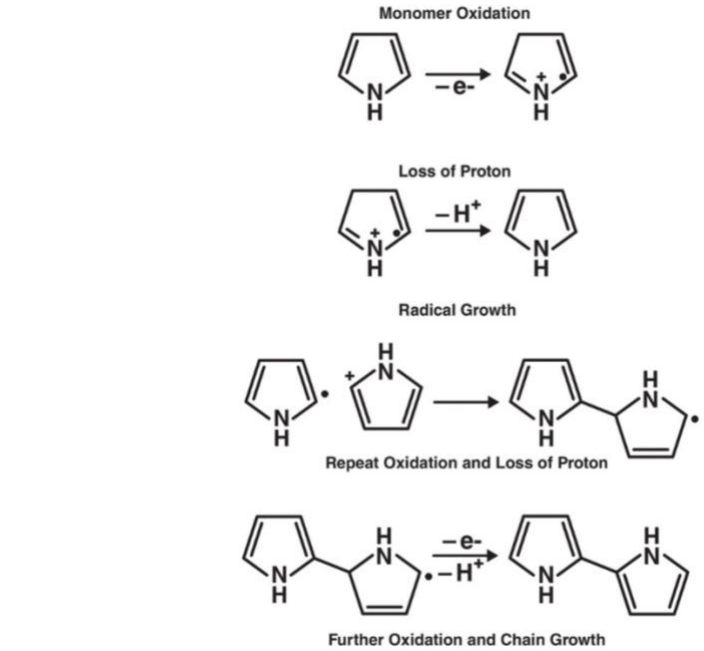

(a)

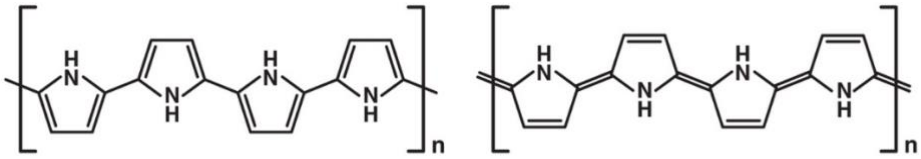

(b)

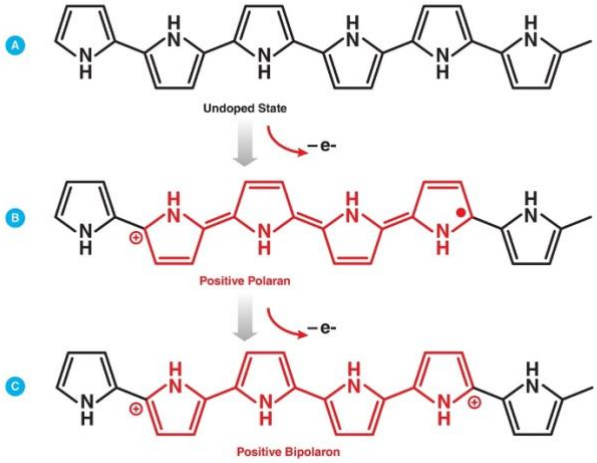

(c)

Figure 1 - 6 (a) Mechanism of electrochemical synthesis of PPy: monomer oxidation, loss of proton and radical growth (Adapted from (Namsheer & Rout, 2021)). (b) benzenoid and quinoid forms of PPy (Adapted from (Mahun et al., 2020)) (c) undoped state, polaran, and bipolaran of PPy (Adapted from (Pang et al., 2021).

Some authors have used conductive nanofillers to improve the functionality of the engineered cardiac tissue. For instance, Liang et al. used PPy blended with silk fibroin electrospun nanofibers for this purpose. Indeed, by working with this material Liang et al. were able to produce low-diameter fibers and achieve a tissue with very similar mechanical properties to those of the native myocardium, which entails that the tissue had enough electrical conductivity and could support cardiomyocyte contractions (Liang et al., 2021).

Zarei et al. for their part, obtained conductive scaffolds composed of chitosan, collagen, and polyethylene oxide with PPy as nanofiller. After evaluating and characterizing this type of fibers, Zarei et al. concluded that they had enhanced conductivity, on the one hand, and promoted cell adhesion, growth, and proliferation (Zarei et al., 2021). In a similar vein, Wang et al. developed nanofibrous sheets composed of PLA and PANI, thus enhancing conductivity while preventing the diameter of the nanofibers from increasing. Moreover, these PLA/PANI nanofibers exhibited a good interaction with cardiomyocytes, which makes them a viable alternative (L. Wang et al., 2017).

Alternatively, there are some reports of other applications nanofibers manufactured with conductive nanofillers. For example, Maharjan et al. developed an *in situ* polymerization of PPy into a PCL solution. Then, the resulting PPy/PCL solution was electrospun, thus its mechanical strength was enhanced, its surface roughness was increased, its fiber diameter was decreased, and its interactions with bone cells were improved (Maharjan et al., 2020).

Moreover, PPy has been combined with polyurethane (PU) and poly-L-lactic acid (PLLA) to obtain a soft conductive, flexible, and easy to handle biomaterial that could be used for biomedical applications that require the proliferation of human skin keratinocytes (S. Cui, Mao, Rouabhia, et al., 2021). Furthermore, PPy has been used in nerve-tissue engineering with PLA to improve the conductivity, hydrophilicity, and mechanical properties of the nerve cells (Imani et al., 2021; S. Li et al., 2022).

Finally, another approach for the fabrication PPy in electrospun scaffolds, Fakhrali et al. made an optimization of the electrospinning variables process to obtain PCL/PGS fibers with a conductive polymer that has been widely used, polypyrrole (PPy), which was *in situ* polymerized from its monomer pyrrole (Py). The synthesis of PGS and PPy was confirmed, achieving a tensile strength of 3.12 ± 0.19 MPa and elongation of 80.26 ± 13.71%. The best concentration of Py to enhance the results in MTT tests and the overall process was 0.05M. Eventually, the diameter under optimal conditions was 283 nm with a range between 357-676 nm, and the electrical conductivity was 3.522-1E-5 S/cm (Fakhrali et al., 2022).

1.5 Main Challenges in CTE

Over the past few decades, CTE has made a considerable progress, with the hope that it will the aim of making it one day become a viable treatment option for heart disease. Despite the significant progress in this field, challenges remain. In this section, we will discuss some of these challenges and the efforts that have been made to overcome them.

1.5.1 Replicate anisotropic structure.

One pivotal challenge in the development of ECM of bioengineered tissues is the replication of the anisotropic structure of cardiac muscle fibers, which promotes the growth and alignment of cardiomyocytes (Camman et al., 2022; Takada et al., 2022; Zhuang et al., 2022), thereby enhancing the contractile function of the heart. Indeed, a successful mimicking of the aligned structure of the myocardium would improve cardiomyocyte maturation and differentiation, regulate cellular function such as morphogenesis, cell the mechanical properties of the tissue, and its flexibility (Kharaziha et al., 2014; Ye & Qiu, 2017).

With many manufacturing techniques of scaffolds is complicated obtain aligned structures, since they work by using general cell-alignment and adhesion patterns that fail to replicate the complexity of actual living tissue (Qasim et al., 2019). The use of electrospun scaffolds provide a solution to align fibers to imitate the cardiac ECM matrix (Camman et al., 2022).

Thanks to the use of electrospinning, it is possible to create scaffolds with random and aligned fibers to better mimic the extracellular matrix (ECM) of cardiomyocytes. For instance, Kai et al. developed aligned and non-aligned scaffolds through electrospinning, combining PCL and gelatin. In their study, they found that aligned nanofibers promoted higher cell attachment and greater cell alignment. Additionally, the aligned nanofibers exhibited anisotropic wetting and mechanical properties that closely resembled those required for native cardiac tissue. Culturing rabbit cardiomyocytes on the electrospun nanofibers confirmed the biocompatibility of the scaffolds and demonstrated their potential in guiding cell attachment and alignment (Kai et al., 2011).

On the other hand, an anisotropic architecture improves electrical conductivity, because there will be an efficient transmission of electrical signals between cardiac cells. For example, the electrical speed of propagation in the ventricle of an adult is 2 or 3 times larger in longitudinal fibers with respect to cross-fiber direction (Bronzino, 2006). Additionally, in cardiac tissue, the conduction velocity is anisotropic, and its orientation is determined by myocytes (Kotadia et al., 2020).

Several studies have demonstrated that the addition of electroconductive nanofillers to aligned nanofibers can significantly enhance the properties of scaffolds for CTE. For instance, Kharaziha et

al. reported that increasing the carbon nanotube (CNT) content in Gel-MA combined with poly(glycerol sebacate) PGS: gelatin (PG) electrospun nanofibers enhances fiber orientation, mimicking the anisotropic alignment of myocardial tissue (with an orientation index value of approximately 40°) (Kharaziha et al., 2014).

In a similar way, Mancino et al. developed an aligned scaffold (APPY), using gelatin, PLGA, and PPy nanoparticles through electrospinning. Compared to non-aligned samples (NAPPY), APPY exhibited improved strength, enabling easier deformation under stress. This is particularly important considering the significant pressure exerted on cardiomyocytes by the heart. Furthermore, the organized structure of APPY promotes cell orientation, resembling the composition of the extracellular matrix (ECM) in the myocardium, which consists of collagen and elastin (Mancino et al., 2022).

1.5.2 Scaffold thickness

The thickness of the scaffold for CTE is an important parameter to consider, as it can influence the performance of the scaffold in the tissue. For example, a very thin scaffold may be fragile and not provide enough mechanical support to maintain the structural integrity of the heart tissue. Likewise, a very thick scaffold limits the diffusion of oxygen and nutrients through the scaffold, this point is very relevant, especially for cardiac cells, due to its continuous contractile activity and its high oxygen demand (Bronzino, 2006).

As a result, the thicker the scaffold, the more cellular viability and function are adversely affected because low oxygen supply to the infracted area prevents cells from being incorporated (Sharma et al., 2021). Some studies claim that oxygen diffusion has a depth limit of 200 μm (Dozois et al., 2017; Qasim et al., 2019) or even less than 100 μm (Suh et al., 2020).

To enhance oxygen transport within the scaffold, vascularization is necessary, and parameters such as porosity play a crucial role (Ye & Qiu, 2017). The electrospinning technique offers an excellent option for obtaining thinner and porous membranes simultaneously, contributing to improved oxygenation within the scaffold.

1.5.3 Chemical properties

The chemical properties of scaffolds must be compatible and safe for use in cardiac cell applications to avoid future immunological reactions. Therefore, it's necessary to consider the material composition of the scaffold, as highlighted in the previous section. Additionally, it's crucial to ensure that the scaffold can gradually degrade as cardiac cells grow and produce their matrix.

The chemical properties of scaffolds are linked to both their chemical composition and the characteristics of their surface. Initially, a scaffold for CTE applications must promote cell adhesion to facilitate the gradual formation of functional tissue, as illustrated in *Figure 1 - 7*. To achieve this, changes in surface chemistry and physical topography are necessary. These changes can be induced by functionalizing the surface, either through chemical or physical means.

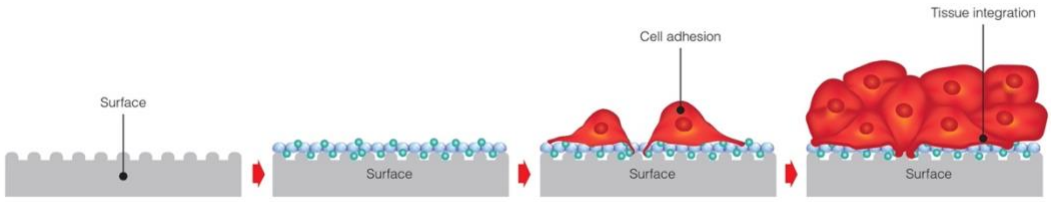

Figure 1 - 7 The Importance of Surface Roughness in Cell Adhesion (author).

Among the options utilized, coatings with bioactive substances that impart properties to the scaffold have been employed. Physical functionalization involves weak interactions between the scaffold ligand and the bioactive molecule through electrostatic interactions, hydrogen bonding, and/or hydrophobic interactions. Chemical functionalization, on the other hand, entails the formation of covalent bonds, resulting in stronger, oriented interactions (Roacho-p et al., 2022). Ultimately, these interactions form the foundation for cellular communication that leads to the development and function of cardiac tissue.

1.5.4 Mechanical properties

To mimic cardiac ECM, the mechanical properties of scaffolds are crucial for maintaining the structural integrity of scaffold necessary for growing tissue and withstanding the biomechanical forces acting on it. Among the most important biomechanical properties is elasticity. Thus, the modulus of elasticity of the scaffold must be close to that of myocardial tissue. In myocardial tissue, Young's modulus is between 200 and 500 kPa (Fleischer et al., 2017; M. Lee et al., 2022; Sigaroodi et al., 2023).

Mechanical properties are also important for the overall biocompatibility of scaffold, because inadequate mechanical properties can cause mechanical stress on cells, which could lead to cell death or unwanted inflammatory responses.

1.5.5 Electrical conduction

Myocardial tissue is electrically active, and many materials used for this application do not conduct electricity, consequently, they would act as a barrier to signals and electrical stimulation in the infarcted area.

Scaffolds made of electro-conductive biomaterials electrically stimulate cardiomyocytes to achieve synchronous contractions, propagate an electrical impulse, promote cell survival, and increase the expression and maturation of cardiomyocyte-specific markers. It is worth noting, that successful integration of the scaffold requires a correct electrical coupling between it and the host, which, in turn, facilitates cell extension (He et al., 2020).

As a reference, in CTE, superior or close to host tissue conductivity must be achieved; in this context, some authors report conductivity of 1 mS/cm (Fakhrali et al., 2022; House et al., 2021; Liang et al., 2021; Ren et al., 2023), other authors report values of 0.5 mS/cm (Sovilj et al., 2014) o 0.54 mS/cm (Gabriel et al., 1996), 40 mS/cm longitudinal and 17.9 mS/cm for transversal heart tissue (Malmivuo & Plonsey, 1995).

1.5.6 Electromechanical couple

Coupled the mechanical strength and electric conductivity, this integration results in the adequate and functional assembly of the cardiac tissue. The aspects mentioned above have been some of the most important challenges for cardiac-tissue engineering in recent years (Bolonduro et al., 2020; Vunjak-Novakovic, 2017; Vunjak-Novakovic et al., 2010).

This coupling is critical because it mimics the inherent operation of the human heart, where electromechanical coupling refers to the process by which electrical activation of myocytes results in mechanical contraction (Pfeiffer et al., 2014). This process involves voltage changes in the cellular membrane, which cause a reorganization in the architecture of hyperpolarization-activated cyclic nucleotide-gated (HCN) ion channels found in the heart and other tissues. These channels, which play a role in the cardiac pacemaker and other electrical activities in the brain and heart, activate in response to membrane hyperpolarization (when the membrane potential becomes more negative) rather than depolarization (when the membrane potential becomes more positive), as is the case with most voltage-activated ion channels (Dai et al., 2021).

Electromechanical coupling ensures that the electrical impulses causing the heart to contract are efficiently transmitted to muscle cells, resulting in a coordinated and effective contraction of the cardiac muscle and adequate blood pumping (Hu et al., 2022). In a healthy heart, the timing of mechanical activation closely follows that of electrical activation, leading to a relatively synchronous

contraction pattern. Myocardial contraction is initiated by electrical activation, with pacemaker cells located in the sinoatrial node or sinus node (SA), and ventricular activation begins with electrical impulses from the atrioventricular node or AV node, traveling through the His bundle, which then divides into right and left branches, leading to the Purkinje fibers located in the subendocardium (Kierszenbaum, Abraham L.; Tres, Laura L.; Fernández Aceñero, 2016).

The conduction velocity is about four times faster in Purkinje fibers than in normal myocardium. Impulse conduction in Purkinje fibers occurs from the base to the apex but exits the Purkinje system near the apex in the subendocardium, causing activation of the septum and the free walls of both the left and right ventricles to occur from the apex to the base and from the endocardium to the epicardium. Due to the rapid transmission of the impulse, normal ventricular activation is relatively synchronous, leading to normal myocardial contraction during systole, which is quite synchronous and efficient.

Given the aforementioned, it's evident that one of the most difficult issues in CTE is achieving electromechanical coupling through the integration of electroconductive scaffolds. The pursuit of this goal serves as a basis for much of the field's research, which seeks to recreate the heart's complex capabilities via synthetic tissues. By comprehending and applying the principles of electromechanical coupling, researchers are making significant progress toward developing scaffolds that can not only support cellular growth but also accurately mimic the electrical and mechanical behavior of the heart, a critical step forward in the quest to treat cardiac diseases with Regenerative Medicine.

1.6 Future Trends in Cardiac Tissue Engineering

Given the preceding section, it is clear that scaffolds designed for Cardiac Tissue Engineering (CTE) must increasingly satisfy highly stringent standards. Currently, no single biomaterial is able to completely recreate all of the characteristics required to mimic the myocardium's architectural, chemistry, and biomechanical attributes (Pomeroy et al., 2020). However, there are numerous studies on biomaterials, constructions, and advancements aiming to fulfill the future objective of improving cardiac pathologies through CTE biomaterials. A simple search on PubMed, filtering results from 2020 with "CARDIAC TISSUE ENGINEERING," yields 5,158 entries, 837 of which include "scaffold" and 372 with "biomaterial," 107 mention "conductive," and 16 "electroconductive."

Despite this number of studies, when comparing the total number of published studies to those that have conducted *in vivo* studies, and even fewer in humans, the numbers decrease significantly. Repeating the search with "CARDIAC TISSUE ENGINEERING" and adding "Clinical Trial" filters yields 37 results. Including "scaffold" in the search narrows the results to just two from 2020.

According to reports on ClinicalTrials.gov, filtering for Myocardial Infarction and scaffold reveals 29 studies worldwide. For Colombia, three studies were found (ClinicalTrials.gov, 2024). Most of the results pertaining to stents, more applicable to Coronary Artery Disease. This highlights the necessity for continued development of new scaffolds that are safe and possess truly implantable properties for real-world applications.

It is important to note that this project focused on nanofibrous scaffolds fabricated via electrospinning. However, other techniques and types of scaffolds are being developed using different methods and biomaterials. Among the emerging techniques is 3D printing, known for its versatility in use and design and the capability to fabricate complex morphologies with a defined and organized three-dimensional structure (Valverde, 2017).

Injectable hydrogels also provide a substrate for directing positive myocardial remodeling in the context of ischemic cardiomyopathies. These injections can easily incorporate cell-derived products to enhance their bioactivity, such as proteins, cells, or controlled release particles of oxygen or drugs. However, this type of material has limited mechanical properties and higher degradability, which are more complex to control, and potential risks of obstruction (Elkhoury et al., 2021).

Decellularization of tissues and organs is also being investigated, using various kinds of physical treatments such as freeze-thaw cycles, perfusion, immersion, and agitation, in addition to chemical treatments using detergents, acids, bases, or saline solutions (Xuewei Zhang et al., 2022). The usage of these scaffolds has several advantages, including the preservation of original structure and fewer immunological rejection. However, there are still hurdles to overcome, such as better decellularization techniques that do not disrupt the structure and preservation of the ECM matrix; it is still not scalable and requires additional ethical and oversight from regulators.

Recently, there has been work combining advanced scaffolds with cellular therapies, using specifically programmed or genetically modified stem cells to enhance cardiac regeneration.

All of this emphasizes how much work needs to be done in the field of CTE to develop and investigate methods and materials that are more and more appropriate for the intended use in order to enhance cardiac tissue regeneration in the future.

2. The Role of Graphene in Electrospun Multi-Layered Scaffolds for Advancing Tissue Engineering

The results presented in this chapter are part of a publication.

Authors:

Ana M. Muñoz-Gonzalez[a], Dianney Clavijo-Grimaldo[a,b]

[a]Universidad Nacional de Colombia, Carrera 45 # 26 – 85, Bogotá Colombia.
[b]Fundación Universitaria Sanitas, Calle 22B # 66-46, Bogotá Colombia

Published in **Chemical Engineering Transactions**, 94, 1423-1428. Sep 2022.

Statement of contribution of co-authors for thesis by published papers:

Contributors	Statement of contribution
Ana M Muñoz-Gonzalez	Designed and perform the experiments Analyzed and interpreted results Conceived and wrote the manuscript Development of research results
Dianney Clavijo-Grimaldo	Involved in the conception of the project Designed the experiments. Assisted with characterization test Provided feedback in the whole process

2.1 Abstract

Graphene is a promising reinforced material used in a vasty of applications due its high mechanical resistance, high electrical and thermal conductivity. These properties could improve the electrical conductivity and mechanical properties of polymeric nanofibers. Nervous, muscular, and cardiac tissues are a challenge for TE not only because of their poor regeneration but because conventional, non-conductive scaffolds are unable to establish an adequate electromechanical coupling. In the present work, graphene was investigated as a nanofiller in a muti-layered polymer scaffold manufactured by electrospinning. The graphene-doped scaffolds were characterized to prospect their use in TE.

2.2 Keywords

Graphene, Tissue Engineering, electrospinning, conductive scaffolds, multi-layer.

2.3 Introduction

Graphene is a promising reinforcement materials for potential applications such as flexible solar panels, batteries and capacitors, sensors, imaging, nanoelectronics, and TE (Ahadian et al., 2016). Furthermore, graphene has an outstanding mechanical resistance, electrical and thermal conductivity (Randviir et al., 2014). Additionally, the honeycomb structures, strong carbon-carbon bonding, elasticity, large specific surface area, and the ability to absorb biomolecules, cells, and tissues, make graphene suitable and practical for TE (Heidari et al., 2019).

TE conflates the engineering and life science to restore the function of damaged tissues using biomaterials. One of the most versatile, promising, and cost-effective method for fabricating nanofibers from a variety of polymers used in TE is electrospinning. Electrospinning scaffolds are capable of mimic the fibrous structure of the extracellular matrix (ECM) (Xue et al., 2019). Nanofibers are generated by the application of an electric field to an injected solution. In this technique, when the electrostatic forces overcome solution surface tension, an accelerated jet arrives at the collector (target) after the formation of a Taylor cone (Chem et al., 2021).

Despite the current solutions for TE, some biomaterials lack in their electrical conductivity (Qasim et al., 2019), and mechanical properties, both relevant to stimulate the adhesion, spreading, and proliferation of cells. For example, conductivity is crucial for cardiomyocytes in myocardium tissue to couple with surrounding cells. Moreover, some of the obtained materials lack fibrous and anisotropic structure, appropriate morphology (porosity, for example, allows oxygen exchange, which it’s

essential for cardiac construction), and show inadequate degradation rate, low mechanical strength, and poor hydrophilicity (Heidari et al., 2019).

Conductive polymeric/graphene nanocomposites could influence and enhance the electrical conduction and mechanical properties of polymeric nanofibers (Bahrami et al., 2019) without any graphene addition. Hence, conductive polymeric nanofibrous scaffolds are a promising solution for heart failure and broken hearts (Qasim et al., 2019) and some other applications such as nerve, osteoblast, or culture and differentiate stem cells. The aim of this study was comparing the properties of a polymeric scaffold with and without graphene made with nanofibers by electrospinning technique.

2.4 Experimental section

2.4.1 Materials

Policaprolactone (PCL) (Sigma-Aldrich, CAS # 134490-19-0 MW=80000 Da), polyvinylpirrolidone (PVP) powder (Sigma-Aldrich, CAS # 9003-39-8 MW=10000 Da), ethanol (Sigma-Aldrich, CAS 64-17-5), isopropyl alcohol (Sigma Aldrich, 99,7 % CAS # 67-66-3), chloroform (Sigma Aldrich, 99,5 %, CAS # 67-66-3) and graphene nanoplatelets was purchased in Bravecount Materials, China (CAS # 7782-42-5).

2.4.2 Polymeric suspensions preparation

For the multi-layer scaffolds obtention by means of the electrospinning technique, it was necessary to prepare:

- PCL suspension: PCL suspension was used at 9% (w/v) in a 50:50 (v/v) chloroform and isopropanol solution. PCL suspension was subjected to an ultrasonic bath (ATU- ATM40-2LCD) with a frequency of 50 Hz per 60 min at 20 °C.
- PVP suspension doped with graphene: PVP was used at 25% (w/v) in 50:50 (v/v) ethanol and water. Afterwards, pristine graphene nanoplatelets solution was added drop by drop at 1% (w/v). PVP with graphene dispersion was stirred in a magnetic stirrer per 60 minutes at room temperature (21 °C). An ultrasonic processor for low volume applications (Cole-Palmer # EW-04714-53) was used to overcome the agglomeration of the graphene nanoplatelets.

2.4.3 Multilayer fabrication by electrospinning and electrospray process and characterization

The fibers were developed into a vertical electrospinning equipment composed by a high voltage source (CZE1000R, Spellman), a dosing pump (KDS100), a syringe, a needle (gauge 21) and a rotary collector (ESD30s). The distance between needle and rotatory collector was maintained in 15 cm. Applied voltage and solution feed rate was chosen as the most relevant electrospinning parameters and were established until uniform and defect-free fibers were obtained.

The PCL suspension was deposited for 45 min at 1.0 ml/h and 14 kV (first layer, nPCL). The graphene-doped PVP suspension was deposited on the nPCL layer for 30 min at 1.5 ml/h and 23 kV (second layer, PVP+G). A final layer of nPCL was deposited under the same conditions as the first layer to seal the PVP+G. This final multi-layer scaffold was named MLS1. To compare the influence of the graphene layer, a control scaffold without graphene was fabricated using the same conditions mentioned above, this sample was named MLS0 (*Figure 2 - 1*). The process was performed at 21 °C room temperature and 55% RH.

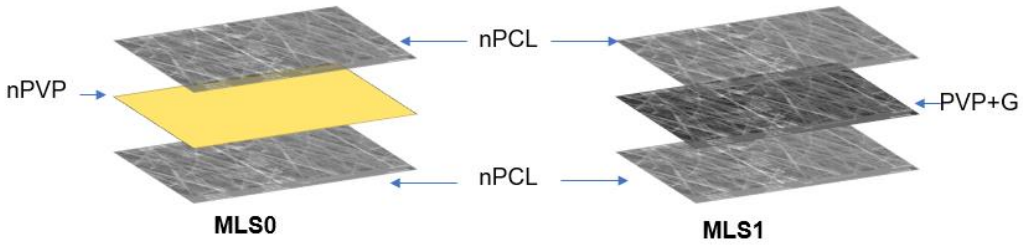

Figure 2 - 1 Configuration of MLS0 and MLS1 (author).

The obtained nanofibers was visualized via scanning electron microscopy (SEM) (Tescan Vega 3 SB) at an accelerating voltage of 15 kV. Based on the SEM images, fiber diameter distribution was determined using Image J software. Statistical analysis was performed for determining the mean diameter and standard deviation at least 100 measurements. The conductivity of each suspension was measured (n=3) using a conductivity sensor (Hanna Instruments HI 5522). Measurements was taken at 17 °C. The mechanical properties of the multilayer scaffold were determined by tensile testing technique (Shimadzu UH-I) with 50 N load capacity of 50 mm/min. Procedure and samples were prepared in rectangular-shape pieces with a length of 120 mm and width of 10 mm, according with the ASTM D882. Five specimens were tested to obtain average values. FTIR spectra were obtained with a Shimadzu® FT-IR solutions spectrometer with attenuated total reflectance (ATR) module and germanium crystal. FTIR spectra were recorded in the transmittance mode in the range

of 4000 – 500 cm-1 and processed with IR Solutions software at environmental temperature conditions.

2.5 Results and discussion

SEM micrographs of nPCL, nPVP, PVP+G and multilayered scaffolds MLS0 and MLS1 are shown in *Figure 2 - 2*. From the images, it can be observed that the fibers, except in PVP+G exhibited a smooth and bead-free surface that was distributed aligned over the scaffold structure. *Figure 2 - 3* shows the mean fiber diameter of the nPCL sample was (620.30 ± 168.42) nm, for the PVP sample was (435.86 ± 151.15) nm and for the PVP+G was (371.42 ± 152.18) nm. According to the results, PVP+G reached a smaller diameter than nPVP and even smaller than nPCL, this could be explained because graphene increases the conductivity of the polymeric suspension making the diameter smaller by the increase in the charge transport (Das et al., 2013) and contributing with the stretching and elasticity of the fibers.

The size reduction of the diameter is a desirable effect as a lower diameter fiber possesses higher surface area for cell attachment and proliferation (Leung Ko, 2011). Despite the decrease in the diameter due to the graphene addition, there are beads along the fibers produced by the difficulty of dispersing the graphene. Other results indicated that the percentage used in PCL/Gelatin/graphene fiber (1%) shows beads caused by the overdispersion of graphene (X. Chen et al., 2019). Further studies with different graphene proportions in polymer suspension and its electrospinning parameters will be addressed to the use of pristine graphene with PVP for TE applications.

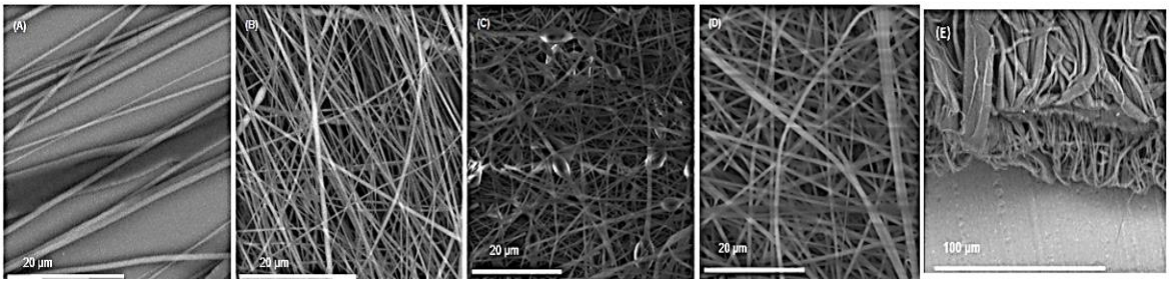

Figure 2 - 2 Morphology observed by SEM of (A) nPCL, (B) nPVP, (C) PVP+G, (D) MLS1 surface, and (E) MLS1 thickness.

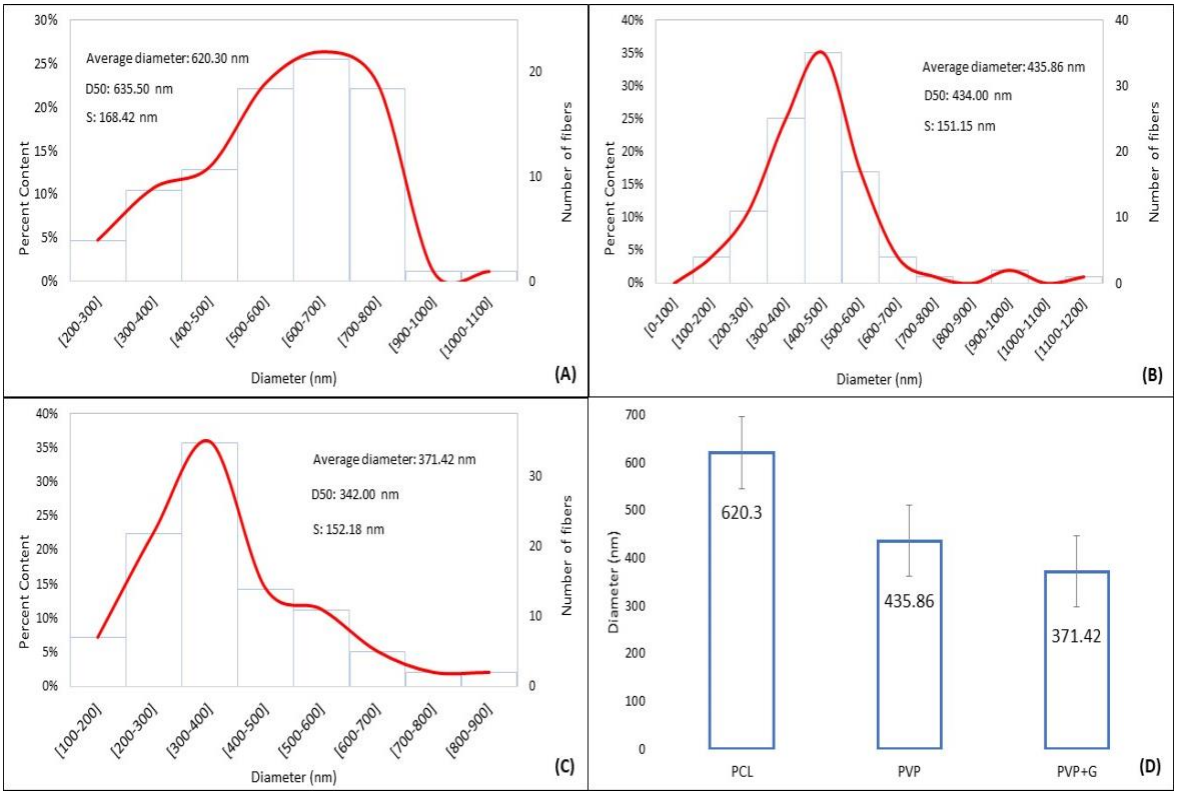

Figure 2 - 3 Fiber diameter distributions of (A) nPCL in the MLS0, (B) nPVP, (C) PVP+G and, (D) average diameters summary. D50 is diameter when the cumulative percentage reaches 50% and S is the standard deviation.

Young's modulus, maximum load, and maximum elongation of the scaffolds are presented in *Figure 2 - 4*. The Young's modulus were determined to be 11.65±7.06 MPa, 138.52±6.87 MPa, 33.75±15.99 MPa, and 34.43±7.90 MPa for the nPCL membrane, PVP+G, MLS0, and MLS1, respectively (*Figure 2 - 4*A). In particular, the modulus of MLS0, compared to MLS1 were not significantly different ($p>0.05$). Pure nPCL was the lowest value for Young's modulus because it was not reinforced and slimmer than the other samples. Further, PVP+G had the highest value Young's modulus despite its thickness, mechanical fragility, and lower diameter as shown in *Figure 2 - 2*. In *Figure 2 - 5* the results show that it is evident the graphene addition reinforces the tensile strength of the polymer matrix.

Other authors with similar material compositions presented similar values. Zhao et al. developed silk biomaterials using controllable surface deposition on the nanoscale to recapitulate electrical microenvironments for CTE reaching 12-13 MPa in tensile tests (Zhao, G, 2018). In the same way, Liu and Xu got values between 10-60 MPa getting with core-sheath fibers loaded with 5% carbon nanotubes (Liu & Xu, 2017). Obtained results demonstrate an enhancement in mechanical properties due to graphene addition and the improving of multilayer configuration with respect to a single polymer nanofiber scaffold. The obtained values overcome physiological values, so the

fabricated material could endure under cyclic stretch due to the rhythmic heartbeat and diastolic and systolic contractions into physiological conditions (Nguyen-truong & Li, 2020).

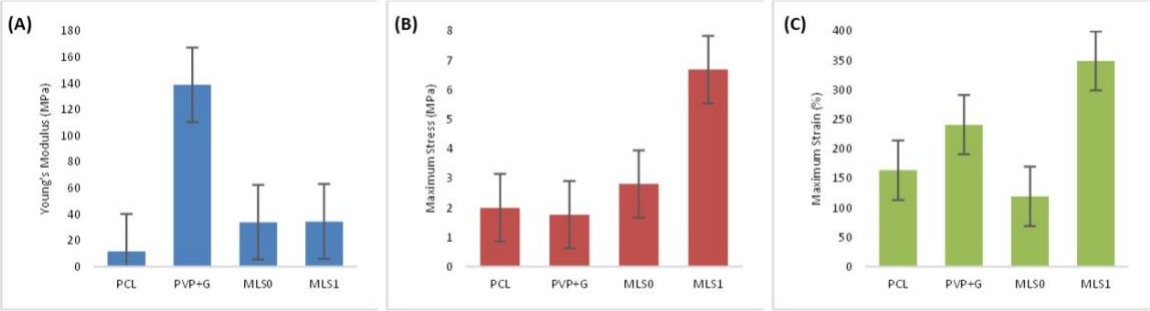

Figure 2 - 4 Mechanical properties of nPCL membrane, PVP+G, MLS0 and MLS1. The columns represent (A) Young's Modulus, (B) maximum stress, and (C) maximum strain.

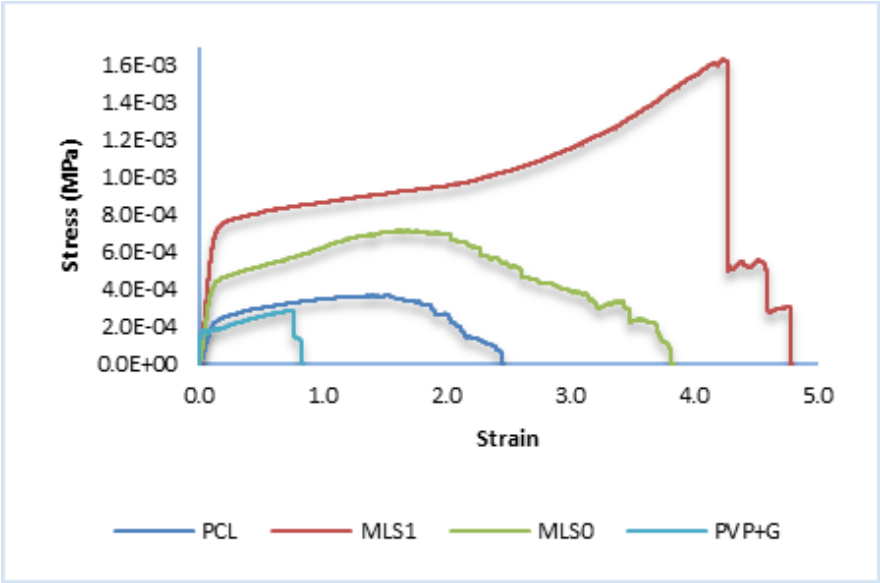

Figure 2 - 5 Stress-Strain profiles of a representative sample of the nPCL, PVP+G, MLS0 and MLS1 groups.

Figure 2 - 6 represents FTIR spectra of PCL, PVP+G and MLS1 scaffold. Characteristics bands of nPCL were identified at 2945, 2868, 1725, 1291, 1239, and 1170 cm^{-1} and attributed to asymmetric vas(CH2), symmetric vs (CH2) stretching, carbonyl (C=O) stretching, C-O and C-C stretching, asymmetric C-O-C stretching, and symmetric C-O-C stretching, respectively. The FTIR spectra of PVP doped with graphene showed bands at 3431, 2954, 1646, 1373, 1287, 1018, 937, and 841 cm^{-1} corresponding to O-H band, asymmetric vas(CH2) of pyrrole ring, C=O band, C-H band, CH2 wagging ν(C-N), C-C, C-C bond and δ(CH2), respectively, characteristics of PVP. Further, there are peaks at 1460, 1422, 1317,1222 and, 1044 cm^{-1} attributed to CH2 bending, C-O, δ (CN), ν(O-H or Ar-OH) and, C-O alkoxy stretching vibrations may be due to the remaining carbonyl groups after the reduction in the fabrication process of graphene. No presence of the O-

H group (3000 and 2500 cm^{-1}), characteristic of the graphene oxide and not of the graphene was detected (Ojrzynska et al., 2020).

All the characteristic peaks of PCL and PVP were identified in the MLS1 scaffold at 2945, 2864, 1725, 1295, 1239, 1165, and 932 cm^{-1}, confirming the structure of the PCL and PVP. Also, peaks at 1417, and 1365 cm^{-1} corresponding to C-O, and δ/β(O–H or C–OH) were observed and are associated with graphene. nPCL, PVP+G and MLS1 curves shown in *Figure 2 - 6* exhibit, presumably, the interaction between layers by the interaction enclosed by nearby peaks and the similar curves; for example, in 1365 cm^{-1} peak in MLS1 exists an interaction between C-OH in graphene and C-H in PVP.

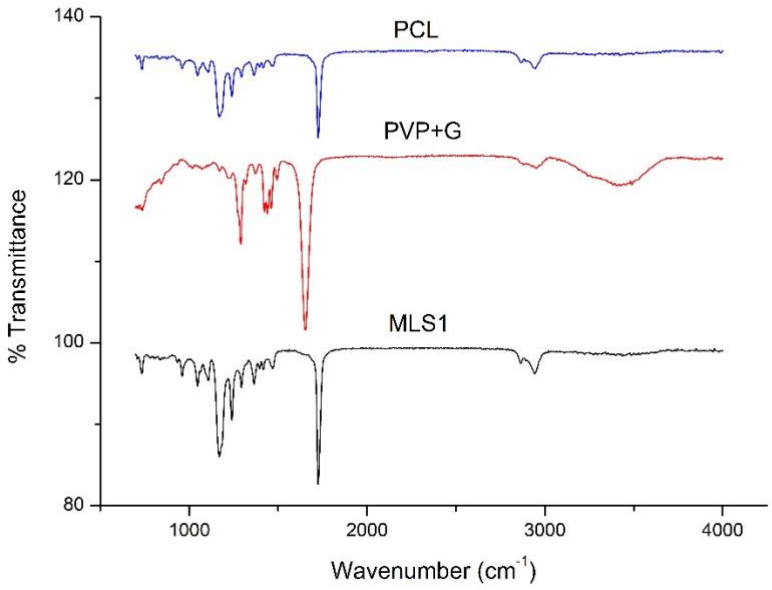

Figure 2 - 6 FTIR of (A) nPCL, (B) PVP+G and, (C) MLS1.

PCL, PVP, and PVP+G solutions conductivity was measured. Results were 0.101±0.018, 83.365±0.592 and, 85.867±0.860 µS/cm for PCL, PVP, and PVP+G, respectively. As observed, the PCL solution is insulating because of its low conductivity value. An increase of conductivity by the addition of graphene in PVP solution is satisfactory considering that the nanofiller is graphene rather than graphene oxide. Conductivity value in PVP+G contributes to low diameters as discussed above.

As long as the graphene/polymer ratio is low, is possible that the critic point of percolation threshold is not reached maybe because of the viscosity, concentration, or time of preparation of the PVP solution that could affect the graphene dispersion having dead zones where particles can arrive, leaving no interaction with the polymer.

2.6 Conclusion

The results of this study demonstrate that doping graphene into polymeric nanofibers resulted in the enhancement of morphological properties such as diameter which was smaller than the polymeric mats without graphene despite the appearance of the beads. Tensile measurements showed that graphene can reinforce the mats and it was demonstrated that the effect of the nPCL layer increases the overall mechanical strength of the MLS1 compound and Young's module was higher and overcome the physiological values. FTIR results confirm the chemical composition of the MLS1 scaffold showing probable interactions between graphene and the polymers. It was demonstrated that the doped polymeric solution with graphene improves the electric conductivity even in a low amount. This study is the initial basis of characterization for an appropriate platform to have cell adhesion, proliferation, and an environment to maintain cell viability for use in cardiac engineering tissue.

2.7 Acknowledgments

This was founded by the Universidad Nacional de Colombia and the Fundación Universidad Sanitas (Internal Research Call 2021-1). Authors express their acknowledgment to the Electrospray and Electrospinning Laboratory of the Universidad Nacional de Colombia for the space for developing this paper.

2.8 References and Notes

Munoz-Gonzalez, A. M., & Clavijo-Grimaldo, D. (2022). Synthesis and Characterization of Graphene-doped Nanofibrous Scaffolds for Tissue Engineering. Chemical Engineering Transactions, 94, 1423-1428. https://doi.org/10.3303/CET2294237. ISBN 978-88-95608-93-8; ISSN 2283-9216

3. Effects of Graphene Nanofiller on Nanofibrous PCL Scaffold Properties for Tissue Engineering

The results presented in this chapter are part of a submitted manuscript in SAGE editorial.

Authors: Ana M. Muñoz-González [1*], Sara Leal-Marin [5,6], Dianney Clavijo-Grimaldo [2,3], Birgit Glasmacher [5,6]

1 Faculty of Engineering, Universidad Nacional de Colombia; Bogotá, Colombia.
2 School of Medicine, Universidad Nacional de Colombia; Bogotá, Colombia.
3 Faculty of Medicine, Grupo INPAC. Fundación Universitaria Sanitas; Bogotá, Colombia
4 Institute for Multiphase Processes, Leibniz University Hannover, Garbsen, Germany
5 Lower Saxony Center for Biomedical Engineering, Implant Research and Development, Hannover, Germany

Acepted in **The International Journal of Artificial Organs**, Jun 2024. doi 10.1177/03913988241266088

Statement of contribution of co-authors for thesis by published papers:

Contributors	Statement of contribution
Ana M Muñoz-Gonzalez	Designed and perform the experiments Analyzed and interpreted results Conceived and wrote the manuscript Development of research results
Dianney Clavijo-Grimaldo	Involved in the conception of the project Designed the experiments. Assisted with characterization test Provided feedback in the whole process
Sara Leal-Marin	Designed and perform the experiments Analyzed and interpreted results Assisted with characterization test
Birgit Glasmacher	Funding and provide equipment, laboratories and materials. Provided feedback in the whole process

3.1 Abstract

The effects of embedding graphene nanoparticles (Gnp) into polycaprolactone (PCL) scaffolds on fiber structure, mechanical properties, and biocompatibility is examined in this study. Gnp insertion significantly decreases the diameter of PCL fibers and generates a more homogeneous, smooth surface that is favorable to cellular activity, according to scanning electron microscopy (SEM) data. Employing Fourier-Transform Infrared Spectroscopy (FTIR) to identify graphene-related bands and validate the presence of distinctive PCL peaks, the incorporation was successful without modifying the chemical identity of PCL. The maximum Young's modulus was obtained from mechanical testing at a concentration of 0.5% Gnp, but larger Gnp levels resulted in stiffer materials and decreased mechanical performance. Hydrophobicity was preserved in contact angle measurements for each scaffold. The non-cytotoxic nature of Gnp-PCL scaffolds was confirmed by cytotoxicity tests using bone marrow mesenchymal stem cells (bmMSCs), which showed increased cell viability at increasing Gnp concentrations. According to the research, Gnp-PCL scaffolds have great potential for CTE. A suitable Gnp concentration can improve scaffold performance without affecting biocompatibility.

3.2 Introduction

In the field of CTE, there is a growing demand for the study and enhancement of the current properties of biomaterials to identify more effective approaches to myocardial restoration, especially following a cardiac event. The heart's minimal regenerating ability after myocardial infarction provides a significant barrier to rehabilitation and function (Fleischer et al., 2017).

Among the materials employed, PCL has shown exceptional performance in TE, owing to its mechanical properties and biocompatibility (Schmitt, Dwyer, & Coulombe, 2022). However, PCL and other commonly used biomaterials lack the required electroconductive properties and have inferior mechanical properties for CTE applications. It has been demonstrated that electroconductive scaffolds play an important role in cardiac recovery because they enhance the morphological, chemical, mechanical, and biological properties required for infarcted tissue repair and regeneration (Morsink et al., 2022).

Graphene, endowed with exceptional mechanical and electrical properties, holds promise as a nanofiller to augment the capabilities of PCL. Graphene-based nanocomposites are increasingly favored in TE due to their conductive electrical properties, robust mechanical integrity, and expansive specific surface area (Eslahi et al., 2022). Moreover, graphene, alone or in combination with other materials, can influence the morphology, function, and maturation of cardiac cells and has been

shown to promote angiogenesis, proliferation, and differentiation of implanted stem cells, along with possessing antibacterial and antioxidant properties (Edrisi et al., 2023; Savchenko et al., 2021).

According to some authors, the influence of graphene in polymeric matrices could provide an optimal balance of scaffold properties. For instance, Chiesa et al. developed electrospun scaffolds from biodegradable polymers (such as the mixture of poly-L-lactide and PCL) reinforced with graphene nanoplatelets, demonstrating improvements in their physical, mechanical, thermal, and degradation properties. These enhancements have been achieved through the alteration of the morphology and composition of the fibers. Furthermore, these improved scaffolds have proven to be biocompatible and effective for biomedical applications, as evidenced by their capacity to support cellular adhesion and proliferation, particularly in fibroblast cells, without showing signs of toxicity or harmful degradation products over a 60-day observation period (Chiesa et al., 2020).

Similarly, Fakli et al. investigated the morphological, chemical, mechanical, and biological properties of nanofibrous scaffolds composed of poly(caprolactone) (PCL), poly(glycerol sebacate) (PGS), and a mixture of both with graphene nanosheets. They found that all the nanofibrous scaffolds are biocompatible and non-toxic. The composite scaffold made of PCL/PGS with 1% by weight of graphene (PCL/PGS/graphene 1) showed the highest cell adhesion and biocompatibility, making it a promising candidate for future research in CTE (Fakhrali et al., 2021).

One of the most promising manufacturing techniques in CTE is electrospinning (Flores-Rojas et al., 2023). Ginestra fabricated PCL scaffolds with graphene nanoplatelet additives and studied the influence of graphene nanoplatelets on PCL. It was found that preparing an optimal graphene suspension in the solution is crucial for enhancing the applicability of the resulting fibers (Ginestra, 2019). Additionally, fibers with graphene oxide nanofiller, based on polyurethane/reduced graphene oxide (PU/RGO), showed that the incorporation of RGO improved the electrical and mechanical properties of the scaffolds, and its entrapment within the PU structure protected cells from cytotoxic concentrations. The scaffolds with RGO enhanced cell adhesion and proliferation. Furthermore, graphene transformed the insulating PU into a conductive nanocomposite (Najafi Tireh Shabankareh et al., 2023).

These PCL and graphene composites are anticipated not only to demonstrate enhanced mechanical integrity but also to support robust cell attachment and growth, without eliciting cytotoxic effects. This research aims to obtain PCL electrospun nanofiber scaffolds incorporating graphene nanoparticles (Gnp) as a filler and to evaluate the influence of various graphene concentrations—0.5%, 1.0%, 1.5%, and 2.0% (w/v)—on the morphological, mechanical, chemical, and biological properties.

3.3 Materials and Methods

3.3.1 Materials

Polycaprolactone (PCL) (Sigma-Aldrich, CAS # 134490-19-0 MW=80000 Da), 2.2.2-Trifluoroethanol (TFE) was purchased from abcr GmbH. Graphene nanopowder (Gnp) (Bravecount Materials). For cell seeding Dulbecco's Modified Eagle Medium (DMEM), glutamine, HEPES, fetal bovine serum (FBS) and Penicillin/Streptomycin (Bio&Sell, Germany) was used.

3.3.2 Gnp-PCL electrospun scaffolds obtention

Gnp-PCL scaffolds obtention involves a two-step process: Preparation of solutions and electrospinning fabrication. In the solution preparation, a 13% (w/v) PCL solution was used with TFE as a solvent and then stirred overnight at room temperature. Then, the Gnp was added to the PCL solution in different concentrations (0.5; 1.0; 1.5 and, 2.0 %(w/v)). To ensure that the Gnp is well dispersed, the different solutions were stirred with a tubular roller (LLG Uniroller 6 easy, Germany), magnetic stirrer (IKA RCT basic, Germany), and ultrasonic bath (Bandelin Sonorex Digitec, Germany) before moving on to the electrospinning process.

The Gnp-PCL scaffolds were fabricated with a horizontal electrospinning device and a rotatory collector to a velocity of 1.1 m/s, using a flow rate 0.5-1 mL/h, an applied voltage between 15-25 kV and, a distance of 26 cm. The process was carried out at 21 °C room temperature and 30% RH.

3.3.3 Characterization of electrospun scaffolds

Scanning electron microscopy (SEM).

The morphology of the Gnp-PCL scaffolds was examined employing SEM (S3400N, Hitachi, Japan). Before observations, all samples were sputter-coated with a thin layer of Au-Pd alloy under vacuum. The samples were then examined at an acceleration voltage of 20 kV and a working distance of 10 cm. The fiber diameter was measured by utilizing an image analysis program (ImageJ software, NIH, Bethesda, MD).

Fourier transform infrared (FTIR) spectroscopy

The chemical composition of PCL, Gnp, and Gnp-PCL scaffolds was determined by using FTIR Spectroscopy analysis (Perkin Elmer Spectrum 100, USA). The FTIR spectrum of the materials was

recorded in the mid-infrared region (4000–650 cm^{-1} wavenumber range) with a resolution of 0.5 cm^{-1}.

Contact angle measurements

The wettability properties of Gnp-PCL scaffolds were determined by evaluating the contact angle of a sessile water droplet on the surface of the samples. Approximately 10 µL of a water drop was placed onto the surface of each sample by using a contact angle instrument (EasyDrop FM40, Krüss, Germany). Images and angle measurements were calculated by image processing with DSA software. The measurements were repeated six times per sample.

Mechanical characterization

For the analysis of mechanical properties, scaffolds were cut into pieces measuring 1x1 cm. The samples were pre-soaked in ethanol and phosphate-buffered saline (PBS) and placed in the grips to initiate the test. Mechanical properties were measured using a uniaxial tensile test with an Instron machine (Instron, Norwood, MA, USA) equipped with a thermal bath (Bioplus, Instron, USA) to conduct the test under wet conditions. All tests were performed in PBS at 37°C and pH 7.4, with a speed of 10 mm/min and a load of 10 N. Stress-strain curves were obtained, and subsequently, Young's modulus, ultimate tensile strength, and maximum strain values were analyzed using the obtained experimental data. The experiments were repeated six times per sample.

Electrical conductivity measurements

With four colinear probes that are in contact with the surface material, the four-point probe was used to measure the electrical conductivity of each scaffold. Sheet resistance measurements were performed using a four-probe resistance meter (HPS2523, Beijing Jiahang Bochuang Technology Co., Beijing, China).

Thickness is the scaffolds was measured with a Mitutoyo micrometer having a precision of 0.1 µm. Five measurements of each sample were taken, and the average result was given. Scaffolds thickness was measured with a were 0.004 to 0.032 mm.

Bone Marrow Mesenquimal Stem Cells (bmMSCs) seeding.

The scaffolds, cut into cylindrical shapes with a surface area of 1.2 cm^2, were sterilized through exposure to ultraviolet light, followed by treatment with 70% ethanol and subsequent rinsing with PBS, and then individually placed in 24-well culture plates. Bone marrow-derived mesenchymal stem cells (bmMSCs) (28,500 cells in 50 µL of culture medium) were seeded onto each scaffold. To facilitate cell adhesion to the scaffold, they were incubated for 2 hours. Afterwards, 700 microliters

of culture medium were added. The samples were maintained in an incubator at 37°C, 95% humidity, and 5% CO_2. The growth medium used was supplemented Dulbecco's Modified Eagle Medium (DMEM) (Bio&Sell, Germany) containing 2.3% (v/v) glutamine, 2.3% (v/v) HEPES, 0.002% (v/v) FGF-2, 11.6% (v/v) fetal bovine serum (FBS) (Bio&Sell, Germany), and 1.2% (v/v) Penicillin/Streptomycin. The medium was renewed every three days.

Cell viability on the material surface

Cell viability of the bmMSCs on/into Gnp-PCL scaffolds was assessed using the Alamar Blue assay, also known as the Resazurin assay. This indicator dye is non-toxic, water-soluble, and remains stable, exhibiting color and fluorescence changes in response to cellular growth due to its chemical reduction in the culture medium (Longhin et al., 2022; O'Brien et al., 2000).

For the assay, a 10% (v/v) resazurin solution was prepared in pre-heated medium, and 750 µL of this solution was applied to each scaffold, discarding previously the culture medium. Following a 2-hour incubation period at 37°C, 100 µL of the reduced resazurin solution was transferred to a 96-well plate to measure fluorescence. The fluorescence measurements were taken at an excitation wavelength of 570 nm and an emission wavelength of 600 nm, using a Tecan Infinite M200PRO plate reader. Fluorescence readings were taken per duplicate at 1-, 3-, 7-, and 14-days post-incubation.

Live/Dead staining

In order to observe cell attachment and growth on and between the fibers of the scaffold, fluorescence microscopy was employed. For imaging, the cultured scaffolds were removed from the incubator, the medium was discarded, and they were washed twice with PBS. Subsequently, the cells were stained with a solution of ethidium homodimer (EthH) and fluorescein diacetate (FDA) in PBS for 15 minutes. Images were then captured on days 1, 7, 10, and 14. The images were taken using a fluorescence microscope (Zeiss Axiovert 200 M, Germany).

Cell–material interactions

To study the cell attachment, the morphology of adherent cells, as well as cell-to-cell and cell-to-scaffold interactions, were effectively observed using SEM. In this process, scaffolds were initially prepared with a 0.1 M sodium cacodylate (CAC) solution and then fixed using a 3% glutaraldehyde solution at room temperature. Then, they were rinsed twice with CAC and miliQ water, and sequentially dehydrated using different graded ethanol solutions at concentrations of 25%, 35%, 50%, 70%, 80%, 90%, and 100%. Once dehydrated, the scaffolds were air-dried. For imaging, the scaffolds were coated with gold, and SEM imaging was performed using a Hitachi S3400N

microscope at an accelerating voltage of 20 kV and a working distance of 10 mm. Images were captured on days 1, 3, 7, 10, and 14.

Statistical analysis

Unless specified otherwise, all data are presented as mean ± standard deviation. Statistical differences among group means were evaluated using a one-way ANOVA analysis, followed by Tukey's multiple comparison test, employing Minitab software for the calculations. For all analyses, $p < 0.05$ was considered statistically significant, and data were indicated with (*).

3.4 Results

3.4.1 Morphological analysis

SEM images of the scaffolds reveal the impact of graphene as a nanofiller on the morphology of PCL fibers. *Figure 3 - 1* demonstrates a wide diameter distribution for pure PCL fibers, averaging 792.42 ± 522.51 nm, showing a high variability.

The incorporation of 0.5% graphene results in a 40% reduction in average diameter in comparison with the PCL fibers, achieving 472.13 ± 309.54 nm. These fibers exhibit smooth and uniform surfaces, with a more defined orientation. Increasing the graphene concentration to 1.0% further reduces the average diameter to 424.76 ± 199.01 nm, with an evident decrease in variability.

At graphene contents of 1.5% and 2.0%, fibers with average diameters of 406.48 ± 214.68 nm and 321.67 ± 88.02 nm, respectively, were obtained, showing a decreasing trend in both diameter and less variability as the graphene percentage increases. However, graphene dispersion and viscosity management in the electrospinning solution were quite more challenging.

The reduced fiber diameter is advantageous for TE applications, as it implies increased surface area, porosity, and topography, crucial for cellular adhesion, migration, and proliferation, as well as for simulating the extracellular matrix (ECM). The graphene, as a conductive filler, promotes the transport of electrical charges in the solution, because the sp2 and sp3 carbon domains, favoring the formation of the Taylor cone in the electrospinning process, which is dependent on the electrostatic force generated by surface charges induced by the applied electric field (Hohman et al., 2001). This facilitates the electrospinning process by stretching the solution, resulting in thinner fibers. Moreover, an increase in solution stretching may reduce the polymer jet travel distance, contributing to the uniformity of fiber diameter. Further, the addition of graphene might increase surface tension, improving fiber elongation during the process.

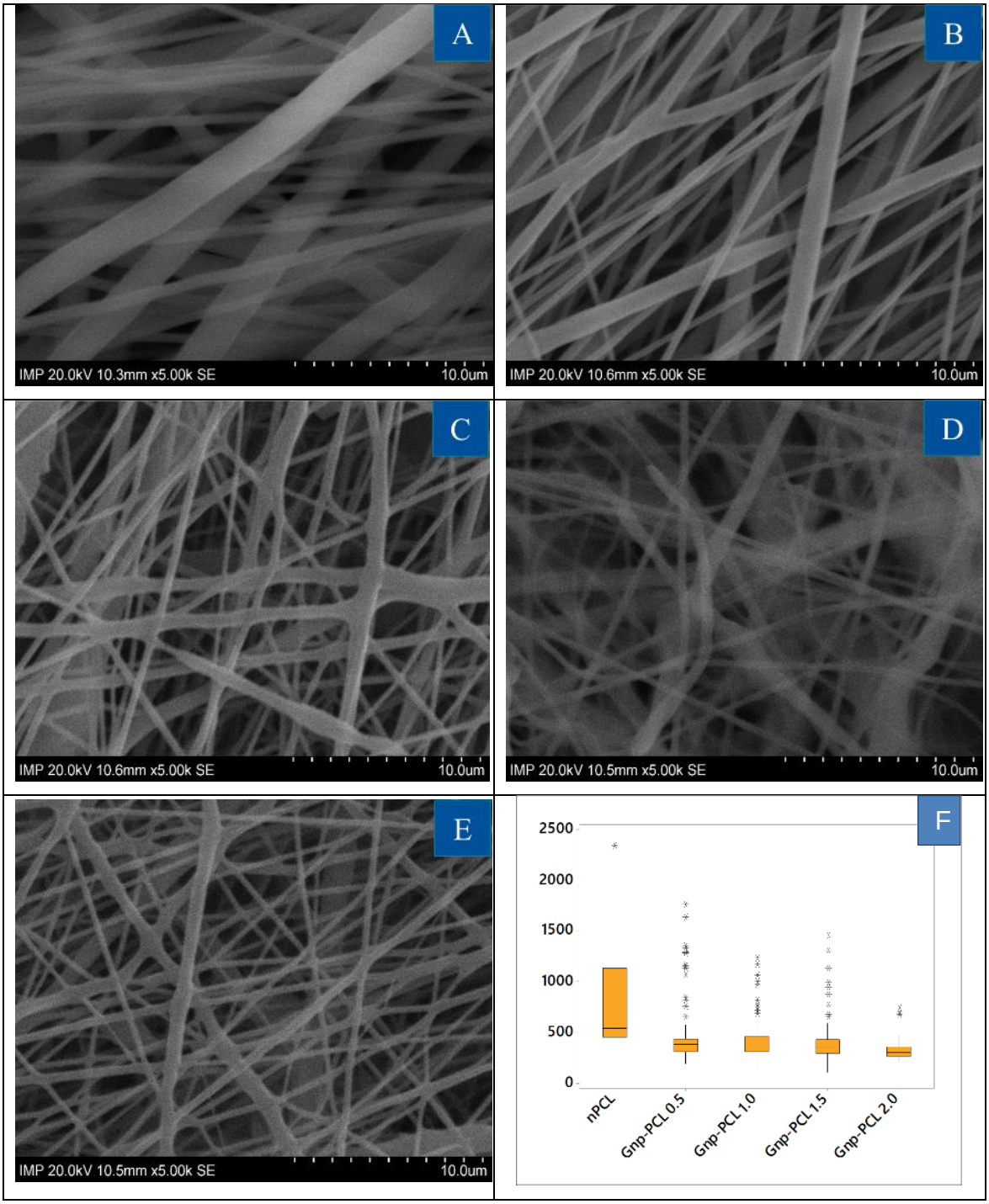

*Figure 3 - 1 Gnp-PCL scaffolds: SEM images and diameter: A. nPCL; B. Gnp-PCL 0,5; C. Gnp-PCL 1,0; D. Gnp-PCL 1,5; F. Gnp-PCL 2,0; G. Diameter sie distribution in nm. *Measurement significantly different.*

Graphene also could increase the stability in the process. The high variability in PCL fibers and those with low graphene percentages is due to the increased stability of the jet with higher graphene

content, resulting in smaller diameters. Finally, graphene is likely to enhance molecular interactions within the solution, positively influencing the electrospinning process.

3.4.2 FTIR characterizations

The FTIR spectra of Gnp, PCL and the different scaffolds with graphene variations are shown in *Figure 3 - 2*. For PCL, characteristic peaks are present at 2942 cm^{-1} for asymmetric vas(CH2), 2863 cm^{-1} for symmetric vs (CH2) stretching, 1722 cm^{-1} for carbonyl (C=O) stretching, 1294 cm^{-1} for C-O and C-C stretching in the crystalline phase, 1236 cm-1 for asymmetric C-O-C stretching and 1103 cm^{-1} for symmetric COC stretching (Heidari et al., 2017; Tayebi et al., 2021; Yuan et al., 2012).

In the case of Gnp, peaks at 1538, 1469, 1367 cm-1 was identified for C=C aromatic stretching; 1236 cm-1 for C-O epoxy stretching vibrations, 1053 cm-1 for C-O alkoxy stretching vibrations, 932 cm-1 for C-C bond and 840 cm-1 for δ(CH2) (Bagheri & Mahmoodzadeh, 2020; Ratih et al., 2018; Surekha et al., 2020).

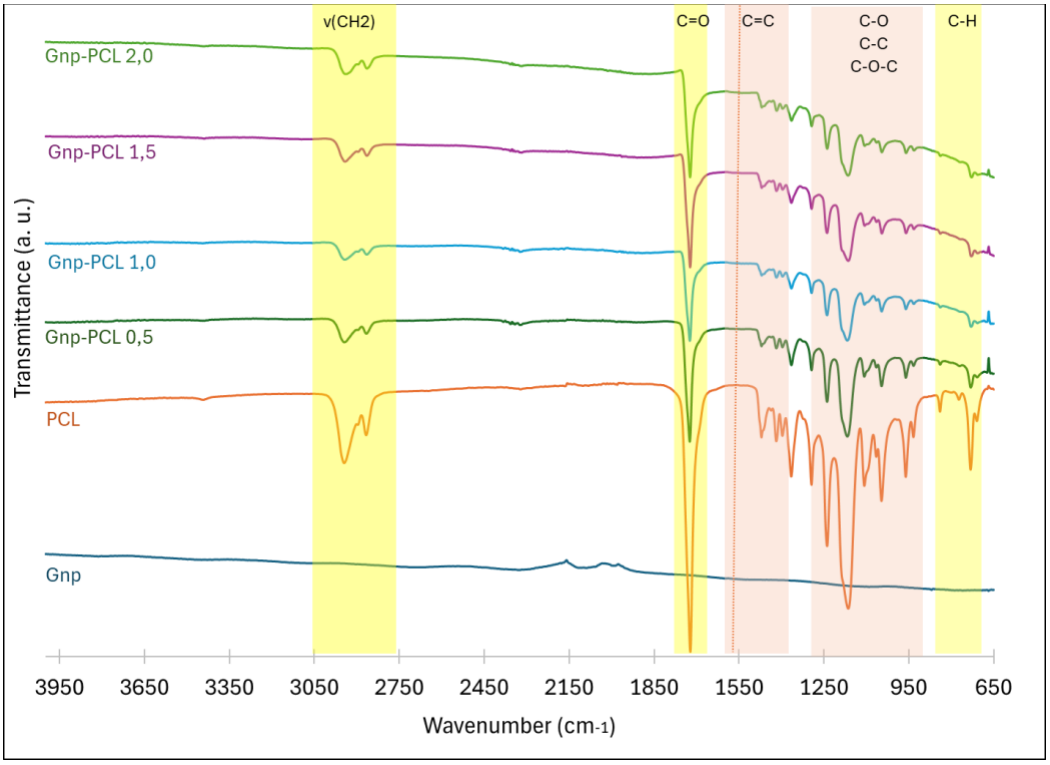

Figure 3 - 2 FTIR spectra Gnp-PCL electrospun scaffolds.

While the characteristic peaks were identified, there are bands that are overlapped, complicating the distinction between the peaks of each material. This is attributed to the relatively low intensity of Gnp bands compared to those of PCL, and the graphene being in not so high percentages, a finding that has been reported by other researchers (Loyo et al., 2023; Serafin et al., 2021). Despite this, it is

observed that graphene does not alter the chemical composition of PCL, as the characteristic peaks are present, but a reduction in peak intensities is observed due to the greater amount of graphene.

3.4.3 Mechanical properties

Figure 3 - 3 presents the stress-strain curves for pure PCL and Gnp-PCL scaffolds with varying graphene concentrations (0.5; 1.0; 1.5; 2.0%). Additionally, the figure presents the calculated mechanical properties such as the Young's Modulus (E), elongation at break (Tensile strain %), and Tensile stress (MPa).

The nPCL scaffold exhibited a Young's Modulus of 4.14 ± 2.73 MPa, which was significative enhanced by the Gnp-PCL 0.5 scaffold ($p<<0.01$), achiving a 55% higher value at 9.23 ± 1.95 MPa—the highest modulus achieved across all graphene concentrations tested. For Gnp-PCL scaffolds with 1.0, 1.5, and 2.0% graphene, the Young's Modulus were 6.40 ± 0.52 MPa, 5.19 ± 0.68 MPa, and 2.62 ± 0.39 MPa, respectively. This trend suggests that as the graphene concentration increases, the Young's Modulus decreases, possibly due to graphene particles reinforcing and increasing stiffness within the PCL fibers, as well as the crystalline nature of graphene.

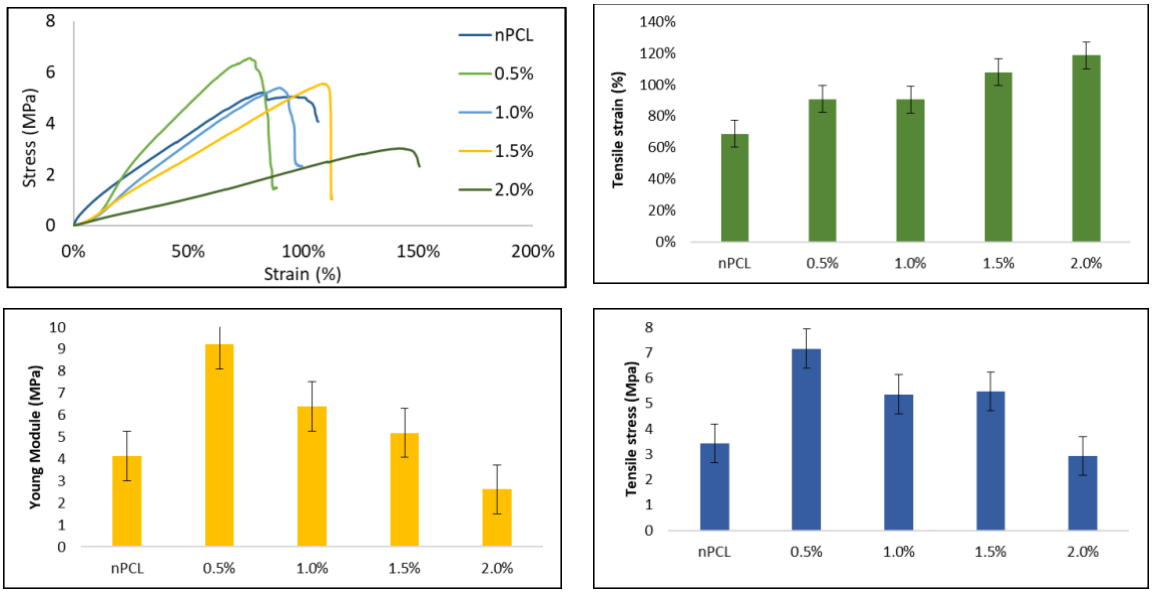

Figure 3 - 3 Mechanical properties of the electrospun PCL scaffolds with different Gnp content.

Tensile stress results followed a similar pattern, with a peak increase for the 0.5% graphene addition (7.16 ± 0.84 MPa), a 52% improvement over nPCL (3.43 ± 1.51 MPa). The Gnp-PCL 1.0 and Gnp-PCL 1.5 scaffolds exhibited very close values of 5.36 ± 0.17 MPa and 5.47 ± 0.53 MPa. For the 2% graphene scaffold (Gnp-PCL 2.0), the value decreased at 2.94 ± 0.55 MPa.

Elongation values displayed an increasing trend with higher graphene concentrations, ranging from 69 to 119%. These findings confirm that mechanical properties are influenced by the nature of the graphene powder, the interaction between PCL and Gnp, and the dispersion of the within the polymer matrix. The lowest graphene concentration resulted in the highest mechanical properties, most likely due to the ease of dispersing graphene particles within the polymer, where it acts as a reinforcement in the polymer matrix. This, however, increases the resistance to PCL chain movement and interaction between the two materials as part of a nanocomposite, as evidenced by FTIR spectrum.

A gradual decrease in mechanical properties with higher graphene percentages may be attributed to increased Van der Waals forces leading to agglomeration within the polymer matrix. Under stress, the particles may delaminate, increasing deformation before rupture, coupled with the observation of decreased fiber diameter at higher graphene concentrations as showing SEM images. Additionally, mechanical properties likely decrease at higher graphene percentages due to the challenges in achieving uniform solution dispersion at higher graphene dispersions. Concentrations below 1% could yield better results, as this percentage appears to offer a balance between strength and elongation, preventing a decline in properties with increased graphene content as observed in the trends of *Figure 3 - 3*.

The results also corroborate the impact of graphene on polymer matrices and its effect on mechanical properties. For instance, Ceretti et al. found that the stiffness of PCL scaffold matrices increased from 9.01 MPa with 0% graphene to 22.1 MPa with 1% added graphene, which tended to decrease at 2% (Ceretti et al., 2017). Similarly, Loyo et al. presented a comparable pattern but using graphene oxide, where increasing graphene oxide concentrations resulted in greater stiffness and elongation. The study also reported an increase in Young's Modulus from 7.85 MPa with 0% graphene oxide to 10.34 and 12.79 MPa for 1 and 2%, respectively (Loyo et al., 2023). Ginestra observed a similar trend in his study with graphene powder, where graphene enhanced resistance, notably at 1% concentration, and mechanical properties appearing to decline in terms of elastic behavior and ultimate tensile strength as graphene content increased (Ginestra, 2019).

3.4.4 Wettability assesment

The contact angles of the nPCL and Gnp-PCL scaffolds were measured to assess their hydrophobicity. The nPCL scaffold exhibited a contact angle of 129.28 ± 6.20°. The contact angles for Gnp-PCL scaffolds with varying graphene concentrations (0.5, 1.0, 1.5, and 2.0%) were also determined, yielding values of 123.98 ± 13.68°, 139.57 ± 8.25°, 143.95 ± 4.24°, and 134.53 ± 5.70°, respectively. All scaffolds were found to be hydrophobic; however, a significant difference was

observed in the scaffold with 0.5% graphene ($p<0.01$). Despite this difference, the scaffold did not attain hydrophilic properties.

3.4.5 Cell viability

The cytotoxicity effects of the Gnp scaffolds were evaluated utilizing bone marrow mesenchymal stem cells (bmMSCs) and the Alamar Blue assay, a redox indicator that shifts in color in response to cellular metabolic activity—a key marker of cell health and viability (Longhin et al., 2022). Upon seeding cells on the top of the scaffolds, their potential to proliferate was monitored over 14 days.

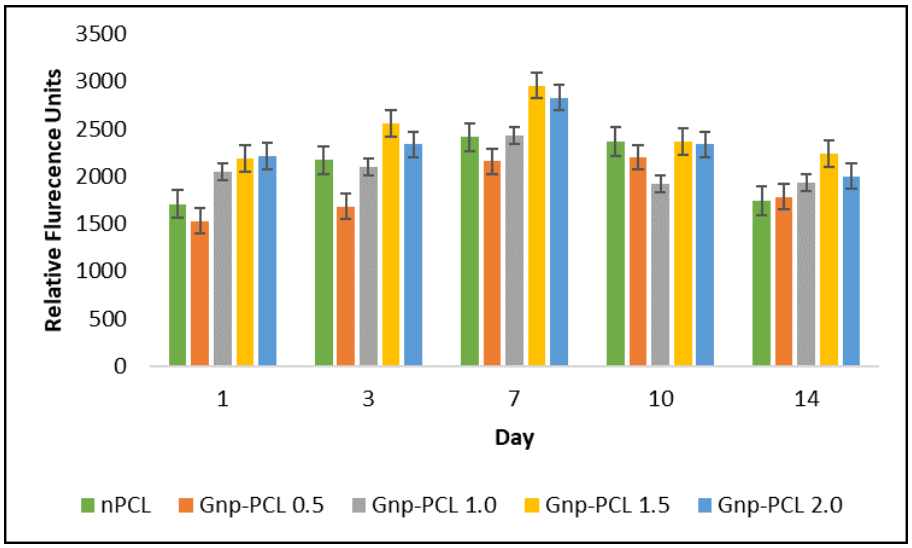

Figure 3 - 4 Metabolic activity on different scaffolds at day 3 and 7 after bmMSCs seeding.

The results, depicted in *Figure 3 - 4*, indicate that initial metabolic activity, indicative of cellular adhesion, was facilitated by the scaffolds. Consistent with prior studies, PCL substrates are known to support cell adhesion and proliferation, particularly PCL fibers, due to their porosity and surface characteristics that are conducive to cell growth imitating the extracellular matrix (ECM) (Sowmya et al., 2021). With the integration of Gnp, there is an enhancement in viability and biocompatibility, particularly evident in concentrations of 1% and higher, which exhibited greater cell viability compared to nPCL and the 0.5% scaffold.

On Day 3, increased proliferation was observed in the Gnp-PCL 1.5 and 2.0 scaffolds, with nPCL outperforming the lower graphene percentages. On Day 7, a peak in cellular activity was reached, following the same trend noted on Day 3, suggesting robust cell proliferation on the scaffolds. These observations suggest that a reduced fiber diameter is beneficial for cellular activity, as the most favorable metabolic outcomes were achieved with scaffolds of smaller diameter. This improvement is likely attributable to the enhanced cellular topography provided by finer fibers.

The assay continued to Day 10 to assess cellular differentiation. However, a general decline in metabolic activity was noted across nearly all scaffolds. This downtrend persisted on Day 14. Statistical analysis, specifically a one-way ANOVA, revealed significant differences only between the 0.5% and 1.5% graphene concentrations.

In conclusion, under all conditions studied, the scaffolds supported the viability of bmMSCs, which successfully adhered and proliferated on the scaffolds. Furthermore, the results validate that graphene, within the tested concentrations, is not cytotoxic to the cells, reinforcing the potential of Gnp-PCL scaffolds for TE applications where cell-scaffold interaction is critical.

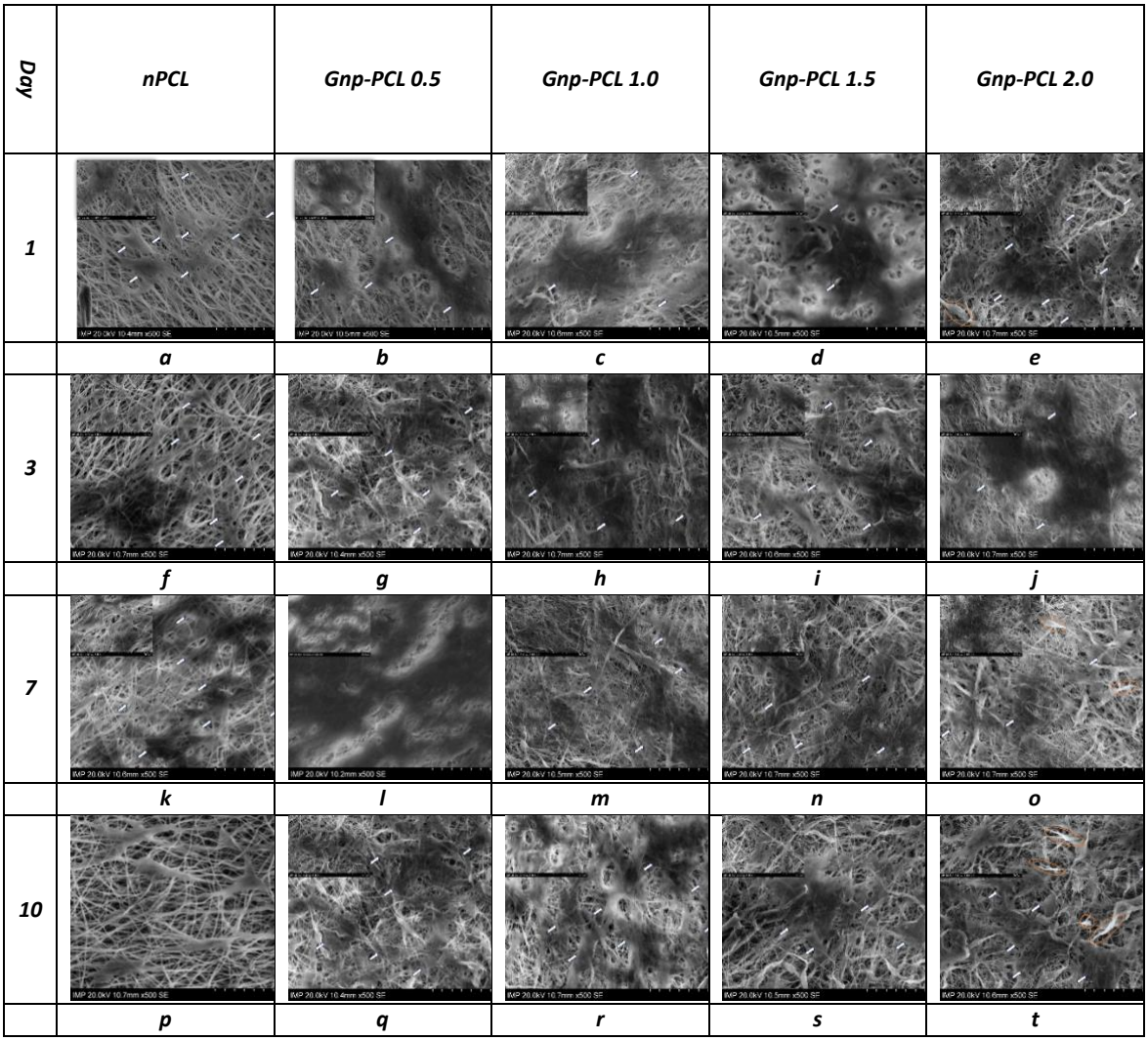

Figure 3 - 5 SEM images of bmMSCs seeded on nPCL, Gnp-PCL 0,5; Gnp-PCL 1,0; Gnp-PCL 1,5; Gnp-PCL 2,0 on day 1, 3, 7 and 10 at 500X.

To verify cell attachment, the morphologies of bmMSCs cultured on nPCL and Gnp-PCL scaffolds were examined using SEM in *Figure 3 - 5*. From the Day 1, cells demonstrated adherence, clustering closely together on the scaffolds, exhibiting an elongated and spread morphology. On day 3, a more

pronounced visual proliferation was evident, with cells increasingly covering the available space, appearing elongated and interconnected.

On day 7, correlating with the peak of cellular metabolism, there was a noticeable enhancement in the cellular population growth across the surface of all scaffolds. However, on day 10, while cells remained present on the scaffolds, they appeared more dispersed.

These observations suggest that the Gnp-PCL scaffolds provide a conducive environment for cell attachment. The cell attachment and proliferation behaviors observed are intimately associated with the biocompatibility of the scaffolds. The Gnp-PCL scaffolds not only support initial cell adhesion but also facilitate subsequent cell proliferation, which is indicative of their potential as suitable substrates in TE applications.

The results of the Live/Dead experiment are shown in *Figure 3 - 6*, where an ongoing increase in red fluorescence is shown starting on Day 1 as the concentration of graphene increases, indicating a higher percentage of dead cells. A significant proportion of green cells relative to red cells can be seen in the Gnp-PCL 0.5 sample, indicating robust cellular viability at this scaffold concentration. The Gnp-PCL 1.0 sample exhibits a modest increase in red cells, although green cells remain predominate. This may signal the beginning of cellular stress or toxicity as the concentration of graphene rises. Red cell presence becomes more noticeable in Gnp-PCL 1.5, which may indicate a decline in cell viability.

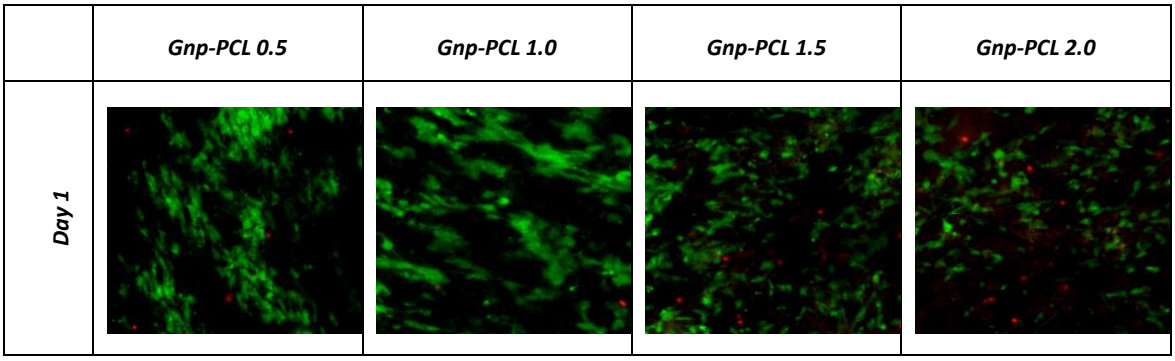

Figure 3 - 6 Live/Dead images for Gnp-PCL scaffolds on Day 1.

This may indicate that the effects of graphene toxicity are starting to become noticeable. The presence of a significant number of red cells in Gnp-PCL 2.0 suggests that the concentration of scaffold may be highly toxic, which would impair cell survival.

For TE applications, the homogenous dispersion of cells across the scaffolds is advantageous. These outcomes are consistent with the other research, emphasizing the significance of maximizing

the concentration of graphene in scaffolds to strike a compromise between improved material properties and the health and viability of cells (X. Chen et al., 2019; J. Li, Zhang, et al., 2018).

3.5 Conclusions

In this research was possible to investigate the effects of graphene nanoparticles on the morphology, mechanical properties, and biocompatibility of PCL scaffolds. SEM research demonstrated that the addition of Gnp resulted in a considerable decrease in fiber diameter and an improvement in surface homogeneity, which may have a major impact on cellular activity. The Young's Modulus results were particularly intriguing since they showed that the scaffolds' mechanical strength—a crucial component for CTE applications—was significantly increased at 0.5% graphene concentration.

The mechanical characterizations supported the hypothesis that graphene gives the scaffolds more rigidity. Although the initial rise in tensile stress and Young's modulus at 0.5% graphene was beneficial, the following fall at greater concentrations demands that scaffold design take Gnp ratios meticulously in order to preserve mechanical integrity.

Although certain overlapping bands made it difficult to distinguish between the peaks, FTIR characterization verified that graphene had been integrated into the PCL matrix without changing its chemical composition. These spectrum results emphasize a successful composite creation that takes advantage of the unique characteristics of PCL and graphene, supporting the morphological findings.

Contact angle measurements used to assess wettability revealed that all scaffold modifications maintained hydrophobic properties, which are necessary for certain TE applications. The cytotoxicity evaluation confirmed that Gnp-PCL scaffolds are not cytotoxic, which is consistent with earlier research on the biocompatibility of graphene.

Lastly, SEM measurements of the cell morphology on bmMSCs grown on these scaffolds supported the conclusion that Gnp-PCL scaffolds provide a favorable substrate for cell adhesion and proliferation, especially at lower graphene concentrations. The scaffolds' promise for Regenerative Medicine is demonstrated by the observed cell behaviors, especially in CTE, where scaffold-cell interactions are crucial.

This work highlights a suitable graphene concentration that maintains biocompatibility while optimizing mechanical benefits, offering insightful information on the complex impacts of graphene incorporation in polymeric scaffolds. These results open up new avenues for future studies on Gnp-PCL scaffolds in clinical settings, where optimizing material characteristics may result in substantial improvements in treatment strategies for cardiac repair.

Acknowledgements

We would like to thank the Lower Saxony Center for Biomedical Engineering, Implant Research and Development, and the Institute for Multiphase Processes for their support. This work was supported by the German Academic Exchange Service (DAAD), which provided financing for the research stay.

4. Incorporating Polypyrrole (PPy) into PolyCaprolactone (PCL) Fibers

The results presented in this chapter will be part of a publication in CET Journal.

Authors:

Ana M. Muñoz-Gonzalez[a], Dianney Clavijo-Grimaldo[a,b]

[a]Universidad Nacional de Colombia, Carrera 45 # 26 – 85, Bogotá Colombia.
[b]Fundación Universitaria Sanitas, Calle 22B # 66-46, Bogotá Colombia

Statement of contribution of co-authors for thesis by published papers:

Contributors	Statement of contribution
Ana M Muñoz-Gonzalez	Designed and perform the experiments Analyzed and interpreted results Conceived and wrote the manuscript Development of research results
Dianney Clavijo-Grimaldo	Involved in the conception of the project Designed the experiments. Assisted with characterization test Provided feedback in the whole process

4.1 Part 1

4.1.1 Abstract

The next chapter shows the results of different experiments looking for the integration of polypyrrole (PPy), a conductive polymer, as a nanofiller into polymeric nanofiber scaffolds, specifically focusing on its application for CTE. The inherent mechanical fragility and difficulty of processability of PPy can be solved by incorporating it as a nanofiller in electrospun nanofiber solution made from Polycaprolactone (PCL). This chapter focus on investigate the effect of different forms of PPy (commercially milled and synthesized) on the properties of PCL-based scaffolds. Electrospinning parameters were stablished, and the scaffolds were characterized using SEM, FTIR, tensile testing, and conductivity measurements. In addition, in this chapter there is some new strategies are required to enhance the properties of PCL-PPy scaffolds.

Keywords: Polypyrrole (PPy), PolyCaprolactone (PCL), Electrospinning, Conductive Polymers, Nanofiber Scaffolds, Tissue Engineering, Mechanical Properties, Polymer Synthesis.

4.1.2 Introduction

The growth of material science, notably in the field of polymers, has resulted in ground-breaking advances in a variety of fields. PPy, a conductive polymer, has emerged as a focal point for interest among these materials due to its large stability, high electrical conductivity, and outstanding intrinsic characteristics. These characteristics have allowed PPy to find a wide range of applications, from supercapacitors and biosensors to antistatic coatings and TE. However, the intrinsic mechanical fragility and problematic processability of PPy frequently impede its practical implementation.

Transitioning into the field of CTE, the use of polymers in electrospun nanofiber scaffolds still reveals certain limitations. Notably, the absence of electrical conductivity, which restricts intercellular interactions. Furthermore, their mechanical properties are weaker or far than those of the natural heart. Achieving the appropriate level of stiffness to prevent matrix failure during tissue contraction, while also maintaining sufficient elasticity to withstand the cyclical stresses of the myocardium, is critical to the success of the scaffold. These parameters play a pivotal role in regulating the behavior of cardiac cells. achieving successful integration of the scaffold with the host tissue requires correct electrical coupling and ideal mechanical resistance.

To address these challenges in CTE, researchers have turned to innovative scaffolds composed of conductive polymers such as poly(3,4 ethylene dioxythiophene) (PEDOT), poly(styrene sulfonate)

(PSS), PPy, and polyaniline (PANI) (Ghovvati et al., 2022; Matysiak et al., 2020; Roshanbinfar et al., 2020), as well as other materials like gold nanoparticles and carbon nanotubes or graphene (Alegret et al., 2019; Bellet et al., 2021; Gelmi et al., 2015; Gómez et al., 2021; B. Guo & Ma, 2018; S. Kumar & Chatterjee, 2016). These developments mark a significant stride in combining material science and biomedical engineering.

In recent years, the integration of conductive nanofillers like PPy into engineered cardiac tissues has shown promising improvements. For example, Liang et al.'s study on blending PPy with silk fibroin in electrospun nanofibers resulted in a reduced fiber diameter, mechanical properties closely matching the native myocardium, and sufficient electrical conductivity to support cardiomyocyte contractions (Liang et al., 2021). Similarly, Zarei et al. obtained conductive scaffolds composed of chitosan, collagen, and polyethylene oxide with PPy as nanofiller; achieving conductivity and cell adhesion, growth, and proliferation (Zarei et al., 2021).

Extending beyond cardiac applications, the versatility of PPy as a nanofiller has been demonstrated in other biomedical areas like bone and nerve tissue engineering. For instance, Maharjan et al. developed an *in situ* polymerization of PPy into a PCL solution; then, the PPy/PCL solution was electrospun, enhancing the mechanical strength, and increased surface roughness, decreased fiber diameter, and better behavior with cells for bone tissue application (Maharjan et al., 2020).

Moreover, PPy has been used with polyurethane (PU) and poly-L-lactic acid (PLLA) to obtain a soft conductive, flexible, and handle biomaterial for biomedical applications that supported the proliferation of human skin keratinocytes (S. Cui, Mao, Rouabhia, et al., 2021). Further, PPy has been used in nerve tissue engineering with PLA to improve the conductivity, hydrophilicity, and mechanical properties of the nerve cells (Imani et al., 2021; S. Li et al., 2022).

The aim of this study is to incorporate PPy into nanofibrous polymeric fibers of Polycaprolactone (PCL), a polymer known for its biocompatibility. The objective is to determine at how PPy particles affect the overall properties of PCL-based scaffolds, perhaps improving their potential in TE. Two types of scaffolds were created using the electrospinning method: a scaffold made of pure PCL nanofibers and a unique combination of PCL and PPy particles (PCL+PPy). Scanning Electron Microscopy (SEM), Fourier Transform Infrared Spectroscopy (FTIR), tensile strength testing, and conductivity studies were used to examine these samples.

This research serves as an initial step towards the fabrication and characterization of a scaffold that could be effectively utilized in TE applications, specialty in CTE. By emphasizing the material properties of PPy and PCL, and their interaction in a nanofibrous format, this study aims to bridge

the gap between material science and biomedical applications, potentially leading to innovative solutions in various engineering disciplines.

4.1.3 Materials and Methods

Materials

Polycaprolactone (PCL) (Sigma-Aldrich, CAS # 134490-19-0 MW=80000 Da), isopropyl alcohol (Sigma Aldrich, 99,7 % CAS # 67-66-3), chloroform (Sigma Aldrich, 99,5 %, CAS # 67-66-3) and, 2.2.2-Trifluoroethanol (TFE) was purchased from abcr GmbH.

Methods

Addition of Electro-Conductive Particles

According *Figure 4 - 1*, to create scaffolds incorporating conductive particles, a 9% (w/v) PCL solution in a 50:50 (v/v) chloroform and isopropanol solvent, prepared at least 48 hours prior to use (Clavijo-Grimaldo et al., 2022). Subsequently, PPy particles, as supplied by the provider and henceforth referred to as PPy, were added at 1% (w/v) to the prepared PCL solution. To ensure uniform dispersion of the particles within the solution, mixing was performed using an ultrasonic probe processor designed for low volume applications (Cole-Palmer # EW-04714-53).

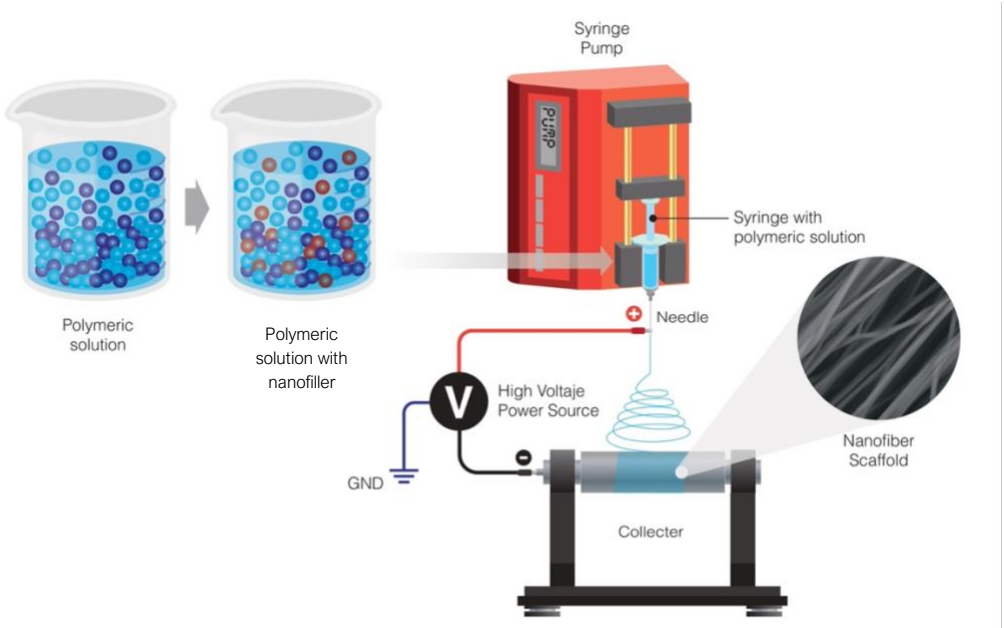

Figure 4 - 1 Electroconductive PPy particles incorporation into the electrospun fibers (author).

To fabricate the scaffold with PCL fibers that include PPy CM particles, an electropinning setup was utilized, comprising a high voltage source (CZE1000R, Spellman, USA), a dosing pump (KDS100, USA) with a 5 mL syringe and an 18-gauge needle. The fibers were collected on a flat aluminum foil collector. Several attempts were made to achieve the desired fibers, with monitoring conducted using an optical microscope (Motic, M300, China). Key electrospinning parameters optimized were the distance between the needle and the rotary collector, the applied voltage, and the solution feed rate. Ultimately, successful deposition was achieved after 60 minutes at 15 cm distance, 15 kV, and 1.0 ml/h, conducted at a room temperature of 20 °C and 50% relative humidity.

It is important to mention that in all the experiments, various methods were used to improve the dispersion of nanofillers in the polymeric solution. Among the methods used were ultrasonic bath, ultrasonic probe, magnetic stirring, agitation in a rotary shaker, and vortex. At the end, the better solution was to combine these methods, transitioning from a less turbulent regime to a more turbulent one, for example from roller agitation to magnetic stirring, and then to ultrasound methods. The vortex was not very efficient.

Characterization of Scaffolds

For morphological characterization of the obtained scaffolds, Scanning Electron Microscopy (SEM) (Tescan Vega 3 SB, Czech Republic / S3400N, Hitachi, Japan). Fiber diameter distribution was determined based on the SEM images, using Image J software. The composition of functional groups present in the scaffolds was analyzed using Fourier Transform Infrared Spectroscopy (FTIR). A Tensile Test was conducted to examine the mechanical properties of the scaffolds, while a Contact Angle Measurement Test was performed to assess wettability. Lastly, the Four-Point Probe method was used to measure the conductivity of the scaffold.

4.1.4 Results and discussion

In *Figure 4 - 2*, SEM images of the PCL+PPy scaffolds and their fiber diameter distribution. The PCL scaffold displays an average fiber diameter of 1471.52 ± 519.22 nm, with considerable size variability. In contrast, the PCL+PPy composite scaffold has a smaller average diameter of 1056.73 ± 238.99 nm, as confirmed by *Figure 4 - 2*b and d, where a narrower diameter distribution is evident.

SEM images also depicts a stochastic and uniform fiber array, creating a 3D network. The fibers are homogenous and defect-free. The PPy polymer affects the fiber diameter as increased conductivity in the solution leads to more charge carriers, elongating the formation for the Taylor cone and consequently reducing fiber diameter. This diameter reduction is advantageous, because it increases the surface area and porosity of the scaffold. These characteristics are essential in CTE applications because they promote cell adhesion, nutrition transportation, and integration with native

tissue. The enhanced porosity also increases the scaffold's capacity to imitate the extracellular matrix, creating a more favorable environment for cell proliferation and the formation of functional tissue constructions.

Furthermore, *Figure 4 - 2*a and c, illustrates that fibers with PPy nanofiller are morphologically more uniform compared to PCL-only fibers. This fact could improve charges transport, having a more consistent electrical conductivity across the scaffold, which is critical for developing more effective scaffolds for CTE, where the electrical signaling is integral for cellular coordination and function.

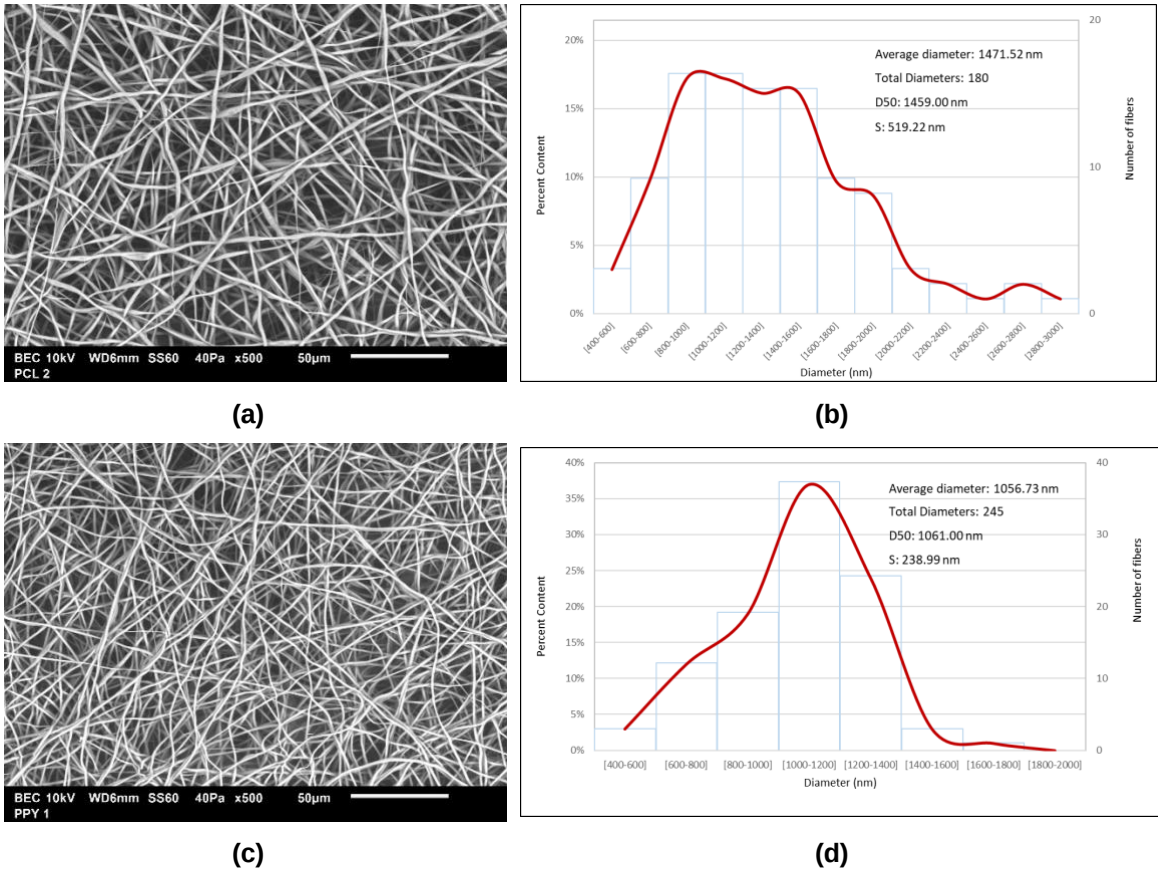

Figure 4 - 2 (a) SEM images of the scaffold composed of PCL fibers, (b) fiber diameter distribution of the scaffold composed of PCL fibers, (c) SEM images of the scaffold composed of PCL fibers with 1% PPy, (d) Distribution of the fiber diameter of the scaffold composed f PCL fibers with PPY 1%. D50 is the diameter when the cumulative percentage reaches 50% and S is the standard deviation.

FTIR assays were used to confirm the presence of the PCL and the PPy particles. In *Figure 4 - 3* are the FTIR spectra for both PCL and PCL+PPy samples. The PCL spectrum is characterized by prominent peaks: asymmetric CH_2 stretching at 2946 cm^{-1}, symmetric CH_2 stretching at 2860 cm^{-1}, carbonyl (C=O) stretching at 1717 cm^{-1}, C-C stretching at 1233 cm^{-1}, asymmetric C-O-C stretching

at 1166 cm^{-1}, and symmetric COC stretching at 1047 cm^{-1}. These peaks are consistent with previous research (Da Silva et al., 2013; Heidari et al., 2017; Tayebi et al., 2021; Yuan et al., 2012).

In the PPy spectrum, characteristic peaks were discerned at 1678 cm^{-1} indicative of C-N bonds, and at 1548 cm^{-1} denoting to C=C and C-C stretching of the polypyrrole ring. Additional peaks at 1420, 1275 and 1132 cm^{-1} are attributed to C-N bonds within the molecule. Subtle peaks ranging between 954 and 725 cm^{-1} imply C-H bonding in both PCL and PPy molecules, aligning with established literature. (S. Cui, Mao, Zhang, et al., 2021; Liang & Goh, 2020; Shinde et al., 2014; Yussuf et al., 2018). Results showed uniformity in the chemical composition of the polymers and the formation of PPy in the scaffolds.

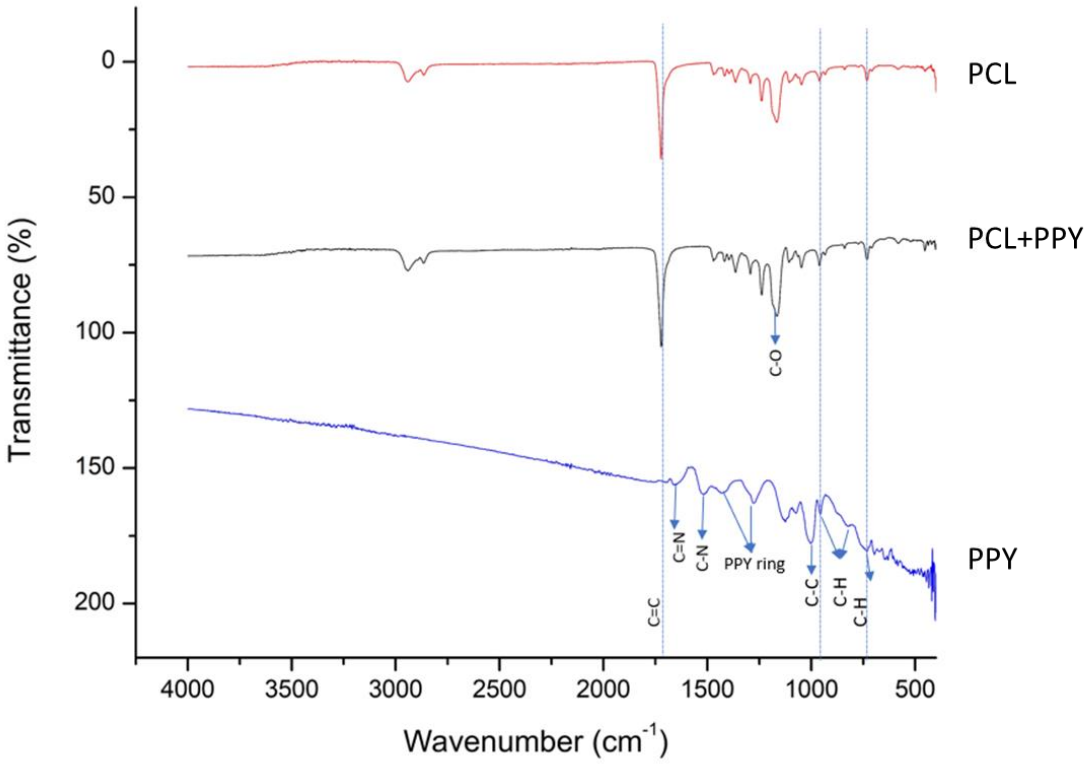

Figure 4 - 3 FTIR spectra of PCL, PCL+PPy and PPy.

The mechanical properties of the scaffolds were analyzed using stress-strain curves, which revealed that PCL and PCL+PPy behaved differently as can be seen in the *Figure 4 - 4*a. Moreover, in *Figure 4 - 4*b, the strain capacity of the PCL+PPy scaffold was 129.79 compared to 102.15 for PCL, indicating higher elasticity. Furthermore, the PCL+PPy had a higher maximum stress of 3.32 MPa compared to 2.50 MPa for PCL scaffold, indicating a more resistance material. The Young's Modulus, increased from 27.01 MPa for PCL to 32.79 MPa for PCL+PPy, indicating a stiffer

composite material. These findings imply that the addition of PPy improves the mechanical properties and elasticity of the PCL scaffold, potentially increasing its value in applications requiring both high strength and flexibility such as the myocardial tissue.

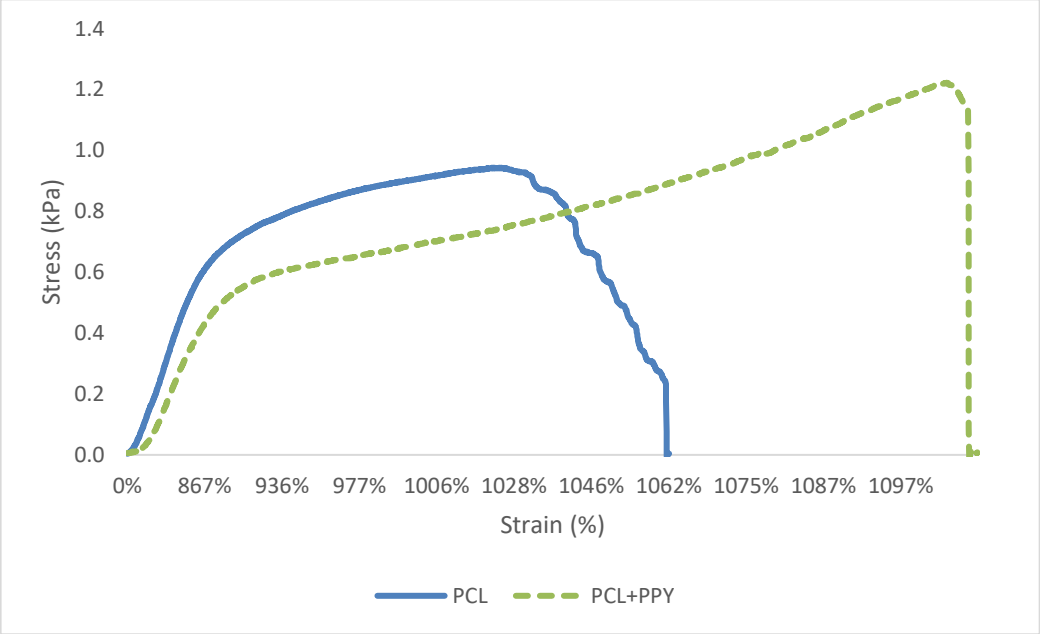

(a)

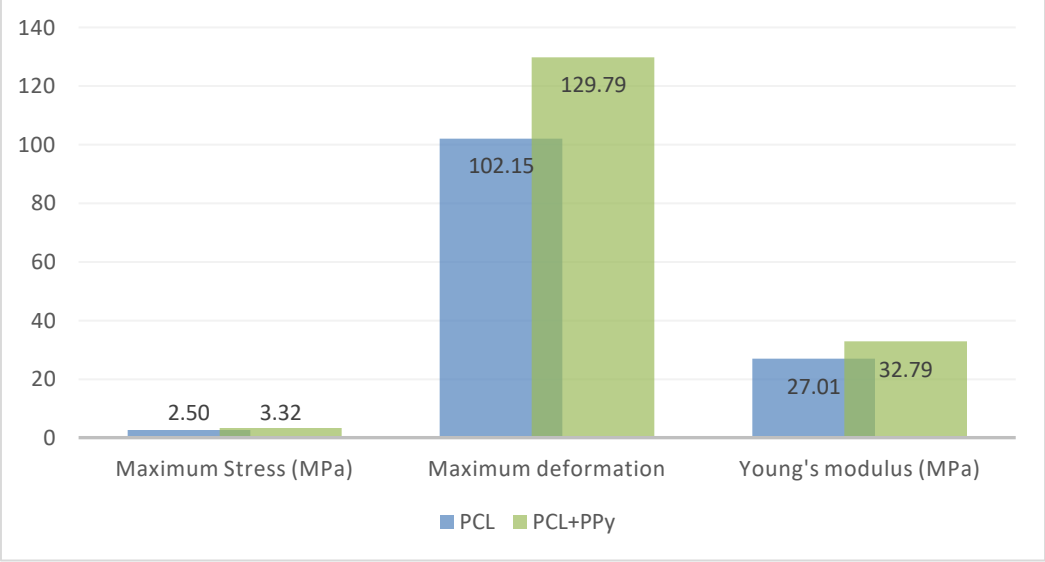

(b)

Figure 4 - 4 (a) Stress-strain diagram for the scaffolds obtained: PCL and PCL+PPy, (b) Mechanical properties of the scaffolds obtained: PCL and PCL+PPy. The columns represent the maximum stress, the maximum strain, and the Young's modulus.

The wettability of the scaffold surfaces can be determined using the contact angle measurements. For the PCL scaffold the contact angle is 125.38±4.89° and the PCL+PPy scaffold at 127.57±4.65°. By the addition of PPy, the contact angle increased, indicating that the surface became more hydrophobic. This could affect how the scaffold interacts with biological components in TE applications. The hydrophobicity of the scaffold may influence cell adherence, protein absorption, and overall bioactivity. These elements have significance for the scaffold's performance in biomedical applications.

Even though the scaffold surfaces are hydrophobic, in the PCL+PPy scaffold water drops tend to attach to the surface as can be seen *Figure 4 - 5*. This phenomenon, in which the water droplet does not flow easily but appears to 'stick' to the surface, may indicate the presence of adhesive forces or surface roughness that increases water retention.

Figure 4 - 5 Contact angle of the PCL+PPy scaffold.

4.1.5 Conclusions

This study examined the addition of PPy to PCL scaffolds, aiming to enhance properties for CTE. PCL+PPy scaffolds displayed reduced fiber diameter and improved porosity, potentially aiding cell adhesion. The incorporation of PPy, confirmed by FTIR analysis, improved mechanical elasticity and electrical conductivity, aligning with cardiac tissue dynamics. Uniform PPy distribution was achieved through optimized mixing methods, indicating that PCL+PPy scaffolds may meet myocardial tissue demands, marking progress in CTE development.

4.2 Part 2: Strategies used for the improvement of PPy incorporation into PCL scaffolds.

Given that the objective was to investigate the effect of a conductive nanofiller on fiber and electrospun scaffold properties and considering that in the first part of this chapter, a unique PPy-PCL solution was used, difficulties were encountered in increasing the nanofiller percentage due to handling and distribution issues within the electrospinning solution, resulting in agglomerations, blockages, and fibers with various defects.

To overcome these challenges, many solutions were used to improve the process and the final scaffold. Mechanical milling of PPy particles was carried out with the assumption that lower particle sizes would result in finer, more uniform fibers and better filler dispersion within the solution and fibers. In addition, synthesis of PPy was also carried out. Then, new PCL fibers were produced using the milled and synthesized PPy, and the process for doing so is described in full below. Results of the experiments was examined using Scanning Electron Microscopy.

4.2.1 Option 1: Enhancing PPy particle size for electrospinning: Milling of Commercial Particles and a new solvent.

To achieve fibers with smaller diameters and improved behavior during the electrospinning process, milling of commercial PPy particles was undertaken to mechanically reduce their size. Mechanical milling involves continuous impact of milling media within a container with powder samples, creating high friction. This process aims to produce smaller particles, as continuous impacts alter their morphology, especially in rigid materials. PPy, being a rigid polymer due to its conjugated chains, is considered suitable for milling (Abbasi et al., 2013).

Additionally, various parameters in mechanical milling influence particle size, including the ball-to-powder weight ratio (BRP), the material and size of the milling media, the container's filling level, and the rotation speed.

For the milling process, a planetary ball mill (Fritsch GmbH, Germany) with a 250 mL stainless steel container and milling media was used. Milling media of two different sizes, 5 mm and 12 mm diameter, were employed. The BRP was set at 125:1, with a rotation speed of 250 rpm, and 15 mL of process control agent (ethanol) per gram of powder was added. Ethanol mitigates temperature rise due to frictional forces during milling, prevents oxidation, and reduces particle agglomeration by soldering. It was chosen for its low boiling point (78.4 °C) and inertness to the components. The experiment was conducted over three different milling durations: 10, 30, and 60 minutes.

Synthesis of PPy

Pyrrole (Py) (Merck, 98%, CAS # 109-97-7), and anhydrous iron (III) chloride (FeCl3) (Merck, CAS # 7705-08-0) were used as an oxidant for the PPy synthesis. Py and $FeCl_3$ solutions were prepared using distilled water.Furthermore, the synthesis of PPy particles was carried out.

First, solutions of Py 0.3 M as a monomer and iron chloride ($FeCl_3$) at 0.73 M as an oxidant in distilled water were prepared. The process involved continuous stirring of the Py solution, to which the oxidant solution was added dropwise, changing color gradually from transparent to black as can be seen in *Figure 4 - 6*. The polymerization time was 230 minutes at room temperature. The black precipitate was filtered and repeatedly washed with distilled water and ethanol to ensure no traces of unreacted reagents remained in the polymer. Finally, the filtered product was dried overnight and stored for later use.

Figure 4 - 6 PPy polymerization process.

Design of Experiments

To fabricate fibers incorporating electroconductive PPy particles with PCL as the base polymer, preparation of the solutions outlined in *Table 4 - 1* was conducted. This part also employed a novel polymeric solution of polycaprolactone (PCL) using Trifluoroethanol (TFE) as an alternative solvent. This was done to ascertain whether the new solvent could offer improved dispersibility for the polypyrrole (PPy) particles within the solution.

To fabricate the scaffold with PCL fibers that include PPy nanofiller, an electrospinning setup develop in the Institute for Multiphase Processes of the Leibniz Universität Hannover, comprising a high voltage source, a dosing pump (KDS200, USA) with a 3 mL syringe and an 0.8-gauge needle. The fibers were collected on a rotatory aluminum foil collector at 580 rpm. Deposition was achieved after 60 minutes at 26 cm distance, conducted at a room temperature of 21 °C and 30% relative humidity. For fiber characterization, SEM (S3400N, Hitachi, Japan) was used to analyze morphology. The samples were then examined at an acceleration voltage of 20 kV and a working distance of 10 cm.

The fiber diameter was measured by utilizing an image analysis program (ImageJ software, NIH, Bethesda, MD).

Table 4 - 1 Solutions with electroconductive PPy particles incorporation into the electrospun fibers.

Polymer	Concentration	PPy particles	Percentage	Nomenclature
PCL	13% Trifluoroethanol (TFE)	PPy CM	1	PCL/TFE+1%PPyCM
			2	PCL/TFE+2%PPyCM
		PPy M	1	PCL/TFE+1%PPyM
			2	PCL/TFE+2%PPyM
	9% Chloroform: Isopropanol	PPy CM	1	PCL/Cl:Is+1%PPyCM
			2	PCL/Cl:Is+2%PPyCM
		PPy M	1	PCL/Cl:Is+1%PPyM
			2	PCL/Cl:Is+2%PPyM

Results

The SEM images presented in the figure reveal the morphology of commercial PPy particles. *Figure 4 - 7*a shows the agglomerated morphology of the particles and a closer view at their individual shapes, which are elongated rather than circular. In the solution for electrospinning process, this morphology suggests a potential increase in solution viscosity, leading to larger fiber diameters. The average particle size is noted as 1.67±1.96 µm.

After 10 minutes of milling, as seen in *Figure 4 - 7*b, there is a noticeable decrease in the size of PPy macroparticles by 25% to 1.24±1.04 µm. In addition, further reduction is observed after 30 and 60 minutes of milling, with sizes reducing to 0.30±0.49 µm (*Figure 4 - 7*c) and 0.15±0.34 µm (*Figure 4 - 7*d), respectively.

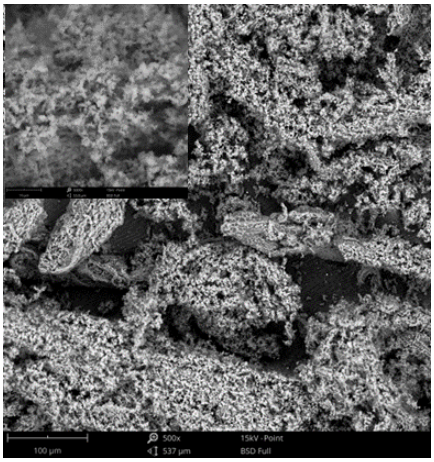

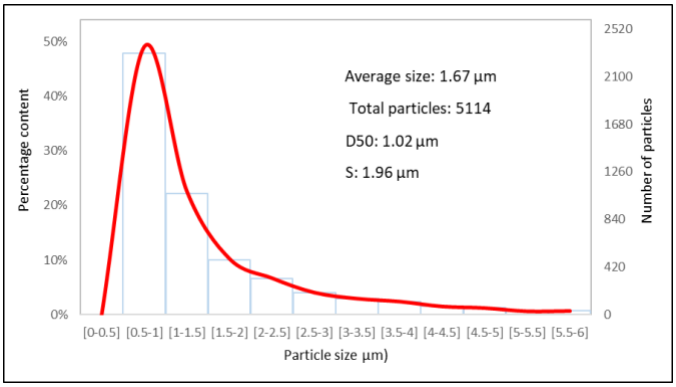
Average size: 1.67 µm
Total particles: 5114
D50: 1.02 µm
S: 1.96 µm
Percentage content
Number of particles
Particle size µm)
[0-0.5] [0.5-1] [1-1.5] [1.5-2] [2-2.5] [2.5-3] [3-3.5] [3.5-4] [4-4.5] [4.5-5] [5-5.5] [5.5-6]

(a)

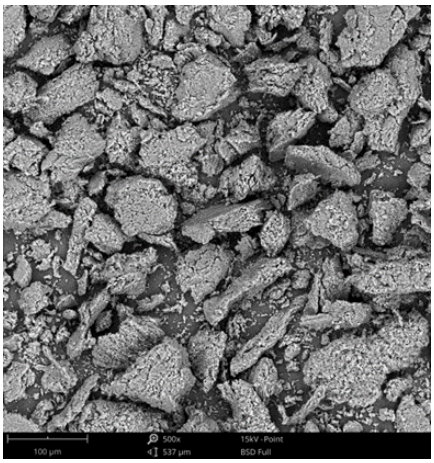

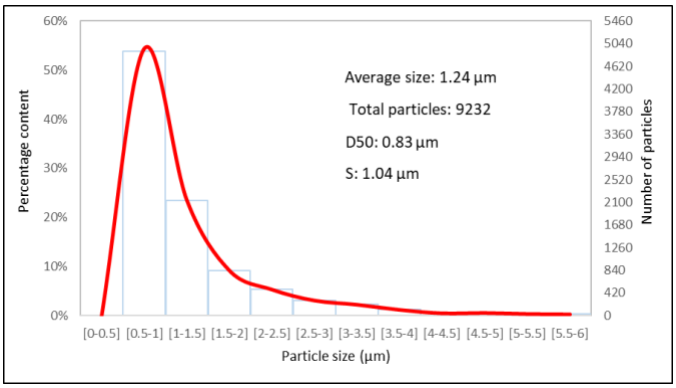
Average size: 1.24 µm
Total particles: 9232
D50: 0.83 µm
S: 1.04 µm
Percentage content
Number of particles
Particle size (µm)
[0-0.5] [0.5-1] [1-1.5] [1.5-2] [2-2.5] [2.5-3] [3-3.5] [3.5-4] [4-4.5] [4.5-5] [5-5.5] [5.5-6]

(b)

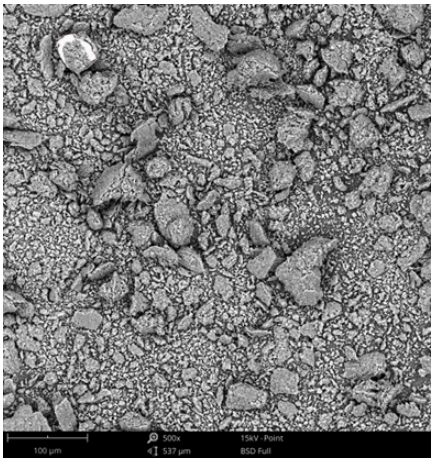

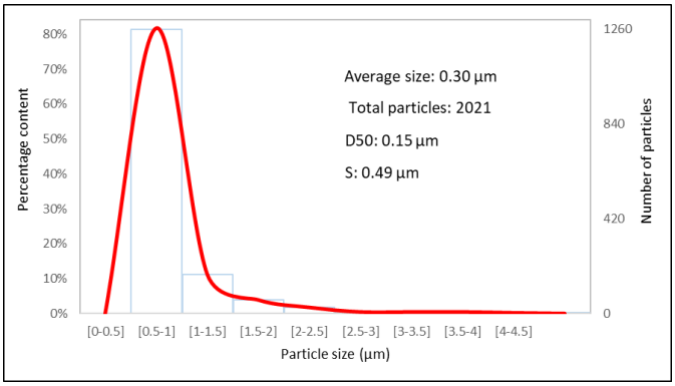
Average size: 0.30 µm
Total particles: 2021
D50: 0.15 µm
S: 0.49 µm
Percentage content
Number of particles
Particle size (µm)
[0-0.5] [0.5-1] [1-1.5] [1.5-2] [2-2.5] [2.5-3] [3-3.5] [3.5-4] [4-4.5]

(c)

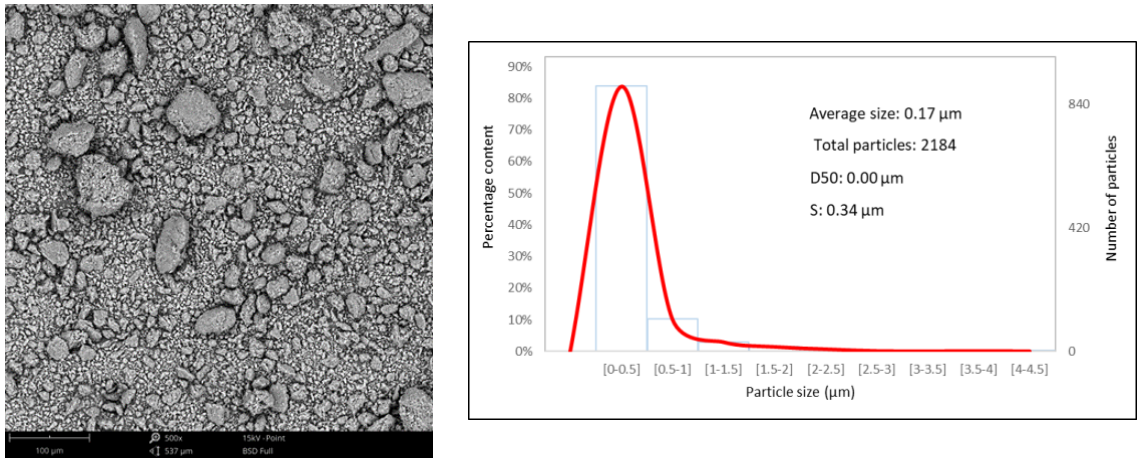

(d)

Figure 4 - 7 (a) SEM images and particle size distribution of PPy commercial particles, (b) SEM images and particle size distribution of PPy 10 min milled, (c) SEM images and particle size distribution of PPy 30 min milled, (d) SEM images and particle size distributof PPy 60 min milled. D50 is the diameter when the cumulative percentage reaches 50% and S is the standard deviation.

The smallest particle size at 60 min, similar to the 30-minute milled particles, shows agglomerations. According to a one-way ANOVA analysis, the particles milled for 30 and 60 minutes do not exhibit significant differences ($p<0.01$), indicating that milling time beyond 30 minutes does not substantially impact the PPy particle size. However, extended milling times could potentially lead to increased particle welding and agglomeration, as well as a possible decrease in electrical conductivity (Abbasi et al., 2013).

Expanding on the analysis of the milling results for PPy particles to be used in an electrospinning process, the SEM images suggest that the particle size reduction resulted from milling would enhance the electrospinning process by favoring the formation of thinner fibers, which is profitable for creating scaffolds with higher surface area-to-volume ratios. The observed agglomerations following milling, particularly at 30 and 60 minutes, could be attributed to the intrinsic stickiness of smaller PPy particles caused by increased surface energy. This could present hurdles in achieving a homogeneous distribution of PPy within the PCL matrix.

The lack of significant size difference between the 30 and 60-minute milled particles, as indicated by the ANOVA test, suggests an optimal milling time that balances size reduction with the risk of excessive agglomeration. Thus, the choice of milling duration may be a trade-off between achieving smaller particle sizes and maintaining the functional properties of PPy, such as electrical conductivity, which is crucial for its application in conductive scaffolds for TE.

The topic, which focuses on the effect of milling on polymer features, is underexplored. As a result, this preliminary contribution lays the framework for future study into the impacts of milling on polymer properties, as well as alternate particle size reduction strategies for conductive polymers.

Results of the synthesis of PPy particles

The images obtained from the SEM in *Figure 4 - 8* show the morphology of the synthesized PPy (PPy M) particles, which are globular, oval, and agglomerated forming a three-dimensional branching structure. The average size of at least 50 particles is 0.82±0.15 µm. This means that the particle size is lower than that of commercial and 10-minute milled particles, but larger than those obtained after 30 or 60 minutes of mechanical milling. However, a one-way ANOVA ($p<<0.01$) shows no significant difference between synthetic particles (PPy M) and those milled for any duration.

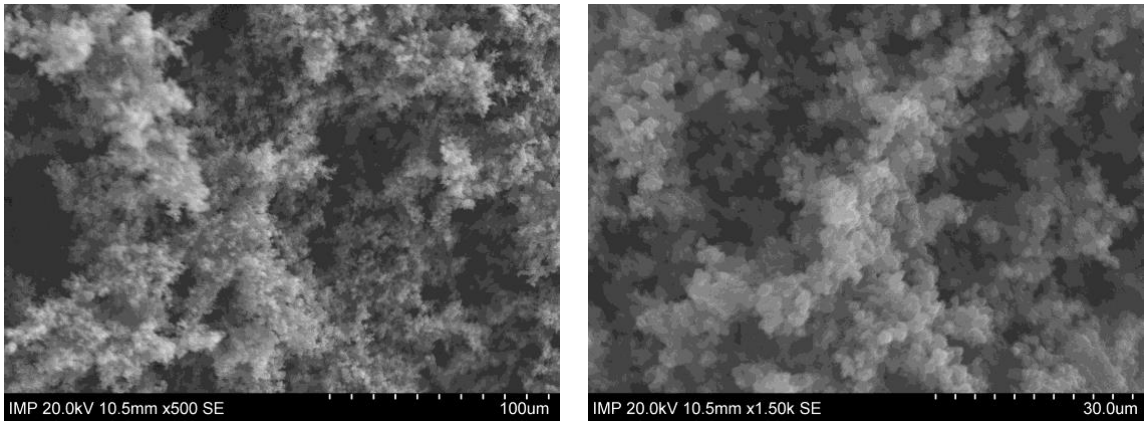

(a) **(b)**

Figure 4 - 8 SEM images of the PPy powder synthesized (a) 500x, (b) 1500x.

Considering the particle size results from both milling and synthesized PPy, the PPy powder milled for 4 hours (PPy CM) and the synthesized PPy (PPy M) were selected as nanofillers for the PCL fibers, in line with the experimental design.

Using milled PPy (PPy CM) and synthesized PPy (PPy M) particles, scaffolds were developed from a PCL solution with chloroform and isopropanol as solvents. This approach yielded fibers with a high degree of uniformity and without defects as can be seen in *Figure 4 - 9*a. The average diameter was relatively large at 2311.27±1507.50 nm, under electrospinning parameters of 1.0 ml/h and 15 kV.

The addition of 1% PPy M resulted in a significant reduction in diameter to 1468.54±639.24 nm, with a more uniform distribution as shown in the *Figure 4 - 9*b. Increasing the PPy M content to 2% further reduced the diameter to 979.86±572.62 nm with. However, this sample exhibited a broader distribution of fiber sizes and contrasts in the SEM images in *Figure 4 - 9*c. It is also noted that the

fibers with 2% PPy M did not perform as well as those with 1% in terms of uniformity and surface quality. The electrospinning parameters in both cases were 0.5 ml/h and 15 kV.

In the *Figure 4 - 9*d, a photograph clearly shows the hose blocked with PPy CM particles during an attempt to fabricate scaffolds with 1 and 2%. This issue arose because the increased particle content heightened the viscosity of the solution, preventing it from flowing through the hose. Additionally, the accumulation of particles at the needle tip in these conditions led to challenging blockages in the electrospinning process, highlighting the practical limitations when working with higher concentrations of PPy CM in the solution.

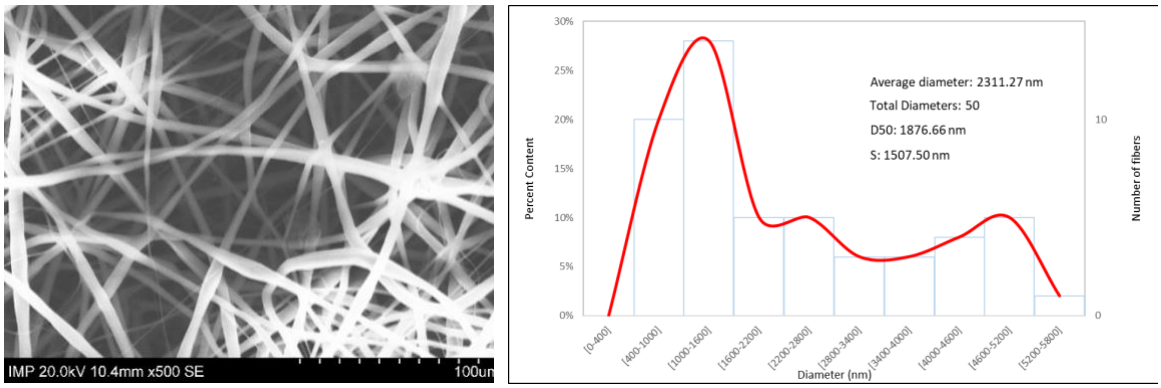

(a)

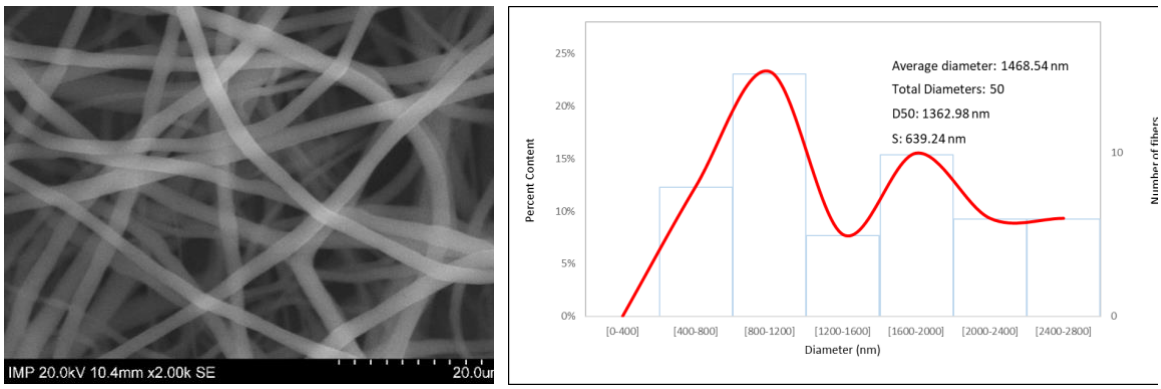

(b)

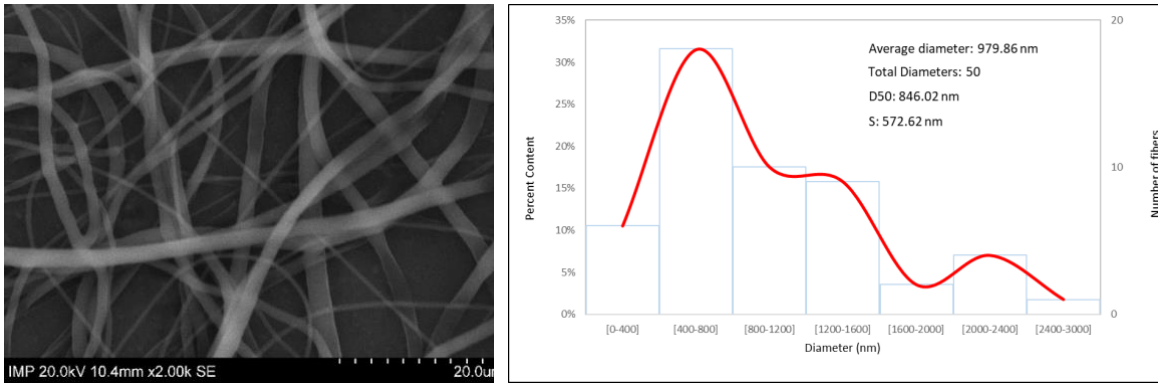

(c)

(d)

Figure 4 - 9 SEM images of (a) PCL/Cl:Is, (b) PCL/Cl:Is+1%PPyCM, (c) PCL/Cl:Is+1%PPyCM scaffolds, (d) blockage found in electrospinning hose.

The ANOVA (Analysis of Variance) and the Tukey post-hoc test were used to examine differences among various fiber groups: PCL/Cl:Is, PCL/Cl:Is+1%PPyCM, and PCL/Cl:Is+2%PPyCM scaffolds. With a significant p-value of $2.74*10^{-9}$, the analysis revealed significant differences between these groups in terms of their diameter. This suggests that the addition of PPy CM have a significant effect on the PCL fibers.

For the PCL/TFE solution (*Figure 4 - 10*a), SEM analysis revealed the formation of uniform, defect-free fibers with an average diameter of 1259.73±704.21 nm, using electrospinning parameters of 0.5 ml/h, 14.3 kV, and a 26 cm needle-to-collector distance. However, the diameter distribution indicated considerable heterogeneity, showing a range of fiber sizes.

The addition of 1% milled PPy (PPy CM) in the PCL/TFE+1%PPyCM sample (*Figure 4 - 9*b) resulted in fibers with a reduced average diameter of 278.46±119.16 nm and a more homogeneous diameter distribution, peaking between 200 and 300 nm. These fibers were also uniform and free of defects.

The electrospinning conditions for this sample were adjusted to 1.0 ml/h, 15 kV, and a 26 cm needle-to-collector distance.

For the PCL/TFE+2%PPyCM sample shown in the *Figure 4 - 10*c, the increase in PPy particles led to less desirable outcomes. SEM images indicated fewer fibers with an irregular, flattened and helical pattern shape, and a non-uniform distribution of PPy, as well as an increase in fiber diameter to 664.37±267.78 nm. The electrospinning process for this sample was challenging due to the high viscosity of the solution. Surface tension, which increases with viscosity, is reason for this morphology. The formation of homogeneous jets is disrupted when the surface tension value is overly high.

The scaffolds containing synthesized PPy particles (PPy M) showed improved results as can be seen in the *Figure 4 - 10*d. The PCL/TFE+1%PPyM sample exhibited uniformly shaped, defect-free fibers, with a decreased average diameter to 422.83±196.84 nm, despite an additional peak in diameter distribution due to a presence of some fibers with larger diameters. The parameters of 0.5 ml/h and 15 kV.

Despite better results on fiber formation with PPy M compared to PPy CM, the electrospinning process had some technical issues due the increase in superficial tension due the higher solution viscosity. Moreover, for the PPy M particles, there was gradual precipitation in the tube from the pump to the needle, suggesting potential uneven distribution of PPy particles in the scaffold fibers.

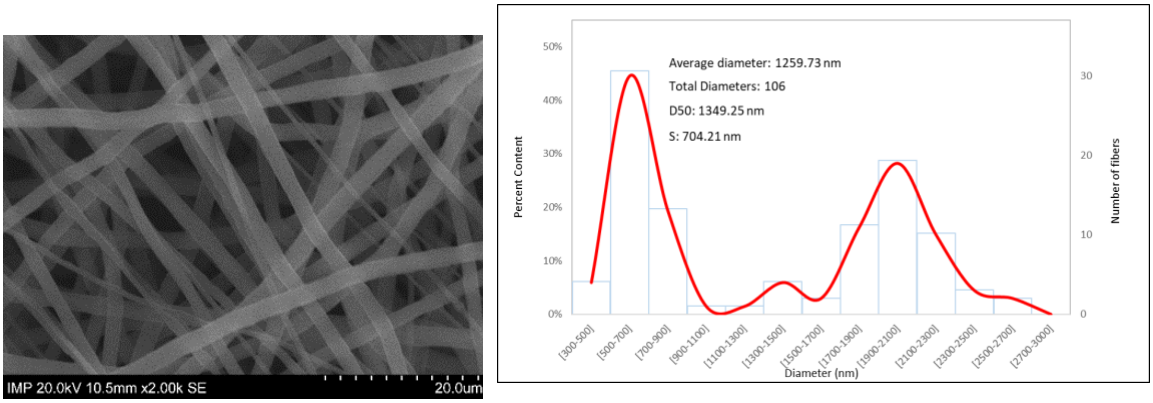

(a)

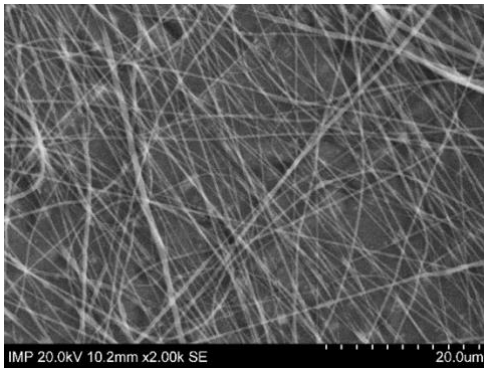
IMP 20.0kV 10.2mm x2.00k SE
20.0um

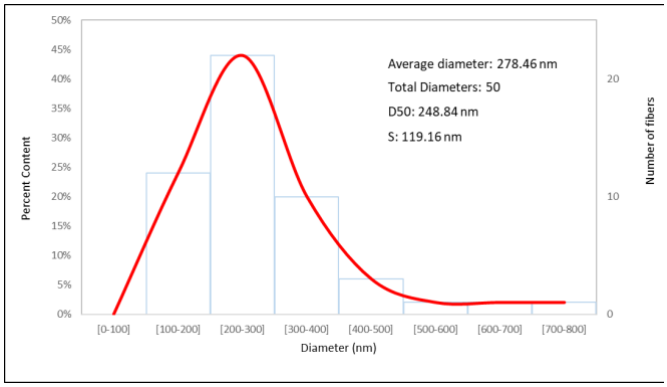
Average diameter: 278.46 nm
Total Diameters: 50
D50: 248.84 nm
S: 119.16 nm
Percent Content
Number of fibers
Diameter (nm)
[0-100]
[100-200]
[200-300]
[300-400]
[400-500]
[500-600]
[600-700]
[700-800]

(b)

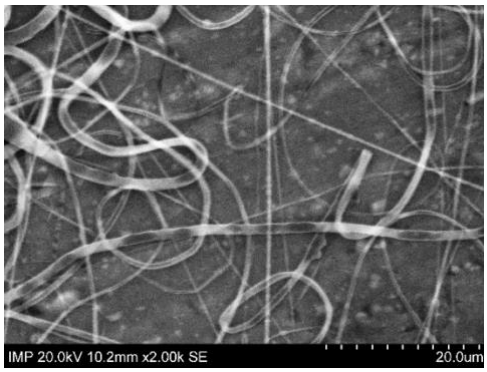
IMP 20.0kV 10.2mm x2.00k SE
20.0um

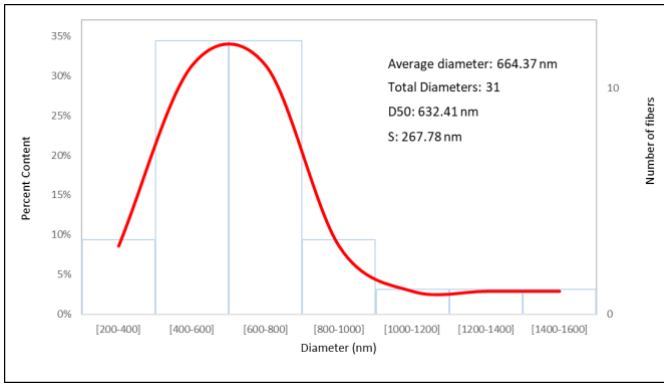
Average diameter: 664.37 nm
Total Diameters: 31
D50: 632.41 nm
S: 267.78 nm
Percent Content
Number of fibers
Diameter (nm)
[200-400]
[400-600]
[600-800]
[800-1000]
[1000-1200]
[1200-1400]
[1400-1600]

(c)

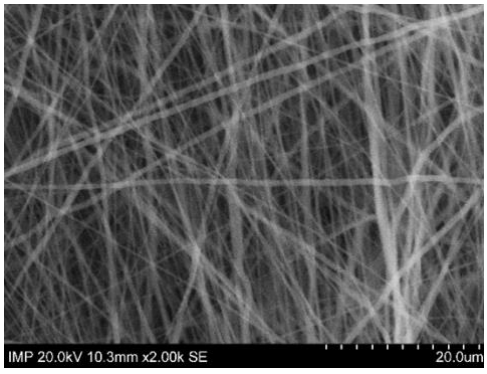
IMP 20.0kV 10.3mm x2.00k SE
20.0um

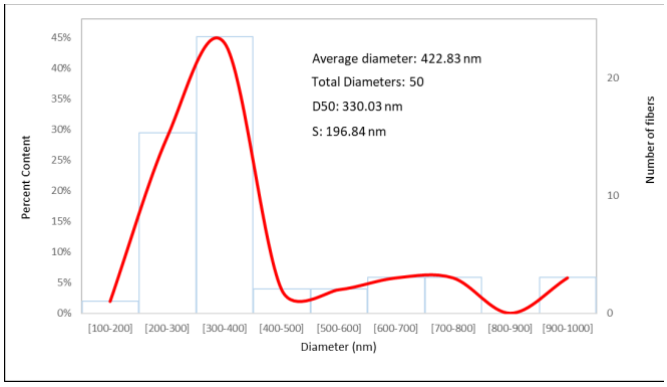
Average diameter: 422.83 nm
Total Diameters: 50
D50: 330.03 nm
S: 196.84 nm
Percent Content
Number of fibers
Diameter (nm)
[100-200]
[200-300]
[300-400]
[400-500]
[500-600]
[600-700]
[700-800]
[800-900]
[900-1000]

(d)

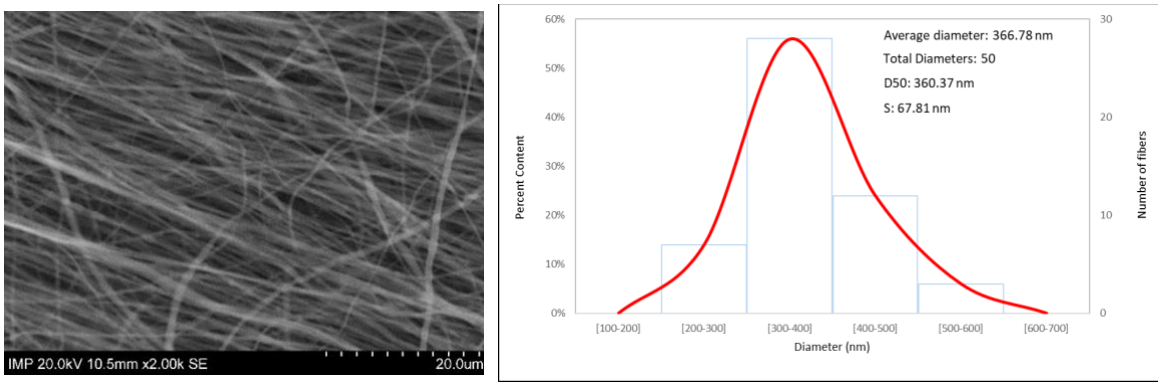

(e)

Figure 4 - 10 SEM images of (a) PCL/TFE, (b) PCL/TFE+1%PPyCM, (c) PCL/TFE+2%PPyCM, (d) PCL/TFE+1%PPyM, (e) PCL/TFE+2%PPyM scaffolds.

To assess the impact of PPy CM and PPy M on PCL/TFE nanofibers, an ANOVA complemented by a Tukey analysis was conducted. The analysis, revealing a negligible p-value, indicates that the incorporation of PPy significantly alters the diameter of PCL/TFE nanofibers. Further, sample with incorporation of 2% of PPy CM, are significant difference between the others, confirming that sample is different than the others as can be seen above. While the PCL/TFE+1%PPyCM, PCL/TFE+1%PPyM, and PCL/TFE+2%PPyM scaffolds do not show significant differences among themselves, they are distinctly different from the PCL/TFE nanofibers, underscoring the significant influence of PPy on the properties of these non-conductive polymer nanofibers.

4.2.2 Option 2: Exploring other solvents and an additional polymer.

According to previous results, the fibers made from PCL with chloroform and isopropanol have a large diameter, and the solution presents issues when addition an increasing amount of nanofiller. That is the reason why TFE was used in the formulation, which produced more favorable results, as observed. However, as the amount of nanofiller increased, the process became much more complex.

Exploring solvents for PCL

In this point, the option of creating fibers containing nanofiller with other solvents or a different polymer was explored, because maybe it could enhance the dispersibility having a more stable and fluidic electrospinning process. One of the options was PCL 10% w/v with dichloromethane (DCM) and dimethylformamide (DMF) in a 1:1 ratio. In this case, as observed in the *Figure 4 - 11*, the best nanofiber obtention are achieved when the parameters are 1 mL/h and 12.7 kV. The achieved diameter in this case was 719.77±169.47 nm, and the fibers have a smooth morphology. However, there is presence of some beads occasionally along the scaffold. This option was also discarded

due to dripping between the needle and collector during the process that could affect the quality of the final scaffolds because it could promote the apparition of defects in macroscale, and there was also not much efficiency in fiber production.

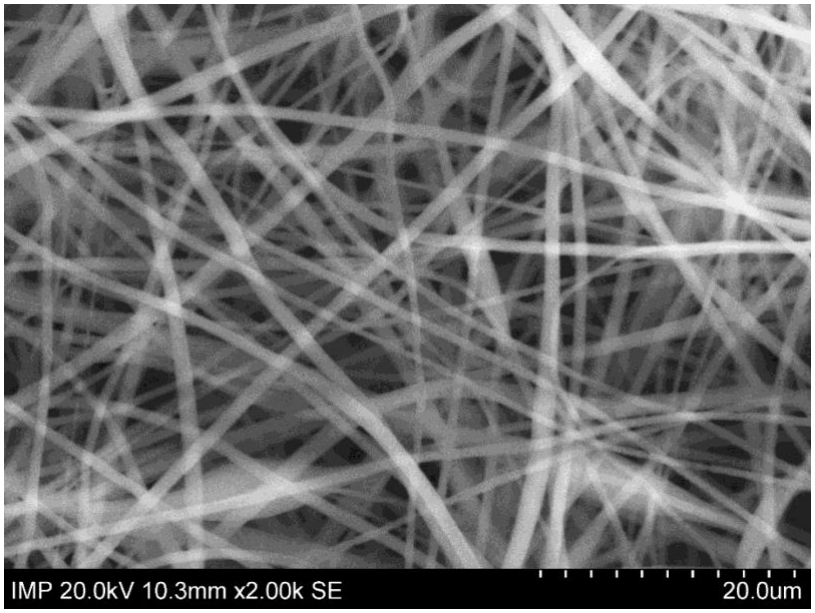

Figure 4 - 11 PCL/DCM:DMF nanofibers.

Another interesting polymer

Another option that was explored was the use of polyvinylidene fluoride (PVDF), as it is a polymer that has interesting properties such as excellent piezoelectric properties, thermal stability, light weight, and mechanical strength with flexibility (Kalimuldina et al., 2020; Zaarour, Zhang, et al., 2019). It has good processability, low cost, and is biocompatible (Saxena & Shukla, 2021), serving both as scaffolds and sensors for cardiac (Adadi et al., 2020) or nervous tissue engineering (Gryshkov et al., 2021).

According to a review in the literature, solvents such as DMF (M. Kumar & Kumari, 2020), tetrahydrofuran (THF), cyclohexane, and acetone (Shao et al., 2015; Zaarour, Zhang, et al., 2019) are used to achieve the PVDF solution for electrospinning. The concentration of this polymer in the solution is typically between 10 and 28%, depending on the molecular weight, which is usually 530,000 g/mol (Shao et al., 2015; Zaarour, Zhu, et al., 2019; Zahari et al., 2021).

In this trial, a 20% w/v PVDF solution was prepared with a solvent system of dichloromethane (DCM) and dimethylformamide (DMF) in a 3:2 ratio, and with electrospinning parameters of 1 mL/h and 15 kV to reach defect-free fibers. Here, the achieved fiber diameter was 1206.04±656.81 nm, and the morphology of the fiber were smooth as can be seen in the *Figure 4 - 12*. The electrospinning process

with this polymer faced several issues, starting with the preparation of the solution, because it is different due to its resinous nature of PVDF, requiring constant stirring and heating at 70°C. That conditions could impact in the entanglement of polymer macromolecular chains in the solution, varying the viscosity as well and the fiber morphology, resulting in a membrane that was not sufficiently resistant and dimensionally stable, thus unmanageable. Additionally, during the fabrication of the scaffold, it was necessary to change the needle every 15 minutes, as it became clogged over time.

Then, the incorporation of PPy into the PVDF fibers, initially there was the challenge, because of the dispersion in the solution, which proved to be difficult despite having several methods for dispersion. When dispersion was possible, the solution had an intermittent jet in the electrospinning process, occasionally ejecting clusters of PPy particles, which led to macroscopic defects in the scaffold.

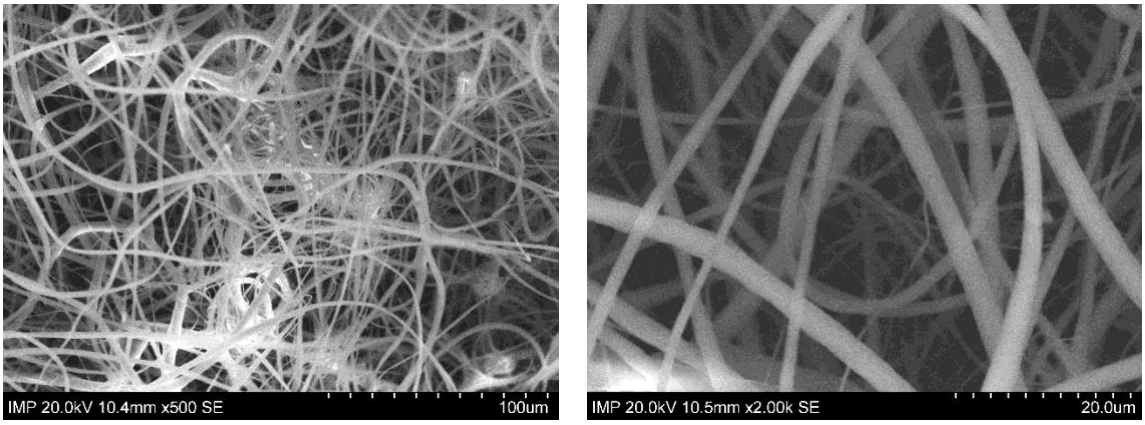

(a) **(b)**

Figure 4 - 12 PVDF nanofibers at (a) 500X and (b) 2.0kX.

4.2.3 Option 3: Use of surfactants or a new way to polymerizate

Surfactants

One possible solution was the use of surfactants in the PCL solution with PPy particles to enhance its dispersion. According to the literature, some surfactants experimented with were stearic acid, Sodium dodecyl sulfate (SDS), PVP, and dodecyl benzenesulfonic acid (Kesornsit et al., 2022; Kim et al., 2018; J. Li, Xu, et al., 2018). For the first two, there was no positive influence on the solutions, and changes in the solvent of the solution had to be considered due to their incompatibility with solvents like chloroform. The fibers made with PVP were not very stable or resistant and presented significant defects. The last option (dodecyl benzenesulfonic), especially for PPy CM particles, was considered because the manufacturer reported this reagent in its production and in one of the

solvents of this polymer. However, the results were not as expected, and contrary to contributing to the new solution, it degraded the PCL polymer, resulting in a significant negative change in the viscosity and composition of the solution.

Polymerization into the polymeric solution for electrospinning.

Lastly, the exploration ventured into polymerizing PPy within a polyvinylpyrrolidone (PVP) solution. PVP, previously utilized as a surfactant (Han et al., 2016), presented a potential dual role as both a supportive polymer matrix and a facilitator for the dispersal of nanofillers. For this investigation, three distinct experimental setups were attempted.

In the initial experiment, the PVP solution was enriched with 5% pyrrole monomer (Py) and 10% iron chloride oxidant. After two hours of polymerization, the solution exhibited a marked increase in viscosity, hindered fiber formation, and occasionally transitioned from electrospinning to dripping. Subsequent experiments adjusted the polymerization duration to one and three hours, respectively. The optimal outcome was observed at the one-hour mark, as depicted in *Figure 4 - 13*. However, the results fell short of expectations. The inclusion of pyrrole and oxidant not only necessitated alterations to the polymeric matrix's properties but also introduced a complex dynamic where the oxidant engaged with both the pyrrole and PVP. This interaction significantly altered the solution's composition and viscosity, rendering it progressively more fluid—a pivotal factor that shifted the methodological focus from electrospinning to electrospray.

Moreover, conducting the polymerization reaction directly within the solution introduced an additional challenge: the potential retention of excess reactants within both the solution and the resultant membranes. For applications in TE, where safety and biocompatibility are paramount, the presence of residual reactants, particularly those with cytotoxic profiles, poses a significant concern.

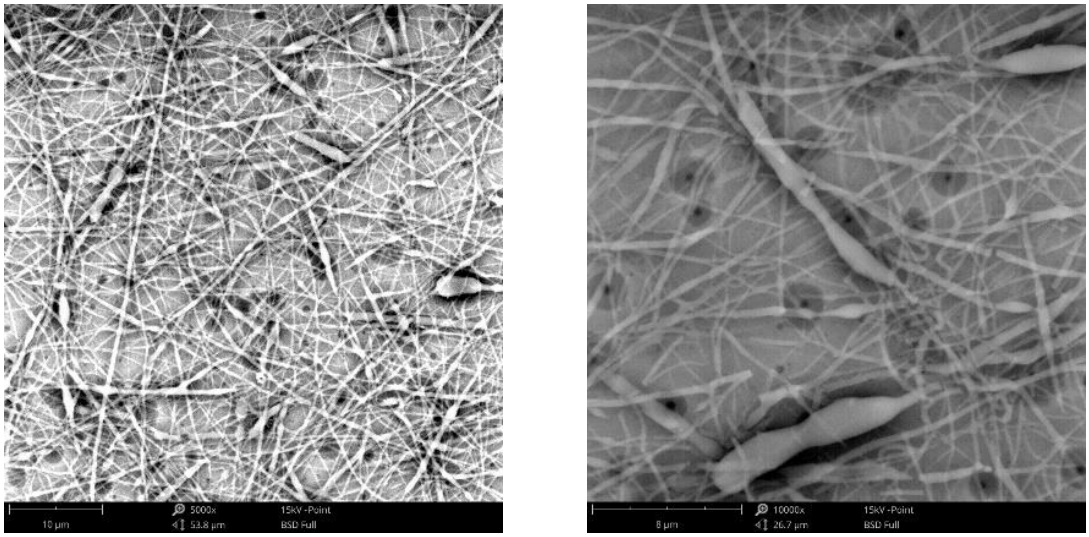

(a)

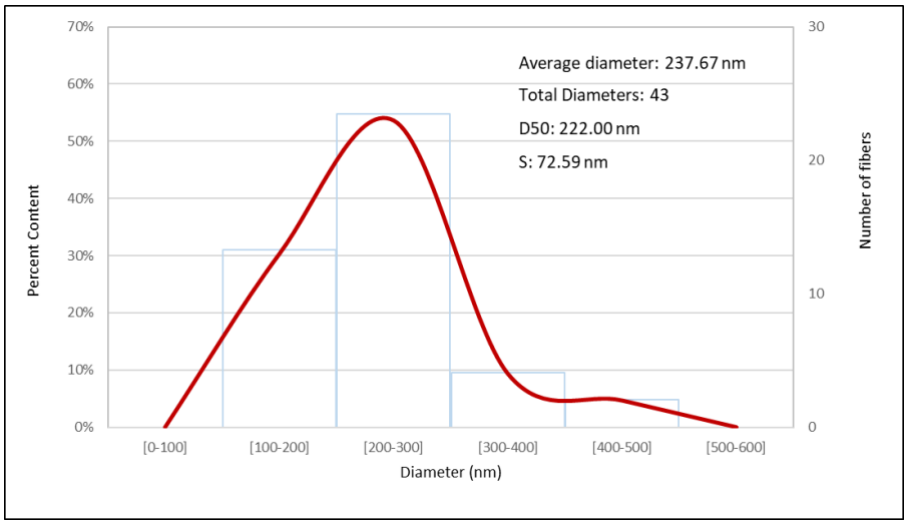

(b)

Figure 4 - 13 (a) SEM images of fibers made of PPy polymerizated into PVP solutions. (b) Nanofibers distribution.

4.3 Conclusions

At the end of this chapter, it is possible to affirm that the incorporation of PPy into PCL fibers affect the morphology of the electrospun scaffolds for TE applications. In addition, the study demonstrated that PPy, both in its milled and synthesized forms (PPy CM and PPy M), can effectively reduce the diameter of PCL fibers, contributing as well to a more uniform and defect-free scaffold structure.

This chapter also delves into the challenges and strategies of incorporating PPy, into PCL scaffolds, aspiring to harness PPy's electrical properties for CTE. Initial attempts with a homogeneous PPy-

PCL blend faced issues like particle aggregation and inconsistent fiber quality during electrospinning, due to difficulties in scaling up the nanofiller content.

Strategies were then devised to refine this process. Mechanical milling aimed to produce finer PPy particles, anticipated to yield more uniform fibers and improve dispersion. In parallel, PPy synthesis was also optimized. SEM provided insight into the morphologies achieved. SEM analyses revealed the impact of particle size reduction on fiber dimensions and the challenges posed by agglomeration. The enhanced milling time emerged as a balance between particle and functionality, crucial for the role of PPy in conductive scaffolds.

Further, the PPy incorporation into PCL using other solvents was examined. Experimenting with trifluoroethanol (TFE) as a solvent offered improved particle dispersal compared to conventional solvents. Dichloromethane and dimethylformamide, among other solvent systems, were tested to assess their ability to support a stable electrospinning process and produce quality nanofibers.

Lastly, alternatives like using surfactants for better dispersion and innovative polymerization methods within the spinning solution were explored, although these approaches met with varying degrees of success.

This investigation underscores the nuanced interplay between material science and scaffold fabrication, setting a preliminary promising alternatives for future advancements in conductive scaffolds for CTE.

Given these challenges and based on a detailed analysis of the results obtained, the need to explore alternative approaches that could overcome these limitations became evident. Consequently, a decision was made to pursue a synthesis method that allowed for greater influence of PPy, thereby optimizing its electrical and mechanical properties. The choice to perform the polymerization of PPy directly on the surface of PCL fibers, as detailed in the subsequent chapter, was motivated by the prospect of significantly improving the interface between PPy and PCL, and consequently, the overall properties of the scaffold.

4.4 Acknowledgments

We would like to thank to the Electrospinning and Electrospray lab in the school of medicine of the Universidad Nacional de Colombia, to the Lower Saxony Center for Biomedical Engineering, Implant Research and Development, Hannover, Germany, and the Institute for Multiphase Processes, Leibniz University Hannover, Garbsen, Germany, for their support, especially in the additional

experiments. Special gratitude is owed to the German Academic Exchange Service (DAAD), which provided financing for the research stay in Germany.

5. From Concept to Application: Optimizing PPy-PCL Scaffolds for Tissue Engineering

The results presented in this chapter are part of a summited publication in WYLEY Editorial.

Authors: Ana M. Muñoz-González [1*], Dianney Clavijo-Grimaldo [2,3], Sara Leal-Marin [5,6], Birgit Glasmacher [5,6]

1 Faculty of Engineering, Universidad Nacional de Colombia; Bogotá, Colombia.
2 School of Medicine, Universidad Nacional de Colombia; Bogotá, Colombia.
3 Faculty of Medicine, Grupo INPAC. Fundación Universitaria Sanitas; Bogotá, Colombia
4 Institute for Multiphase Processes, Leibniz University Hannover, Garbsen, Germany
5 Lower Saxony Center for Biomedical Engineering, Implant Research and Development, Hannover, Germany

Submitted in **Journal of Biomedical Materials Research: Part B - Applied Biomaterials,** may 2024.

Statement of contribution of co-authors for thesis by published papers:

Contributors	Statement of contribution
Ana M Muñoz-Gonzalez	Designed and perform the experiments Analyzed and interpreted results Conceived and wrote the manuscript Development of research results
Dianney Clavijo-Grimaldo	Involved in the conception of the project Designed the experiments. Assisted with characterization test Provided feedback in the whole process
Sara Leal-Marin	Designed and perform the experiments Assisted with characterization test
Birgit Glasmacher	Funding and provide equipment, laboratories and materials. Provided feedback in the whole process

5.1 Abstract

Incorporating electrically conductive materials has emerged as an enticing new frontier in the ongoing search for effective tissue regeneration. This research focused on creating electroconductive scaffolds with PPy-PCL (polypyrrole-polycaprolactone) through the application of optimal process parameters. The development in-volved *in situ* chemical polymerization of PPy, employing Box-Behnken response surface methodology (RSM). The optimal conductivity obtained was 2,542 mS/cm. The parameters studied were monomer concentration, oxidant concentration, and polymerization time. Scanning electron microscopy (SEM) revealed a uniform morphology with globular PPy particles arranged in a dendrimer-like fashion in the PCL fibers. In addition, Fourier Transform Infrared (FTIR) and Energy Dispersive X-ray spectroscopy (EDX) analysis con-firmed the presence of PPy and PCL on the scaffolds. Mechanical evaluation showed higher tensile strength and Young's modulus in the optimized scaffolds compared to pure PCL fibers. The optimized hydrophilicity of the scaffolds was improved considerably, transitioning from initially hydrophobic to fully hydrophilic for the optimum scaffold, making it suitable for TE applications. The MTT assay performed on L929 fibroblasts showed adequate cell viability with no adverse effects of the optimized PPy-PCL scaffold. Furthermore, evaluation of bone marrow mesenchymal stem cells (bmMSCs) on the scaffold with Alamar Blue assay showed a considerable increase in metabolic activity over 7 days, indicating increased cell viability and potential for supporting cellular functions in TE applications. In conclusion, the *in situ* synthesis of PPy in the PCL matrix by optimizing the fabrication parameters resulted in conductive scaffolds with promising structural and functional properties for TE.

Keywords: scaffolds, electrically conductive, polypyrrole, electrospinning.

5.2 Introduction

The increasing life expectancy and the prevalence of degenerative and chronic diseases have heightened the need for organ and/or tissue replacement strategies. Given the limited availability of donors and the morbidity and mortality associated with transplants, TE has emerged as a promising field. TE comprises three components: cells, scaffolds, and chemical environment. The role of scaffolds is to mimic the extracellular matrix, a multifaceted material with nano/microstructure that is essential for maintaining tissue viability, morphology, regeneration, and functional characteristics (Clavijo-Grimaldo et al., 2022). The growing global demand for functional tissue substitutes has led to outstanding advances in the field of TE. The global market for scaffold technology was estimated

at US$ 1.14 billion in 2021 and is projected to reach approximately US$ 2.63 billion by 2030 (Research, 2022).

The demand for electroconductive scaffolds and the search for more efficient production methods has increased recently. In TE, electroconductive scaffolds could facilitate electrochemical communication between cells as electrical stimulation activates signaling pathways. Besides electrical conductivity, cell migration, proliferation, and differentiation are also affected (C. Chen et al., 2019; Saberi et al., 2019). Some processes to develop electroconductive scaffolds include solvent casting, thermic separation phase, freeze drying, 3D printing, vapor phase polymerization, *in situ* polymerization, and electrospinning (Asri et al., 2022; Mutepfa et al., 2022).

Myocardial regeneration is one of TE's most important applications for electroconductive scaffolds. According to the World Health Organization (WHO), CVD is the leading cause of death worldwide, accounting for approximately 32% of all deaths. During a heart attack, one to two million cardiomyocytes (CMs) are lost. CM's death disrupts the myocardium's electrical conductivity, as the injured tissue is replaced by hard, electrically inactive, and non-contractile scar tissue due to the limited regenerative capacity of the myocardium (Fleischer et al., 2017). The electrical conduction system of the heart may be altered due to the size and location of the infarct, which can lead to ventricular fibrillation and sudden death. In this context, conductive scaffolds could promote the expression of cardiac markers and allow stem cells to differentiate into CM (Ye & Qiu, 2017). Conductive scaffolds foster CM regeneration and facilitate proper propagation of electrical activity, promoting electromechanical coupling and reducing the likelihood of arrhythmias and other complications (Kharaziha et al., 2014).

Many other human cells are electrically active, which shows the multiple scenarios in which conductive scaffolds are functional in TE. For example, these scaffolds support nerve cell growth and regeneration and restore injured or damaged neuronal connections. This makes conductive scaffolds applicable in addressing spinal cord injury (SCI), a severe and debilitating condition for which there is no permanent cure for the complete recovery of neurological function (Mutepfa et al., 2022; Zhao et al., 2023). Since electroconductive scaffolds modulate bone cell activity and improve mechanical properties, they have also been used to restore bone tissue and treat degenerative bone diseases, as they are essential for maintaining a favorable bioelectric microenvironment that could promote osteogenesis in certain pathological conditions (Heng et al., 2023; Nekounam et al., 2021; Saberi et al., 2019).

Polymers are the most commonly used biomaterials for scaffold fabrication in TE. Conjugated electrons or alternating bonds are often found in the chemical structure of conductive polymers. Polypyrrole (PPy) is a conjugated polymer because the secondary bond in its main chain alternates

between carbon atoms. This type of bond allows it to contain some delocalized electrons that can move freely along the polymer chain, resulting in a cloud of charged electrons that spreads across the entire substance. In addition to electrical conductivity, other advantages of PPy include its organized structure (which optimizes the flow of electrical charge and allows localized electron movement), ease of synthesis, chemical stability, and biocompatibility (Pang et al., 2021). However, the shape and brittleness of PPy scaffolds can pose challenges that limit their suitability for specific applications in TE (Balint et al., 2014; Mao & Zhang, 2018; Namsheer & Rout, 2021; Pang et al., 2021).

For instance, PPy is difficult to process once synthesized, and fabricating a conductive scaffold from pure PPy is also challenging (C. Chen et al., 2019), so its combination with other biocompatible polymers is common. Due to its low glass transition, compatibility with other materials, and numerous applications in TE, polycaprolactone (PCL), a biodegradable polyester, exhibits good strength and flexibility, properties that compensate for the disadvantages of PPy scaffolds (Deshmukh et al., 2017; Reshmy et al., 2021). For example, Shafei et al. fabricated scaffolds made of electrospun PCL nanofibers, then, vapor phase polymerization of the pyrrole occurred by electrospraying the oxidant on the PCL fibers at different times (0, 1, 2, 3, and 4 hours). The PPy-PCL membranes were reported to have a higher electrical conductivity (1.9 S/cm) than the results obtained by other authors. Moreover, Young's modulus for the aligned fibers was 11.6 MPa. In an *in vitro* assay, L929 fibroblast cells showed viability and PC12 cell differentiation, which improved the results for the PPy-PCL membranes (Shafei, Foroughi, Stevens, et al., 2017).

Khatti et al. fabricated PCL-Gelatin nanofiber scaffolds with different ratios and fiber orientations made by electrospinning followed by a polymerization coating. Nanofiber diameters were 162 to 207 nm, and scaffolds have a high conductivity in the range of 4.6–5.8 S/cm. Reaction time and oxidant concentration affected surface porosity, and monomer concentration deeply influenced coating thickness(Khatti et al., 2019). Sudwilai et al. fabricated aligned and random PLA nanofibrous scaffolds with and without PPy, demonstrating that aligned fibers showed better properties than random fibers (Sudwilai et al., 2014). Lee et al. also fabricated conductive PPy-PLGA meshes with aligned and random nanofibers. The results showed good cellular compatibility interactions and stimulation of PC12 cells and embryonic hippocampal neurons (J. Y. Lee et al., 2009). For their part, Fakhrali et al. developed an ideal scaffold made of nanofibers of poly (glycerol sebacate)/poly (caprolactone)/poly (pyrrole) (PPy), which was then polymerized after analyzing the effects of variables such as monomer concentration and polymerization time. The following scaffold was developed and evaluated for use in applications as heart patches (Fakhrali et al., 2022).

This research aims to optimize the fabrication parameters of PPy-PCL scaffolds using a Design of Experiments (DoE) approach to determine the ideal conditions that maximize electrical conductivity and improve scaffold morphology. DoE is a statistical tool used to evaluate the effect of many variables on a process. Box-Behnken designs are a response surface methodology (RSM) used in DoE to develop a robust model for predicting a higher-order response using fewer runs than a factorial DoE, making it a cost-effective strategy. Electrospinning was used to fabricate nanofiber scaffolds of PCL. The produced PCL fibers were then subjected to *in situ* chemical synthesis of PPy, and the synthesis conditions were then tuned to obtain the optimal characteristics and properties for the chosen scaffold. The morphology, chemical composition, and hydrophilicity of the obtained scaffolds were investigated using scanning electron microscopy (SEM), energy dispersive X-ray spectroscopy (EDX), Fourier Transform Infrared (ATR-FTIR) spectroscopy, and contact angle. Electrical conductivity was measured using a four-point probe device. Finally, mechanical properties were measured by tensile test, and the scaffold's cell adhesion, proliferation, and possible cytotoxic effects on the Fibroblast L929 and bone marrow mesenchymal stem cells (bmMSCs) were investigated.

This study offers a novel approach to TE by optimizing the synthesis of electroconductive PPy-PCL scaffolds using a Box-Behnken design, resulting in a unique combination of enhanced electrical conductivity, superior mechanical properties, and improved hydrophilicity, demonstrating substantial prospects for advanced cellular support and tissue regeneration.

5.3 Materials and Methods

5.3.1 Materials

Polycaprolactone (PCL) (Sigma-Aldrich, CAS # 134490-19-0 MW=80000 Da), isopropyl alcohol (Sigma Aldrich, 99,7 % CAS # 67-66-3), chloroform (Sigma Aldrich, 99,5 %, CAS # 67-66-3) are used for the fabrication of the nanofibers. Pyrrole (Py) (Merck, 98%, CAS # 109-97-7) is used as a monomer, and synthesis-grade anhydrous iron (III) chloride (FeCl3) (Merck, CAS # 7705-08-0) is used as an oxidant for the PPy synthesis. Py and FeCl3 solutions were prepared using distilled water.

5.3.2 Nanofibers fabrication

For the manufacture of PCL nanofibers, a 9% (w/v) PCL solution was used in a 50:50 (v/v) chloroform and isopropanol solution, which was stored at room temperature for 48 hours (Clavijo-Grimaldo et al., 2022).

The PCL nanofiber scaffold was fabricated using a vertical electrospinning device consisting of a high voltage source (CZE1000R, Spellman, USA), a dosing pump (KDS100, USA) with a 5 mL syringe with a needle (gauge 18), and a rotary collector (ESD30s, Nanolab Instruments Sdn. Bhd, Malaysia) at 2000 rpm wrapped with aluminum foil and. The most important electrospinning parameters to fabricate the electrospun nanofibers were the distance between the needle and the rotatory collector, the applied voltage, and the solution feed rate maintained to obtain uniform and bead-free fibers. Therefore, PCL deposition was performed for 90 min at 17 cm, 14 kV, and 1.0 ml/h. The process was conducted at 20 °C room temperature and 50% relative humidity.

5.3.3 PPy-PCL scaffold obtention

PCL nanofiber scaffold served as a template to obtain the PPy-PCL scaffolds. Initially, PCL nanofibers were immersed in the Py solution. Due to the hydrophilicity of PCL, fibers are carefully immersed and wet to ensure that the PCL fibers were completely soaked. Subsequently, the selected oxidant, iron chloride ($FeCl_3$), was gradually introduced to initiate the *in situ* chemical oxidative PPy polymerization, as depicted in *Figure 5 - 1*. The synthesis of PPy-PCL scaffolds occurred within a temperature range of 2 to 4 °C. The polymerization reaction occurs inside a freezer to control the temperature, which it is vital to moderate the exothermic reaction and enhance the reaction yield (Song et al., 2016).

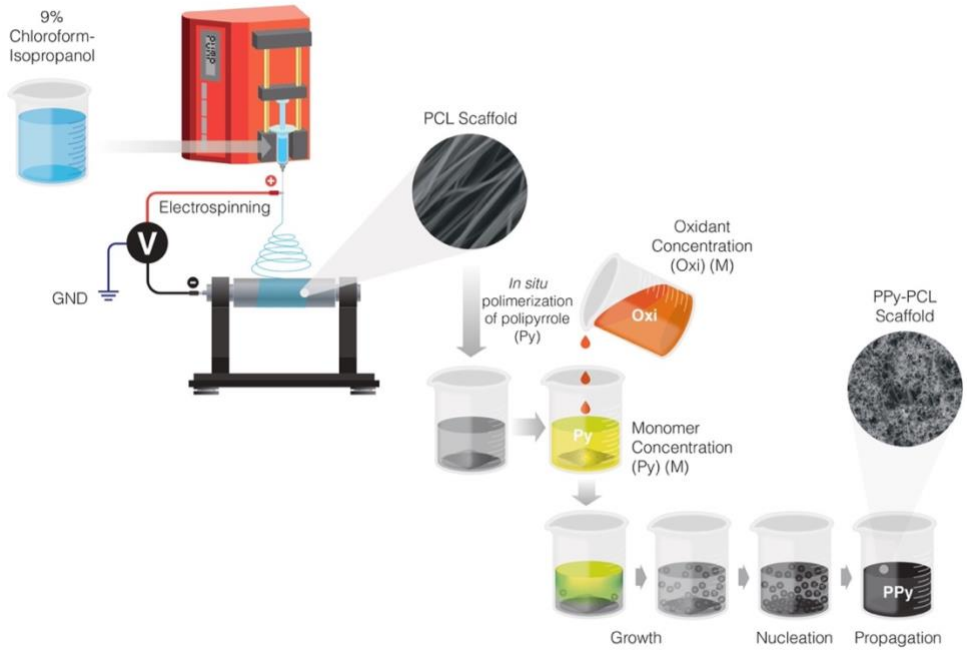

Figure 5 - 1 PPy-PCL scaffolds obtention process (author).

Box-Behnken response surface design was used to study the effects of PPy on the polymeric nanofiber scaffold properties. *Table 5 - 1* shows the variables and parameters of the response surface experimental design used to fabricate PPy-PCL scaffolds. Each factor delineated in *Table 5 - 1* was explored across three levels: low, medium, and high, based on insights from the existing literature. As previously mentioned, three process parameters were considered during the fabrication of PPy-PCL scaffolds: the molar concentration of the Py solution (Py) prepared at 0.1, 0.2, and 0.3 M; the molar concentration of the oxidant (Oxi) designed at varying concentrations (0.15, 0.45, and 0.75 M) in distilled water; and the polymerization time (Time) set at 30, 165, and 300 minutes. The experimental runs according to 33 Box-Behnken design are shown in *Table 5 - 2*.

Table 5 - 1 Process parameters and levels.

Factors	**Levels**		
	Low	Medium	High
Pyrrole concentration (M)	0.1	0.2	0.3
Oxidant concentration (M)	0.15	0.45	0.75
Polymerization time (min)	30	165	300

.

Table 5 - 2 Experimental runs for Box-Behnken DoE.

Run	**[Py] (M)**	**[Oxi] (M)**	**Time (min)**
PPy1	0.3	0.45	30
PPy2	0.2	0.15	30
PPy3	0.2	0.75	30
PPy4	0.1	0.45	30
PPy5	0.1	0.45	300
PPy6	0.2	0.75	300
PPy7	0.2	0.15	300
PPy8	0.3	0.45	300
PPy9	0.3	0.15	165
PPy10	0.1	0.75	165
PPy11	0.1	0.15	165
PPy12	0.2	0.45	165
PPy13	0.2	0.45	165
PPy14	0.3	0.75	165
PPy15	0.2	0.45	165

5.3.4 Characterization of the fabricated scaffolds.

Conductivity/resistivity measurement

Electrical conductivity was measured using the four-point probe, a conventional test for measuring thin films, conductive coatings, and semiconductor materials (Waremra & Betaubun, 2018). The technique uses four equally spaced and colinear probes in contact with the material. Current and voltage sensing are separated, with a constant current applied through the two external probes, while voltage is measured between two internal probes.

In the case of the obtained samples, which are thin membranes, these are 40% smaller than probe separation. With a sufficiently large size, it becomes feasible to calculate the sheet resistance using the following equation:

$$R_s = \left(\frac{\pi}{\ln(2)}\right)\left(\frac{V}{I}\right) = 4.53236\ \left(\frac{V}{I}\right) \quad (1)$$

Rs is the sheet resistance, V is the voltage measured between the inner probes, and I is the current applied between the outer probes. If the thickness of the measured material is known, the strength of the sheet can be used to calculate its resistivity:

$$\rho = R_S * t, \quad (2)$$

where ρ is the resistivity, and t is the thickness of the material.

As the conductivity (σ) can be calculated employing resistivity, since it is defined as the inverse of the value of the resistivity (ρ), thus,

$$\sigma = \frac{1}{\rho} \quad (3)$$

Therefore, conductivity is determined in $m\Omega^{-1}$ cm^{-1} or mS/cm (S is Siemens, where 1 S = 1 Ω^{-1}). Sheet resistance measurements were performed using a four-probe resistance meter (HPS2523, Beijing Jiahang Bochuang Technology Co., Beijing, China).

The scaffold thickness was measured with a Mitutoyo micrometer with a precision of 0.1 µm. Five measurements of each sample were taken, and the average result was obtained.

Scanning Electron Microscope (SEM)

Scanning electron microscopy (SEM) (Tescan Vega 3 SB) at an accelerating voltage of 15 kV under 1000X and 5000X was used to study the morphology, structure, and porosity of the PCL and PPy-PCL scaffolds. Based on the SEM images, fiber diameter distribution was determined using Image

J software. All measurements were subjected to statistical analysis to calculate the mean diameter and standard deviation.

Electronic dispersive X-ray spectroscopy (EDX) with detectors for EDS analysis in SEM was employed to analyze elemental composition of the samples.

Optimum scaffold porosity

The porosity of the PPy-PCL scaffolds was estimated using a weighting technique through the following equation:

$$\%P = \frac{d_B - d_A}{d_B} * 100 \quad (4)$$

The dB was determined by dividing the difference between the PPy-PCL and PCL by the percentage of each component. According to the provider, the PCL density is 1.145 g/cm3, and the PPy density is 1.5 g/cm3. The apparent density, denoted by the symbol dA, is computed using the following equation:

$$d_A = \frac{mass\ of\ PPy\ PCL\ scaffolds\ (g)}{scaffold\ thickness\ (cm) * scaffold\ area\ (cm^2)} \quad (5)$$

For each sample, three measures of porosity were taken.

Fourier Transform Infrared (ATR-FTIR) spectroscopy.

In order to confirm that the monomer was polymerized during the synthesis process and that the produced polypyrrole conductive polymer contained functional groups, FTIR investigations were conducted. A Shimadzu® FT-IR solution spectrometer with an Attenuated Total Reflectance (ATR) module and a germanium crystal was used to produce the FTIR spectra. At ambient temperature settings, FTIR spectra were recorded in the transmission mode in the 4000 - 500 cm^{-1} range and analyzed using IR Solutions software.

Mechanical properties

Tensile testing (Shimadzu UH-I) with a load capacity of 50 N at 50 mm/min was used to determine the mechanical properties of the multilayer scaffold. The procedure and specimens were prepared in rectangular-shaped sections with a length of 120 mm and a width of 10 mm following ASTM D882. Five specimens were tested to obtain the average results.

Wettability evaluation

Surface hydrophilicity was evaluated by sessile drop water contact angle measurement using 10 µl deionized water droplets. The drop test was repeated for three randomly selected points on each

sample. Sample measurements were taken with the contact angle plug-in of ImageJ, which calculates the angle of a drop on a flat surface using the sphere approximation and the ellipse approximation (Brugnara et al., 2006). Results are reported as the mean and standard deviation of these points.

Cytotoxicity Assessment

To assess the cytotoxicity of the optimized PPy-PCL scaffold, an MTT assay was conducted in accordance with ISO 10993-5 guidelines using L929 fibroblast cells. Initially, the scaffolds were cut into pieces with a diameter of 1 cm. These pieces were then incubated for 24 hours, after which the supernatant was collected for cellular testing. Subsequently, 1 x 105 cells in 100 µL of medium were seeded into each well of a 96-well plate containing Dulbecco's Modified Eagle's Medium (DMEM) supplemented with fetal bovine serum (FBS). The plate was incubated at 37°C in a 5% CO2 atmosphere for 24 hours.

After 24 hours, the medium was removed, and the wells were washed with PBS twice. Subsequently, 100 µL of serum-free DMEM were added to each well. Additionally, 10 µL of MTT solution was added, and the plate was incubated for 4 hours. After the 4-hour incubation period, the MTT solution was aspirated, and 100 µl of dimethyl sulfoxide (DMSO) was added to each well. The optical density (OD) was measured at 560 nm and normalized to the control OD (TRIAD Multimode Microplate Reader). The MTT assay was repeated three times for each sample, and the average measurements were reported. Sterile DMEM supplemented with 25% DMSO and DMEM incubated with 0.2 g/mL silicone were used as positive and negative controls, respectively.

Cellular Metabolic Activity

Cell cytotoxicity was also evaluated by measuring metabolic activity using Alamar Blue assay with human bone marrow mesenchymal stem cells (bmMSCs) seeded onto both PCL and optimum scaffolds over a 3- and 7-day period. For the testing procedure, scaffolds of PCL fibers and the optimal scaffold of PPy-PCL were seeded, but the optimum scaffold was seeded on both sides. The side with the highest concentration of polymerized PPy was termed Optimum PPy-PCL (UP), while the opposite side was called Optimum PPy-PCL (DOWN).

Cells were seeded onto circular 1.2 cm^2 scaffolds at 60,000 cells per cm^2 density. PCL scaffolds without PPy served as control. The seeded scaffolds were cultivated in 24 well plates in supplemented growth medium made of Dulbecco’s modified Eagle’s medium (DMEM) (Bio&Sell, Germany) with 2.3 % (v/v) glutamine, 2.3% (v/v) HEPES, 0.002 % (v/v) FGF-2, 11.6 % (v/v) fetal

bovine serum (Bio&Sell, Germany), and 1.2 % (v/v) Penicillin/Streptomycin; medium was replaced every 3 days and kept in an incubator at 37°C and 5% CO_2 with 95% relative humidity.

On days 3 and 7, the metabolic activity of bmMSCs on the scaffolds was assessed using the Alamar Blue assay (also known as the Resazurin assay). Alamar Blue, a water-soluble and stable indicator dye, changes color and fluorescence in response to cell growth due to chemical reduction in the growth medium (O'Brien et al., 2000). This assay is non-toxic, permeable through cell membranes, and advantageous over other methods for measuring cell viability and proliferation, including being robust, simple, and cost-effective (Longhin et al., 2022).

After preparation of the solution at 10% (v/v) resazurin in the prewarmed medium, 750 µL was added to each scaffold. Following a 2-hour incubation at 37°C, 100 µL of the reduced resazurin was transferred to 96-well plate for fluorescence measurements at an excitation wavelength of 570 nm and an emission wavelength of 600 nm using an Infinite M200PRO plate reader from Tecan. Readings were recorded on days 3 and 7.

The morphology of the adherent cells was visualized using Scanning electron microscopy (SEM). The scaffolds were washed with sodium cacodylate (CAC) 0.1 M for the SEM preparation and underwent fixation using a 3% glutaraldehyde solution. Afterward, they were rinsed twice with CAC and miliQ water and dehydrated through graded ethanol concentrations (25%, 35%, 50%, 70%, 80%, 90%, and 100%). After dehydration, the scaffolds were dried. Scaffolds were then gold-coated for imaging purposes, and SEM images (S3400N, Hitachi, Japan) were taken at an accelerating voltage of 20 kV. A working distance of 10 mm was also used to study the morphology.

5.4 Results

The outcomes of the process variable optimization that improved the electrical conductivity of the scaffolds developed through the DoE are presented in this section. After this, the examination of the optimum scaffold's morphological, chemical, mechanical, and biocompatibility characteristics is provided.

5.4.1 Morphology and structure of PCL fibers

Polymeric nanofibers play a significant role in TE and offer several advantages. A fibrous polymeric matrix exhibits a unique structure resembling the ECM and directs cell development. Additionally, it acts as an essential support system for cells, enabling correct alignment in the optimal direction and encouraging subsequent tissue signaling. As a result, numerous tests were required for this investigation to generate homogeneous, smooth, and defect-free PCL fibers (PCLf).

Figure 5 - 2 illustrates the aligned PCL fibers' morphology, average, and diameter distribution. The average diameter is 1114.68 ± 351.74 nm. This in-depth distribution insight highlights the fibers' broad diametric spectrum, their polydispersity, and the range where most fibers fall.

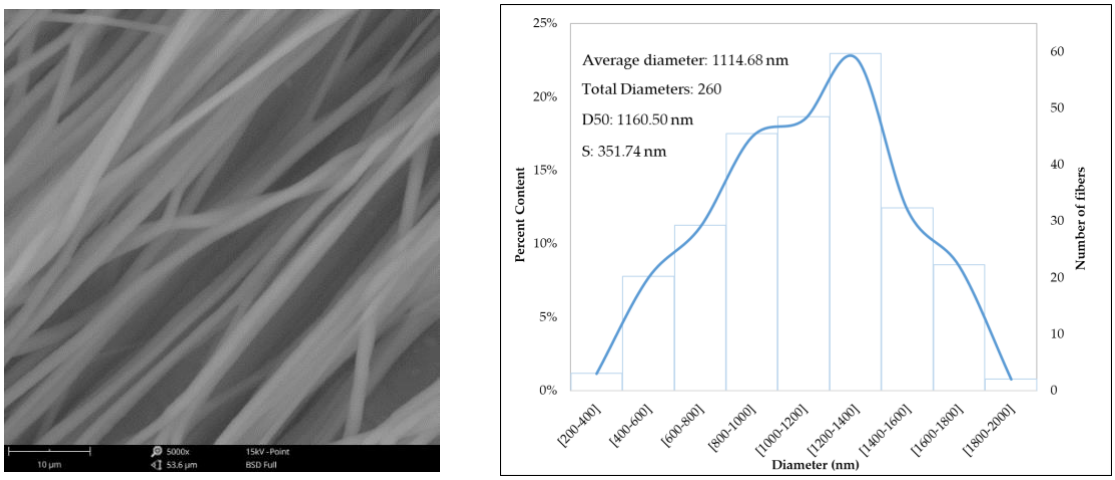

(a) **(b)**

Figure 5 - 2 (a) SEM image of pure PCL fibers, (b) fiber diameter distribution.

5.4.2 Polymerization Process Parameter Optimization for Enhanced Conductivity

After the fabrication of PPy-PCL scaffolds through *in situ* PPy polymerization using the experimental design detailed in *Table 5 - 2*, each scaffold's conductivity measurement was conducted. The measured values are presented in *Table 5 - 3*. Notably, within these results, it is evident that the conductivity of the scaffold produced using the parameters for PPy2 is insufficient. However, scaffolds PPy14 and PPy8 exhibit the highest conductivity levels.

An ANOVA analysis was performed to analyze the factors exerting more influence on higher electric conductivity levels, and the results are presented in *Table 5 - 3*. The p-value and F-value derived from the ANOVA results indicate the significance of the model. Additionally, the values of S and R^2 (0.44 and 81.71%, respectively) confirm the model's accuracy in predicting the experimental data.

Moreover, based on the ANOVA results in the *Figure 5 - 3* depicts the RSM results and the contour plot of the PPy-PCL scaffolds fabrication. *Figure 5 - 3*a illustrates the interaction between Py and Time. This graph indicated that an increase in polymerization time by more than 187 minutes, coupled with high concentrations of Py (greater than 0.28 M), leads to a higher conductivity. Similarly, *Figure 5 - 3*b shows that as the polymerization time increases, so does the conductivity value, with

better results from 130 min. However, with a prolonged increase in time, conductivity decreases again.

Equivalently, *Figure 5 - 3*c confirms that the higher values of Py (more than 0.26 M) and Oxi (greater than 0.49 M) increase scaffold conductivity.

In order to optimize the variables of the process through RSM, the coefficients of the model were determined, and the mathematical equation of the relationship between conductivity and manufacturing factors is described next:

*Conductivity = 1,056 - 18,79 Py + 4,90 Oxi + 0,00875 Time + 19,4 Py*Py - 4,81 Oxi*Oxi - 0,000041 Time*Time + 12,26 Py*Oxi + 0,05093 Py*Time - 0,00702 Oxi*Time*

Using the model solution, the optimal process values to maximize conductivity were calculated as Py = 0.3 M, Oxi = 0.73 M and Time = 232 min. These values resulted in an adjusted conductivity value for this solution, which is 3.050 mS/cm (desirability = 0.84).

Table 5 - 4, it is apparent that the most influential parameters are oxidant concentration (Oxi), polymerization time (Time*Time) interaction, and the interaction between monomer concentration and polymerization time (Py*Time). On the other hand, the interaction of monomer concentration (Py*Py) is not significant.

Table 5 - 3 Mean conductivity and thickness data for samples.

Scaffold	**Conductivity (mS/cm)**	**Scaffold thickness (mm)**
PPy1	0.365±0.012	0.013±0.003
PPy2	0.000±0.000	0.004±0.002
PPy3	0.944±0.086	0.004±0.005
PPy4	1.589±0.069	0.005±0.004
PPy5	0.956±0.099	0.016±0.005
PPy6	0.876±0.010	0.015±0.010
PPy7	1.069±0.050	0.007±0.001
PPy8	2.482±0.215	0.022±0.006
PPy9	0.861±0.007	0.013±0.003
PPy10	1.723±0.131	0.016±0.002
PPy11	0.596±0.011	0.013±0.001
PPy12	1.390±0.069	0.014±0.004

PPy13	1.882±0.155	0.020±0.002
PPy14	3.460±0.146	0.023±0.004
PPy15	2.425±0.144	0.019±0.005

Figure 5 - 3 depicts the RSM results and the contour plot of the PPy-PCL scaffolds fabrication. *Figure 5 - 3*a illustrates the interaction between Py and Time. This graph indicated that an increase in polymerization time by more than 187 minutes, coupled with high concentrations of Py (greater than 0.28 M), leads to a higher conductivity. Similarly, *Figure 5 - 3*b shows that as the polymerization time increases, so does the conductivity value, with better results from 130 min. However, with a prolonged increase in time, conductivity decreases again.

Equivalently, *Figure 5 - 3*c confirms that the higher values of Py (more than 0.26 M) and Oxi (greater than 0.49 M) increase scaffold conductivity.

In order to optimize the variables of the process through RSM, the coefficients of the model were determined, and the mathematical equation of the relationship between conductivity and manufacturing factors is described next:

*Conductivity = 1,056 - 18,79 Py + 4,90 Oxi + 0,00875 Time + 19,4 Py*Py - 4,81 Oxi*Oxi - 0,000041 Time*Time + 12,26 Py*Oxi + 0,05093 Py*Time - 0,00702 Oxi*Time*

Using the model solution, the optimal process values to maximize conductivity were calculated as Py = 0.3 M, Oxi = 0.73 M and Time = 232 min. These values resulted in an adjusted conductivity value for this solution, which is 3.050 mS/cm (desirability = 0.84).

Table 5 - 4 ANOVA table for response surface model for conductivity of PPy-PCL scaffolds.

Source	**df**	**Sum of square**	**Mean square**	**F-value**	**p-value**	
Model	11	28.66	2.61	13.41	3.25E-09	
Blocks	2	0.00	0.00	0.00	9.98E-01	
Lineal	3	11.82	3.94	20.27	1.25E-07	
Py	1	1.99	1.99	10.25	3.02E-03	
Oxi	1	7.51	7.51	38.66	5.09E-07	Significant
Time	1	2.32	2.32	11.92	1.54E-03	
Square	3	8.57	2.86	14.70	3.00E-06	
Py*Py	1	0.42	0.42	2.14	1.53E-01	
Oxi*Oxi	1	2.07	2.07	10.66	2.55E-03	
Time*Time	1	6.14	6.14	31.59	2.95E-06	

2-factor interaction	3	8.27	2.75	14.18	4.19E-06	
Py*Oxi	1	1.62	1.62	8.35	6.76E-03	
Py*Time	1	5.67	5.67	29.19	5.62E-06	
Oxi*Time	1	0.97	0.97	4.99	3.24E-02	
Error	33	6.41	0.19			
Lack of adjustment	27	4.72	0.17	0.62	8.19E-01	No significant
Pure error	6	1.69	0.28			
Total	44	35.07				

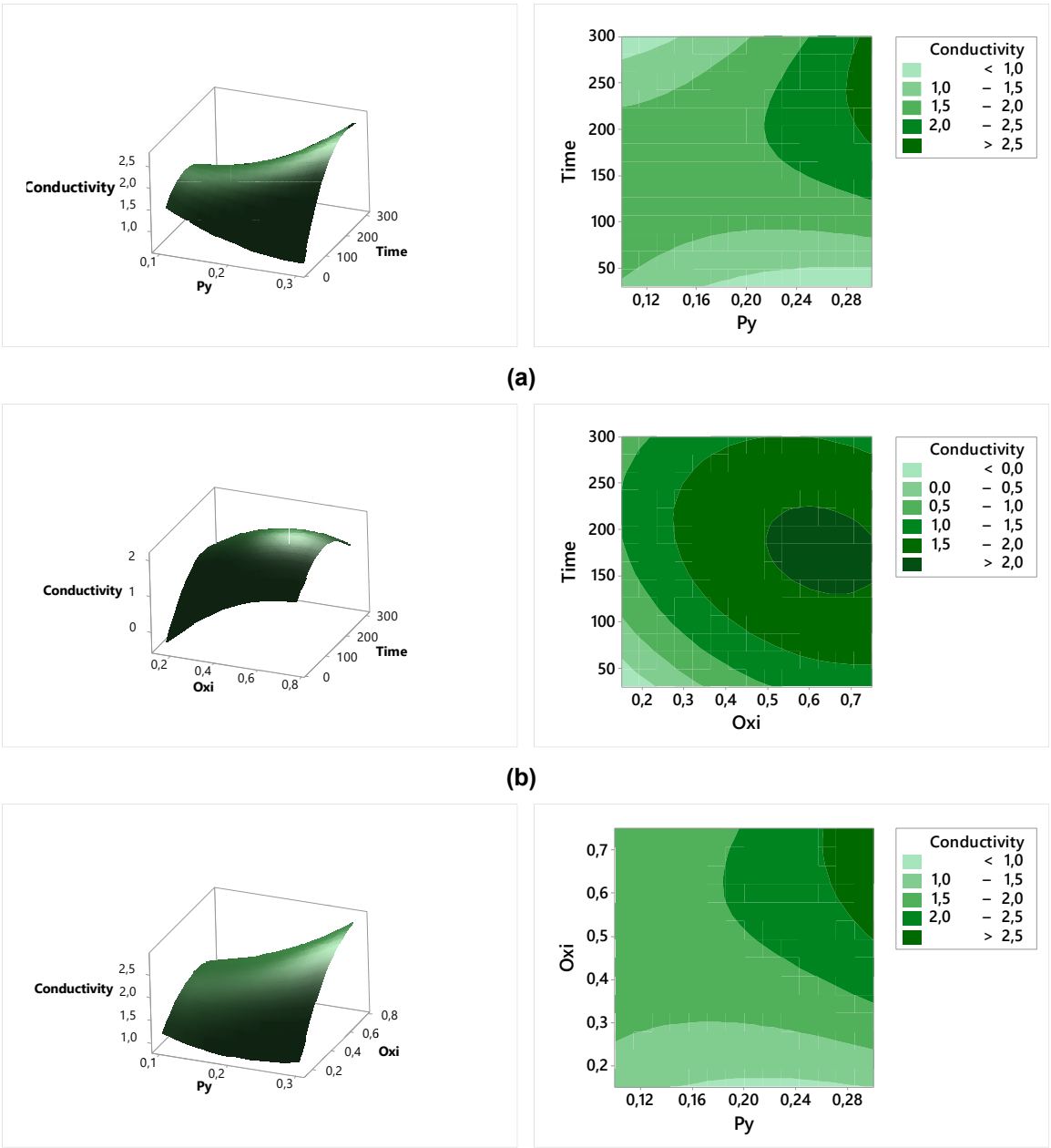

Figure 5 - 3 (a) Response surface and contour plot on the conductivity effect of monomer (PY) and polymerization time (TIME). (b) Response surface and contour plot on the conductivity effect of oxidant concentration (OXI) and polymerization time (TIME). (c) Response surface and contour plot on the conductivity, effect of monomer (PY) and oxidant concentration (OXI).

Subsequently, three new samples were manufactured under these optimized conditions. To measure conductivity, at least ten resistivity values were taken for each sample, and the average conductivity measurement obtained was 2.542 ± 0.139 mS/cm, differing 16.6% from the theoretical

value. Nevertheless, this achieved value surpasses most values obtained in the analysis devices, as indicated in *Table 5 - 3*.

5.4.3 Morphology and structure of PPy-PCL scaffolds

Following the *in situ* polymerization process detailed in *Table 5 - 3* across fifteen runs, the morphology of these scaffolds was examined using SEM. Initially, *Figure 5 - 4*a to d illustrate PPy-PCL scaffolds fabricated under varying monomer and oxidant concentrations but with a consistent and shorter PPy polymerization time (30 minutes), as outlined in *Table 5 - 1*. This accounts for the comparatively lower PPy content within the PCL fibers.

Moving on to *Figure 5 - 4*e to *Figure 5 - 4*h, these images display PPy-PCL scaffolds produced with different monomer and oxidant concentrations employing an extended polymerization time (300 minutes). In the case of PPy5, using 0.1 M monomer and 0.45 M oxidant, a more pronounced presence of PPy is evident within the fibrous structure compared to samples PPy1 through PPy4. Here, the distribution of PPy along the PCL fibers and within the fibrous matrix becomes apparent. Notably, the particle structure of the conductive polymer and its interaction with the PCL fibers are more effectively characterized, illustrating a tendency for the polymer to aggregate and coil around the PCL fibers.

For the PPy6 experiment in *Figure 5 - 4*f, which was conducted using 0.2 M monomer and 0.75 M oxidant and 300 min of polymerization, a greater amount of PPy was placed on the surface of the fibrous matrix of PCL, covering it almost completely and more uniformly.

*Figure 5 - 4*g shows the PPy7 experiment, which was prepared using a monomer concentration of 0.2 M and an oxidant concentration of 0.15 M. In this instance, there is a distribution and interaction between the two polymers and optically less PPy than in the PPy6 sample.

At this point, it becomes evident that, at the same polymerization time, variations in monomer and oxidant concentrations significantly impact the morphology and visual attributes of the PPy-PCL scaffold. Notably, a higher oxidant concentration yields a superior distribution and quantity of the conductive polymer within the fibrous matrix. This observation of the role of oxidant concentration in enhancing the dispersion and presence of the conductive polymer throughout the scaffold.

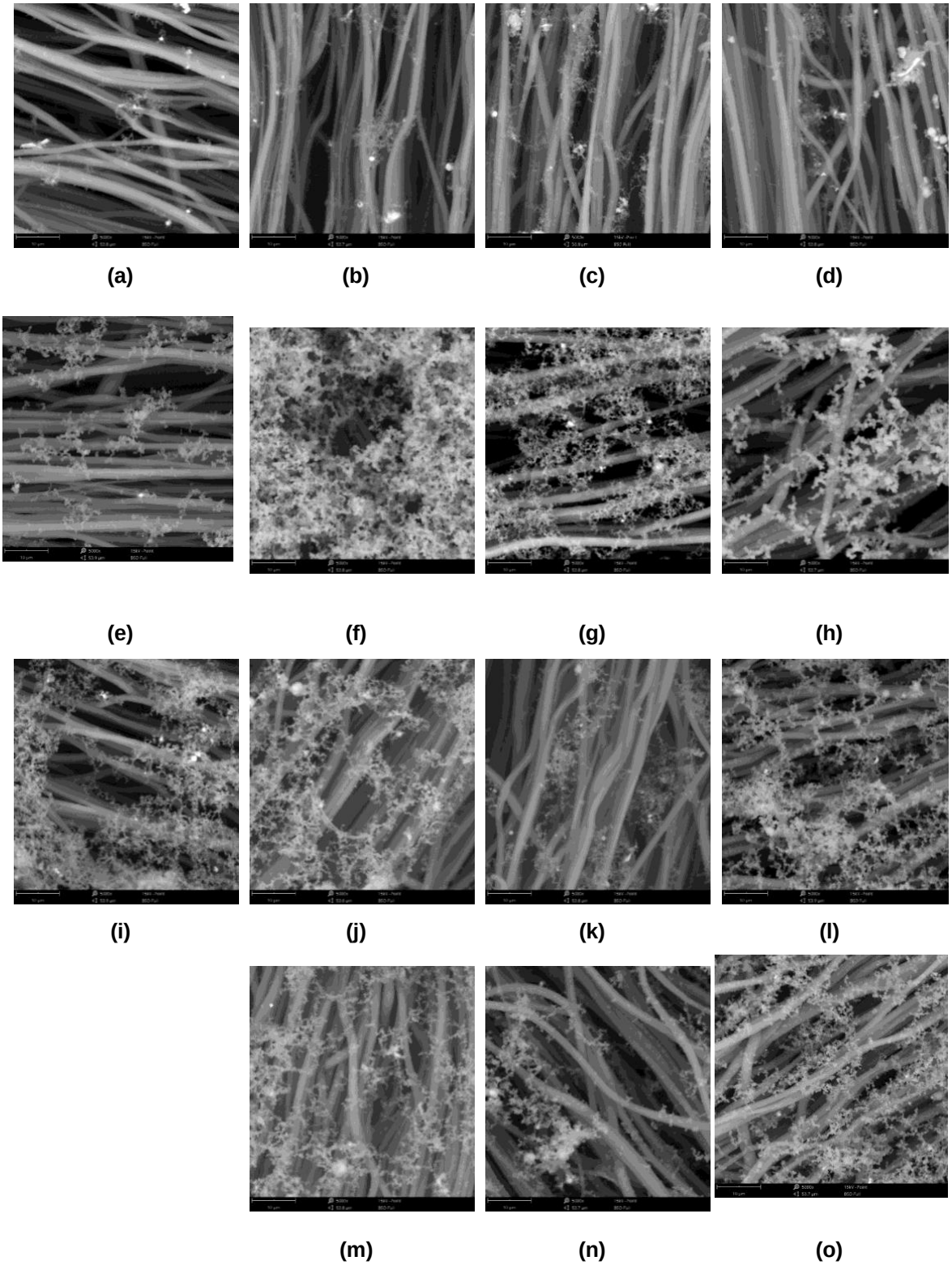

Figure 5 - 4 SEM images of PPy-PCL scaffolds (a) PPy1, (b) PPy2, (c) PPy3, (d) PPy4, (e) PPy5, (f) PPy6, (g) PPy7, (h) PPy8, (i) PPy9, (j) PPy10, (k) PPy11, (l) PPy12, (m) PPy13, (n) PPy14, (o) PPy15.Scale bar: 10µm.

*Figure 5 - 4*h depicts the final experiment PPy8, conducted at 300 minutes. In this case, the distribution and appearance of the conductive polymer closely resemble those of the sample PPy5, with shared oxidant content and polymerization time.

In *Figure 5 - 4*i, the conductive polymer is not distributed equally in the fibrous matrix for the PPy9 experiment with a monomer concentration of 0.3 M, an oxidant concentration of 0.15 M, and a polymerization time of 165 min, interacting better with the fibers farther apart from it. There is also an agglomeration trend in *Figure 5 - 4*j of the PPy10 experiment.

*Figure 5 - 4*k depicts the PPy11 experiment with the lower monomer and oxidant concentrations. In this situation, the conductive polymer is placed in the porosity of the fibrous matrix of PCLf, and the distribution of PPy particles along the fibers is observed. However, despite this achievement, there remains a limited uniformity of PPy within the PCL fibers.

The presence of PPy in samples PPy12 in *Figure 5 - 4*l, PPy13 in *Figure 5 - 4*m, and PPy15 in *Figure 5 - 4*o confirms the tendency of PPy to agglomerate and distribute the PPy particles. In those situations, a better dispersion is noticeable, characterized by a coating-like appearance on the PCL fibers but in a smaller percentage than PPy6, reinforcing the influential role of oxidant concentration for a better PPy filler in the PCL fibers. Finally, in *Figure 5 - 4*n, PPy14 shows a superior PPy distribution in the PCL matrix compared to the previous samples.

In general, SEM images revealed that PPy interacts with PCL fibers, especially the thinner ones. Nevertheless, in some cases, PPy is not homogeneously distributed along the PCL matrix, and PPy tends to clump around PCL fibers. Furthermore, it is observed that the PPy tends to occupy vacant volumes left in the porosity of the PCL fibrous matrix and PPy structure exhibits a dendrimer-like structure.

Figure 5 - 5 presents SEM images showcasing the PPy-PCL scaffold manufactured under optimal parameters. The images reveal a notably more uniform surface regarding conductive polymer distribution, forming a cohesive layer of the conductive polymer across all the scaffold surface, maintaining a porosity of 43.30 ± 0.12%. The particulate structure of the conductive polymer and the interaction between both polymers facilitate the formation of a three-dimensional structure. This aspect proves advantageous, contributing to increased roughness, surface area, and enhanced uniformity in the electrical conductivity of the scaffold.

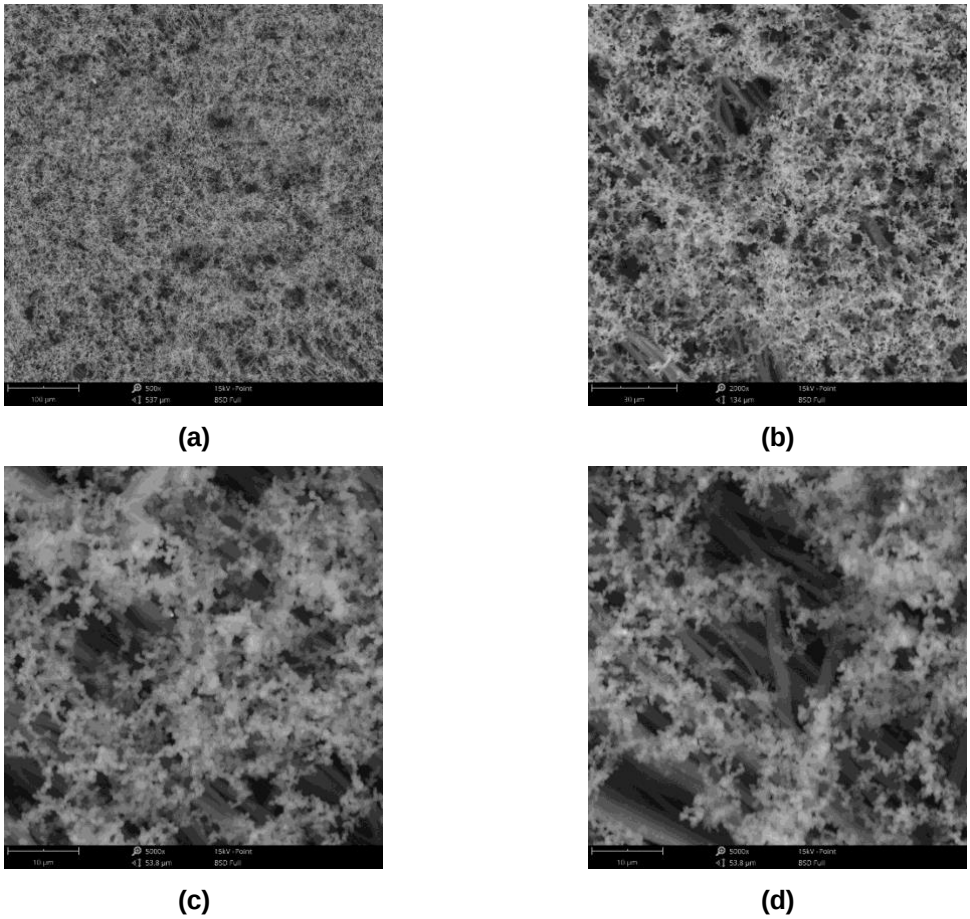

(a) **(b)**

(c) **(d)**

Figure 5 - 5 SEM images of the optimum scaffold (a) 500x, (b) 2000x, (c, d) 5000x.

5.4.4 Chemical analysis of PPy-PCL scaffolds

In addition to observing the change from white to black in the color of the scaffold, the presence of the atoms present in the molecules of the scaffold polymers was observed through energy-dispersive X-ray spectroscopy (EDX). Additionally, FTIR analysis was employed to identify the characteristic peaks of both polymers.

Initially, FTIR assays were used to confirm the presence of the PCL and the polymerized PPy. *Figure 5 - 6* shows the ATR-FTIR spectra of all the samples carried out in the experimental design and the fabricated PCL nanofibers. For the PCL spectra, denoted by a dot line, characteristics peaks at 2933, 2860, 1718, 1292, 1237, 1157 and 1044 cm^{-1} were identified. These peaks correspond to asymmetric vas(CH_2), symmetric vs(CH2) stretching, carbonyl (C=O) stretching, C-O, C-C stretching, asymmetric C-O-C stretching, and symmetric COC stretching, respectively (Heidari et al., 2017; Tayebi et al., 2021; Yuan et al., 2012).

PPy peaks, indicated with a dashed line in *Figure 5 - 6*, were also identified. For the samples of the DoE, PPy characteristic peaks between 1504 to 1537 cm^{-1} and 1453-1469 cm^{-1} were observed, corresponding to C=C stretching of the polypyrrole ring. Further, peaks in 1360 cm^{-1} correspond to C-N bonds in the molecule. Additionally, tiny peaks near 3400 cm^{-1} indicated N-H bonding, while a peak around 2100 cm-1 is attributed to C-H stretching. Minor peaks between 725 and 959 cm^{-1} suggest C-H bonding for PCL and PPy molecules. The identified peaks align with the findings available in literature (S. Cui, Mao, Zhang, et al., 2021; Liang & Goh, 2020; Yussuf et al., 2018). Results showed uniformity in the chemical composition of the polymers and the formation of PPy in the scaffolds. Furthermore, the presence of oxidants did not show significant changes.

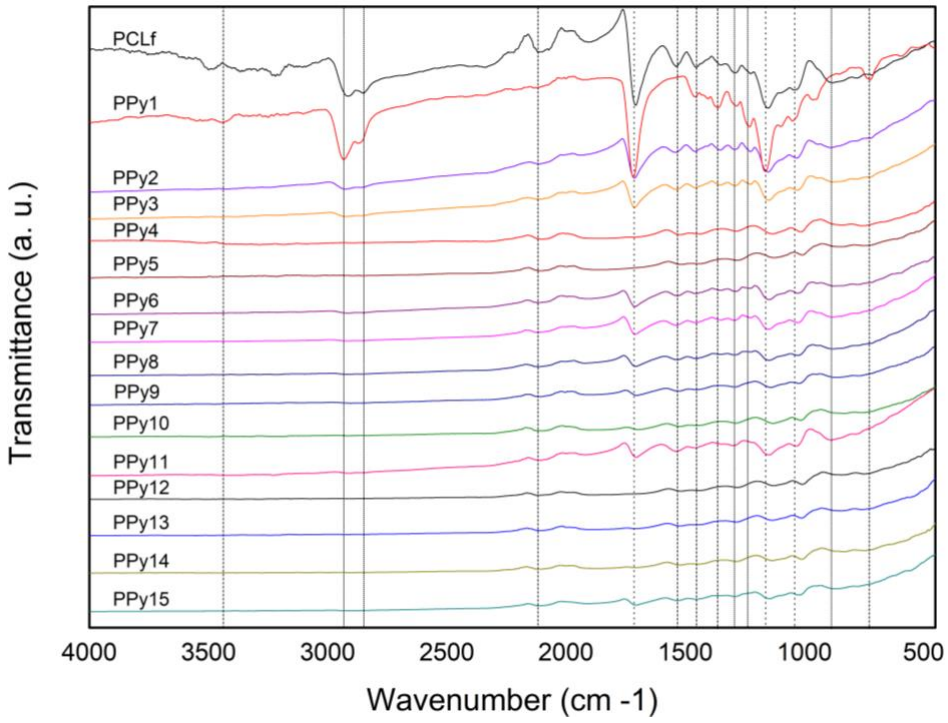

Figure 5 - 6 ATR-FTIR spectra of the PCLf and PPy-PCL samples.

*Figure 5 - 7*a shows the FTIR spectra of the optimum PPy-PCL scaffolds. There is a mild peak at 3659 cm-1 corresponding to N-H bonding in the PPy molecule as shown in *Figure 5 - 7*b. The next peak at 2375 and 2111 cm^{-1} corresponds to C-H stretching. Moreover, peaks at 1812 cm^{-1} correspond to the ester group (C=O) of PCL, and a peak at 1296 cm^{-1} corresponds to C-O and C-C stretching in the crystalline phase in PCL. A peak at 1531 cm^{-1} is a characteristic of C=C vibrations, while 1159 cm^{-1} is attributed to C-N stretching, and 1031 cm^{-1} is the band of C-H and N-H in-plane deformation of the polypyrrole ring. The last peak at 771 cm^{-1} corresponds to out-of-plane ring deformation of the C-H bond. The FTIR results supported previous research by other authors and proved the chemical interaction between PCL and PPy (Číková et al., 2018; Da Silva et al., 2013;

Fakhrali et al., 2022; Ibrahim et al., 2013; Maharjan et al., 2020; Sadeghi et al., 2019; Shinde et al., 2014; H. Xu et al., 2014).

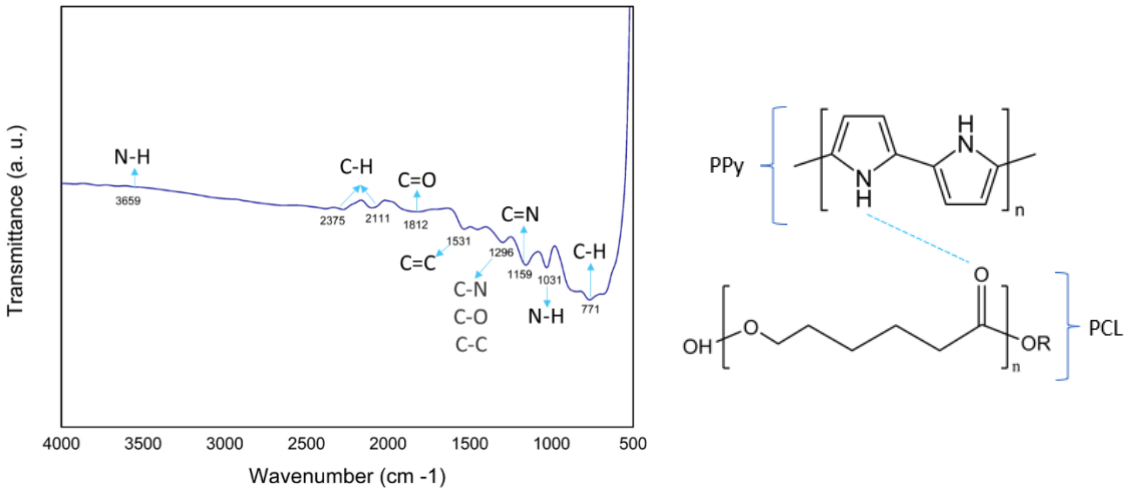

(a) **(b)**

Figure 5 - 7 (a) ATR-FTIR spectra of the optimum PPy-PCL scaffold, (b) PPy-PCL interaction.

On the other hand, the chemical composition of the polymers in the optimum PPy-PCL scaffold was analyzed with the energy dispersive X-ray spectroscopy (EDX). The peaks of O, C and N were identified with a relative weight percentage of 33.89±3.28%, 28.37±0.61%, 22.91±0.58%, respectively. The Cl was also identified because it is the anion that dissociates the oxidant ($FeCl_3$) with a 14.83±2.13%. Moreover, the negligible Fe peak indicates the absence of residual oxidant in PPy polymerization.

5.4.5 Mechanical strength of the optimum PPy-PCL scaffold

The mechanical properties of engineered tissue scaffolds are notably important in providing structural support, transmitting charges, directing cell growth, stimulating cellular response, and establishing compatibility with surrounding tissue. As a result, the mechanical properties of the optimum scaffold were evaluated.

*Figure 5 - 8*a shows the stress-strain curves of the pure PCL fibers compared with the PPy-PCL scaffold. The high percentage at break (1215.65) indicated by the PCLf curve confirms the elastic nature of the PCL and the well-known plastic deformation before breakage. The mechanical properties of the PCLf and the optimum scaffold are shown in *Figure 5 - 8*b, with a higher stroke for the PCLf.

In the case of the PPy-PCL scaffold, it is evident that the percentage strain at break is considerably lower than that of the PCLf. However, as shown in *Figure 5 - 8*, the optimum scaffold exhibits higher tensile strength and Young modulus, making it a more rigid scaffold, to which more force had to be applied. The force used for the test was 2.30 N, compared to the force applied to the PCLf of 1.80 N, which is nearly double.

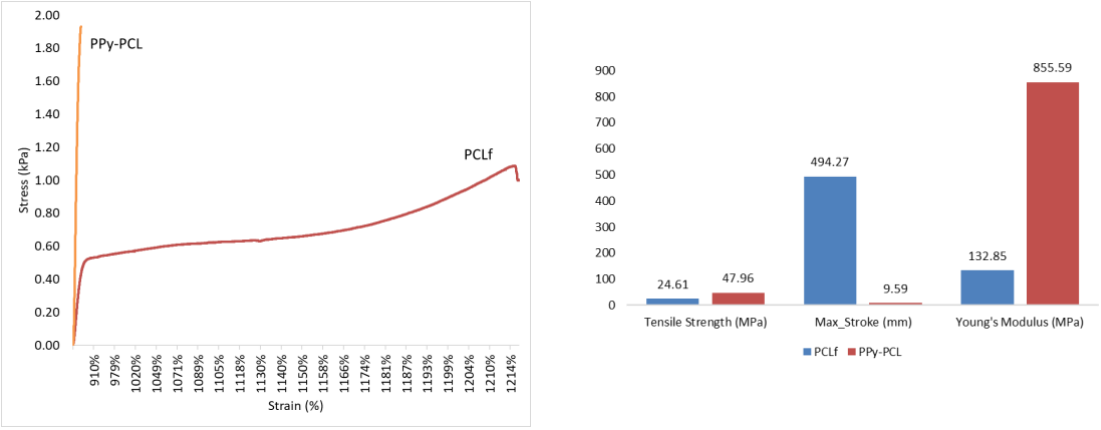

(a) **(b)**

Figure 5 - 8 (a) Stress-strain curves, (b) Tensile strength, maximum stroke, and Young's modulus of the optimum PPy-PCL scaffold compared with PCL fibers.

5.4.6 Wettability properties

The water contact angle value evaluated surface wettability of the scaffolds. As established by previous scientists, the lower contact angle verifies the improved hydrophilic property of the scaffolds, which is favorable because it promotes higher cell feasibility (Shafei, Foroughi, Chen, et al., 2017).

Table 5 - 5 shows contact angle measurement of the pure PCL fibers and the PPy-PCL scaffolds. The contact angle for pure PCL fibers is 108.68±7.54°, corresponding to a hydrophobic surface because PCL is naturally hydrophobic (Arakawa & DeForest, 2017). Moreover, PPy5, PPy8, PPy10, PPy13, PPy14, and PPy15 have a contact angle of zero degrees, indicating that the liquid is fully spread over these surfaces. Many other measurements of the contact angle are hydrophobic; for example, PPy1 to PPy4 showed similar values to pure PCLf, particularly PPy2, which has the lowest oxidant value (0.15 M) and a shorter polymerization time (30 min), which had less impact on the production of PPy, according to the results of manufacturing parameter optimization. Other hydrophobic values shown by the PPy7 and PPy9 scaffolds, which were likewise synthesized with low oxidant concentration values, are as follows.

Table 5 - 5 Contact angle of PCLf and PPy-PCL scaffolds.

Sample	Contact angle
PCLf	108.68±7.54
PPy1	110.82±16.95
PPy2	108.60±11.62
PPy3	107.30±11.17
PPy4	98.57±1.71
PPy5	0.00±0.00
PPy6	119.75±13.84
PPy7	123.00±14.02
PPy8	0.00±0.00
PPy9	125.32±16.77
PPy10	0.00±0.00
PPy11	106.06±2.08
PPy12	108.95±18.75
PPy13	0.00±0.00
PPy14	0.00±0.00
PPy15	0.00±0.00

An ANOVA was performed to analyze whether there are significant differences between the measurements of contact angles. The analysis results show no significant differences in means (p-value is $3.75*10^{-3}$ for Time and p-value is $1.35*10^{-4}$ for Oxi factor), but Oxi and Time were the most relevant factors. *Figure 5 - 9* illustrates the contour plot of the factors and the contact angle as the response variable. Graphs show that the Oxi must be larger than 0.33 M and the polymerization duration must be around than 100 min to ensure hydrophilicity on the scaffolds. The monomer concentration (Py) has little effect on the contact angle.

At the end, for the optimum PPy-PCL scaffold with the optimum fabrication parameters, results showed that this optimum scaffold was hydrophilic as shown in *Figure 5 - 10*. According with contact angles analysis and the fabrication parameters for optimum PPy-PCL scaffold, results agree with the values showed before.

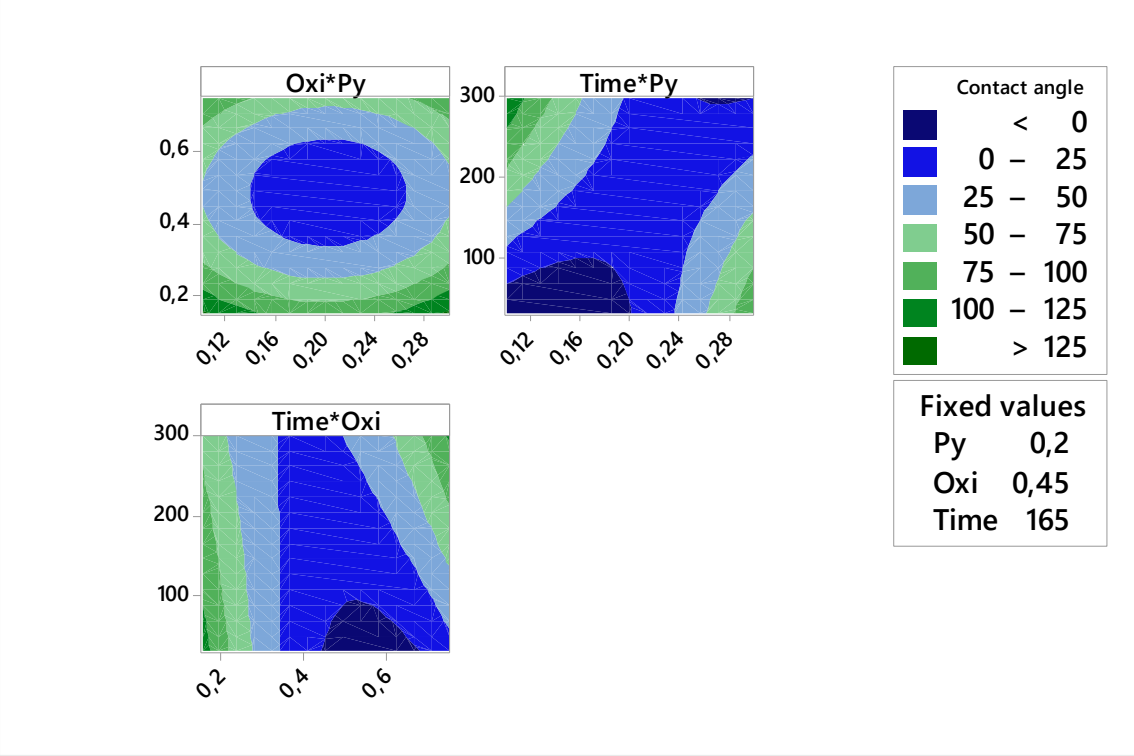

Figure 5 - 9 Contour plot of polymerization factors for contact angle.

(a) **(b)**

Figure 5 - 10 The wettability characteristics of the optimum PPy-PCL scaffold at (a) 0 s and (b) 1 s, respectively, illustrate that water has completely permeated the scaffold.

5.4.7 Cytotoxicity results

In *Figure 5 - 11*, the MTT assay results depict the morphological characteristics of fibroblast cells in both the negative and positive control groups and the cellular viability within the PCL and PPy-PCL scaffolds.

Visually discernible from the imagery is the absence of any appreciable distinction between the control and PCL scaffold groups. Furthermore, within the samples containing PPy, evident cellular viability is observed. Notably, *Figure 5 - 11*d reveals the presence of PPy particles intimately

associated with the cells, indicative of the interaction of the material with fibroblasts, without harmful effects on cell viability.

Following the protocol stipulated by ISO 10993-5 standards, cellular viability exceeding 70% indicates a non-cytotoxic environment. In this study, the cellular viability, determined from the control group and obtained through triplicate measurements for the PCL scaffold, is quantified at 123 ± 0.60%. Meanwhile, for the PPy-PCL scaffold, cellular viability reaches 107 ± 0.34%. These results collectively suggest the absence of any adverse effects stemming from the scaffolds under investigation, with particular emphasis on the optimized PPy-PCL scaffold but are still above the PCL results.

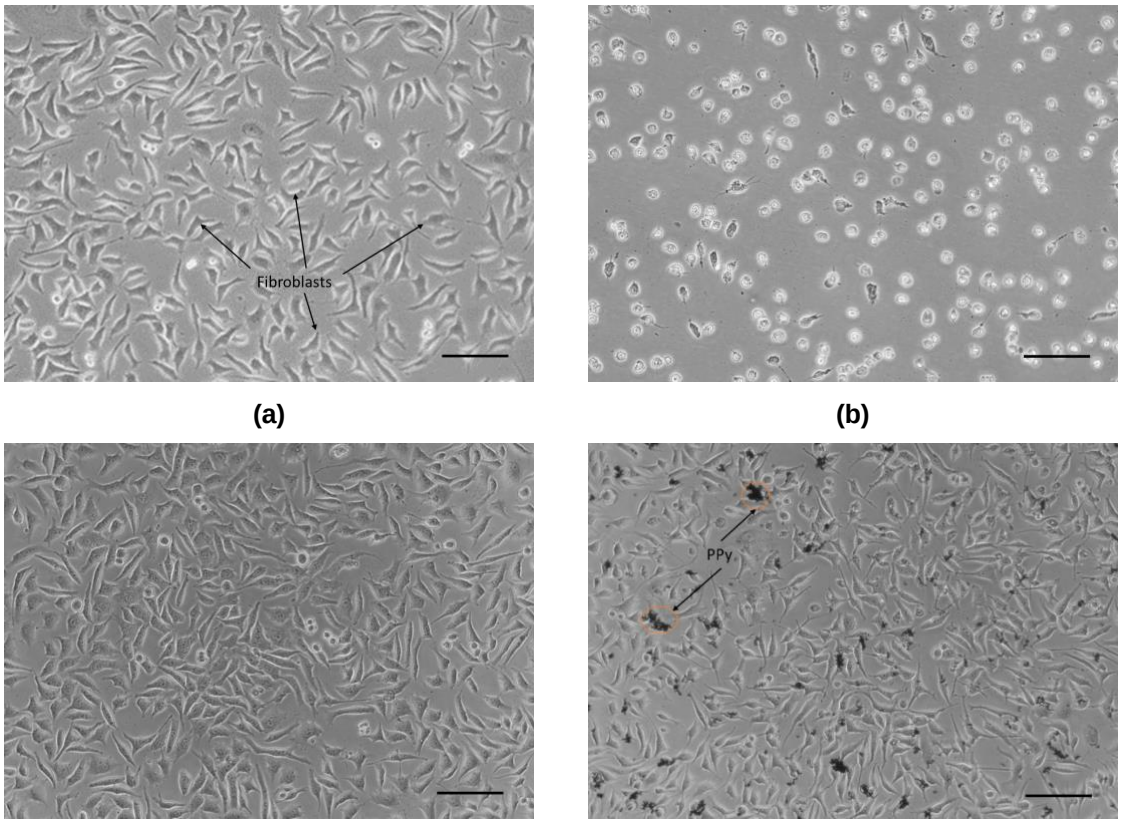

Figure 5 - 11 MTT assay results. (a) Fibroblast cells (blank), (b) positive control, (c) PCL scaffold, (d) PPy-PCL scaffold viability. Scale bar 100 µm.

For the metabolic activity of bmMSCs measured with Alamar Blue, the results of the One-way ANOVA indicated no significant differences between the PCLf scaffolds and both PPy-PCL (UP) and PPy-PCL (DOWN) scaffolds (see *Figure 5 - 12*). However, a significant difference was observed between the two distinct PPy-PCL scaffolds. Furthermore, cell proliferation on the opposite side of

the optimal membrane has been consistently higher since day 3 compared to the area with the highest concentration of PPy, followed by the PCL fibers.

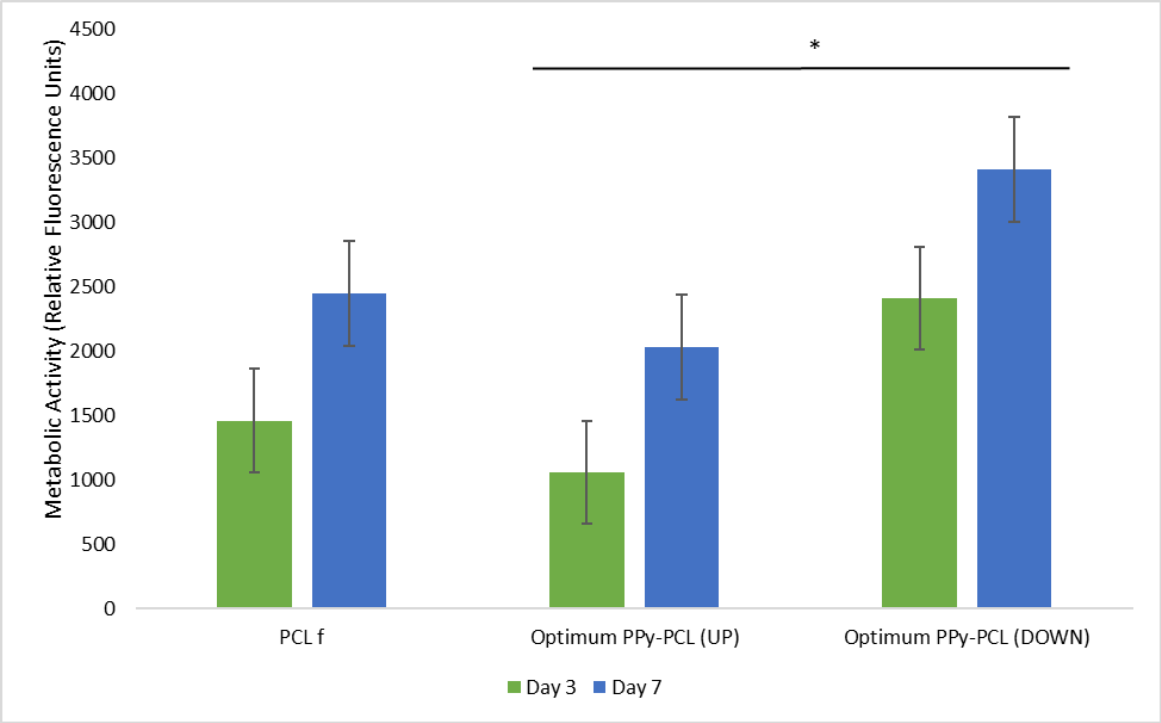

*Figure 5 - 12 Metabolic activity on different scaffolds at days 3 and 7 after bmMSCs seeding. Values are expressed as mean, with asterisks representing significant differences between scaffolds (*p < 0.01).*

In *Figure 5 - 13*, the interaction between cells and scaffolds is depicted. As observable, cellular growth and a cell layer formation on the surface can be seen for the scaffold with PCL fibers and both optimal scaffolds. Cell growth for PCL fibers increased significantly from day 3 to day 7. The white arrows indicate the contact points between the fibers and the cells positioned and interacting within the fiber matrix.

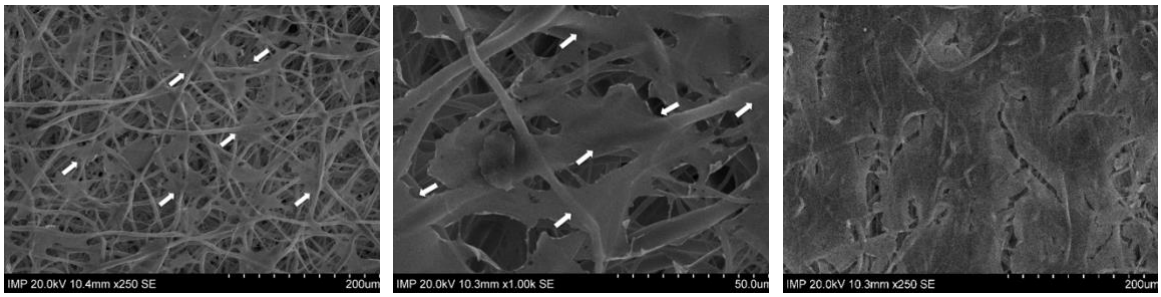

(a) **(b)** **(c)**

Figure 5 - 13 SEM images of bmMSCs seeded on (a) PCL fiber scaffold on day 3 at 250X, (b) PCL fiber scaffold on day 3 at 1.0kX, (c) PCL fiber scaffold on day 7 at 250X.

For the Optimum PPy-PCL scaffold (UP), it can be observed that cells are situated on the surface of the PPy particles, showing increased proliferation by Day 7, as depicted in *Figure 5 - 14*. However, as illustrated in *Figure 5 - 5*, due to the morphology of the PPy particles and the positioning of the PCL fibers beneath, a profound adherence below the PPy particles is not evident, which likely explains the lower values of metabolic activity with Alamar Blue.

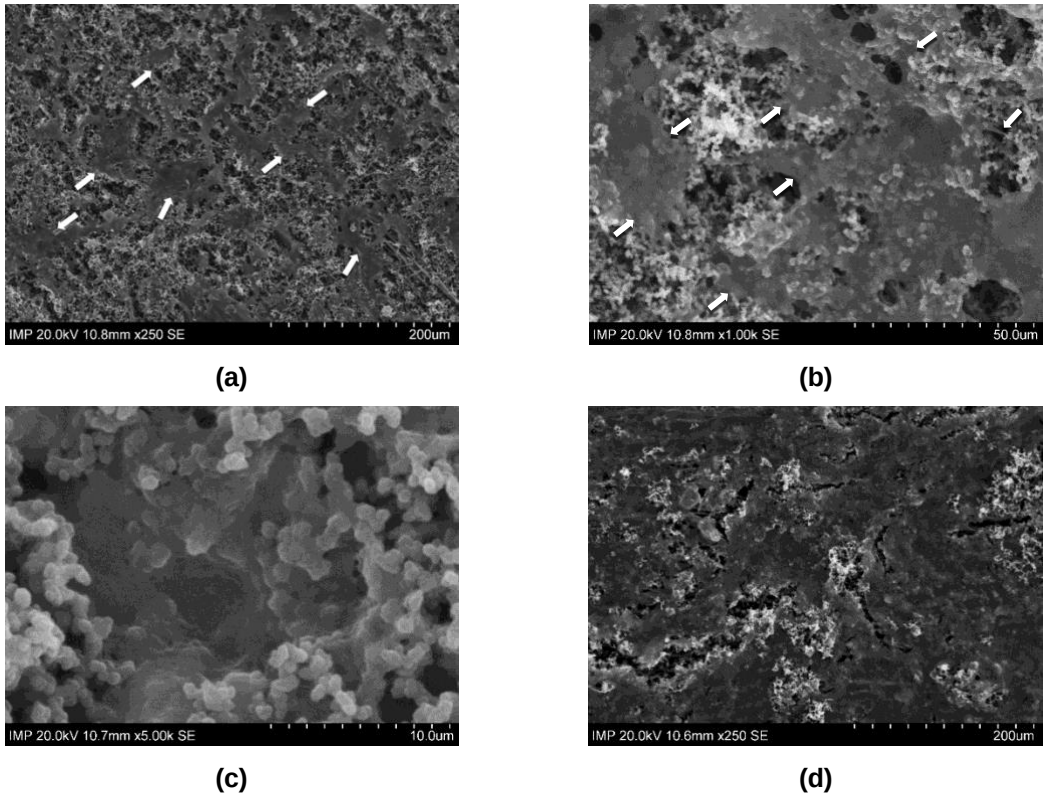

Figure 5 - 14 SEM images of bmMSCs seeded on (a) Optimum PPy-PCL (UP) scaffold on day 3 at 250X, (b) Optimum PPy-PCL (UP) scaffold on day 3 at 1.0kX, (c) Optimum PPy-PCL (UP) scaffold on day 3 at 5.0kX, (d) Optimum PPy-PCL (UP) scaffold on day 7 at 250X.

Regarding the Optimum PPy-PCL scaffold (DOWN) showed in *Figure 5 - 15*, greater adhesion and proliferation of cells along the matrix are observed. Additionally, as depicted, cells tend to adhere to the PCL fibers while interacting with the surrounding PPy particles.

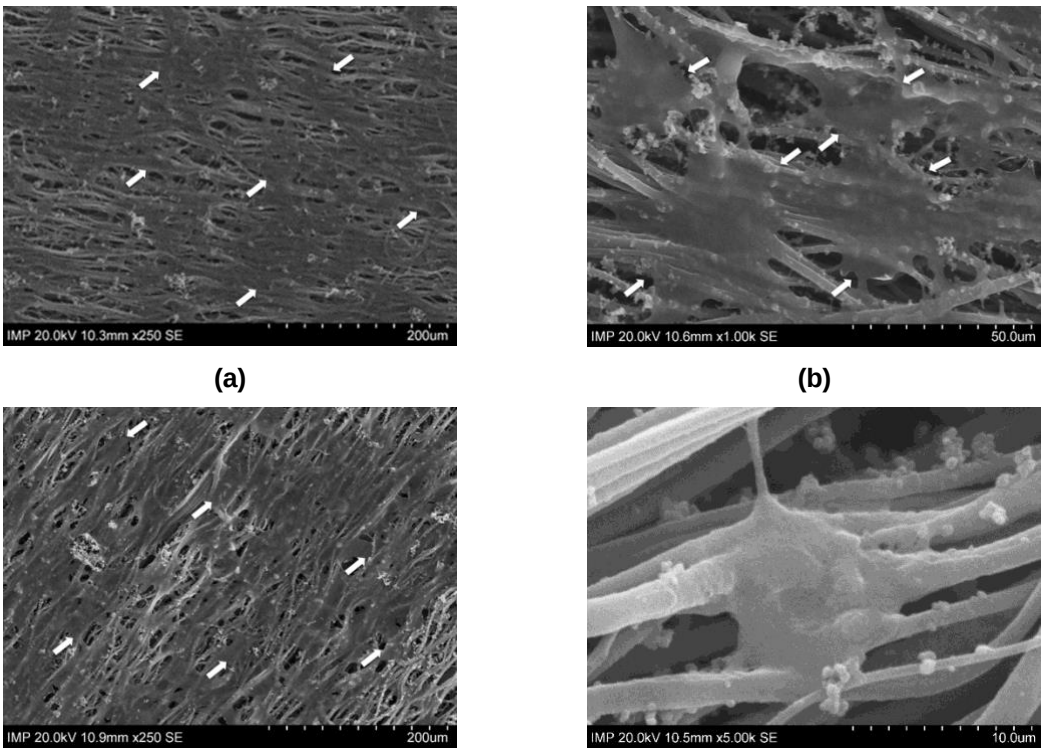

Figure 5 - 15 SEM images of bmMSCs seeded on (a) Optimum PPy-PCL (DOWN) scaffold on day 3 at 250X, (b) Optimum PPy-PCL (DOWN) scaffold on day 3 at 1.0kX, (c) Optimum PPy-PCL (DOWN) scaffold on day 7 at 250X, (d) Optimum PPy-PCL (DOWN) cell on day 7 at 1.0kX

5.5 Discussion

To provide a promising solution to overcome some challenges in TE, the main goal of this study was to develop and characterize a conductive scaffold for potential use in TE applications. The results have shown that the *in situ* synthesis of polypyrrole (PPy) in a polycaprolactone (PCL) fiber matrix improves scaffold properties.

As detailed in the results section, a polymeric matrix made of PCL fibers obtained by electrospinning was characterized. Despite exhibiting larger diameters compared to previous studies, microfibers have an advantage over nanofibers in specific applications, such as CTE, since a scaffold built of microfibers often has a greater pore size, facilitating better cell penetration into the scaffold (Jana et al., 2019).

The PCL fiber matrix was fabricated with aligned fibers. According to other authors, having aligned fibers replicated the anisotropic structure of heart or muscle tissue (Qasim et al., 2019). The properties of a scaffold with anisotropic construction can improve cell maturation, regulation of critical

cellular functions such as morphogenesis, and mechanical properties (Fleischer et al., 2017; Kharaziha et al., 2014; Ye & Qiu, 2017).

After the PPy polymerization, the optimum PPy-PCL scaffold with a conductivity of 2.542 mS/cm was obtained by optimizing manufacturing parameters (Py, Oxi, and Time) using a Box-Behnken response surface design. Results show the more significant parameters are oxidant concentration (Oxi), polymerization time (Time*Time) interaction, and monomer concentration with polymerization time interaction (Py*Time). The interaction between monomer concentration and (Py*Py) was not significant.

In this study, oxidant concentration (Oxi) was the most influential factor in the manufacturing process of PPy-PCL scaffolds. Anhydrous FeCl3 was employed as a oxidant because, according to various authors (Jain et al., 2023; Tavakkol et al., 2017; Yussuf et al., 2018), it produces better electrical conductivity results. Another advantage of using anhydrous FeCl3 is that its ions (Cl- and ClO4-) decompose and dissociate, serving as a dopant during polymerization and reducing the number of parameters and materials to consider during the polymerization process (Pang et al., 2021). Furthermore, anhydrous FeCl3 is the substance that will remove electrons and start the polymerization of PPy. Then, the higher the oxidant concentration, the more negative charges are delocalized, resulting in greater charge mobility in the scaffold. As previously stated, FeCl3 is a strong oxidant with high redox potential, which allows it to gain electrons and quickly oxidize Py. Still, it is also possible that it can degrade the new PPy, generating cross-linking interchains (Sasso et al., 2011). In this context, time plays a vital importance because it greatly affects the final conductivity of the material.

The second significant parameter is Time*Time interaction. According to this study, the polymerization time to achieve conductive scaffolds ranged from 30 to 300 minutes. Based on the conductivity results of the scaffolds conducted (see *Table 5 - 2*), a conductive scaffold may be achieved within 30 minutes regardless of the concentration of oxidant or monomer. Other authors have demonstrated that a conductive scaffold (5.06±1.1 S/cm) can be generated in at least seven minutes (Khatti et al., 2019). Other researchers, on the other hand, have achieved good conductivity results with polymerization times of 4 hours (Číková et al., 2018; Yussuf et al., 2018) or 5 hours (Boutry et al., 2012; H. Xu et al., 2014) with good conductivity results. In fact, Agrawal et al. (Agrawal et al., 2020) studied different polymerization times ranging from 0.3 to 1, 2, 4, 6, 8, 10, and 24 hours, achieving better results at 8 h (2 S/cm) because conductivity declines with longer times. However, undesirable reactions may occur during prolonged polymerization times, which is why it is necessary to optimize the polymerization time to avoid disruptions in conjugation, such as overoxidation reactions (Lewis, 1998) (degradation of the PPy chain) and the development of the PPy conjugate

system (Pang et al., 2021). Furthermore, as shown in *Figure 5 - 1*, the times to achieve appropriate propagation, nucleation, and growth of PPy in the PCL matrix may not be sufficient.

Similarly, a parameter to consider for the polymerization reaction is the oxidant/monomer ratio. As discussed before, higher concentration of oxidant and longer polymerization time could be detrimental to conductivity. Therefore, achieving a balance between the oxidant and Py is crucial, since the former must remove electrons from the Py, but an excess of oxidant can lead to overoxidation. Some authors suggest that the optimal values in this molar ratio should be between 2.25 and 2.40 when FeCl3 is used as an oxidant (Ansari, 2006; Pang et al., 2021). In the present study, the optimal scaffold has a ratio of 0.73/0.30=2.43, which is close to the optimal range reported in the literature.

On the other hand, the temperature of the polymerization process was considered and remained a fixed parameter. Some authors have performed the process at room temperature (Shafei, Foroughi, Stevens, et al., 2017; Yussuf et al., 2018). Others, however, have done it at low temperatures, such as 4°C (20) or 5°C (Agrawal et al., 2020; Talebi et al., 2019). Agrawal et al. (Agrawal et al., 2020) performed the process at room temperature (27°C), 20 and 5°C, finding that lower temperatures improved conductivity. The temperature was regulated to a maximum of 4 °C for the technique used in this study. According to previous reports, low temperatures favor the decrease in the kinetics of the reaction, promoting the formation of linear PPy because charge transport movements are preferred, better regulating the conjugation, and finally, favoring the electrical conductivity of the PPy (Pang et al., 2021).

The scaffold developed during the current investigation could be helpful in the search for electro-conductive materials for TE, which is one of the primary objectives of this research. For example, in CTE, superior or close to host tissue conductivity must be achieved. In this context, various authors report conductivity of 1 mS/cm (Fakhrali et al., 2022; House et al., 2021; Liang et al., 2021; Ren et al., 2023), while others say values of 0.5 mS/cm (Sovilj et al., 2014) or 0.54 mS/cm (Gabriel et al., 1996), 40 mS/cm longitudinal and 17.9 mS/cm for transversal heart tissue (Malmivuo & Plonsey, 1995). In nervous tissues, conductivity falls within the range of ≈0.8-13 mS/cm (Manousiouthakis et al., 2022). Since the electric conductivity achieved in this case exceeds some physiological levels, it should be noted that when the scaffold is exposed to a physiological environment, handled with other materials that improve tissue-implant interaction or used practically, conductivity may decrease or vary. As a result, it is critical to recognize that scaffolding is suitable for electrical conductivity.

As observed in *Figure 5 - 4* and *Figure 5 - 5* the particle morphology of the scaffolds is homogeneous and granulated, even without surfactants (L. Hao et al., 2022). The interaction between the PPy particles appears to produce a dendrimer-like shape. Notably, only a few writers achieved similar

morphologies to the one obtained in this research. For instance, Číková et al. (39) presented globular morphologies, and Fan et al. (60) achieved soft nanoparticles. The circular and uniform morphology of the optimum scaffold described in this work suggests several advantages for its application to TE. The surface morphology, for example, would have a larger surface area than other morphologies, allowing for more contact between biologically active cells and substances. Furthermore, this structure may provide a free volume where drugs or additional compounds could be incorporated for specific uses. As a result, the optimum scaffold features a 3D structure ideal for recreating the ECM environment. It should be noted that there is no overall uniformity of PPy in the structure of PCL fibers in all scaffold images. This is both a disadvantage and an opportunity for future work, as other writers have already observed a problem with comparable methods (Laforgue & Robitaille, 2010; Pang et al., 2021). Despite this, this method produces thin scaffolds, which increase cell penetration and diffusion of nutrients and oxygen from the surrounding environment into growing tissue cells (Bronzino, 2006; Jana et al., 2019; Qasim et al., 2019).

Whether it relates to mechanical properties, Young's modulus increased from 132.85 MPa for PCL fibers to 855.59 MPa for the optimum scaffold. It also improved its resistance to strain and applied force. However, the PPy-PCL scaffold's breaking point was anticipated. These findings can be explained by the fact that PPy contains conjugate chains, which are related to PPy stiffness; hence, the scaffold possesses rigidity as well (Maharjan et al., 2020). Since the maximum breaking point of the PCL structure with PPy was much more significant (494.27 mm) compared to that of the scaffold with PPy (9.59 mm), this confirms that the elastic/viscoelastic nature of PCL (Alexeev et al., 2020; Baker et al., 2016) became more rigid. The presence of PPy in the fibers also causes cross-links in the PCL fibers and agglomerations like those shown in the SEM images (Fakhrali et al., 2022).

In tissues such as the myocardium, Young's modulus falls within the range of 200-500 KPa (Fleischer et al., 2017; M. Lee et al., 2022), and the optimal scaffold of this study exceeds the value in this case. However, as the scaffolds were not exposed to physiological fluids or cell culture, the mechanical properties may vary since they were tested dry. It should be highlighted that the optimum PPy-PCL scaffold has superior manipulability than the scaffold produced just of PCL fibers, which is advantageous in real-world applications (Shafei, Foroughi, Stevens, et al., 2017). These findings demonstrate that the mechanical properties of the scaffold made of PCL fibers can be significantly influenced by the incorporation of PPy and tailored for various applications, such as bone or tendon TE (Mckee et al., 2011).

Natural polymers could be added, as has been done in previous studies, to decrease Young's modulus for specific applications (Fakhrali et al., 2022; Kai et al., 2011b; Khatti et al., 2019).

According to the literature, the conductivity obtained in the present study could be suitable for skeleton muscle, cardiac, nerve, and liver tissue (Haq et al., 2021). When considering the relationship between conductivity and Young's modulus, cardiac tissue emerges as the most promising candidate for applying the optimum scaffold (Haq et al., 2021; Saberi et al., 2019).

The chemical analysis of the scaffolds shows the interaction between the two polymers, in which intermolecular hydrogen bonds can be formed between the molecular chains of both polymers, as observed in *Figure 5 - 7*b.

Regarding wettability, it was determined that the optimum scaffold was completely hydrophilic, and the influence of PPy predominantly contributed to this improvement. The presence of hydroxyl groups and the hydrophilic amino group of the PPy molecule, the scaffold PPy-PCL promotes the hydrogen bond with water molecules. Other publications show similar findings on the increases in hydrophilicity influenced by PPy on the surface (S. Li et al., 2022; Maharjan et al., 2020). Additionally, the roughness in the scaffolds allows the drop to disperse in the structure. As evident in the SEM images, there is a greater contact area than the PCL fibers, as PPy is present not only on the surface but also within the matrix of PCL fibers. Because some of the manufactured scaffolds that turned out to be hydrophobic exhibited drop adhesion on the surface, the scaffold's roughness might fit the Wenzel state model. The fact that the optimum scaffold is hydrophilic is a significant advantage as it promotes cell attachment, proliferation, and subsequent growth (Ferreira et al., 2019; Tian et al., 2016).

The *in vitro* tests indicate that all scaffolds, PCL fibers, and optimized PPy-PCL scaffolds are not cytotoxic. Cellular growth was observed on all scaffolds up to day 7. The optimum scaffold, specifically on the side opposite to where the Ppy was polymerized, exhibited superior performance compared to the scaffold side containing a higher concentration of polymerized Ppy particles and compared to PCL fibers alone without PPy particles.

SEM images further confirm cellular growth on the scaffolds, highlighting the cell-scaffold interaction where cells tend to align and position themselves among the fibers. This optimal scaffold, comprising both fibers and PPy particles, appears to encourage cells to bridge the gaps between these elements. Particularly, when cells adhere to the scaffold side with more polymerized PPy particles (Optimum PPy (UP)), their adherence is evident but not as robust as their attachment to the fibers themselves or the opposite side of the scaffold (Optimum PPy (DOWN)). This behavior may be driven by cells preferring to adhere more readily to areas rich in fibers. Furthermore, the PPy particles may not provide equal stability, guiding cells toward the fibers via mechanotransduction. For example, the bmMSCs, there is a preference of a rigid substrate (M. Sun et al., 2018). Moreover, there is a natural inclination of cells to bridge gaps in a rougher surface or a dense fiber network,

where they can establish stable connections (Q. Chen et al., 2020), unlike with the side with more quantity but less stable PPy particles. Therefore, this scaffold configuration could be more effectively employed on the opposite side facing the host tissue.

Finally, the optimized conductive PPy-PCL scaffold demonstrated excellent cell viability with fibroblasts and bmMSCs. Both tests indicate cell survival and proliferation, suggesting that these materials are suitable for TE applications. Other studies have also supported the cellular suitability of similar materials for such applications (Fakhrali et al., 2022; Sadeghianmaryan et al., 2019; Zarei et al., 2021).

The optimum PPy-PCL scaffold fabricated (Py=0.3M; Oxi=0.73 M and Time=232 min) in this study showed good electric conductivity (2.542 ± 0.139 mS/cm), proving the effective interaction between the two polymers and resulting in a 3D structure suitable for TE applications. This scaffold enables a greater replication of the natural environment, solid structural support, greater surface area, improved nutrition, oxygen transport, and cellular behavior like that found *in vivo*.

5.6 Conclusions

This study highlighted the effectiveness of optimizing PPy polymerization parameters, leading to heightened electrical conductivity. The *in situ* polymerization of polypyrrole within PCL fibers has a pronounced influence on the characteristics of PPy-PCL scaffolds. These scaffolds showcased notably high electrical conductivity, indicating their potential for bioelectrical applications. Specifically, our optimized scaffold exhibited an electrical conductivity of 2.54 mS/cm. Key factors impacting conductivity included oxidant concentration (Oxi), polymerization time (Time*Time), and the interrelation between monomer concentration and polymerization time (PyTime).

SEM analysis verified the successful integration and interaction between PPy and PCL, revealing a consistent morphology and a globular particle arrangement. Additionally, the optimized scaffolds exhibited improved tensile strength and Young's modulus compared to pure PCL fibers, suggesting applications in supporting polymeric rigid tissue. The heightened hydrophilicity in the optimized scaffolds was demonstrated to enhance cell adhesion and nutrient conveyance, essential for advancing engineered tissue development and functionality. Cell seeding experiments affirmed the biocompatibility of the fabricated PPy-PCL scaffolds. However, to validate these results, future research should concentrate on optimizing electrical conductivity, enhancing mechanical properties, and investigating biological responses. This study establishes a foundation for future assessments of these scaffolds in specific applications such as myocardial or neuronal regeneration.

5.7 Annex

5.7.1 Developing a Custom Electrical Conductivity Measurement Device

To address a significant challenge in this project - the measurement of electrical conductivity of the developed materials - we ventured beyond conventional methodologies due to the constraints of physical and financial resources. Scientific literature frequently referenced the four-point probe test for such measurements; however, the unavailability of appropriate equipment prompted an innovative approach. We embarked on designing a custom device capable of facilitating simpler conductivity measurements.

The initial phase involved qualitative evaluations of the scaffold's ability to conduct electricity, employing a basic circuit setup as illustrated in Figure 5 - 16. This preliminary experiment confirmed that the fabricated scaffolds could indeed conduct electrical current, as indicated by the illumination of a bulb within the circuit.

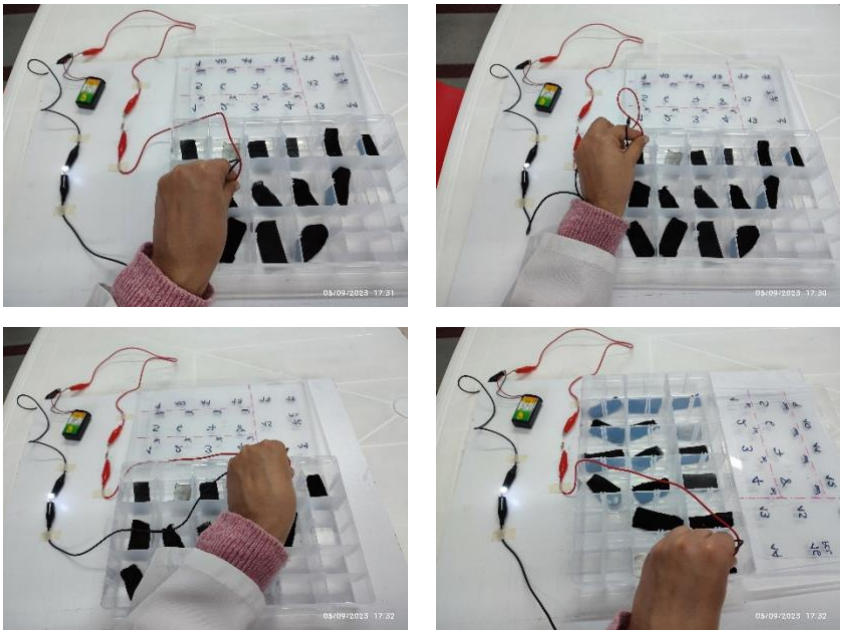

Figure 5 - 16 Basic circuit setup to evaluate electric conductivity of scaffolds (author).

Progressing through various configurations, the final assembly emulated the four-point probe principle, a standard approach for measuring conductivity in thin films, conductive coatings, and semiconductor materials. This technique utilizes four linearly aligned probes in contact with the material under test. By applying a constant current through the outer probes and measuring the voltage across the inner probes, as depicted in Figure 5 - 17, it is possible to assess conductivity with precision. The constructed device comprised a DC power source (YX-1502DS), two separate multimeters for voltage and current measurement (XL830L), a 1 Ω resistor, and four co-linear probes

spaced 1 mm apart, supported by a holder fabricated through 3D printing. Film thickness was accurately gauged using a micrometer (M120-25 Mitutoyo).

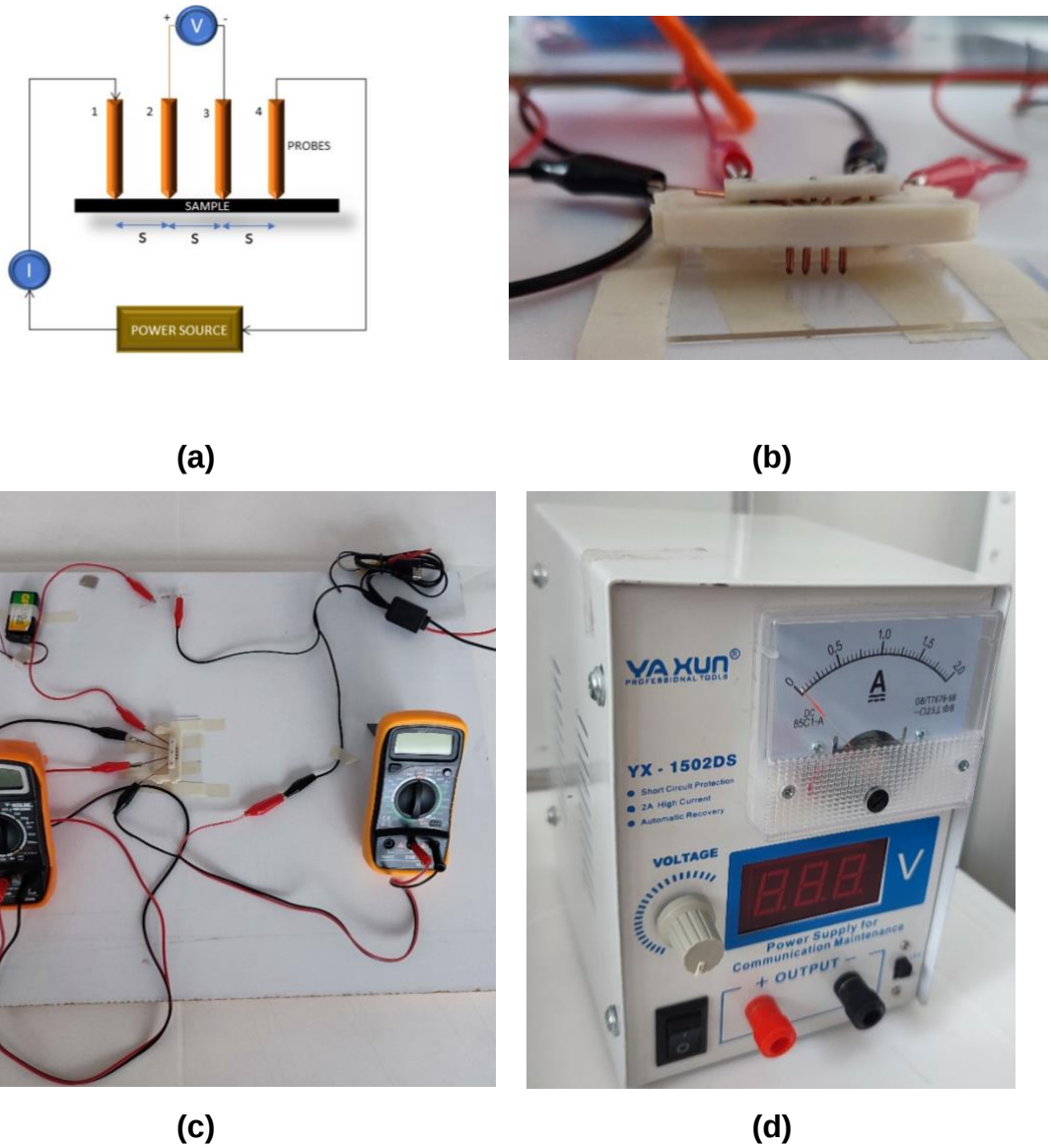

Figure 5 - 17 (a) Four point probe diagram, (b) four point probes build, (c) Four point probe handmade setup, (d) Power supply sed in the setup.

Despite the custom setup enabling the measurement of electrical conductivity, the results significantly diverged from those reported in established literature, highlighting a lack of comparability. Nevertheless, the gathered data, though not accurate, exhibited a high degree of precision, as evidenced by the standard deviations detailed in Table 5 - 6. To achieve this level of precision, between 10 to 20 measurements were taken for each scaffold. Outliers were identified

and excluded through statistical tests, normalizing the data to 10 measurements per scaffold. This methodological approach underscored the urgent need for standardized equipment for future evaluations. Notably, the values recorded using this makeshift method were considerably higher than those obtained with the subsequently acquired standardized equipment (Table 5 - 3) and those cited in the literature, an outcome that defies logical expectation.

This inconsistency emphasizes the critical importance of utilizing standardized, calibrated equipment for electrical conductivity measurements in TE research. The discrepancies observed with the improvised setup reiterate the challenges in replicating the nuanced conditions and precise control afforded by dedicated scientific instruments.

Table 5 - 6 Electric conductivity measurements with the handmade setup.

Scaffold	Electric conductivity (S/cm)
PPy1	0.072±0.0005
PPy2	0.023±0.0005
PPy3	0.407±0.049
PPy4	0.098±2.59
PPy5	0.154±0.001
PPy6	0.204±2.764
PPy7	0.025±0.003
PPy8	0.558±11.832
PPy9	0.172±0.001
PPy10	0.246±0.003
PPy11	0.082±0.002
PPy12	0.216±0.001
PPy13	0.63±0.004
PPy14	0.075±0.021
PPy15	0.491±0.008

5.7.2 Scaffold Limitations and Mechanical Property Concerns

Upon reviewing previous chapters, it becomes apparent that producing fibers that not only incorporate particles but also achieve high electrical conductivity presents significant challenges. The method described in this chapter, while seemingly simpler and requiring careful fabrication, marks a crucial advancement in scaffold development. However, the resultant mechanical properties, though superior, far exceed those of native myocardium, which could potentially hinder the scaffold's contractility (Liang et al., 2021).

Importantly, literature reviews, such as those conducted by Liu and Wu in 2023, suggest that scaffolds enhanced with a PPy coating significantly improve electrical conductivity, charge storage

capacity, photothermal properties, and biocompatibility (Liu & Wu, 2023). This highlights the importance of continued exploration and innovation in CTE, aiming to overcome current limitations and pave the way for groundbreaking advancements in Regenerative Medicine.

6. Final Insights and Path Forward in Cardiac Tissue Engineering

This chapter focuses on choosing the best scaffold for CTE, summarizing key findings and suggesting avenues for future research. It highlights the scaffold that showed the most promise for CTE applications, drawing on comprehensive evaluations. The chapter concludes with strategic recommendations for advancing scaffold technology in cardiac regeneration.

6.1 Scaffold Selection for Electromechanical Integration with Myocardial Tissue

In the extensive journey of this research, numerous scaffolds were crafted, with a select few standing out due to their exceptional performance. These distinguished scaffolds, which are underscored for their favorable results within this document, were meticulously chosen for their potential application in cardiac tissue engineering (CTE). The selection criteria were meticulously extracted from a thorough literature review, anchoring the decision-making in a materials engineering framework. This literature review included a bibliometric study, utilizing the entire body of work consulted for the project. As illustrated in the word cloud shown in the *Figure 6 - 1*a, certain criteria, and challenges that scaffolds must meet to have the potential for electromechanical coupling were emphasized. Additionally, the *Figure 6 - 1*b depicts the scholarly works considered over time in the bibliometric study, reflecting the rigorous methodological approach taken to establish the selection criteria for these pivotal components of tissue engineering.

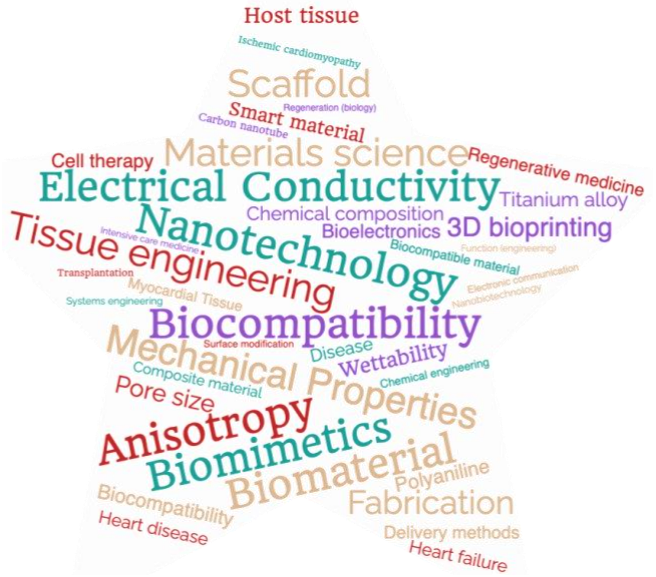

(a)

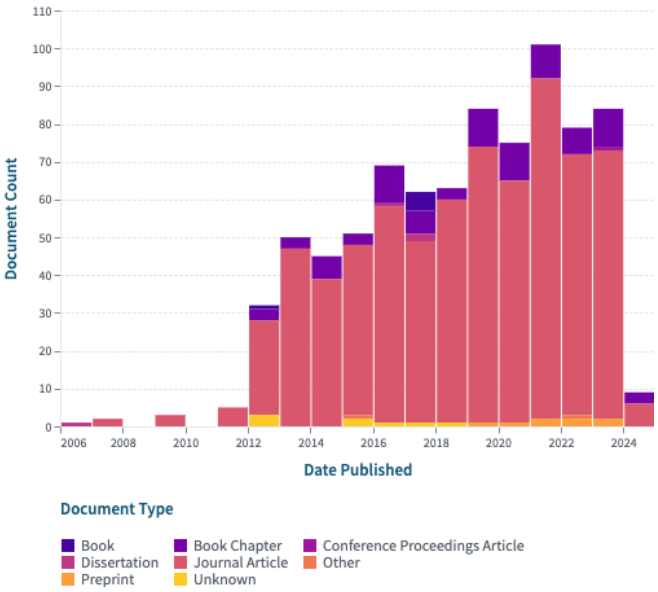

(b)

Figure 6 - 1 Word Cloud Derived from the Bibliometric Study and Literature Timeline in the Field of Research.

1. **Chemical Properties of the Scaffold:** The evaluation focuses on the scaffold's chemical composition and interactions between components, such as the nanofiller and the polymeric matrix. It is critical to understand how these interactions influence the scaffold's overall chemical

stability, degradation rate (scaffold should be decomposed when damage is complete restored), and safety that can support cellular functions.

In this project, PCL and/or PVP were employed as the polymeric matrix, which numerous studies have affirmed as suitable for biomedical applications (Bejaoui et al., 2021; Kurakula & Koteswara Rao, 2020; J. Li, Zhang, et al., 2018; Schmitt, Dwyer, Minor, et al., 2022). Additionally, as reviewed in previous chapters, graphene and PPy are suitable for such applications as long as they do not exceed critical percentages at which they could become cytotoxic (Mota & Corrêa, 2021; J. Wang, 2021).

2. **Replication of Myocardial Anisotropy and Topography:** This criterion assessed the scaffold's ability to replicate the anisotropic structure of the myocardial extracellular matrix (ECM), which is essential for fostering organized development and functionality of cardiac cells. In this project, scaffolds produced using the electrospinning technique on both flat and rotary collectors were studied. However, those manufactured using a rotary collector demonstrated superior properties, achieving a degree of fiber alignment crucial for mimicking the anisotropic nature of myocardial tissue.

   The surface topography of the scaffold was also critical in supporting cell adhesion, protein proliferation, and subsequent cellular growth. The microarchitecture required to be highly porous and interconnected, featuring a high surface-to-volume ratio. Such structural complexities created an environment that closely simulated the natural ECM, thereby promoting effective tissue integration and regeneration. These properties were evaluated through SEM microscopy images, where porosity and pore interconnectivity were assessed. Additionally, the diverse surface morphology was examined to ensure it supported cellular adherence, a fundamental step toward successful tissue engineering.

3. **Biocompatibility:** In the realm of cardiac tissue engineering (CTE), fibroblasts play a pivotal role in tissue remodeling and repair post-injury, largely due to their collagen and elastin-producing capabilities within the extracellular matrix. This function is crucial in the context of healing and regenerative processes following cardiac injuries. Moreover, bone marrow-derived mesenchymal stem cells (bmMSCs) are employed for their differentiation potential into cardiomyocytes and have been directly seeded in patients post-myocardial infarction. These cells are instrumental in evaluating scaffold biocompatibility due to their significant role in cardiac repair and regeneration, further validating the scaffold’s suitability for therapeutic applications (Biscaia et al., 2022; Deliormanlı, 2019).

4. **Wettability and Surface Energy:** The wettability, governed by the scaffold's surface energy, significantly affects cell attachment. Cells generally adhere more effectively to surfaces with moderate hydrophilicity, which facilitates the initial cell-scaffold interactions critical for subsequent cell proliferation and tissue formation. There are studies that have shown that increasing nanofiller, e.g. graphene, improves scaffolding hydrophilicity (Mcivor et al., 2022).

5. **Electrical Conductivity:** The electrical properties of the scaffold, particularly those introduced by nanofillers, can distinctly influence cell behavior compared to non-conductive fibers. Certain cells, including cardiac myocytes, respond to electrical stimuli, which can affect their adhesion, orientation, and proliferation, emphasizing the importance of electrical conductivity for scaffolds intended for CTE. Reference values for myocardial tissue are detailed in Chapter 1 of this thesis. For materials similar to those discussed in this project, the electrical conductivity values are significantly higher than those of native tissues, which largely depend on the quantity of nanofiller incorporated.

6. **Mechanical Properties:** The mechanical properties, including stiffness and elasticity, of the scaffold materials are evaluated to match or exceed those of native tissue. Cells can sense the mechanical properties of their substrate through mechanotransduction, affecting their differentiation and functional maturation. Thus, the scaffold's mechanical environment should closely mimic that of the target tissue to support the desired cellular activities.

   For healthy myocardial tissue, the Young's modulus typically ranges from 10 to 500 kPa (Echegaray et al., 2017). Notably, in pathological conditions like myocardial fibrosis, the Young's modulus can increase as the tissue becomes stiffer due to excessive extracellular matrix deposition. This change underscores the importance of developing scaffolds with mechanical properties that are not only suitable for healthy myocardial tissue but also adaptable to varying pathological conditions to ensure optimal integration and functionality within the cardiac environment (Chang et al., 2016; Y. Sun et al., 2021).

7. **Manipulability:** This criterion assesses the scaffold's potential to be manipulated under real-world conditions as an implant. The scaffold must be easily handled, shaped, and positioned without compromising its structural integrity or biological functionality, ensuring its practical applicability in clinical settings.

Based on the aforementioned criteria, the following scaffolds were selected:

1. **Graphene Multilayer Scaffold (MLS1)-Chapter 2**:

    - This multilayer scaffold consists of two outer layers of PCL and an inner layer of PVP with graphene nanoplatelets.
    - Mechanical Properties: Young's Modulus: 33.75 MPa, % Max Strain: 348.65, Max Stress: 6.68 MPa.
    - Chemical Composition: Polymers with addition of graphene.
    - Electrical Conductivity: Direct measurement not possible, but solution before electrospinning had a conductivity of 85.867 microS/cm.
    - Cellular Testing: Not conducted, though presumed biocompatible due to PCL composition in outer layers.

2. **Embedded Graphene-PCL Scaffold-Chapter 3**:

    - Manufactured with PCL fibers containing varying concentrations of graphene powder.
    - Mechanical Properties: Young's Modulus varies with graphene concentration.
    - Chemical Composition: Polymers with addition of graphene.
    - Electrical Conductivity: Not specified.
    - Cellular Testing: Metabolic activity observed in bmMSCs.

3. **Embedded PPy-PCL Scaffolds-Chapter 4**:

    - Manufactured with PCL fibers containing polypyrrole (PPy) powder.
    - Mechanical Properties: Young's Modulus: 32.79 MPa, % Max Strain: 129.79, Max Stress: 3.32 MPa.
    - Chemical Composition: Polymers with addition of PPy.
    - Electrical Conductivity: Not specified.
    - Cellular Testing: Not conducted, but hydrophobicity was observed in tests.

4. ***In situ* PPy-PCL Scaffold-Chapter 5**:

    - Manufactured by *in situ* polymerization of PPy onto PCL fibers.
    - Mechanical Properties: Young's Modulus: 855.59 MPa, Max Stress: 47.96 MPa.
    - Chemical Composition: Polymers with addition of PPy.
    - Electrical Conductivity: 2.542 ± 0.139 mS/cm.
    - Cellular Testing: Metabolic activity observed in fibroblasts and bone marrow stem cells.

The selection of the most promising scaffold for CTE was conducted using a weighted scoring table, which is presented in *Table 6 - 1*. The selection criteria, previously discussed, were applied to four chosen scaffolds. Based on the bibliometric study's keyword findings, each criterion was assigned a significance level ranging from one to eight, with eight being the most critical and one the least. This ranking of each criterion's importance is noted in the table.

Subsequently, each scaffold was rated against these criteria on a scale from one to five, with five indicating superior properties compared to the others, and one representing the lowest score. These ratings for each scaffold are listed in the following four columns of the table. The score for each scaffold is then calculated by multiplying the significance level of each criterion by the given rating. The cumulative score for each scaffold, indicating its overall suitability for CTE applications, is shown in the last row of their respective columns.

In this table, each scaffold has been evaluated according to the established criteria, with a rating assigned for each. The total score is then calculated by multiplying the importance of each criterion by the corresponding rating and summing these values.

Table 6 - 1 Scaffold Selection Table.

Criterion	Importance	MLS 1	Embedded Graphene-PCL	Embedded PPy-PCL	*In situ* PPy-PCL	MLS 1	Embedded Graphene-PCL	Embedded PPy-PCL	*In situ* PPy-PCL
1. Chemical Composition	3	3	3	4	4	9	9	12	12
2. Anisotropy	4	4	4	2	3	16	16	8	12
3. Biocompatibility	8	2	3	2	4	16	24	16	32
4. Wettability	2	1	1	1	4	2	2	2	8
5. Electrical Conductivity	6	1	3	2	5	6	18	12	30
6. Mechanical Properties	7	3	4	3	2	21	28	21	14
7. Manipulability	1	2	3	1	4	2	3	1	4
		Total				**72**	**100**	**72**	**112**

Based on this assessment, the "*In situ* PPy-PCL" scaffold obtains the highest total score, making it the preferred choice according to these specific criteria. The comprehensive evaluation underscores the "*In situ* PPy-PCL" scaffold's strengths in key areas crucial for myocardial tissue engineering, particularly its biocompatibility, electrical conductivity, and wettability. While it shows areas for improvement, notably in anisotropy, its overall performance aligns with the goal of achieving effective, theoretically, electromechanical coupling with myocardial tissue. Future work could focus

on optimizing fiber alignment to enhance anisotropy without compromising the scaffold's existing advantages, paving the way for its application in CTE.

6.2 Conclusions

In synthesizing the extensive research and development efforts detailed in this thesis, we arrive at a pivotal juncture in the field of CTE. The journey undertaken in this work aimed to illuminate the path toward designing scaffold materials that not only match but potentially exceed the native properties required for effective myocardial tissue regeneration. Herein, we encapsulate the essence of our findings, integrating the insights gained from each chapter to construct a coherent narrative of progress and potential.

Graphene's Role in Scaffold Enhancement

Our exploration into the realm of conductive nanofillers began with the investigation of graphene, a material renowned for its exceptional mechanical, electrical, and thermal properties. The incorporation of graphene into polymeric nanofibers, as detailed in our studies, significantly improved the scaffolds' morphological, and mechanical properties. This enhancement is particularly critical in the context of CTE, where the establishment of adequate electromechanical coupling is paramount. Our findings underscore graphene's potential to serve as a pivotal component in the development of next-generation scaffolds, capable of supporting the complex requirements of myocardial tissue regeneration.

Polypyrrole Integration

The integration of polypyrrole (PPy), another conductive polymer, into polymeric scaffolds represented a further step toward achieving scaffolds with enhanced electrical properties. While challenges related to the dispersion of PPy particles and scaffold uniformity were encountered, the pursuit of *in situ* polymerization techniques emerged as a promising strategy to optimize the electrical and mechanical properties of the PPy-PCL scaffolds. This methodological shift not only addressed the encountered obstacles but also highlighted the potential for creating scaffolds with superior functionalities for biomedical applications.

Optimization of Scaffold Properties

The culmination of our research efforts was marked by the optimization of the PPy polymerization process within PCL fibers, which led to scaffolds exhibiting markedly high electrical conductivity and improved mechanical properties. These advancements are critical for applications that require bioelectrical integration, such as myocardial or neuronal regeneration. Our optimized scaffolds

demonstrated the potential to provide a conducive environment for cell adhesion, proliferation, and differentiation, essential factors for successful TE.

The collective insights gleaned from this thesis elucidate the significant potential of conductive nanofillers, specifically graphene and polypyrrole, in enhancing the properties of polymeric scaffolds for CTE. While the journey has unveiled promising strategies and materials, it also lays bare the complexity of mimicking the native myocardial environment. The optimized scaffold, characterized by its electrical conductivity, mechanical strength, and biocompatibility, stands as a testament to the feasibility of this endeavor.

6.3 Future directions

As we look toward the future, it is evident that while significant strides have been made in the field of CTE, considerable work remains to refine scaffold properties further and enhance their functionality for clinical applications. The journey chronicled in this thesis, from conceptualization to optimization of scaffold design, underscores the dynamic and evolving nature of this research area. The following directions are proposed to guide future investigations:

Improving Particle Dispersion: Achieving a uniform dispersion of nanoparticles within polymeric matrices for electrospinning remains a persistent challenge not only in this field but other as well. Future studies should focus on innovative mixing techniques or chemical modifications to enhance the compatibility and distribution of conductive particles within the scaffold matrix, thereby optimizing their electrical and mechanical properties.

Incorporating Natural Polymers: Exploring the integration of natural polymers into scaffold formulations could offer a promising avenue to modulate scaffold stiffness and enhance biocompatibility. By blending synthetic and natural polymers, it may be possible to create scaffolds with tunable properties that better mimic the natural myocardial environment, facilitating improved cell adhesion and function.

Adding Biochemical Signals: Introducing biochemical cues, such as growth factors or cell-adhesion molecules, onto scaffold fibers or within the conductive particles themselves could significantly influence cell-scaffold interactions. Such biochemical modifications have the potential to direct cell behavior more effectively, promoting targeted adhesion, proliferation, and maturation of cardiac cells.

Evaluating Different Cell Types: The specific requirements of different cell types for adhesion, proliferation, and maturation necessitate a tailored approach to scaffold design. Future research

should consider the unique preferences of various cardiac cells, including cardiomyocytes, fibroblasts, and stem cells, to optimize scaffold compositions for diverse cellular environments.

Continued Challenges: The challenges discussed throughout this thesis, including optimizing fabrication processes and material composition, remain at the forefront of the field. Persistent efforts to address these challenges are crucial for advancing scaffold technology and realizing its full potential in Regenerative Medicine.

In Vivo Testing: A critical next step is the translation of scaffold technologies to *in vivo* models. Conceptual designs for *in vivo* studies, as proposed for future postdoctoral research, are essential for assessing the scaffolds' efficacy, biocompatibility, and integration within the myocardial tissue. Despite the plethora of materials and scaffolds developed globally, the scarcity of *in vivo* testing represents a significant barrier to clinical translation. Bridging this gap will be instrumental in moving from laboratory research to human clinical trials.

A. Annex: Conceptual Desing: Assessment and Ethical Considerations of *In Vivo* Electromechanical Coupling in Myocardial Tissue Using Conductive Polymeric Nanofiber

The results presented in this chapter are part of a comprehensive procedure approved by the Bioethics Committee. This a conceptual design for this thesis.

Authors:

Ana M. Muñoz-Gonzalez[a], Dianney Clavijo-Grimaldo[a,b,*], Vladimir Galindo Zamora[c]

[a]Universidad Nacional de Colombia, Carrera 45 # 26 – 85, Bogotá Colombia.
[b]Fundación Universitaria Sanitas, Calle 22B # 66-46, Bogotá Colombia.
[c] Faculty of Veterinary Medicine, Universidad Nacional de Colombia, Carrera 45 # 26 – 85, Bogotá Colombia.

Statement of contribution of co-authors:

Ana M Muñoz-Gonzalez	Writing and Research of Conceptual Design
Dianney Clavijo-Grimaldo	Approval and Contributions to the Methodology. Management for the Approval of the Bioethics Committee
Vladimir Galindo Zamora	Approval and Methodology of the Experiment

Introduction

This chapter presents a comprehensive conceptual design for a study aimed at investigating the electromechanical coupling of *in vivo* conductive scaffolds in myocardial tissue. The concept design explores the potential of *in vivo* trials using sheep models, selected for their physiological similarities to human cardiac systems, to assess the efficacy of these scaffolds in myocardial regeneration and their capability to integrate electromechanically with the host's myocardial electrical system.

While the design and methodology are thoroughly developed, encompassing pre-surgical protocols, surgical procedures, and post-operative care, the actual execution of the study remains pending. This is due to a combination of technical, temporal, and financial constraints that have prevented the realization of the *in vivo* experiments.

Despite the lack of practical implementation, this concept design stands as a significant theoretical contribution to the field. It offers a well-structured framework for future studies and lays the groundwork for potential breakthroughs in treating cardiac pathologies. The study's objective to evaluate the electromechanical integration of conductive scaffolds in myocardial tissue holds promise for improving the treatment and quality of life for patients with CVDs, marking a step forward in the realm of cardiac health and TE.

By presenting this conceptual design, the chapter not only addresses a critical gap in cardiac therapy but also sets a precedent for future research endeavors, paving the way for advancements in CTE and Regenerative Medicine.

Justification and Objectives

An estimated 17.9 million people die annually from CVDs, representing approximately 31% of all global deaths. In the United States, projections indicate that by 2035, 46.1% of the population will be affected by some form of CVD, potentially incurring healthcare costs of around 1.1 trillion dollars (Qasim, Arunkumar, Powell, & Khan, 2019).

The situation in Colombia mirrors this trend. According to the latest Vital Statistics from DANE, the leading cause of death is cardiac ischemia, accounting for 17.1% of fatalities (Dane, 2018). This condition involves a partial obstruction of blood flow in the coronary arteries and is marked by ionic and biochemical changes, which can culminate in a heart attack or death. The heart's capacity for regeneration is limited (Kazu Kikuchi & Poss, 2008), and typically, infarcted areas are replaced with non-contractile fibrotic scar tissue, which is rigid and electrically inactive. This forms an unstable electrical substrate that isolates cardiomyocytes and blocks electrical conduction, potentially leading

to arrhythmias (Ghuran & Camm, 2001; Solazzo, O'Brien, Nicolosi, & Monaghan, 2019; Tortora & Derrickson, 2006). Cardiac arrhythmias are a common clinical problem, encompassing rhythm disorders such as sinoatrial (SA) node dysfunction and atrioventricular (AV) conduction abnormalities.

In a cardiac infarction, up to nearly a million cardiomyocytes can be lost (Qasim et al., 2019), leading to death or heart failure. Traditionally, this has been managed clinically using medications that increase myocyte contractility and/or reduce myocardial oxygen consumption, depending on the patient's condition and comorbidities. However, none of these alternatives have proven to enhance the scant regeneration of the tissue. In this regard, TE aims to offer promising solutions to improve the quality of life.

TE essentially utilizes three components: scaffolds (frameworks mimicking the extracellular matrix), cells, and a chemical environment (hormones, growth factors, etc.). *In vitro* TE is conducted entirely in the laboratory: the scaffold is fabricated, autologous cells are seeded onto it, and a conducive environment is maintained. Given the challenge of replicating the biological chemical environment, the current trend is in vivo TE, which involves implanting scaffolds at the site of pathology. Here, cells migrate from the edges of the lesion and, in the natural chemical environment, differentiate and divide, promoting regeneration. However, some biomaterials used in scaffolds developed so far have exhibited limitations such as the lack of electromechanical coupling between adjacent cells, due to a mismatch in the physicochemical properties of the material, insufficient tissue regeneration, inappropriate mechanical properties, poor replication of an anisotropic structure, and primarily, lack of electrical conductivity.

Given that the implanted scaffold must be evaluated in terms of cell migration at the edge of the lesion (infarct) and the subsequent electro-mechanical coupling, *in vivo* evaluation using an animal model already approved and recognized by the scientific community as a preclinical study is imperative. In these models, cardiac ischemia is first induced in the species, followed by infarct, and then the scaffold is implanted to assess the degree of recovery of heart function compared to the initial condition. In this proposal, the use of a scaffold of conductive nanofibers will generate contributions in the understanding and development of new approaches in the comprehension, prediction, and subsequent treatment and improvement of cardiac pathologies, particularly heart failure. This will enable the research results to guide their application in human myocardial tissue.

In vitro trials in studies like this do not meet the objectives set out in the present project, as the *in vitro* approach is reductionist (Lindsey et al., 2018). The viability of cardiomyocytes cannot predict changes in the infarcted area as effectively as *in vivo* trials. Furthermore, cultivating adult cardiomyocytes presents a significant technical challenge; it is costly, observations and analyses,

especially of the electromechanical coupling sought in this project, are limited (Chorro & López-merino, 2009; Qasim et al., 2019; Tsui et al., 2019). Another *in vitro* evaluation method for similar biomaterials involves studying proteins involved in establishing cellular contacts identified through histological studies; however, quantifying molecules cannot be considered evidence of electromechanical coupling with myocardial tissue involved in conducting action potentials throughout the cardiac muscle and its influence on heart function as an organ (Zhou et al., 2014).

On the other hand, the use of mathematical models requires experimental data from *in vivo* trials as input. Such solutions, therefore, require a significant number of animals, which contradicts the 3Rs principle of animal experimentation. To study the sought-after electromechanical integration with the intended implant, a complex mathematical model accounting for a wide variety of variables would be required. Moreover, most models related to heart disease (e.g., finite element models) focus on studying the left ventricle because it is under the greatest stress (higher pressures) and thus more prone to failure (Heikhmakhtiar & Lim, 2018).

There are computational models that have succeeded in simulating the behavior of the left ventricle, some simulate both ventricles with a greater degree of difficulty, but there are no recognized models that can simulate the behavior of the entire heart with all four cardiac chambers (Baillargeon et al., 2014; Sack et al., 2016). Given this, such an alternative method would not be suitable, as the control and disease variables would be diverse, and a reliable real approximation could not be achieved, considering that the project's objective is to evaluate electromechanical integration as a system in myocardial tissue.

In conclusion, considering the objectives and approaches of the research, an *in vivo* case study becomes necessary. The central challenge of this trial is to evaluate the electromechanical integration capability of innovative scaffolds, specifically designed for myocardial tissue regeneration. Beyond generating spontaneous contraction, the aim is to determine whether the fabricated scaffold, once implanted, achieves effective connection with the host's myocardial electrical system. This objective addresses one of the major challenges in TE and the use of biomaterials for cardiac regeneration: achieving proper electromechanical integration, which is essential for the complete restoration of cardiac tissue functionality (Vunjak-Novakovic et al., 2010). Through this study, we aim to provide an innovative solution that not only regenerates tissue but also harmoniously integrates with the electrical properties of the host's heart. This is a crucial step towards the effective treatment of cardiac diseases and improving the quality of life for patients.

Description of the Trial

Selection of the Animal Specie

For the assessment of the scaffold to be implanted, choosing the appropriate animal model is a significant factor. Among the animal models used in CTE are rodents, rabbits, dogs, pigs, and sheep, with the latter being the suggested species for this study.

Smaller models, such as rodents and rabbits, despite being more frequently used (Riehle & Bauersachs, 2019), present several limitations. These include the anatomical size of the heart and significant structural differences compared to the human system, making surgical manipulation during the procedure challenging (Zimmermann et al., 2002). Additionally, differences in heart rate, oxygen consumption, contractility, protein expression, and stem cell population render them less suitable for studies on electromechanical coupling and arrhythmia risk due to differences in electrical properties between rodent and human cells (Zaragoza et al., 2011). Furthermore, variations in inflammatory response and scar formation are critical in angiogenesis, host cell recruitment, and the overall regeneration process. High surgical and postsurgical mortality rates have also been reported in these models (Lindsey et al., 2018).

Conversely, larger animal models like pigs offer advantages such as the durability and functionality of the implanted scaffold, rapid growth, and coronary circulation and arterial anatomy very similar to humans. Moreover, the size of the infarcted areas can be predicted with high reliability due to their size (Rashid et al., 2004; Zaragoza et al., 2011). However, they are prone to arrhythmias and desynchronization under electrical stimuli (Diaz et al., 2016). Like the dog model, they have a much more extensive coronary collateral circulation than humans (Ikram et al., 1997), making the extent of myocardial damage and left ventricular recovery unpredictable (Rashid et al., 2004).

Sheep are considered in the literature as an excellent post-infarction model, as ischemic cardiomyopathy is very similar to that in humans (Diaz et al., 2016). Other advantages of this animal model include its anatomical size and body weight similar to humans (McMillen, 2001), and the reduction of early mortality since the coronary circulation is practically identical to humans (Ikram et al., 1997). The similarity of their heart valves in terms of mechanical properties and hemodynamic flow parameters to humans has already been studied (Rashid et al., 2004). Additionally, it is an animal model with a high recovery rate and allows frequent blood sampling in both short-term studies via intravascular catheters and long-term studies via isolated loops of the carotid artery (McMillen, 2001). Also, the contractile and relaxation kinetics of sheep cardiomyocytes are similar to those of human heart cells, with both showing a positive force-frequency relationship. Moreover, the resting heart rate in sheep (60–120 bpm), systolic pressure (~90–115 mmHg), and diastolic pressure (~100

mmHg) are relatively similar to average human values (70-100 bpm, 120 mmHg, and 80 mmHg, respectively) (Camacho et al., 2016).

Despite the notable advantages of sheep as an animal model, one of the limitations is the need for constant veterinary monitoring of vital functions during all surgical procedures (Sartoretto et al., 2016), and although their size is an advantage, it requires costly work and maintenance infrastructure (McMillen, 2001). Despite these limitations, this species meets the scientifically required animal model objective, as its advantages outweigh the limitations, which is why this animal model is suggested for the present study.

Species	Ovina (*Ovis orientalis aries)*
Raza/estirpe	Criolla
Sex	Male o Female
Age	6-7 months old
Body Size	Weight-based
Weight	50± 10 kg
Origin	Centro Agropecuario Marengo (UN)

Table A - 1 Characteristics of the animal species to be used.

Determination of the number of animals

To determine the number of animals and the surgical procedure to be performed, a review of the literature was conducted. Some of the articles are mentioned in *Table A - 2*, where it can be seen that the number of animals used is significant and open-chest techniques are commonly employed.

Animal Model	Number of Animals	Surgical Procedure	Number of Surviving Animals	Results	Reference
Pig	42	INFARCTION: Anterolateral free wall infarction of the left ventricle (LV) was induced by catheter embolization with collagen or gel spheres in the first or second diagonal branch of the left anterior descending coronary artery. SCAFFOLD IMPLANTATION: At 6 or 8 weeks, a 4-layer multilaminated extracellular matrix derived from the urinary bladder and expanded polytetrafluoroethylene (ePTFE) as a control were implanted.	0, Cardiotomy for tissue culture. 37 survived the infarction and implantation. 31 survived during rest. 15 survived after 3 days of surgery. 12 survived the fourth day.	One-week and one-month patches were intact with thrombosis and inflammation. At 3 months, the urinary bladder matrix was bioresorbed, and a collagen-rich vascularized tissue with numerous myofibroblasts was present. The ePTFE at 3 months had a foreign body response with necrosis and calcification. Flow cytometry showed urinary bladder matrix cells were	(Robinson et al., 2005)

				similar to normal myocardium, while ePTFE had limited cardiomyocyte markers.	
Pig	25	INFARCTION: 60-minute balloon catheter occlusion of the left circumflex artery. SCAFFOLD IMPLANTATION: After 2 weeks, biodegradable porous polyurethane PEUU was implanted. Animals with a risk area over 25% of the LV free wall were randomly assigned to PEUU patch placement (MI + PEUU) or sham surgery (MI + sham).	0, 7 (28%) deaths during the occlusion procedure. The final analysis included 7 animals in the MI + PEUU group and 8 in the MI sham group.	PEUU patch implantation prevented adverse left ventricular remodeling and cardiac functional loss over an 8-week period post-placement on an ischemia-reperfusion injury in a porcine model. The implanted PEUU patch partially degraded during this period. Cells marked similarly were observed under the patch, along with a significant increase in neovascularization and left ventricular wall thickening.	(Hashizume et al., 2013)
Pigs	4	INFARCTION: Ligation of the left anterior descending coronary artery (LAD) for 50 min. SCAFFOLD IMPLANTATION: Five minutes after LAD ligation, the patch was sutured in the ischemic area of the myocardium and secured with four 5.0 prolene stitches.	0, Three animals were sacrificed after 24 hours of the intervention and one after 3 months of follow-up. The first was used for setting up the surgical technique, testing the appropriate number of biopsy samples, and verifying ischemic areas post-procedure.	The primary finding is that gelatin/PLGA bilayer cardiac patch functionalization with adenosine allows targeted delivery to the ischemia-reperfused heart area, promoting several beneficial effects. Besides activating pro-survival signaling pathways, the adenosine functionalized patch seemingly promotes more pronounced cellularization at 24 hours of follow-up and a non-fibrotic outcome at 3 months of follow-up.	(Cristallini et al., 2019b)
Pigs	14	INFARCTION: Myocardial infarction (MI)	0, Four pigs died after the operation.	The success rate of patch implantation	(J. Cui et al., 2005)

		was created by embolizing the diagonal branch (DA) of the left anterior descending coronary artery with a collagen suspension. SCAFFOLD IMPLANTATION: After 4 to 6 weeks, 14 pigs received a patch implant (ECM or expanded polytetrafluoroethylene). Six pigs were infarcted in the first DA and seven pigs in the second DA.	After 1 month, 10 pigs were sacrificed, and the patch locations were examined.	in the second DA (85.7%) was higher than the first DA group (50%). The infarct size in the second DA was smaller than in the first DA (4.6 ± 1.2 vs. 10.8 ± 2.4 cm^2, P <.05). The second DA had a more anterior position, allowing easier access from the thoracotomy. However, the first DA was located more laterally and required more heart manipulation during surgery.	
Sheep	20	INFARCTION: Microembolization of the left coronary arteries with 0.5 ml of 90-micron polystyrene beads.	13	This ovine model mimics the hemodynamic and neurohumoral characteristics of acute myocardial infarction, resulting in left ventricular dysfunction, and should be suitable for studying interventions in various conditions.	(Ikram et al., 1997)
Sheep	55	INFARCTION: Myocardial infarction was induced by Gelfoam embolism through this catheter and confirmed by electrocardiographic (ECG) changes.	18 (15 met the objective, 3 underwent repeated embolizations)	Baseline EF was 68%, with a final average EF of 33%. This resulted in a 54% reduction in EF (range 44% to 68%) from baseline values. Two animals developed late symptomatic heart failure and died, while EF was stable at 3 months of follow-up echocardiography in the remaining animals without significant spontaneous improvement.	(Devlin et al., 2000)
Sheep	12	INFARCTION: Ligation of the main diagonal branch of the left anterior descending (LAD) coronary artery (i.e.,	12	Cyanotic discoloration and hypokinesia in cardiac tissue were detected immediately after	(Rabbani et al., 2008)

		homonymous artery in sheep).		vessel ligation. Pathological Q waves were present 2 months later. Echocardiographic evaluations showed an average relative decrease of 30% in cardiac ejection fraction. Wall motion analysis showed anteroseptal hypokinesia and akinesia at 1 day and 2 months post-operation, respectively. Thin-walled infarcted areas with tissue fibrosis were evident in pathological investigations 2 months post-surgery.	
Sheep	4	INFARCTION: Artery ligation. Ischemia-reperfusion model.	0, (1 case of intraoperative death due to ventricular fibrillation)	Ischemia for 90 minutes of the distal anterior descending artery beyond the origin of the second diagonal has been shown to generate a considerable and coincident infarct size by SPECT study and pathological anatomy.	(Dayan V, Benech A, Rodríguez C, Ado S, Guedes I, Sotelo V, Laguzzi F, Kapitán M, Langhain M, Ferrando R, 2011)
Pig	15	INFARCTION: Surgical coronary ligation versus coil embolization MI models.	15, sacrificed after 37 days.	Infarct size, scar fibrosis, inflammation, myocardial vascularization, and cardiac function were assessed by magnetic resonance imaging (MRI).	(Gálvez-Montón et al., 2014)

Table A - 2 Large Animal Models for Myocardial Infarction.

Experimental procedure

In *Figure A - 1*, the flow diagram of the experimental design is depicted in spanish, which includes the procedures to be carried out in the animal model.

Highlighted in blue is the pre-surgical care protocol, beginning with an initial electrocardiogram and echocardiogram. Sedation will be performed for cleaning and hair trimming in the areas of interest, followed by intravenous anesthetic induction.

The boxes highlighted in pink display the surgical procedure according to the protocol mentioned (Rabbani et al., 2008), which includes:

- Intubation and maintenance with inhaled anesthesia.
- Continuous electrocardiogram monitoring throughout the procedure.
- Administration of anticholinergic and antibiotic.
- Performing a 15-20 cm long left lateral thoracotomy incision through the fourth intercostal space.
- Administering lidocaine as an intravenous bolus dose before ligating the diagonal branch (2 mg/kg) and 15-20 minutes afterwards (1 mg/kg) for antiarrhythmic prophylaxis.
- Ligation of the main diagonal branch (i.e., the second branch of the right LAD coronary artery): tied using a curved round needle and 6-0 prolene suture approximately 40% from its base.
- Clinical and electrocardiographic confirmation of myocardial changes: cyanosis of cardiac tissue and ventricular hypokinesia, ST segment and Q wave changes in ECG.
- Maintenance of surgical conditions for 60 minutes.
- Implantation of the scaffold in the infarcted area.
- Closing the thoracotomy (pericardium with 5-0 prolene, muscles and skin with 2-0 Vicryl sutures) and placement of a chest tube.

The boxes highlighted in lilac show the post-surgical management of the animals:

- Pain management with Butorphanol 0.1 mg/kg + Flunixin meglumine 1.1 mg/kg every 12 hours for 48 hours.
- Hospitalization in the animal intensive care unit for 24 hours post-surgery.
- Hospitalization in the clinic as per each patient's needs for post-surgical care (monitoring for signs of pain and infection, daily dressing change, etc).
- Once the animals are discharged, their follow-up continues (boxes highlighted in green):
- Housing in the Vivarium with daily clinical monitoring and electrocardiographic and echocardiographic control every two weeks.
- Eight weeks after the surgical procedure, the final stages of the experimental design are carried out (boxes highlighted in yellow):
- Euthanasia.
- Autopsy and heart extraction.

- Histological study of the myocardium in the infarcted area, the edges of the lesion, and at the biomaterial (scaffold)-tissue interface.
- Final disposition of the animal.

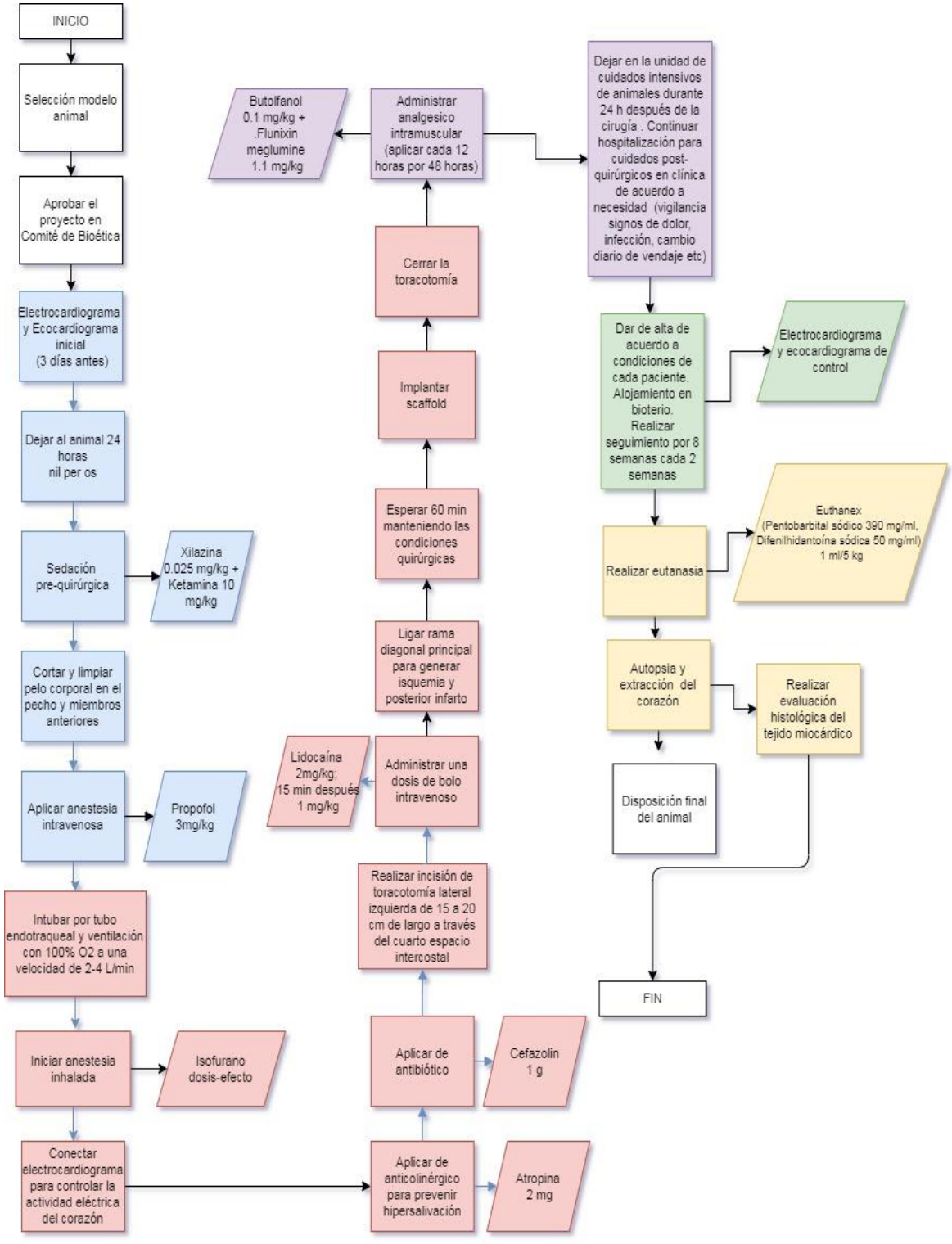

Figure A - 1 Experimental Design Flowchart.

Animal Pain Relief

Pain management will be conducted during and after the surgical procedure with Butorphanol 0.1 mg/kg + Flunixin meglumine 1.1 mg/kg every 12 hours for 48 hours.

The need for additional analgesia will be determined based on the following considerations:

Generally, signs of pain in sheep and goats are similar to those in cattle. Changes in posture and movement are often evident, and a change in facial expression can be observed. There is a general reluctance to move. Goats are more likely than cattle to vocalize in response to pain. Teeth grinding and grunting sounds are also heard (National Research Council., 1992). Animals in pain display reliable, albeit sometimes very subtle, signs of distress. A recently developed Sheep Pain Facial Expression Scale (SPFES) can help handlers to accurately and objectively assess the degree of pain an animal is experiencing. The SPFES was developed using animals with mastitis and foot rot; however, the expressions identified are common to other conditions that cause pain and distress in sheep (AWIN et al., 2014; Manteca et al., 2017; Nostril & Lip, n.d.).

The SPFES includes five features, each scored as 0 (not present), 1 (partially present), or 2 (present). These features are:

● Orbital tightening: there is closure of the palpebral fissure by the eyelids and a narrowing of the eye opening.
● Cheek flattening: there is a more convex shape of the cheek in the area of the masseter muscle.
● Abnormal ear posture: the ears rotate completely ventrally and caudally.
● Abnormal lip and jaw profile: the jaw profile appears straight to concave.
● Abnormal nasal bridge and crease: there is a "V" shape between the openings of the nostrils.

Each area is scored separately, with the total from the five areas combined for an overall 'pain score.' The maximum possible score is 10 (i.e., the assessment of each feature scores '2'). Researchers who developed the SPFES considered a score of 5 or more to justify the consideration of the use of analgesics.

When observing the sheep, it's necessary to view the face from both a lateral and frontal view to properly assess each area. The assessment should not be performed while the animal is chewing or has food in its mouth.

Figure A - 2 Lateral view (left) and frontal view of a sheep (right).

- Orbital Tightening: Observe the shape of the eye, the muscles around the eye, and how much the upper eyelid is closed.
- Cheek Stretching: Observe the area of the cheek muscle used for chewing food, differentiating it from the process of clenching with a food bolus in the mouth. When there is tension, the muscle that runs from the corner of the mouth area along the jawline up to the cheekbone is more prominent. There may also be tension from the cheek to the ear along the edge of the eye.
- Abnormal Ear Posture: Normally, the ears are held upright, and the inner part of the ear is visible when viewed from the front. As the position becomes abnormal, the ears droop and turn towards the face, so the inner part of the ear is not visible. The ear may be held in a backward position. The normal ear position will vary depending on the breed; however, the changes that occur are the same for all breeds.
- Abnormal Lip and Jaw Profile: Normally, the corner of the mouth turns slightly upwards. The lips flatten as tension increases, reducing the "smile" characteristic. The chin and jawline are rounded when there is no tension. The line becomes straighter and curved inward (concave) when there is clenching.
- Abnormal Nasal Bridge and Crease: Normally, there is a shallow "U" shape between the nostrils' openings. The surrounding muzzle follows this "U" shape. As the position becomes abnormal, the area between the nostrils (and surrounding muzzle) increasingly appears in a "V" shape.

Regular animal monitoring

Regular monitoring of the sheep should begin from the initial signs of a change in facial expression within at least one of the five areas. Observations should be made as discreetly as possible to avoid "masking" the pain and should be repeated every half hour. Observations should last a few minutes to monitor the fluctuating nature of pain (Krista McLennan, n.d.).

To keep a record of the animal's follow-up, a format will be maintained with the information shown below:

Fecha hora	Identificación Oveja	Puntaje total		Detalles del alivio del dolor proporcionado	Otros comportamientos destacables	Signos de enfermedad
		Estrechamiento orbitario				
		Estiramiento de las mejillas				
		Postura anormal de la oreja				
		Perfil anormal de labios y mandíbulas				
		Fosa y surco nasales anormales				
		TOTAL				

If pain relief is provided, the facial expression score should be recorded before treatment and again 12-24 hours later to assess the effectiveness of the treatment. Additional treatment may be required, and the facial expression should be re-evaluated.

If a sheep scores above 5 on the pain scale, considering pain relief is recommended. If analgesics are administered, the animal will be monitored in the following hours to assess effectiveness. The facial expression is re-evaluated 24 hours later. If the score is greater than 6 points, the points described in the 'Experiment Endpoint Criteria' will be considered for euthanasia.

Experiment Endpoint Criterion and Euthanasia

At this point, the symptoms identified in the previous section and the following are considered (National Farm Animal Care Council, 2013):

- Weak, unable to stand
- Unable to eat or drink
- Severe injury
- Broken leg with exposed bone
- Exposed internal organs
- Moderate to severe lameness
- Severe body weight loss (20% or more)

Failure in pain management according to the protocol mentioned in the previous point.

Approved method of euthanasia to be used

Euthanasia will be performed on the animal with Euthanex (Pentobarbital sodium 390 mg/ml, Diphenylhydantoin sodium 50 mg/ml) at a dose of 1 ml/5 kg, followed by necropsy.

Final disposition of experimental animals

This will be carried out according to protocols established by the Universidad Nacional de Colombia with the contracted company (Ecocapital).

Maintenance conditions of the animals

Do they require confinement? Yes

Where and how will they be housed? Sufficient floor space is required so that all the sheep can lie down at the same time in a normal resting posture, adjust their position, move freely, and find a comfortable place to rest and ruminate.

It must be ensured that the sheep have sufficient access to food (including salt and minerals) and water of adequate quality and quantity to meet their nutritional and physiological needs.

Do they require special housing? No

Environmental conditions (temperature, humidity, lighting, noise, odors, equipment of the housing premises): In confinement, ventilation systems that ensure adequate airflow to avoid excessive heat are necessary to minimize the risk of heat stress. Sheep should be provided a proper rest period without artificial light (e.g., 6 hours) but should not be kept in permanent darkness.

Sheep should not be housed on solid concrete floors without providing adequate bedding. Various materials can be used as bedding for sheep, such as straw, wood shavings, paper products, peat, and hemp.

Ethical aspects

Regarding the ethical aspects of this *in vivo* trial, the complete procedure outlined above was submitted to the Bioethics Committee of the Faculty of Veterinary Medicine and Zootechnics at the Universidad Nacional de Colombia. In a regular session, and in accordance with the Minutes 1 of 2021, approval was granted for the project under the name: “Nanofibras poliméricas conductoras: fabricación, caracterización y evaluación del acople electromecánico en tejido miocárdiaco” as can be seen in the *Figure A - 3*.

Comité de Bioética
Facultad de Medicina Veterinaria y de Zootécnia
Sede Bogotá

UNIVERSIDAD NACIONAL DE COLOMBIA

Bogotá D.C, febrero 3 de 2021 **[CB-FMVZ-UN-003-2021]**

Doctores
DIANNEY CLAVIJO GRIMALDO
VLADIMIR GALINDO ZAMORA
Investigadores principales

Respetados doctores:

Amablemente les comunico que el Comité de Bioética en sesión ordinaria, Acta 01 de 2021, luego de la revisión de la documentación al siguiente proyecto, acordó emitir el respectivo concepto, así:

Proyecto	**"Nanofibras poliméricas conductoras: fabricación, caracterización y evaluación del acople electromecánico en tejido miocárdiaco"**
Responsables del proyecto	Investigadores Principales: Dianney Clavijo Grimaldo-Vladimir Galindo Zamora Estudiante: ANA MARIA MUÑOZ GONZALEZ / Doctorado en Ingeniería – Ciencia y Tecnología de Materiales
Concepto	**AVALADO**

Es importante tener en cuenta que **este concepto sólo aplica para los procedimientos en las condiciones y con las características indicadas en el formato final y documentos presentados**. El investigador deberá informar sobre cualquier cambio que se proponga incluir y que esté relacionado con la ubicación, el cuidado y bienestar de los animales, estas modificaciones no podrán ejecutarse sin el aval previo del Comité; así mismo, se debe dar aviso sobre cualquier situación imprevista que se considere implique algún riesgo para los animales o la comunidad o el medio en el cual se lleva a cabo el estudio.

Cordialmente,

LUCÍA BOTERO ESPINOSA
Coordinadora Comité de Bioética

[Página **1** de 1]
Elaboró: Diana M Cendales

Carrera 30 No. 45-03. Ciudad Universitaria.
Edificio 561B, piso 2, oficina 22
Teléfono directo: 57-1-3165693 | Conmutador: 57-1-3165000 Ext. 19469
Email: comibio_fmvzbog@unal.edu.co
Bogotá D.C., Colombia

Patrimonio de todos los colombianos

Figure A - 3 Letter of endorsement Ethics Committee.

References

Abbasi, A. M. R., Marsalkova, M., & Militky, J. (2013). Conductometry and Size Characterization of Polypyrrole Nanoparticles Produced by Ball Milling. *Journal of Nanoparticles*, *2013*, 1–4. https://doi.org/10.1155/2013/690407

Abdul Rahman, N., & Bahruji, H. (2022). Plastics in Biomedical Application. In M. S. J. Hashmi (Ed.), *Encyclopedia of Materials: Plastics and Polymers* (pp. 114–125). Elsevier. https://doi.org/https://doi.org/10.1016/B978-0-12-820352-1.00071-7

Adadi, N., Yadid, M., Gal, I., Asulin, M., Feiner, R., Edri, R., & Dvir, T. (2020). Electrospun Fibrous PVDF-TrFe Scaffolds for Cardiac Tissue Engineering, Differentiation, and Maturation. *Advanced Materials Technologies*, *5*(3), 1–11. https://doi.org/10.1002/admt.201900820

Agrawal, R., Shah, J., Gupta, G., Srivastava, R., Sharma, C., & Kotnala, R. (2020). Significantly high electromagnetic shielding effectiveness in polypyrrole synthesized by eco-friendly and cost-effective technique. *Journal of Applied Polymer Science*, *137*(48), 1–12. https://doi.org/10.1002/app.49566

Ahadian, S., Zhou, Y., Yamada, S., Estili, M., Liang, X., Nakajima, K., Shiku, H., & Matsue, T. (2016). Graphene induces spontaneous cardiac differentiation in embryoid bodies. *Nanoscale*, *8*(13), 7075–7084. https://doi.org/10.1039/c5nr07059g

Ajith, G., Tamilarasi, G. P., Sabarees, G., Gouthaman, S., Manikandan, K., Velmurugan, V., Alagarsamy, V., & Solomon, V. R. (2023). Recent Developments in Electrospun Nanofibers as Delivery of Phytoconstituents for Wound Healing. *Drugs and Drug Candidates*, *2*(1), 148–171. https://doi.org/10.3390/ddc2010010

Al-Abduljabbar, A., & Farooq, I. (2023). Electrospun Polymer Nanofibers: Processing, Properties, and Applications. *Polymers*, *15*(1). https://doi.org/10.3390/polym15010065

Alcon, A., Cagavi Bozkulak, E., & Qyang, Y. (2012). Regenerating functional heart tissue for myocardial repair. *Cellular and Molecular Life Sciences*, *69*(16), 2635–2656. https://doi.org/10.1007/s00018-012-0942-4

Alegret, N., Dominguez-Alfaro, A., & Mecerreyes, D. (2019). 3D Scaffolds Based on Conductive Polymers for Biomedical Applications. *Biomacromolecules*, *20*(1), 73–89. https://doi.org/10.1021/acs.biomac.8b01382

Alexeev, D., Goedecke, N., Snedeker, J., & Ferguson, S. (2020). Mechanical evaluation of electrospun poly (ε -caprolactone) single fi bers. *Materials Today Communications*, *24*(April),

101211. https://doi.org/10.1016/j.mtcomm.2020.101211

Amariei, N., Manea, L. R., Bertea, A. P., Bertea, A., & Popa, A. (2017). The Influence of Polymer Solution on the Properties of Electrospun 3D Nanostructures. *IOP Conference Series: Materials Science and Engineering*, *209*(1). https://doi.org/10.1088/1757-899X/209/1/012092

Amaya, J. B. (2018). Estudio De La Degradabilidad Del Pcl (Policaprolactona) Dosificado Con La Lignina De La Fibra De Banano. *Revista Iberoamericana de Polimeros y MAteriales*, *19*(4), 128–141.

Ansari, R. (2006). Polypyrrole Conducting Electroactive Polymers: Synthesis and Stability Studies. *E-Journal of Chemistry*, *3*(4), 186–201. https://doi.org/10.1155/2006/860413

Arakawa, C. K., & DeForest, C. A. (2017). *Chapter 19 - Polymer Design and Development* (A. Vishwakarma & J. M. B. T.-B. and E. of S. C. N. Karp (eds.); pp. 295–314). Academic Press. https://doi.org/https://doi.org/10.1016/B978-0-12-802734-9.00019-6

Asri, N. A. N., Mahat, M. M., Zakaria, A., Safian, M. F., & Abd Hamid, U. M. (2022). Fabrication Methods of Electroactive Scaffold-Based Conducting Polymers for Tissue Engineering Application: A Review. *Frontiers in Bioengineering and Biotechnology*, *10*(July), 1–13. https://doi.org/10.3389/fbioe.2022.876696

Avouris, P., & Dimitrakopoulos, C. (2012). Graphene: synthesis and applications. *Materials Today*, *15*(3), 86–97. https://doi.org/https://doi.org/10.1016/S1369-7021(12)70044-5

AWIN, Mclennan, K. M., Rebelo, C. J. R., Corke, M. J., Holmes, M. A., & Constantino-Casas. (2014). *Using facial expression to assess pain in sheep*. *9*, 92281.

Aziz, R., Falanga, M., Purenovic, J., Mancini, S., Lamberti, P., & Guida, M. (2023). A Review on the Applications of Natural Biodegradable Nano Polymers in Cardiac Tissue Engineering. *Nanomaterials*, *13*(8), 1–28. https://doi.org/10.3390/nano13081374

Baei, P., Jalili-Firoozinezhad, S., Rajabi-Zeleti, S., Tafazzoli-Shadpour, M., Baharvand, H., & Aghdami, N. (2016). Electrically conductive gold nanoparticle-chitosan thermosensitive hydrogels for cardiac tissue engineering. *Materials Science and Engineering C*, *63*, 131–141. https://doi.org/10.1016/j.msec.2016.02.056

Bagbi, Y., Pandey, A., & Solanki, P. R. (2019). Chapter 10 - Electrospun Nanofibrous Filtration Membranes for Heavy Metals and Dye Removal. In S. Thomas, D. Pasquini, S.-Y. Leu, & D. A. Gopakumar (Eds.), *Nanoscale Materials in Water Purification* (pp. 275–288). Elsevier. https://doi.org/https://doi.org/10.1016/B978-0-12-813926-4.00015-X

Bagheri, M., & Mahmoodzadeh, A. (2020). Polycaprolactone/Graphene Nanocomposites: Synthesis, Characterization and Mechanical Properties of Electrospun Nanofibers. *Journal of Inorganic and Organometallic Polymers and Materials*, *30*(5), 1566–1577. https://doi.org/10.1007/s10904-019-01340-8

Bahrami, S., Solouk, A., Mirzadeh, H., & Seifalian, A. M. (2019). Electroconductive polyurethane/graphene nanocomposite for biomedical applications. *Composites Part B:*

Engineering, *168*(March), 421–431. https://doi.org/10.1016/j.compositesb.2019.03.044

Baillargeon, B., Rebelo, N., Fox, D. D., Taylor, R. L., & Kuhl, E. (2014). The Living Heart Project: A robust and integrative simulator for human heart function. *European Journal of Mechanics. A, Solids*, *48*, 38–47. https://doi.org/10.1016/j.euromechsol.2014.04.001

Baker, S. R., Banerjee, S., Bonin, K., & Guthold, M. (2016). Determining the mechanical properties of electrospun poly-ε-caprolactone (PCL) nanofibers using AFM and a novel fiber anchoring technique. *Materials Science and Engineering C*, *59*, 203–212. https://doi.org/10.1016/j.msec.2015.09.102

Balint, R., Cassidy, N. J., & Cartmell, S. H. (2014). Conductive polymers: Towards a smart biomaterial for tissue engineering. *Acta Biomaterialia*, *10*(6), 2341–2353. https://doi.org/10.1016/j.actbio.2014.02.015

Barba Evia, J. R. (2009). Cardiomioplastia: El papel de las células madre en la regeneración miocárdica. *Revista Latinoamericana de Patología Clínica y Medicina de Laboratorio*, *56*(1), 50–65.

Bejaoui, M., Galai, H., Touati, F., & Kouass, S. (2021). Multifunctional Roles of PVP as a Versatile Biomaterial in Solid State. In U. Ahmad (Ed.), *Dosage Forms*. IntechOpen. https://doi.org/10.5772/intechopen.99431

Bellet, P., Gasparotto, M., Pressi, S., Fortunato, A., Scapin, G., Mba, M., Menna, E., & Filippini, F. (2021). *Graphene-Based Scaffolds for Regenerative Medicine*.

Beltran-Vargas, N. E., Peña-Mercado, E., Sánchez-Gómez, C., Garcia-Lorenzana, M., Ruiz, J. C., Arroyo-Maya, I., Huerta-Yepez, S., & Campos-Terán, J. (2022). Sodium Alginate/Chitosan Scaffolds for Cardiac Tissue Engineering: The Influence of Its Three-Dimensional Material Preparation and the Use of Gold Nanoparticles. *Polymers*, *14*(16). https://doi.org/10.3390/polym14163233

Bertuoli, P. T., Ordono, J., Armelin, E., Pérez-Amodio, S., Baldissera, A. F., Ferreira, C. A., Puiggalí, J., Engel, E., Del Valle, L. J., & Alemán, C. (2019). Electrospun Conducting and Biocompatible Uniaxial and Core-Shell Fibers Having Poly(lactic acid), Poly(ethylene glycol), and Polyaniline for Cardiac Tissue Engineering. *ACS Omega*, *4*(2), 3660–3672. https://doi.org/10.1021/acsomega.8b03411

Biscaia, S., Silva, J. C., Moura, C., Viana, T., Tojeira, A., Mitchell, G. R., Pascoal-Faria, P., Ferreira, F. C., & Alves, N. (2022). Additive Manufactured Poly(ε-caprolactone)-graphene Scaffolds: Lamellar Crystal Orientation, Mechanical Properties and Biological Performance. *Polymers*, *14*(9). https://doi.org/10.3390/polym14091669

Blachowicz, T., & Ehrmann, A. (2020). Conductive electrospun nanofiber mats. *Materials*, *13*(1). https://doi.org/10.3390/ma13010152

Bolonduro, O. A., Duffy, B. M., Rao, A. A., Black, L. D., & Timko, B. P. (2020). From biomimicry to bioelectronics: Smart materials for cardiac tissue engineering. *Nano Research*, *12*(1). https://doi.org/10.1007/s12274-020-2682-3

Borges, M. H. R., Nagay, B. E., Costa, R. C., Souza, J. G. S., Mathew, M. T., & Barão, V. A. R. (2023). Recent advances of polypyrrole conducting polymer film for biomedical application: Toward a viable platform for cell-microbial interactions. In *Advances in Colloid and Interface Science* (Vol. 314, Issue February). https://doi.org/10.1016/j.cis.2023.102860

Boroumand, S., Haeri, A., Nazeri, N., & Rabbani, S. (2021). Review Insights In Cardiac Tissue Engineering: Cells, Scaffolds and Pharmacological Agents. *Iranian Journal of Pharmaceutical Research*, *20*(4), 467–496. https://doi.org/10.22037/IJPR.2021.114730.15012

Boutry, C. M., Müller, M., & Hierold, C. (2012). Junctions between metals and blends of conducting and biodegradable polymers (PLLA-PPy and PCL-PPy). *Materials Science and Engineering C*, *32*(6), 1610–1620. https://doi.org/10.1016/j.msec.2012.04.051

Bronzino, J. D. (2006). *Tissue Engineering and Artificial Organs (1st ed.)* (1st ed.). CRC Press. https://doi.org/https://doi.org/10.1201/9781420003871

Brugnara, M., Della Volpe, C., Siboni, S., & Zeni, D. (2006). Contact angle analysis on polymethylmethacrylate and commercial wax by using an environmental scanning electron microscope. *Scanning*, *28*(5), 267–273. https://doi.org/10.1002/sca.4950280504

Butt, H.-J., & Kappl, M. (2018). *Surface and Interfacial Forces*. Wiley VCH.

Camacho, P., Fan, H., Liu, Z., & He, J. Q. (2016). Small mammalian animal models of heart disease. *American Journal of Cardiovascular Disease*, *6*(3), 70–80. https://doi.org/10.3390/jcdd3040030

Camman, M., Joanne, P., Agbulut, O., & Hélary, C. (2022). 3D models of dilated cardiomyopathy: Shaping the chemical, physical and topographical properties of biomaterials to mimic the cardiac extracellular matrix. *Bioactive Materials*, *7*, 275–291. https://doi.org/10.1016/j.bioactmat.2021.05.040

Centers for Disease Control and Prevention. (2022). *Heart Disease Facts*. https://www.cdc.gov/heartdisease/facts.htm#print

Ceretti, E., Ginestra, P. S., Ghazinejad, M., Fiorentino, A., & Madou, M. (2017). Electrospinning and characterization of polymer–graphene powder scaffolds. *CIRP Annals - Manufacturing Technology*, *66*(1), 233–236. https://doi.org/10.1016/j.cirp.2017.04.122

Chakraborty, M. (2020). *Chitosan Biopolymer on Plant Growth. Encyclopedia*. https://encyclopedia.pub/entry/3639

Chang, W.-T., Chen, J.-S., Tsai, M.-H., Tsai, W.-C., Juang, J.-N., & Liu, P.-Y. (2016). Interplay of Aging and Hypertension in Cardiac Remodeling: A Mathematical Geometric Model. *PloS One*, *11*(12), e0168071. https://doi.org/10.1371/journal.pone.0168071

Chem, G., Thomas, M. S., Pillai, P. K. S., Farrowc, S. C., Pothan, L. A., & Thomas, S. (2021).

Electrospinning as an Important Tool for Fabrication of Nanofibers for Advanced Applications — a Brief Review. *Figure 1*, 1–7. https://doi.org/10.21127/yaoyigc20200022

Chen, C., Bai, X., Ding, Y., & Lee, I. S. (2019). Electrical stimulation as a novel tool for regulating cell behavior in tissue engineering. *Biomaterials Research*, *23*(1), 1–12. https://doi.org/10.1186/s40824-019-0176-8

Chen, Q., Xiao, S., Shi, S. Q., & Cai, L. (2020). Synthesis, Characterization, and Antibacterial Activity of N-substituted Quaternized Chitosan and Its Cellulose-based Composite Film. *BioResources*, *15*(1), 415.

Chen, X., Feng, B., Zhu, D. Q., Chen, Y. W., Ji, W., Ji, T. J., & Li, F. (2019). Characteristics and toxicity assessment of electrospun gelatin/PCL nanofibrous scaffold loaded with graphene *in vitro* and *in vivo*. *International Journal of Nanomedicine*, *14*, 3669–3678. https://doi.org/10.2147/IJN.S204971

Chiesa, E., Dorati, R., Pisani, S., Bruni, G., Rizzi, L. G., Conti, B., Modena, T., & Genta, I. (2020). Graphene nanoplatelets for the development of reinforced PLA-PCL electrospun fibers as the next-generation of biomedical mats. *Polymers*, *12*(6). https://doi.org/10.3390/polym12061390

Chorro, F. J., & López-merino, L. S. V. (2009). *Modelos animales de enfermedad cardiovascular*. *62*(I), 69–84.

Číková, E., Mičušík, M., Šišková, A., Procházka, M., Fedorko, P., & Omastová, M. (2018). Conducting electrospun polycaprolactone/polypyrrole fibers. *Synthetic Metals*, *235*(December 2017), 80–88. https://doi.org/10.1016/j.synthmet.2017.11.011

Clavijo-Grimaldo, D., Casadiego-Torrado, C. A., Villalobos-Elías, J., Ocampo-Páramo, A., & Torres-Parada, M. (2022). Characterization of Electrospun Poly(ε-caprolactone) Nano/Micro Fibrous Membrane as Scaffolds in Tissue Engineering: Effects of the Type of Collector Used. *Membranes*, *12*(6). https://doi.org/10.3390/membranes12060563

ClinicalTrials.gov. (2024). *ClinicalTrials.gov*. https://clinicaltrials.gov/search?term=scaffold&cond=Myocardial Infarction&city=

Cristallini, C., Barberis, R., Bellotti, E., Vaccari, G., Falzone, M., Cabiale, K., Perona, G., Rastaldo, R., Pascale, S., Pagliaro, P., & Giachino, C. (2019a). *Cardioprotection of PLGA / gelatine cardiac patches functionalised with adenosine in a large animal model of ischaemia and reperfusion injury : A feasibility study*. *March*, 1253–1264. https://doi.org/10.1002/term.2875

Cristallini, C., Barberis, R., Bellotti, E., Vaccari, G., Falzone, M., Cabiale, K., Perona, G., Rastaldo, R., Pascale, S., Pagliaro, P., & Giachino, C. (2019b). *Cardioprotection of PLGA / gelatine cardiac patches functionalised with adenosine in a large animal model of ischaemia and reperfusion injury : A feasibility study*. *April*, 1253–1264. https://doi.org/10.1002/term.2875

Cui, J., Li, J., Mathison, M., Tondato, F., Mulkey, S. P., Micko, C., Chronos, N. A. F., & Robinson, K.

A. (2005). A clinically relevant large-animal model for evaluation of tissue-engineered cardiac surgical patch materials. *Cardiovascular Revascularization Medicine*, *6*(3), 113–120. https://doi.org/10.1016/j.carrev.2005.07.006

Cui, S., Mao, J., Rouabhia, M., Elkoun, S., & Zhang, Z. (2021). A biocompatible polypyrrole membrane for biomedical applications. *RSC Advances*, *11*(28), 16996–17006. https://doi.org/10.1039/d1ra01338f

Cui, S., Mao, J., Zhang, Z., & Rouabhia, M. (2021). *A biocompatible polypyrrole membrane for biomedical applications*. 16996–17006. https://doi.org/10.1039/d1ra01338f

Da Silva, A. B., Marini, J., Gelves, G., Sundararaj, U., Gregório, R., & Bretas, R. E. S. (2013). Synergic effect in electrical conductivity using a combination of two fillers in PVDF hybrids composites. *European Polymer Journal*, *49*(10), 3318–3327. https://doi.org/10.1016/j.eurpolymj.2013.06.039

Dai, G., Aman, T. K., DiMaio, F., & Zagotta, W. N. (2021). Electromechanical coupling mechanism for activation and inactivation of an HCN channel. *Nature Communications*, *12*(1), 2802. https://doi.org/10.1038/s41467-021-23062-7

Dane. (2018). *Estadísticas vitales*. https://www.dane.gov.co/index.php/estadisticas-por-tema/demografia-y-poblacion/nacimientos-y-defunciones

Das, S., Wajid, A. S., Bhattacharia, S. K., Wilting, M. D., Rivero, I. V., & Green, M. J. (2013). Electrospinning of polymer nanofibers loaded with noncovalently functionalized graphene. *Journal of Applied Polymer Science*, *128*(6), 4040–4046. https://doi.org/10.1002/app.38694

Dayan V, Benech A, Rodríguez C, Ado S, Guedes I, Sotelo V, Laguzzi F, Kapitán M, Langhain M, Ferrando R, T. C. (2011). MODELO DE INFARTO AGUDO DE MIOCARDIO MEDIANTE ISQUEMIA-REPERFUSIÓN EN OVEJAS. *Revista Uruguaya de Cardiología*, 31–93. http://www.scielo.edu.uy/scielo.php?pid=S1688-04202011000400007&script=sci_arttext

De Vrieze, S., Van Camp, T., Nelvig, A., Hagström, B., Westbroek, P., & De Clerck, K. (2009). The effect of temperature and humidity on electrospinning. *Journal of Materials Science*, *44*(5), 1357–1362. https://doi.org/10.1007/s10853-008-3010-6

Deitzel, J. M., Kleinmeyer, J., Harris, D., & Beck Tan, N. C. (2001). The effect of processing variables on the morphology of electrospun nanofibers and textiles. *Polymer*, *42*(1), 261–272. https://doi.org/https://doi.org/10.1016/S0032-3861(00)00250-0

del Maria Javier, M. F., Delmo, E. M. J., & Hetzer, R. (2021). Evolution of heart transplantation since Barnard's first. *Cardiovascular Diagnosis and Therapy*, *11*(1), 171–182. https://doi.org/10.21037/CDT-20-289

Deliormanlı, A. M. (2019). Direct Write Assembly of Graphene/Poly(ε-Caprolactone) Composite Scaffolds and Evaluation of Their Biological Performance Using Mouse Bone Marrow Mesenchymal Stem Cells. *Applied Biochemistry and Biotechnology*, *188*(4), 1117–1133. https://doi.org/10.1007/s12010-019-02976-5

Deshmukh, K., Basheer Ahamed, M., Deshmukh, R. R., Khadheer Pasha, S. K., Bhagat, P. R., & Chidambaram, K. (2017). 3 - Biopolymer Composites With High Dielectric Performance: Interface Engineering. In K. K. Sadasivuni, D. Ponnamma, J. Kim, J.-J. Cabibihan, & M. A. AlMaadeed (Eds.), *Biopolymer Composites in Electronics* (pp. 27–128). Elsevier. https://doi.org/https://doi.org/10.1016/B978-0-12-809261-3.00003-6

Devlin, G., Matthews, K., McCracken, G., Stuart, S., Jensen, J., Conaglen, J., & Bass, J. (2000). An ovine model of chronic stable heart failure. *Journal of Cardiac Failure*, *6*(2), 140–143. https://doi.org/10.1054/jcaf.2000.7279

Diaz, A., Ignacio, E., & Fischer, C. (2016). *Modelos Experimentales de Insuficiencia Cardiaca en Grandes Animales* (Issue February).

Ding, B., Wang, X., & Yu, J. (2019). *Electrospinning and nanofabrication and applications*. Elsevier.

Dozois, M. D., Bahlmann, L. C., Zilberman, Y., & Tang, X. (Shirley). (2017). Carbon nanomaterial-enhanced scaffolds for the creation of cardiac tissue constructs: A new frontier in cardiac tissue engineering. *Carbon*, *120*, 338–349. https://doi.org/10.1016/j.carbon.2017.05.050

Echegaray, K., Andreu, I., Lazkano, A., Villanueva, I., Sáenz, A., Elizalde, M. R., Echeverría, T., López, B., Garro, A., González, A., Zubillaga, E., Solla, I., Sanz, I., González, J., Elósegui-Artola, A., Roca-Cusachs, P., Díez, J., Ravassa, S., & Querejeta, R. (2017). Role of Myocardial Collagen in Severe Aortic Stenosis With Preserved Ejection Fraction and Symptoms of Heart Failure. *Revista Espanola de Cardiologia (English Ed.)*, *70*(10), 832–840. https://doi.org/10.1016/j.rec.2016.12.038

Edrisi, F., Baheiraei, N., Razavi, M., Roshanbinfar, K., Imani, R., & Jalilinejad, N. (2023). Potential of graphene-based nanomaterials for cardiac tissue engineering. *Journal of Materials Chemistry B*, *11*(31), 7280–7299. https://doi.org/10.1039/d3tb00654a

El-Sayed, N. M., El-Bakary, M. A., Ibrahim, M. A., Elgamal, M. A., & Hamza, A. A. (2021). Characterization of the mechanical and structural properties of PGA/TMC copolymer for cardiac tissue engineering. *Microscopy Research and Technique*, *84*(7), 1596–1606. https://doi.org/10.1002/jemt.23720

Elamparithi, A., Punnoose, A. M., Paul, S. F. D., & Kuruvilla, S. (2017). Gelatin electrospun nanofibrous matrices for cardiac tissue engineering applications. *International Journal of Polymeric Materials and Polymeric Biomaterials*, *66*(1), 20–27. https://doi.org/10.1080/00914037.2016.1180616

Elkhoury, K., Morsink, M., Sanchez-Gonzalez, L., Kahn, C., Tamayol, A., & Arab-Tehrany, E. (2021). Biofabrication of natural hydrogels for cardiac, neural, and bone Tissue engineering Applications. *Bioactive Materials*, *6*(11), 3904–3923. https://doi.org/https://doi.org/10.1016/j.bioactmat.2021.03.040

Eroğlu, N. S. (2022). *Production of Nanofibers from Plant Extracts by Electrospinning Method* (T. Tański & P. Jarka (eds.); p. Ch. 3). IntechOpen. https://doi.org/10.5772/intechopen.102614

Eslahi, N., Lotfi, R., Zandi, N., Mazaheri, M., Soleimani, F., & Simchi, A. (2022). 8 - Graphene-based polymer nanocomposites in biomedical applications. In S. M. Rangappa, J. Parameswaranpillai, V. Ayyappan, M. G. Motappa, S. Siengchin, & C. Soutis (Eds.), *Innovations in Graphene-Based Polymer Composites* (pp. 199–245). Woodhead Publishing. https://doi.org/https://doi.org/10.1016/B978-0-12-823789-2.00016-9

Fakhrali, A., Nasari, M., Poursharifi, N., Semnani, D., Salehi, H., Ghane, M., & Mohammadi, S. (2021). Biocompatible graphene-embedded PCL/PGS-based nanofibrous scaffolds: A potential application for cardiac tissue regeneration. *Journal of Applied Polymer Science*, *138*(40), 1–14. https://doi.org/10.1002/app.51177

Fakhrali, A., Semnani, D., Salehi, H., & Ghane, M. (2022). Electro-conductive nanofibrous structure based on PGS/PCL coated with PPy by *in situ* chemical polymerization applicable as cardiac patch: Fabrication and optimization. *Journal of Applied Polymer Science*, *139*(19), 1–20. https://doi.org/10.1002/app.52136

Ferreira, C. L., Valente, C. A., Zanini, M. L., Sgarioni, B., Henrique, P., Tondo, F., Chagastelles, P. C., Braga, J., Campos, M. M., Malmonge, A., Regina, N., & Basso, D. S. (2019). *Biocompatible PCL / PLGA / Polypyrrole Composites for Regenerating Nerves*. *1800028*, 1–8. https://doi.org/10.1002/masy.201800028

Flaig, F., Ragot, H., Simon, A., Revet, G., Kitsara, M., Kitasato, L., Hébraud, A., Agbulut, O., & Schlatter, G. (2020). Design of Functional Electrospun Scaffolds Based on Poly(glycerol sebacate) Elastomer and Poly(lactic acid) for Cardiac Tissue Engineering. *ACS Biomaterials Science and Engineering*, *6*(4), 2388–2400. https://doi.org/10.1021/acsbiomaterials.0c00243

Fleischer, S., Feiner, R., & Dvir, T. (2017). Cardiac tissue engineering: From matrix design to the engineering of bionic hearts. *Regenerative Medicine*, *12*(3), 275–284. https://doi.org/10.2217/rme-2016-0150

Flores-Rojas, G. G. ., Gómez-Lazaro, B. ., López-Saucedo, F. ., Vera-Graziano, R. ., Bucio, E. ., & Mendizábal, E. (2023). Electrospun Scaffolds for Tissue Engineering : A Review. *Macromol*, *3*, 524–553. https://doi.org/https://doi.org/10.3390/macromol3030031

Forward, K., & Rutledge, G. (2012). Free surface electrospinning from a wire electrode. *Chemical Engineering Journal*, *183*, 492–503. https://doi.org/10.1016/j.cej.2011.12.045

Fujihara, K., Teo, E., Teik-Cheng, L., & Ma, Z. (2005). An Introduction To Electrospinning And Nanofibers. In *World Scientific: Singapore* (Vol. 3). https://doi.org/10.1142/9789812567611_0003

Fujita, B., & Zimmermann, W. H. (2017). Engineered Heart Repair. *Clinical Pharmacology and Therapeutics*, *102*(2), 197–199. https://doi.org/10.1002/cpt.724

Furth, M. E., & Atala, A. (2014). Chapter 6 - Tissue Engineering: Future Perspectives. In R. Lanza,

R. Langer, & J. Vacanti (Eds.), *Principles of Tissue Engineering (Fourth Edition)* (Fourth Edi, pp. 83–123). Academic Press. https://doi.org/https://doi.org/10.1016/B978-0-12-398358-9.00006-9

Gabriel, S., Lau, R. W., & Gabriel, C. (1996). The dielectric properties of biological tissues: II. Measurements in the frequency range 10 Hz to 20 GHz. *Physics in Medicine and Biology*, *41*(11), 2251–2269. https://doi.org/10.1088/0031-9155/41/11/002

Gálvez-Montón, C., Prat-Vidal, C., Díaz-Güemes, I., Crisóstomo, V., Soler-Botija, C., Roura, S., Llucià-Valldeperas, A., Perea-Gil, I., Sánchez-Margallo, F. M., & Bayes-Genis, A. (2014). Comparison of two preclinical myocardial infarct models: Coronary coil deployment versus surgical ligation. *Journal of Translational Medicine*, *12*(1), 1–9. https://doi.org/10.1186/1479-5876-12-137

Gálvez-Montón, C., Prat-Vidal, C., Roura, S., Soler-Botija, C., & Bayes-Genis, A. (2013). Ingeniería tisular cardiaca y corazón bioartificial. *Revista Espanola de Cardiologia*, *66*(5), 391–399. https://doi.org/10.1016/j.recesp.2012.11.013

Gelmi, A., Zhang, J., Cieslar-Pobuda, A., Ljunngren, M. K., Los, M. J., Rafat, M., & Jager, E. W. H. (2015). Electroactive 3D materials for cardiac tissue engineering. *Electroactive Polymer Actuators and Devices (EAPAD) 2015*, *9430*, 94301T. https://doi.org/10.1117/12.2084165

Ghovvati, M., Kharaziha, M., Ardehali, R., & Annabi, N. (2022). Recent Advances in Designing Electroconductive Biomaterials for Cardiac Tissue Engineering. *Advanced Healthcare Materials*, *2200055*.

Ghuran, A. V., & Camm, A. J. (2001). Ischaemic heart disease presenting as arrhythmias. *British Medical Bulletin*, *59*, 193–210. https://doi.org/10.1093/bmb/59.1.193

Ginestra, P. (2019). Manufacturing of polycaprolactone - Graphene fibers for nerve tissue engineering. *Journal of the Mechanical Behavior of Biomedical Materials*, *100*(July), 103387. https://doi.org/10.1016/j.jmbbm.2019.103387

Gómez, J., Vásquez, M., Mantione, D., & Alegret, N. (2021). *Carbon Nanomaterials Embedded in Conductive Polymers : A State of the Art*.

Greenlund, K. J., Giles, W. H., Keenan, N. L., Malarcher, A. M., Zheng, Z. J., Casper, M. L., & Croft, J. B. (2006). 381Heart Disease and Stroke Mortality in the Twentieth Century. In J. W. Ward & C. Warren (Eds.), *Silent Victories: The History and Practice of Public Health in Twentieth Century America* (p. 0). Oxford University Press. https://doi.org/10.1093/acprof:oso/9780195150698.003.18

Gryshkov, O., Al Halabi, F., Kuhn, A. I., Leal-Marin, S., Freund, L. J., Förthmann, M., Meier, N., Barker, S. A., Haastert-Talini, K., & Glasmacher, B. (2021). Pvdf and p(Vdf-trfe) electrospun scaffolds for nerve graft engineering: A comparative study on piezoelectric and structural

properties, and *in vitro* biocompatibility. *International Journal of Molecular Sciences*, *22*(21), 1–27. https://doi.org/10.3390/ijms222111373

Grzeszczuk, M. (2018). Polymer electrodes: Preparation, properties, and applications. In *Encyclopedia of Interfacial Chemistry: Surface Science and Electrochemistry*. Elsevier. https://doi.org/10.1016/B978-0-12-409547-2.11676-2

Gu, H., Huang, J., Li, N., Yang, H., Wang, Y., Zhang, Y., Dong, C., Chen, G., & Guan, H. (2022). Polystyrene-Modulated Polypyrrole to Achieve Controllable Electromagnetic-Wave Absorption with Enhanced Environmental Stability. *Nanomaterials*, *12*(15). https://doi.org/10.3390/nano12152698

Guo, B., & Ma, P. X. (2018). Conducting Polymers for Tissue Engineering [Review-article]. *Biomacromolecules*, *19*(6), 1764–1782. https://doi.org/10.1021/acs.biomac.8b00276

Guo, Q.-Y., Yang, J.-Q., Feng, X.-X., & Zhou, Y.-J. (2023). Regeneration of the heart: from molecular mechanisms to clinical therapeutics. *Military Medical Research*, *10*(1), 18. https://doi.org/10.1186/s40779-023-00452-0

Hagen, R. (2012). 10.12 - Polylactic Acid. In K. Matyjaszewski & M. Möller (Eds.), *Polymer Science: A Comprehensive Reference* (pp. 231–236). Elsevier. https://doi.org/https://doi.org/10.1016/B978-0-444-53349-4.00269-7

Haider, A., Haider, S., & Kang, I. K. (2018). A comprehensive review summarizing the effect of electrospinning parameters and potential applications of nanofibers in biomedical and biotechnology. *Arabian Journal of Chemistry*, *11*(8), 1165–1188. https://doi.org/10.1016/j.arabjc.2015.11.015

Han, J., Li, H., Xu, X., Yuan, L., Wang, N., & Yu, H. (2016). Cu2(OH)PO4 pretreated by composite surfactants for the micro-domino effect: A high-efficiency Fenton catalyst for the total oxidation of dyes. *Materials Letters*, *166*, 71–74. https://doi.org/https://doi.org/10.1016/j.matlet.2015.12.046

Hao, D., Swindell, H. S., Ramasubramanian, L., Liu, R., Lam, K. S., Farmer, D. L., & Wang, A. (2020). Extracellular Matrix Mimicking Nanofibrous Scaffolds Modified With Mesenchymal Stem Cell-Derived Extracellular Vesicles for Improved Vascularization. *Frontiers in Bioengineering and Biotechnology*, *8*(June). https://doi.org/10.3389/fbioe.2020.00633

Hao, L., Dong, C., Zhang, L., Zhu, K., & Yu, D. (2022). Polypyrrole Nanomaterials: Structure, Preparation and Application. *Polymers*, *14*(23). https://doi.org/10.3390/polym14235139

Haq, A. U., Carotenuto, F., De Matteis, F., Prosposito, P., Francini, R., Teodori, L., Pasquo, A., & Di Nardo, P. (2021). Intrinsically conductive polymers for striated cardiac muscle repair. *International Journal of Molecular Sciences*, *22*(16). https://doi.org/10.3390/ijms22168550

Harlin, A., & Ferenets, M. (2006). Introduction to conductive materials. *Intelligent Textiles and Clothing*, 217–238. https://doi.org/10.1533/9781845691622.3.217

Hashizume, R., Fujimoto, K. L., Hong, Y., Guan, J., Toma, C., Tobita, K., & Wagner, W. R. (2013).

Biodegradable elastic patch plasty ameliorates left ventricular adverse remodeling after ischemia-reperfusion injury: A preclinical study of a porous polyurethane material in a porcine model. *Journal of Thoracic and Cardiovascular Surgery*, *146*(2), 391-399.e1. https://doi.org/10.1016/j.jtcvs.2012.11.013

He, S., Wu, J., Li, S., Wang, L., Sun, Y., Xie, J., & Ramnath, D. (2020). The conductive function of biopolymer corrects myocardial scar conduction blockage and resynchronizes contraction to prevent heart failure. *Biomaterials*, 120285. https://doi.org/10.1016/j.biomaterials.2020.120285

Heidari, M., Bahrami, H., & Ranjbar-Mohammadi, M. (2017). Fabrication, optimization and characterization of electrospun poly(caprolactone)/gelatin/graphene nanofibrous mats. *Materials Science and Engineering C*, *78*, 218–229. https://doi.org/10.1016/j.msec.2017.04.095

Heidari, M., Bahrami, S. H., Ranjbar-Mohammadi, M., & Milan, P. B. (2019). Smart electrospun nanofibers containing PCL/gelatin/graphene oxide for application in nerve tissue engineering. *Materials Science and Engineering C*, *103*(May), 109768. https://doi.org/10.1016/j.msec.2019.109768

Heikhmakhtiar, A. K., & Lim, K. M. (2018). Computational Prediction of the Combined Effect of CRT and LVAD on Cardiac Electromechanical Delay in LBBB and RBBB. *Computational and Mathematical Methods in Medicine*, *2018*(September), 10–12. https://doi.org/10.1155/2018/4253928

Heng, B. C., Bai, Y., Li, X., Lim, L. W., Li, W., Ge, Z., Zhang, X., & Deng, X. (2023). Electroactive Biomaterials for Facilitating Bone Defect Repair under Pathological Conditions. *Advanced Science*, *10*(2), 2204502. https://doi.org/https://doi.org/10.1002/advs.202204502

Hirenkumar, M., & Steven, S. (2012). Poly Lactic-co-Glycolic Acid (PLGA) as Biodegradable Controlled Drug Delivery Carrier. *Polymers*, *3*(3), 1–19. https://doi.org/10.3390/polym3031377.Poly

Hohman, M., Shin, M., Rutledge, G., & Brenner, M. (2001). Electrospinning and Electrically Forced Jets. I. Stability Theory. *Physics of Fluids - PHYS FLUIDS*, *13*. https://doi.org/10.1063/1.1383791

House, A., Atalla, I., Lee, E. J., & Guvendiren, M. (2021). *Designing Biomaterial Platforms for Cardiac Tissue and Disease Modeling*. *2000022*, 1–16. https://doi.org/10.1002/anbr.202000022

Hu, S., Mi, L., Fu, J., Ma, W., Ni, J., Zhang, Z., Li, B., Guan, G., Wang, J., & Zhao, N. (2022). Model Embraced Electromechanical Coupling Time for Estimation of Heart Failure in Patients With Hypertrophic Cardiomyopathy. *Frontiers in Cardiovascular Medicine*, *9*, 895035. https://doi.org/10.3389/fcvm.2022.895035

Huang, C., Niu, H., Wu, J., Ke, Q., Mo, X., & Lin, T. (2012). Needleless Electrospinning of

Polystyrene Fibers with an Oriented Surface Line Texture. *Journal of Nanomaterials*, *2012*, 473872. https://doi.org/10.1155/2012/473872

Huang, P., Liu, Y., Chen, Z., Zheng, Y., Vasilovna, K. V., Faritovich, G. R., & Xin, B. (2023). Preparation and Characterization of PU/PDA/PPy Flexible Composite Film for Electric Heating. *Fibers and Polymers*. https://doi.org/10.1007/s12221-023-00416-0

Huang, Z.-M., Zhang, Y.-Z., Kotaki, M., & Ramakrishna, S. (2003). A review on polymer nanofibers by electrospinning and their applications in nanocomposites. *Composites Science and Technology*, *63*(15), 2223–2253. https://doi.org/https://doi.org/10.1016/S0266-3538(03)00178-7

Ibrahim, I. M., Yunus, S., & Hashim, M. A. (2013). Relative performance of isoproopylamine, pyrrole and pyridine as corrosion inhibitors for carbon steels in saline water at mildly elevated temperatures. *International Journal of Scientific & Engineering Research*, *4*(2), 1–12.

Ikram, H., Rogers, S. J., Charles, C. J., Sands, J., Richards, A. M., Bridgman, P. G., & Gooneratne, R. (1997). An ovine model of acute myocardial infarction and chronic left ventricular dysfunction. *Angiology*, *48*(8), 679–688. https://doi.org/10.1177/000331979704800803

Imani, F., Karimi-Soflou, R., Shabani, I., & Karkhaneh, A. (2021). PLA electrospun nanofibers modified with polypyrrole-grafted gelatin as bioactive electroconductive scaffold. *Polymer*, *218*(September 2020), 123487. https://doi.org/10.1016/j.polymer.2021.123487

Jain, A., Nabeel, A. N., Bhagwat, S., Kumar, R., Sharma, S., Kozak, D., Hunjet, A., Kumar, A., & Singh, R. (2023). Fabrication of polypyrrole gas sensor for detection of NH3 using an oxidizing agent and pyrrole combinations: Studies and characterizations. *Heliyon*, *9*(7), e17611. https://doi.org/10.1016/j.heliyon.2023.e17611

Jana, S., Bhagia, A., & Lerman, A. (2019). Optimization of polycaprolactone fibrous scaffold for heart valve tissue engineering. *Biomedical Materials (Bristol)*, *14*(6). https://doi.org/10.1088/1748-605X/ab3d24

Jang, Y., Park, Y., & Kim, J. (2020). Engineering Biomaterials to Guide Heart Cells for Matured Cardiac Tissue. *Coatings*, *10*, 925. https://doi.org/10.3390/coatings10100925

Jiang, L., Chen, D., Wang, Z., Zhang, Z., Xia, Y., Xue, H., & Liu, Y. (2019). Preparation of an Electrically Conductive Graphene Oxide/Chitosan Scaffold for Cardiac Tissue Engineering. *Applied Biochemistry and Biotechnology*, *188*(4), 952–964. https://doi.org/10.1007/s12010-019-02967-6

John, J., & Jayalekshmi, S. (2023). Polypyrrole with appreciable solubility, crystalline order and electrical conductivity synthesized using various dopants appropriate for device applications. *Polymer Bulletin*, *80*(6), 6099–6116. https://doi.org/10.1007/s00289-022-04354-4

Jung, H.-S., Kim, M. H., Shin, J. Y., Park, S. R., Jung, J.-Y., & Park, W. H. (2018). Electrospinning and wound healing activity of β-chitin extracted from cuttlefish bone. *Carbohydr. Polym.*, *193*, 205.

Kai, D., Prabhakaran, M. P., Jin, G., & Ramakrishna, S. (2011a). Guided orientation of cardiomyocytes on electrospun aligned nanofibers for cardiac tissue engineering. *Journal of Biomedical Materials Research - Part B Applied Biomaterials*, *98 B*(2), 379–386. https://doi.org/10.1002/jbm.b.31862

Kai, D., Prabhakaran, M. P., Jin, G., & Ramakrishna, S. (2011b). Polypyrrole-contained electrospun conductive nanofibrous membranes for cardiac tissue engineering. *Journal of Biomedical Materials Research - Part A*, *99 A*(3), 376–385. https://doi.org/10.1002/jbm.a.33200

Kalimuldina, G., Turdakyn, N., Abay, I., Medeubayev, A., Nurpeissova, A., Adair, D., & Bakenov, Z. (2020). A review of piezoelectric pvdf film by electrospinning and its applications. *Sensors (Switzerland)*, *20*(18), 1–42. https://doi.org/10.3390/s20185214

Kariduraganavar, M. Y., Kittur, A. A., & Kamble, R. R. (2014). Chapter 1 - Polymer Synthesis and Processing. In S. G. Kumbar, C. T. Laurencin, & M. Deng (Eds.), *Natural and Synthetic Biomedical Polymers* (pp. 1–31). Elsevier. https://doi.org/https://doi.org/10.1016/B978-0-12-396983-5.00001-6

Karimi, S. N. H., Aghdam, R. M., Ebrahimi, S. A. S., & Chehrehsaz, Y. (2022). Tri-layered alginate/poly(epsilon-caprolactone) electrospun scaffold for cardiac tissue engineering. *POLYMER INTERNATIONAL*, *71*(9), 1099–1108. https://doi.org/10.1002/pi.6371

Karkan, S. F., Davaran, S., Rahbarghazi, R., Salehi, R., & Akbarzadeh, A. (2019). Electrospun nanofibers for the fabrication of engineered vascular grafts. *Journal of Biological Engineering*, *7*, 1–13.

Kashou, A. H., & Chhabra, H. B. L. (2020). Physiology, Sinoatrial Node. *StatPearls [Internet]*, 1–6.

Kausar, A. (2021). Chapter 5 - Perspectives on nanocomposite with polypyrrole and nanoparticles. In A. Kausar (Ed.), *Conducting Polymer-Based Nanocomposites* (pp. 103–128). Elsevier. https://doi.org/https://doi.org/10.1016/B978-0-12-822463-2.00006-3

Kazu Kikuchi, & Poss, K. D. (2008). Cardiac Regenerative Capacity and Mechanisms. *Annual Review of Cell and Developmental Biology*, *28*(1), 719–741. https://doi.org/doi.org/10.1146/annurev-cellbio-101011-155739

Kesornsit, S., Direksilp, C., Phasuksom, K., Thummarungsan, N., Sakunpongpitiporn, P., Rotjanasuworapong, K., Sirivat, A., & Niamlang, S. (2022). Synthesis of Highly Conductive Poly(3-hexylthiophene) by Chemical Oxidative Polymerization Using Surfactant Templates. *Polymers*, *14*(18), 1–19. https://doi.org/10.3390/polym14183860

Kharaziha, M., Shin, S. R., Nikkhah, M., Topkaya, S. N., Masoumi, N., Annabi, N., Dokmeci, M. R., & Khademhosseini, A. (2014). Tough and flexible CNT-polymeric hybrid scaffolds for engineering cardiac constructs. *Biomaterials*, *35*(26), 7346–7354. https://doi.org/10.1016/j.biomaterials.2014.05.014

Khatti, T., Naderi-Manesh, H., & Kalantar, S. M. (2019). Polypyrrole-Coated Polycaprolactone-Gelatin Conductive Nanofibers: Fabrication and Characterization. *Materials Science and Engineering B: Solid-State Materials for Advanced Technology*, *250*(October), 114440. https://doi.org/10.1016/j.mseb.2019.114440

Kierszenbaum, Abraham L.; Tres, Laura L.; Fernández Aceñero, M. J. (2016). *Histología y biología celular : introducción a la anatomía patológica* (Elsevier (ed.)).

Kim, S., Tserengombo, B., Choi, S.-H., Noh, J., Huh, S., Choi, B., Chung, H., Kim, J., & Jeong, H. (2018). Experimental investigation of dispersion characteristics and thermal conductivity of various surfactants on carbon based nanomaterial. *International Communications in Heat and Mass Transfer*, *91*, 95–102. https://doi.org/https://doi.org/10.1016/j.icheatmasstransfer.2017.12.011

Kotadia, I., Whitaker, J., Roney, C., Niederer, S., O'Neill, M., Bishop, M., & Wright, M. (2020). Anisotropic Cardiac Conduction. *Arrhythmia & Electrophysiology Review*, *9*(4), 202–210. https://doi.org/10.15420/aer.2020.04

Krista McLennan. (n.d.). Recognising, assessing and alleviating pain in sheep. *Farm Animal Well Being*.

Kumar, A., & Kumar, A. (2019). Poly(lactic acid) and poly(lactic-co-glycolic) acid nanoparticles: Versatility in biomedical applications. In *Materials for Biomedical Engineering: Absorbable Polymers*. Elsevier Inc. https://doi.org/10.1016/B978-0-12-818415-8.00007-3

Kumar, M., & Kumari, P. (2020). The effect of reciprocating motion of drum collector on electrospun PVDF nanofiber for energy harvesting application. *WCMNM*, 18–21.

Kumar, S., & Chatterjee, K. (2016). Comprehensive Review on the Use of Graphene-Based Substrates for Regenerative Medicine and Biomedical Devices. In *ACS Applied Materials and Interfaces* (Vol. 8, Issue 40, pp. 26431–26457). American Chemical Society. https://doi.org/10.1021/acsami.6b09801

Kurakula, M., & Koteswara Rao, G. S. N. (2020). Moving polyvinyl pyrrolidone electrospun nanofibers and bioprinted scaffolds toward multidisciplinary biomedical applications. *European Polymer Journal*, *136*(July). https://doi.org/10.1016/j.eurpolymj.2020.109919

Laforgue, A., & Robitaille, L. (2010). Deposition of ultrathin coatings of polypyrrole and poly(3,4-ethylenedioxythiophene) onto electrospun nanofibers using a vapor-phase polymerization method. *Chemistry of Materials*, *22*(8), 2474–2480. https://doi.org/10.1021/cm902986g

Langer, R., & Vacanti, J. P. (1993). Tissue Engineering. *Science*, *260*(5110), 920–926. https://doi.org/10.1126/science.8493529

Le, T. H., Kim, Y., & Yoon, H. (2017). Electrical and electrochemical properties of conducting polymers. *Polymers*, *9*(4). https://doi.org/10.3390/polym9040150

Lee, J. K. Y., Chen, N., Peng, S., Li, L., Tian, L., Thakor, N., & Ramakrishna, S. (2018). Polymer-based composites by electrospinning: Preparation & functionalization with nanocarbons.

Progress in Polymer Science, *86*, 40–84. https://doi.org/10.1016/j.progpolymsci.2018.07.002

Lee, J. Y., Bashur, C. A., Goldstein, A. S., & Schmidt, C. E. (2009). Polypyrrole-coated electrospun PLGA nanofibers for neural tissue applications. *Biomaterials*, *30*(26), 4325–4335. https://doi.org/10.1016/j.biomaterials.2009.04.042

Lee, M., Kim, M. C., & Lee, J. Y. (2022). Nanomaterial-Based Electrically Conductive Hydrogels for Cardiac Tissue Repair. *International Journal of Nanomedicine*, *17*, 6181–6200. https://doi.org/10.2147/IJN.S386763

Leung, V., & Ko, F. (2011). Biomedical applications of nanofibers. *Polymers for Advanced Technologies*, *22*, 350–365. https://doi.org/10.1002/pat.1813

Lewis, T. W. (1998). *A Study of The Overoxidation of The Conducting Polymer Polypyrrole*. 230.

Li, J., Xu, C., Tian, H., Zha, F., Qi, W., & Wang, Q. (2018). Blend-electrospun poly(vinylidene fluoride)/stearic acid membranes for efficient separation of water-in-oil emulsions. *Colloids and Surfaces A: Physicochemical and Engineering Aspects*, *538*, 494–499. https://doi.org/https://doi.org/10.1016/j.colsurfa.2017.11.043

Li, J., Zhang, X., Jiang, J., Wang, Y., Jiang, H., Zhang, J., Nie, X., & Liu, B. (2018). Systematic Assessment of the Toxicity and Potential Mechanism of Graphene Derivatives *In Vitro* and *In Vivo*. *Toxicological Sciences*, *167*(1), 269–281. https://doi.org/10.1093/toxsci/kfy235

Li, S., Yu, X., & Li, Y. (2022). Conductive polypyrrole-coated electrospun chitosan nanoparticles / poly (D , L-lactide) fibrous mat : influence of drug delivery and Schwann cells proliferation Conductive polypyrrole-coated electrospun chitosan nanoparticles / poly (D , L-lactide) fi. *Biomedical Physics & Engineering Express*, *8*.

Li, T. T., Yan, M., Zhong, Y., Ren, H. T., Lou, C. W., Huang, S. Y., & Lin, J. H. (2019). Processing and characterizations of rotary linear needleless electrospun polyvinyl alcohol(PVA)/Chitosan(CS)/Graphene(Gr) nanofibrous membranes. *Journal of Materials Research and Technology*, *8*(6), 5124–5132. https://doi.org/10.1016/j.jmrt.2019.08.035

Li, Y., Wei, L., Lan, L., Gao, Y., Zhang, Q., Dawit, H., Mao, J., Guo, L., Shen, L., & Wang, L. (2022). Conductive biomaterials for cardiac repair: A review. *Acta Biomaterialia*, *139*, 157–178. https://doi.org/10.1016/j.actbio.2021.04.018

Liang, Y., & Goh, J. C.-H. (2020). Polypyrrole-Incorporated Conducting Constructs for Tissue Engineering Applications: A Review. *Bioelectricity*, *2*(2), 101–119. https://doi.org/10.1089/bioe.2020.0010

Liang, Y., Mitriashkin, A., Lim, T. T., & Goh, J. C. H. (2021). Conductive polypyrrole-encapsulated silk fibroin fibers for cardiac tissue engineering. *Biomaterials*, *276*(January), 121008. https://doi.org/10.1016/j.biomaterials.2021.121008

Liau, B., Zhang, D., & Bursac, N. (2012). Functional cardiac tissue engineering. *Regenerative*

Medicine, *7*(2), 187–206. https://doi.org/10.2217/rme.11.122

Lindsey, M. L., Bolli, R., Canty, J. M., Du, X. J., Frangogiannis, N. G., Frantz, S., Gourdie, R. G., Holmes, J. W., Jones, S. P., Kloner, R. A., Lefer, D. J., Liao, R., Murphy, E., Ping, P., Przyklenk, K., Recchia, F. A., Longacre, L. S., Ripplinger, C. M., Van Eyk, J. E., & Heusch, G. (2018). Guidelines for experimental models of myocardial ischemia and infarction. *American Journal of Physiology - Heart and Circulatory Physiology*, *314*(4), H812–H838. https://doi.org/10.1152/ajpheart.00335.2017

Liu, H., Paul, C., & Xu, M. (2017). Optimal environmental stiffness for stem cell mediated ischemic myocardium repair. *Adult Stem Cells*, 293–304.

Liu, Y., & Wu, F. (2023). Synthesis and application of polypyrrole nanofibers: a review. *Nanoscale Advances*, 3606–3618. https://doi.org/10.1039/d3na00138e

Longhin, E. M., El Yamani, N., Rundén-Pran, E., & Dusinska, M. (2022). The alamar blue assay in the context of safety testing of nanomaterials. *Frontiers in Toxicology*, *4*, 981701. https://doi.org/10.3389/ftox.2022.981701

Loyo, C., Cordoba, A., Palza, H., Canales, D., Melo, F., Vivanco, J. F., Baier, R. V., Millán, C., Corrales, T., & Zapata, P. A. (2023). Effect of Gelatin Coating and GO Incorporation on the Properties and Degradability of Electrospun PCL Scaffolds for Bone Tissue Regeneration. *Polymers*, *16*(1), 129. https://doi.org/10.3390/polym16010129

Lu, H., Li, X., & Lei, Q. (2021). Conjugated Conductive Polymer Materials and its Applications: A Mini-Review. *Frontiers in Chemistry*, *9*(September), 6–11. https://doi.org/10.3389/fchem.2021.732132

Lukin, I., Erezuma, I., Maeso, L., Zarate, J., Desimone, M. F., Al-Tel, T. H., Dolatshahi-Pirouz, A., & Orive, G. (2022). Progress in Gelatin as Biomaterial for Tissue Engineering. *Pharmaceutics*, *14*(6), 1–19. https://doi.org/10.3390/pharmaceutics14061177

Ma, Z., Shi, W., Yan, K., Pan, L., & Yu, G. (2019). Doping engineering of conductive polymer hydrogels and their application in advanced sensor technologies. *Chemical Science*, *10*(25), 6232–6244. https://doi.org/10.1039/c9sc02033k

MacDonald, E. A., Rose, R. A., & Quinn, T. A. (2020). Neurohumoral Control of Sinoatrial Node Activity and Heart Rate: Insight From Experimental Models and Findings From Humans. *Frontiers in Physiology*, *11*. https://doi.org/10.3389/fphys.2020.00170

Maharjan, B., Kaliannagounder, V. K., Jang, S. R., Awasthi, G. P., Bhattarai, D. P., Choukrani, G., Park, C. H., & Kim, C. S. (2020). In-situ polymerized polypyrrole nanoparticles immobilized poly(ε-caprolactone) electrospun conductive scaffolds for bone tissue engineering. *Materials Science and Engineering C*, *114*(April), 111056. https://doi.org/10.1016/j.msec.2020.111056

Mahmoudi, T., Wang, Y., & Hahn, Y.-B. (2018). Graphene and its derivatives for solar cells application. *Nano Energy*, *47*, 51–65. https://doi.org/https://doi.org/10.1016/j.nanoen.2018.02.047

Mahun, A., Abbrent, S., Bober, P., Brus, J., & Kobera, L. (2020). Effect of structural features of polypyrrole (PPy) on electrical conductivity reflected on 13C ssNMR parameters. *Synthetic Metals*, *259*, 116250. https://doi.org/https://doi.org/10.1016/j.synthmet.2019.116250

Majid, Q. A., Fricker, A. T. R., Gregory, D. A., Davidenko, N., Hernandez Cruz, O., Jabbour, R. J., Owen, T. J., Basnett, P., Lukasiewicz, B., Stevens, M., Best, S., Cameron, R., Sinha, S., Harding, S. E., & Roy, I. (2020). Natural Biomaterials for Cardiac Tissue Engineering: A Highly Biocompatible Solution. *Frontiers in Cardiovascular Medicine*, *7*(October), 1–32. https://doi.org/10.3389/fcvm.2020.554597

Malmivuo, J., & Plonsey, R. (1995). *Bioelectromagnetism: Principles and Applications of Bioelectric and Biomagnetic Fields*. Oxford University Press. https://doi.org/10.1093/acprof:oso/9780195058239.001.0001

Mancino, C., Hendrickson, T., Whitney, L. V., Paradiso, F., Abasi, S., Tasciotti, E., Taraballi, F., & Guiseppi-Elie, A. (2022). Electrospun electroconductive constructs of aligned fibers for cardiac tissue engineering. *Nanomedicine: Nanotechnology, Biology, and Medicine*, *44*, 102567. https://doi.org/10.1016/j.nano.2022.102567

Mannhardt, I., Breckwoldt, K., Letuffe-Brenière, D., Schaaf, S., Schulz, H., Neuber, C., Benzin, A., Werner, T., Eder, A., Schulze, T., Klampe, B., Christ, T., Hirt, M. N., Huebner, N., Moretti, A., Eschenhagen, T., & Hansen, A. (2016). Human Engineered Heart Tissue: Analysis of Contractile Force. *Stem Cell Reports*, *7*(1), 29–42. https://doi.org/10.1016/j.stemcr.2016.04.011

Manousiouthakis, E., Park, J., Hardy, J. G., Lee, J. Y., & Schmidt, C. E. (2022). Towards the translation of electroconductive organic materials for regeneration of neural tissues. *Acta Biomaterialia*, *139*, 22–42. https://doi.org/https://doi.org/10.1016/j.actbio.2021.07.065

Manteca, X., Temple, D., Mainau, E., & Llonch, P. (2017). Evaluación del dolor en el ganado ovino. *Fawec*, *17*(1), 1–2. https://doi.org/10.13130/AWIN

Mao, J., & Zhang, Z. (2018). Polypyrrole as Electrically Conductive Biomaterials: Synthesis, Biofunctionalization, Potential Applications and Challenges. *Advances in Experimental Medicine and Biology*, *1078*, 347–370. https://doi.org/10.1007/978-981-13-0950-2_18

Margerrison, E., Argentieri, M., Kommala, D., & Schabowsky, C. N. (2021). *Polycaprolactone (PCL) Safety Profile Report Details Date of Submission ECRI Corporate Governance Project Manager*. *540*.

Markowitz, S. M., & Lerman, B. B. (2018). A contemporary view of atrioventricular nodal physiology. *Journal of Interventional Cardiac Electrophysiology*, *52*(3), 271–279. https://doi.org/10.1007/s10840-018-0392-5

Matysiak, W., Tański, T., Smok, W., Gołombek, K., & Schab-Balcerzak, E. (2020). Effect of

conductive polymers on the optical properties of electrospun polyacrylonitryle nanofibers filled by polypyrrole, polythiophene and polyaniline. *Applied Surface Science*, *509*(December 2019). https://doi.org/10.1016/j.apsusc.2019.145068

Mbayachi, V. B., Ndayiragije, E., Sammani, T., Taj, S., Mbuta, E. R., & ullah khan, A. (2021). Graphene synthesis, characterization and its applications: A review. *Results in Chemistry*, *3*, 100163. https://doi.org/https://doi.org/10.1016/j.rechem.2021.100163

McClelland, R., Dennis, R., Reid, L. M., Palsson, B., & Macdonald, J. M. (2005). 7 - TISSUE ENGINEERING. In J. D. Enderle, S. M. Blanchard, & J. D. Bronzino (Eds.), *Introduction to Biomedical Engineering (Second Edition)* (Second Edi, pp. 313–402). Academic Press. https://doi.org/https://doi.org/10.1016/B978-0-12-238662-6.50009-4

Mcivor, M. J., Maolmhuaidh, F. Ó., Meenagh, A., Hussain, S., Bhattacharya, G., Fishlock, S., Ward, J., Mcferran, A., Acheson, J. G., Cahill, P. A., Forster, R., Mceneaney, D. J., Boyd, A. R., & Meenan, B. J. (2022). *3D Fabrication and Characterisation of Electrically Receptive Tissue Models*.

Mckee, C. T., Last, J. A., Russell, P., & Murphy, C. J. (2011). Indentation versus tensile measurements of Young's modulus for soft biological tissues. *Tissue Engineering. Part B, Reviews*, *17 3*, 155–164.

McKeen, L. (2021). Chapter11 - The effect of heat aging on the properties of sustainable polymers. In L. McKeen (Ed.), *The Effect of Long Term Thermal Exposure on Plastics and Elastomers (Second Edition)* (Second Edi, pp. 313–332). William Andrew Publishing. https://doi.org/https://doi.org/10.1016/B978-0-323-85436-8.00001-1

McMahan, S., Taylor, A., Copeland, K. M., Pan, Z., Liao, J., & Hong, Y. (2020). Current advances in biodegradable synthetic polymer based cardiac patches. *Journal of Biomedical Materials Research - Part A*, *108*(4), 972–983. https://doi.org/10.1002/jbm.a.36874

McMillen, C. (2001). The sheep - an ideal model for biomedical research? *Anzccart News*, *14*(2), 1–4.

Megelski, S., Stephens, J. S., Chase, D. B., & Rabolt, J. F. (2002). Micro- and Nanostructured Surface Morphology on Electrospun Polymer Fibers. *Macromolecules*, *35*(22), 8456–8466. https://doi.org/10.1021/ma020444a

Mehta, P. P., & Pawar, V. S. (2018). 22 - Electrospun nanofiber scaffolds: Technology and applications. In Inamuddin, A. M. Asiri, & A. Mohammad (Eds.), *Applications of Nanocomposite Materials in Drug Delivery* (pp. 509–573). Woodhead Publishing. https://doi.org/https://doi.org/10.1016/B978-0-12-813741-3.00023-6

Mit-uppatham, C., Nithitanakul, M., & Supaphol, P. (2004). Ultrafine Electrospun Polyamide-6 Fibers: Effect of Solution Conditions on Morphology and Average Fiber Diameter. *Macromolecular Chemistry and Physics*, *205*(17), 2327–2338. https://doi.org/https://doi.org/10.1002/macp.200400225

Mittal, T. (2005). Pacemakers- A journey through the years. *Indian Journal of Thoracic and Cardiovascular Surgery*, *21*, 236–249. https://doi.org/doi.org/10.1007/s12055-005-0060-0

Mohan, V. B., Lau, K., Hui, D., & Bhattacharyya, D. (2018). Graphene-based materials and their composites: A review on production, applications and product limitations. *Composites Part B: Engineering*, *142*, 200–220. https://doi.org/https://doi.org/10.1016/j.compositesb.2018.01.013

Montes, A., Valor, D., Penabad, Y., Dom, M., Pereyra, C., Mart, E., & Ossa, D. (2023). *Formation of PLGA – PEDOT : PSS Conductive Scaffolds by Supercritical Foaming*. 1–20.

Morsink, M., Severino, P., Luna-Ceron, E., Hussain, M. A., Sobahi, N., & Shin, S. R. (2022). Effects of electrically conductive nano-biomaterials on regulating cardiomyocyte behavior for cardiac repair and regeneration. *Acta Biomaterialia*, *139*, 141–156. https://doi.org/10.1016/j.actbio.2021.11.022

Mota, K. O., & Corrêa, C. B. (2021). *Effect of Preparation Additives on the Antimicrobial Activity and Cytotoxicity of Polypyrrole*. *32*(6), 1203–1212.

Murugan, S. S., Dalavi, P. A., Devi G.V., Y., Chatterjee, K., & Venkatesan, J. (2022). Natural and Synthetic Biopolymeric Biomaterials for Bone Tissue Engineering Applications. In M. S. J. Hashmi (Ed.), *Encyclopedia of Materials: Plastics and Polymers* (pp. 746–757). Elsevier. https://doi.org/https://doi.org/10.1016/B978-0-12-820352-1.00246-7

Mutepfa, A. R., Hardy, J. G., & Adams, C. F. (2022). Electroactive Scaffolds to Improve Neural Stem Cell Therapy for Spinal Cord Injury. *Frontiers in Medical Technology*, *4*(February). https://doi.org/10.3389/fmedt.2022.693438

Nag, A., Mitra, A., & Mukhopadhyay, S. C. (2018). Graphene and its sensor-based applications: A review. *Sensors and Actuators A: Physical*, *270*, 177–194. https://doi.org/https://doi.org/10.1016/j.sna.2017.12.028

Nagiah, N., El Khoury, R., Othman, M. H., Akimoto, J., Ito, Y., Roberson, D. A., & Joddar, B. (2022). Development and Characterization of Furfuryl-Gelatin Electrospun Scaffolds for Cardiac Tissue Engineering. *ACS Omega*, *7*(16), 13894–13905. https://doi.org/10.1021/acsomega.2c00271

Nair, N. R., Sekhar, V. C., Nampoothiri, K. M., & Pandey, A. (2017). 32 - Biodegradation of Biopolymers. In A. Pandey, S. Negi, & C. R. Soccol (Eds.), *Current Developments in Biotechnology and Bioengineering* (pp. 739–755). Elsevier. https://doi.org/https://doi.org/10.1016/B978-0-444-63662-1.00032-4

Najafi Tireh Shabankareh, A., Samadi Pakchin, P., Hasany, M., & Ghanbari, H. (2023). Development of a new electroconductive nanofibrous cardiac patch based on polyurethane-reduced graphene oxide nanocomposite scaffolds. *Materials Chemistry and Physics*, *305*(May), 127961. https://doi.org/10.1016/j.matchemphys.2023.127961

Namsheer, K., & Rout, C. S. (2021). Conducting polymers: a comprehensive review on recent

advances in synthesis, properties and applications. *RSC Advances*, *11*(10), 5659–5697. https://doi.org/10.1039/d0ra07800j

Nasr, S. M., Rabiee, N., Hajebi, S., Ahmadi, S., Fatahi, Y., Hosseini, M., Bagherzadeh, M., Ghadiri, A. M., Rabiee, M., Jajarmi, V., & Webster, T. J. (2020). Biodegradable nanopolymers in cardiac tissue engineering: From concept towards nanomedicine. *International Journal of Nanomedicine*, *15*, 4205–4224. https://doi.org/10.2147/IJN.S245936

National Farm Animal Care Council. (2013). Code of practice for the care and handling of sheep. In *Practice*.

National Research Council. (1992). 4 Recognition and Assessment of Pain, Stress, and Distress. In *Recognition and Alleviation of Pain and Distress in Laboratory Animals.* The National Academies Press. https://doi.org/doi: 10.17226/1542

Nekounam, H., Gholizadeh, S., Allahyari, Z., Samadian, H., Nazeri, N., Shokrgozar, M. A., & Faridi-Majidi, R. (2021). Electroconductive scaffolds for tissue regeneration: Current opportunities, pitfalls, and potential solutions. *Materials Research Bulletin*, *134*(June 2020), 111083. https://doi.org/10.1016/j.materresbull.2020.111083

Nguyen-truong, M., & Li, Y. V. (2020). *Mechanical Considerations of Electrospun Sca ff olds for Myocardial Tissue and Regenerative Engineering*. 1–22.

Nguyen, T. D., Roh, S., Thi, M., Nguyen, N., & Lee, J. S. (2023). *Structural Control of Nanofibers According to Electrospinning Process Conditions and Their Applications*.

Nikkhah, M., Akbari, M., Paul, A., Memic, A., Dolatshahi-Pirouz, A., & Khademhosseini, A. (2016). Gelatin-Based Biomaterials For Tissue Engineering And Stem Cell Bioengineering. In *Biomaterials from Nature for Advanced Devices and Therapies* (pp. 37–62). John Wiley & Sons, Ltd. https://doi.org/https://doi.org/10.1002/9781119126218.ch3

Nostril, A., & Lip, A. (n.d.). *Sheep Pain Facial Expression Scale * Sheep Pain Facial Expression Scale (SPFES)*. 0–1.

O'Brien, J., Wilson, I., Orton, T., & Pognan, F. (2000). Investigation of the Alamar Blue (resazurin) fluorescent dye for the assessment of mammalian cell cytotoxicity. *European Journal of Biochemistry*, *267*(17), 5421–5426. https://doi.org/10.1046/j.1432-1327.2000.01606.x

Ojrzynska, M., Wroblewska, A., Judek, J., Malolepszy, A., Duzynska, A., & Zdrojek, M. (2020). Study of optical properties of graphene flakes and its derivatives in aqueous solutions. *Optics Express*, *28*(5), 7274. https://doi.org/10.1364/oe.382523

Oprea, A. E., Ficai, A., & Andronescu, E. (2019). Electrospun nanofibers for tissue engineering applications. In *Materials for Biomedical Engineering*. Elsevier Inc. https://doi.org/10.1016/b978-0-12-816909-4.00004-x

Pang, A. L., Arsad, A., & Ahmadipour, M. (2021). Synthesis and factor affecting on the conductivity of polypyrrole: a short review. *Polymers for Advanced Technologies*, *32*(4), 1428–1454. https://doi.org/10.1002/pat.5201

Park, D. W., Ness, J. P., Brodnick, S. K., Esquibel, C., Novello, J., Atry, F., Baek, D. H., Kim, H., Bong, J., Swanson, K. I., Suminski, A. J., Otto, K. J., Pashaie, R., Williams, J. C., & Ma, Z. (2018). Electrical Neural Stimulation and Simultaneous *in Vivo* Monitoring with Transparent Graphene Electrode Arrays Implanted in GCaMP6f Mice. *ACS Nano*, *12*(1), 148–157. https://doi.org/10.1021/acsnano.7b04321

Patino, M. G., Neiders, M. E., Andreana, S., Noble, B., & Cohen, R. E. (2002). *Collagen : An Overview*. 280–285. https://doi.org/10.1097/01.ID.0000019547.50849.3B

Pfeiffer, E. R., Tangney, J. R., Omens, J. H., & McCulloch, A. D. (2014). Biomechanics of cardiac electromechanical coupling and mechanoelectric feedback. *Journal of Biomechanical Engineering*, *136*(2), 21007. https://doi.org/10.1115/1.4026221

Pomeroy, J. E., Helfer, A., & Bursac, N. (2020). Biomaterializing the promise of cardiac tissue engineering. *Biotechnology Advances*, *42*, 107353. https://doi.org/https://doi.org/10.1016/j.biotechadv.2019.02.009

Potdar, A., Kale, A., Marathe, P., Talekar, P., & Yadav, S. (2020). A Review On Applications Of Graphene. *IJRAR1AA1390 International Journal of Research and Analytical Reviews (IJRAR) Www.Ijrar.Org*, *80*(4), 80–85. www.ijrar.org

Precedence Research. (2022). *Transplantation Market Size, Share and Growth Analysis*.

Pushp, P., Bhaskar, R., Kelkar, S., Sharma, N., Pathak, D., & Gupta, M. K. (2021). Plasticized poly(vinylalcohol) and poly(vinylpyrrolidone) based patches with tunable mechanical properties for cardiac tissue engineering applications. *Biotechnology and Bioengineering*, *118*(6), 2312–2325. https://doi.org/10.1002/bit.27743

Qasim, M., Arunkumar, P., Powell, H. M., & Khan, M. (2019). Current research trends and challenges in tissue engineering for mending broken hearts. *Life Sciences*, *229*(March), 233–250. https://doi.org/10.1016/j.lfs.2019.05.012

Rabbani, S., Ahmadi, H., Fayazzadeh, E., Sahebjam, M., Boroumand, M. A., Sotudeh, M., & Nassiri, S. M. (2008). Development of an ovine model of myocardial infarction. *ANZ Journal of Surgery*, *78*(1–2), 78–81. https://doi.org/10.1111/j.1445-2197.2007.04359.x

Randviir, E. P., Brownson, D. A. C., & Banks, C. E. (2014). A decade of graphene research: Production, applications and outlook. In *Materials Today* (Vol. 17, Issue 9, pp. 426–432). Elsevier. https://doi.org/10.1016/j.mattod.2014.06.001

Rashid, S. T., Salacinski, H. J., Hamilton, G., & Seifalian, A. M. (2004). The use of animal models in developing the discipline of cardiovascular tissue engineering: A review. *Biomaterials*, *25*(9), 1627–1637. https://doi.org/10.1016/S0142-9612(03)00522-2

Ratih, D., Siburian, R., & Andriayani. (2018). The performance of graphite/n-graphene and graphene/n-graphene as electrode in primary cell batteries. *Rasayan Journal of Chemistry*,

11(4), 1649–1656. https://doi.org/10.31788/RJC.2018.1145007

Ray, S. S., Chen, S.-S., Nguyen, N. C., & Nguyen, H. T. (2019). Chapter 9 - Electrospinning: A Versatile Fabrication Technique for Nanofibrous Membranes for Use in Desalination. In S. Thomas, D. Pasquini, S.-Y. Leu, & D. A. Gopakumar (Eds.), *Nanoscale Materials in Water Purification* (pp. 247–273). Elsevier. https://doi.org/https://doi.org/10.1016/B978-0-12-813926-4.00014-8

Refate, A., Mohamed, Y., Mohamed, M., Sobhy, M., Samhy, K., Khaled, O., Eidaroos, K., Batikh, H., El-Kashif, E., El-Khatib, S., & Mehanny, S. (2023). Influence of electrospinning parameters on biopolymers nanofibers, with emphasis on cellulose & chitosan. *Heliyon*, *9*(6), e17051. https://doi.org/https://doi.org/10.1016/j.heliyon.2023.e17051

Ren, X., Jiang, Z., & Tang, M. (2023). *Application of conductive hydrogels in cardiac tissue engineering*. *4*(2), 1–7.

Reneker, D. H., & Yarin, A. L. (2008). Electrospinning jets and polymer nanofibers. *Polymer*, *49*(10), 2387–2425. https://doi.org/10.1016/j.polymer.2008.02.002

Reneker, D. H., Yarin, A. L., Fong, H., & Koombhongse, S. (2000). Bending instability of electrically charged liquid jets of polymer solutions in electrospinning. *Journal of Applied Physics*, *87*(9), 4531–4547. https://doi.org/10.1063/1.373532

Research, P. (2022). *Scaffold Technology Market (By Product: Hydrogels, Micropatterned Surface Microplates, and Nanofiber Based Scaffolds; By Application: Neurology, Orthopedics, Dental, Cardiology & Vascular, Cancer, Skin & Integumentary, GI & Gynecologyand Urology; By End-U*. https://www.precedenceresearch.com/scaffold-technology-market

Reshmy, R., Philip, E., Vaisakh, P. H., Sindhu, R., Binod, P., Madhavan, A., Pandey, A., Sirohi, R., & Tarafdar, A. (2021). *Chapter 14 - Biodegradable polymer composites* (P. Binod, S. Raveendran, & A. B. T.-B. Pandey Biofuels, Biochemicals (eds.); pp. 393–412). Elsevier. https://doi.org/https://doi.org/10.1016/B978-0-12-821888-4.00003-4

Riehle, C., & Bauersachs, J. (2019). *Small animal models of heart failure*. 1838–1849. https://doi.org/10.1093/cvr/cvz161

Roacho-p, J. A., Garza-treviño, E. N., Moncada-saucedo, N. K., Carriquiry-chequer, P. A., Valencia-g, L. E., Matthews, E. R., G, V., Simental-mend, M., Delgado-gonzalez, P., Delgado-gallegos, J. L., Padilla-rivas, G. R., & Islas, J. F. (2022). *Artificial Scaffolds in Cardiac Tissue Engineering*. 1–21.

Robinson, K. A., Li, J., Mathison, M., Redkar, A., Cui, J., Chronos, N. A. F., Matheny, R. G., & Badylak, S. F. (2005). Extracellular matrix scaffold for cardiac repair. *Circulation*, *112*(9 SUPPL.), 135–143. https://doi.org/10.1161/CIRCULATIONAHA.104.525436

Rodrigues, I. C. P., Kaasi, A., Maciel Filho, R., Jardini, A. L., & Gabriel, L. P. (2018). Cardiac tissue engineering: current state-of-the-art materials, cells and tissue formation. *Einstein (Sao Paulo, Brazil)*, *16*(3), eRB4538. https://doi.org/10.1590/S1679-45082018RB4538

Roser, M., & Ritchie, H. (2023). How has world population growth changed over time? *Our World in Data*.

Roshanbinfar, K., Vogt, L., Ruther, F., Roether, J. A., Boccaccini, A. R., & Engel, F. B. (2020). *Nanofibrous Composite with Tailorable Electrical and Mechanical Properties for Cardiac Tissue Engineering*. *1908612*. https://doi.org/10.1002/adfm.201908612

Saberi, A., Jabbari, F., Zarrintaj, P., Saeb, M. R., & Mozafari, M. (2019). Electrically conductive materials: Opportunities and challenges in tissue engineering. In *Biomolecules* (Vol. 9, Issue 9). https://doi.org/10.3390/biom9090448

Sack, K. L., Baillargeon, B., Acevedo-Bolton, G., Genet, M., Rebelo, N., Kuhl, E., Klein, L., Weiselthaler, G. M., Burkhoff, D., Franz, T., & Guccione, J. M. (2016). Partial LVAD restores ventricular outputs and normalizes LV but not RV stress distributions in the acutely failing heart in silico. *The International Journal of Artificial Organs*, *39*(8), 421–430. https://doi.org/10.5301/ijao.5000520

Sadeghi, A., Moztarzadeh, F., & Aghazadeh Mohandesi, J. (2019). Investigating the effect of chitosan on hydrophilicity and bioactivity of conductive electrospun composite scaffold for neural tissue engineering. *International Journal of Biological Macromolecules*, *121*, 625–632. https://doi.org/10.1016/j.ijbiomac.2018.10.022

Sadeghianmaryan, A., Karimi, Y., Naghieh, S., Alizadeh Sardroud, H., Gorji, M., & Chen, X. (2019). Electrospinning of Scaffolds from the Polycaprolactone/Polyurethane Composite with Graphene Oxide for Skin Tissue Engineering. *Applied Biochemistry and Biotechnology*. https://doi.org/10.1007/s12010-019-03192-x

Sartoretto, S. C., Uzeda, M. J., Miguel, F. B., Nascimento, J. R., Ascoli, F., & Calasans-Maia, M. D. (2016). Sheep as an experimental model for biomaterial implant evaluation. *Acta Ortopedica Brasileira*, *24*(5), 262–266. https://doi.org/10.1590/1413-785220162405161949

Sasso, C., Beneventi, D., Zeno, E., Chaussy, D., Petit-Conil, M., & Belgacem, N. (2011). Polypyrrole and polypyrrole/wood-derived materials conducting composites: A review. *BioResources*, *6*(3), 3585–3620. https://doi.org/10.15376/biores.6.3.3585-3620

Savchenko, A., Yin, R. T., Kireev, D., Efimov, I. R., & Molokanova, E. (2021). Graphene-Based Scaffolds: Fundamentals and Applications for Cardiovascular Tissue Engineering. *Frontiers in Bioengineering and Biotechnology*, *9*(December), 1–8. https://doi.org/10.3389/fbioe.2021.797340

Saxena, P., & Shukla, P. (2021). A comprehensive review on fundamental properties and applications of poly(vinylidene fluoride) (PVDF). *Advanced Composites and Hybrid Materials*, *4*(1), 8–26. https://doi.org/10.1007/s42114-021-00217-0

Scheetz, S. D., & Upadhyay, G. A. (2022). Physiologic Pacing Targeting the His Bundle and Left

Bundle Branch: a Review of the Literature. *Current Cardiology Reports*, *24*(8), 959–978. https://doi.org/10.1007/s11886-022-01723-3

Schmitt, P. R., Dwyer, K. D., & Coulombe, K. L. K. (2022). Current Applications of Polycaprolactone as a Scaffold Material for Heart Regeneration. *ACS Applied Bio Materials*, *5*(6), 2461–2480. https://doi.org/10.1021/acsabm.2c00174

Schmitt, P. R., Dwyer, K. D., Minor, A. J., & Coulombe, K. L. K. (2022). *Wet-Spun Polycaprolactone Scaffolds Provide Customizable Anisotropic Viscoelastic Mechanics for Engineered Cardiac Tissues*.

Sell, S. A., McClure, M. J., Garg, K., Wolfe, P. S., & Bowlin, G. L. (2009). Electrospinning of collagen/biopolymers for regenerative medicine and cardiovascular tissue engineering. *Advanced Drug Delivery Reviews*, *61*(12), 1007–1019. https://doi.org/https://doi.org/10.1016/j.addr.2009.07.012

Senthil, T., & Anandhan, S. (2017). *Effect of Solvents on the Solution Electrospinning of Discover more interesting articles and news on the subject ! Entdecken Sie weitere interessante Artikel und News zum Thema !*

Serafin, A., Murphy, C., Rubio, M. C., & Collins, M. N. (2021). Printable alginate/gelatin hydrogel reinforced with carbon nanofibers as electrically conductive scaffolds for tissue engineering. *Materials Science and Engineering C*, *122*(January), 111927. https://doi.org/10.1016/j.msec.2021.111927

Shafei, S., Foroughi, J., Chen, Z., Wong, C. S., & Naebe, M. (2017). Short oxygen plasma treatment leading to long-term hydrophilicity of conductive PCL-PPy nanofiber scaffolds. *Polymers*, *9*(11). https://doi.org/10.3390/polym9110614

Shafei, S., Foroughi, J., Stevens, L., Wong, C. S., Zabihi, O., & Naebe, M. (2017). Electroactive nanostructured scaffold produced by controlled deposition of PPy on electrospun PCL fibres. *Research on Chemical Intermediates*, *43*(2), 1235–1251. https://doi.org/10.1007/s11164-016-2695-4

Shang, L., Qi, Y., Lu, H., Pei, H., Li, Y., Paul, J. A., Chool, S. O. N. S., Engineering, O. F., & S, A. P. P. S. C. (2019). 7. Graphene and Graphene Oxide for Tissue Engineering and Regeneration. In *Theranostic Bionanomaterials*. Elsevier Inc. https://doi.org/10.1016/B978-0-12-815341-3.00007-9

Shao, H., Fang, J., Wang, H., & Lin, T. (2015). Effect of electrospinning parameters and polymer concentrations on mechanical-to-electrical energy conversion of randomly-oriented electrospun poly(vinylidene fluoride) nanofiber mats. *RSC Advances*, *5*(19), 14345–14350. https://doi.org/10.1039/c4ra16360e

Sharma, V., Dash, S. K., Govarthanan, K., Gahtori, R., Negi, N., Barani, M., Tomar, R., Chakraborty, S., Mathapati, S., Bishi, D. K., Negi, P., Dua, K., Singh, S. K., Gundamaraju, R., Dey, A., Ruokolainen, J., Thakur, V. K., Kesari, K. K., Jha, N. K., … Ojha, S. (2021). Recent advances

in cardiac tissue engineering for the management of myocardium infarction. In *Cells* (Vol. 10, Issue 10). https://doi.org/10.3390/cells10102538

Shinde, S. S., Gund, G. S., Dubal, D. P., Jambure, S. B., & Lokhande, C. D. (2014). Morphological modulation of polypyrrole thin films through oxidizing agents and their concurrent effect on supercapacitor performance. *Electrochimica Acta*, *119*, 1–10. https://doi.org/10.1016/j.electacta.2013.10.174

Shokrollahi, P., Omidi, Y., Cubeddu, L. X., & Omidian, H. (2023). Conductive polymers for cardiac tissue engineering and regeneration. *Journal of Biomedical Materials Research - Part B Applied Biomaterials*, *111*(11), 1979–1995. https://doi.org/10.1002/jbm.b.35293

Sigaroodi, F., Rahmani, M., Parandakh, A., Boroumand, S., Rabbani, S., & Khani, M. M. (2023). Designing cardiac patches for myocardial regeneration–a review. *International Journal of Polymeric Materials and Polymeric Biomaterials*, *0*(0), 1–19. https://doi.org/10.1080/00914037.2023.2180510

Socci, M. C., Rodríguez, G., Oliva, E., Fushimi, S., Takabatake, K., Nagatsuka, H., Felice, C. J., & Rodríguez, A. P. (2023). Polymeric Materials, Advances and Applications in Tissue Engineering: A Review. *Bioengineering*, *10*(2). https://doi.org/10.3390/bioengineering10020218

Solazzo, M., O'Brien, F. J., Nicolosi, V., & Monaghan, M. G. (2019). The rationale and emergence of electroconductive biomaterial scaffolds in cardiac tissue engineering. *APL Bioengineering*, *3*(4), 041501. https://doi.org/10.1063/1.5116579

Son, W. K., Youk, J. H., Lee, T. S., & Park, W. H. (2004). The effects of solution properties and polyelectrolyte on electrospinning of ultrafine poly(ethylene oxide) fibers. *Polymer*, *45*(9), 2959–2966. https://doi.org/10.1016/j.polymer.2004.03.006

Song, H., Li, T., Han, Y., Wang, Y., Zhang, C., & Wang, Q. (2016). Optimizing the polymerization conditions of conductive polypyrrole. *Journal of Photopolymer Science and Technology*, *29*(6), 803–808. https://doi.org/10.2494/photopolymer.29.803

Sovilj, S., Magjarević, R., Al Abed, A., Lovell, N. H., & Dokos, S. (2014). Simplified 2D bidomain model of whole heart electrical activity and ECG generation. *Measurement Science Review*, *14*(3), 136–143. https://doi.org/10.2478/msr-2014-0018

Sowmya, B., Hemavathi, A. B., & Panda, P. K. (2021). Poly (ε-caprolactone)-based electrospun nano-featured substrate for tissue engineering applications: a review. *Progress in Biomaterials*, *10*(2), 91–117. https://doi.org/10.1007/s40204-021-00157-4

Sudwilai, T., Ng, J. J., Boonkrai, C., Israsena, N., Chuangchote, S., & Supaphol, P. (2014). Polypyrrole-coated electrospun poly(lactic acid) fibrous scaffold: Effects of coating on electrical conductivity and neural cell growth. *Journal of Biomaterials Science, Polymer Edition*, *25*(12),

1240–1252. https://doi.org/10.1080/09205063.2014.926578

Suh, T. C., Amanah, A. Y., & Gluck, J. M. (2020). *Electrospun Sca ff olds and Induced Pluripotent Stem Cell-Derived Cardiomyocytes for Cardiac Tissue Engineering Applications*. 1–21.

Sun, M., Chi, G., Li, P., Lv, S., Xu, J., Xu, Z., Xia, Y., Tan, Y., Xu, J., Li, L., & Li, Y. (2018). Effects of Matrix Stiffness on the Morphology, Adhesion, Proliferation and Osteogenic Differentiation of Mesenchymal Stem Cells. *International Journal of Medical Sciences*, *15*(3), 257–268. https://doi.org/10.7150/ijms.21620

Sun, Y., Liu, J., Xu, Z., Lin, X., Zhang, X., Li, L., & Li, Y. (2021). *Matrix stiffness regulates myocardial differentiation of human umbilical cord mesenchymal stem cells*. *13*(2), 2231–2250.

Surekha, G., Krishnaiah, K. V., Ravi, N., & Padma Suvarna, R. (2020). FTIR, Raman and XRD analysis of graphene oxide films prepared by modified Hummers method. *Journal of Physics: Conference Series*, *1495*(1). https://doi.org/10.1088/1742-6596/1495/1/012012

Szewczyk, P. K., & Stachewicz, U. (2020). The impact of relative humidity on electrospun polymer fibers: From structural changes to fiber morphology. *Advances in Colloid and Interface Science*, *286*, 102315. https://doi.org/https://doi.org/10.1016/j.cis.2020.102315

Takada, T., Sasaki, D., Matsuura, K., Miura, K., Sakamoto, S., Goto, H., Ohya, T., Iida, T., Homma, J., Shimizu, T., & Hagiwara, N. (2022). Aligned human induced pluripotent stem cell-derived cardiac tissue improves contractile properties through promoting unidirectional and synchronous cardiomyocyte contraction. *Biomaterials*, *281*, 121351. https://doi.org/https://doi.org/10.1016/j.biomaterials.2021.121351

Talebi, A., Labbaf, S., & Karimzadeh, F. (2019). A conductive film of chitosan-polycaprolcatone-polypyrrole with potential in heart patch application. *Polymer Testing*, *75*(December 2018), 254–261. https://doi.org/10.1016/j.polymertesting.2019.02.029

Tamimi, M., Rajabi, S., & Pezeshki-Modaress, M. (2020). Cardiac ECM/chitosan/alginate ternary scaffolds for cardiac tissue engineering application. *International Journal of Biological Macromolecules*, *164*, 389–402. https://doi.org/10.1016/j.ijbiomac.2020.07.134

Tavakkol, E., Tavanai, H., Abdolmaleki, A., & Morshed, M. (2017). Production of conductive electrospun polypyrrole/poly(vinyl pyrrolidone) nanofibers. *Synthetic Metals*, *231*(July), 95–106. https://doi.org/10.1016/j.synthmet.2017.06.017

Tayebi, T., Baradaran-Rafii, A., Hajifathali, A., Rahimpour, A., Zali, H., Shaabani, A., & Niknejad, H. (2021). Biofabrication of chitosan/chitosan nanoparticles/polycaprolactone transparent membrane for corneal endothelial tissue engineering. *Scientific Reports*, *11*(1), 1–12. https://doi.org/10.1038/s41598-021-86340-w

Tenreiro, M. F., Louro, A. F., Alves, P. M., & Serra, M. (2021). Next generation of heart regenerative therapies: progress and promise of cardiac tissue engineering. *Npj Regenerative Medicine*, *6*(1). https://doi.org/10.1038/s41536-021-00140-4

Tian, L., Prabhakaran, M. P., Hu, J., Chen, M., Besenbacher, F., & Ramakrishna, S. (2016).

Synergistic effect of topography, surface chemistry and conductivity of the electrospun nanofibrous scaffold on cellular response of PC12 cells. *Colloids and Surfaces B: Biointerfaces*. https://doi.org/10.1016/j.colsurfb.2016.05.032

Tiwari, S. K., & Venkatraman, S. S. (2012). Importance of viscosity parameters in electrospinning: Of monolithic and core–shell fibers. *Materials Science and Engineering: C*, *32*(5), 1037–1042. https://doi.org/https://doi.org/10.1016/j.msec.2012.02.019

Topuz, F., Abdulhamid, M. A., Holtzl, T., & Szekely, G. (2021). Nanofiber engineering of microporous polyimides through electrospinning: Influence of electrospinning parameters and salt addition. *Materials & Design*, *198*, 109280. https://doi.org/https://doi.org/10.1016/j.matdes.2020.109280

Torabi, M., Abazari, M. F., Zare Karizi, S., Kohandani, M., Hajati-Birgani, N., Norouzi, S., Nejati, F., Mohajerani, A., Rahmati, T., & Mokhames, Z. (2021). Efficient cardiomyocyte differentiation of induced pluripotent stem cells on PLGA nanofibers enriched by platelet-rich plasma. *Polymers for Advanced Technologies*, *32*(3), 1168–1175. https://doi.org/10.1002/pat.5164

Tortora, G., & Derrickson, B. (2006). Principios de Anatomía y Fisiología. In *Editorial Panamericana* (Vol. 1). https://doi.org/10.1017/CBO9781107415324.004

Tsao, Connie W; Aday, Aaron W.; Almarzooq, Z. I. (2022). Heart Disease and Stroe Statistics-2022 Update: A Report From the american Heart Association. *Circulation*, *145*(8). https://doi.org/10.1161/IR.0000000000001052

Tsui, J. H., Leonard, A., Camp, N. D., Long, J. T., Nawas, Z. Y., Chavanachat, R., Choi, J. S., Wolf-Yadlin, A., Murry, C. E., Sniadecki, N. J., & Kim, D.-H. (2019). Functional Maturation of Human iPSC-based Cardiac Microphysiological Systems with Tunable Electroconductive Decellularized Extracellular Matrices. *BioRxiv*, 786657. https://doi.org/10.1101/786657

Ţucureanu, V., Matei, A., & Avram, A. M. (2016). FTIR Spectroscopy for Carbon Family Study. *Critical Reviews in Analytical Chemistry*, *46*(6), 502–520. https://doi.org/10.1080/10408347.2016.1157013

U.S. FDA Center for Devices and Radiological Health. (2020). *Medical Device Material Performance Study Poly Lactic-co-Glycolic Acid [P (L / G) A] Safety Profile Submitted to*. *804*.

United Nations, Department of Economic and Social Affairs, P. D. (2022). *World Population Prospects 2022*.

Vacanti, C. (2006). The history of tissue engineering. *Journal of Cellular and Molecular Medicine*, *1*(3), 569–576. https://doi.org/10.2755/jcmm010.003.20

Valdoz, J. C., Johnson, B. C., Jacobs, D. J., Franks, N. A., Dodson, E. L., Sanders, C., Cribbs, C. G., & Van Ry, P. M. (2021). The ECM: To scaffold, or not to scaffold, that is the question. *International Journal of Molecular Sciences*, *22*(23). https://doi.org/10.3390/ijms222312690

Valverde, I. (2017). *Impresión tridimensional de modelos cardiacos : aplicaciones en el campo de la*

educación y el intervencionismo estructural. *70*(4), 282–291.

Vogt, L., Rivera, L. R., Liverani, L., Piegat, A., El Fray, M., & Boccaccini, A. R. (2019). Poly(ε-caprolactone)/poly(glycerol sebacate) electrospun scaffolds for cardiac tissue engineering using benign solvents. *Materials Science and Engineering C*, *103*(February), 109712. https://doi.org/10.1016/j.msec.2019.04.091

Vunjak-Novakovic, G. (2017). Tissue engineering of the heart: An evolving paradigm. *Journal of Thoracic and Cardiovascular Surgery*, *153*(3), 593–595. https://doi.org/10.1016/j.jtcvs.2016.08.057

Vunjak-Novakovic, G., Tandon, N., Godier, A., Maidhof, R., Marsano, A., Martens, T. P., & Radisic, M. (2010). Challenges in cardiac tissue engineering. *Tissue Engineering. Part B, Reviews*, *16*(2), 169–187. https://doi.org/10.1089/ten.teb.2009.0352

Wang, J. (2021). *Meta-analysis of Cellular Toxicity for Graphene via Data-Mining the Literature and Machine Learning*.

Wang, L., Wu, Y., Hu, T., Guo, B., & Ma, P. X. (2017). Electrospun conductive nanofibrous scaffolds for engineering cardiac tissue and 3D bioactuators. *Acta Biomaterialia*, *59*, 68–81. https://doi.org/10.1016/j.actbio.2017.06.036

Wang, Y., & Feng, W. (2022). Conductive Polymers and Their Composites. In *Conductive Polymers and their Composites*. https://doi.org/10.1007/978-981-19-5363-7

Waremra, R. S., & Betaubun, P. (2018). Analysis of Electrical Properties Using the four point Probe Method. *E3S Web of Conferences*, *73*, 1–4. https://doi.org/10.1051/e3sconf/20187313019

Wee, J. H., Yoo, K. D., Sim, S. B., Kim, H. J., Kim, H. J., Park, K. N., Kim, G. H., Moon, M. H., You, S. J., Ha, M. Y., Yang, D. H., Chun, H. J., Ko, J. H., & Kim, C. H. (2022). Stem cell laden nano and micro collagen / PLGA bimodal fibrous patches for myocardial regeneration. *Biomaterials Research*, 1–17. https://doi.org/10.1186/s40824-022-00319-w

WHO, W. H. O. (2022). *Cardiovascular diseases (CVDs)*. 11 June 2021. https://www.who.int/news-room/fact-sheets/detail/cardiovascular-diseases-(cvds)

World Heart Federation. (2022). *World Heart Vision 2030*. 4–9.

Xu, B., Li, Y., Deng, B., Liu, X., Wang, L., & Zhu, Q. L. (2017). Chitosan hydrogel improves mesenchymal stem cell transplant survival and cardiac function following myocardial infarction in rats. *Experimental and Therapeutic Medicine*, *13*(2), 588–594. https://doi.org/10.3892/etm.2017.4026

Xu, H., Holzwarth, J. M., Yan, Y., Xu, P., Zheng, H., Yin, Y., Li, S., & Ma, P. X. (2014). Conductive PPY/PDLLA conduit for peripheral nerve regeneration. *Biomaterials*, *35*(1), 225–235. https://doi.org/10.1016/j.biomaterials.2013.10.002

Xu, M., Qin, M., Cheng, Y., Niu, X., Kong, J., Zhang, X., Huang, D., & Wang, H. (2021). Alginate microgels as delivery vehicles for cell-based therapies in tissue engineering and regenerative medicine. *Carbohydrate Polymers*, *266*, 118128.

https://doi.org/10.1016/j.carbpol.2021.118128

Xue, J., Wu, T., Dai, Y., & Xia, Y. (2019). Electrospinning and electrospun nanofibers: Methods, materials, and applications. *Chemical Reviews*, *119*(8), 5298–5415. https://doi.org/10.1021/acs.chemrev.8b00593

Yalcinkaya, F., Yalcinkaya, B., & Jirsak, O. (2015). Influence of Salts on Electrospinning of Aqueous and Nonaqueous Polymer Solutions. *Journal of Nanomaterials*, *2015*, 134251. https://doi.org/10.1155/2015/134251

Yang, Q., Li, Z., Hong, Y., Zhao, Y., Qiu, S., Wang, C., & Wei, Y. (2004). Influence of Solvents on the Formation of Ultrathin Uniform Poly(Vinyl Pyrrolidone) Nanofibers with Electrospinning. *Journal of Polymer Science Part B: Polymer Physics*, *42*, 3721–3726. https://doi.org/10.1002/polb.20222

Ye, G., & Qiu, X. (2017). Conductive biomaterials in cardiac tissue engineering. *Biotarget*, *1*(5), 9–9. https://doi.org/10.21037/biotarget.2017.08.01

You, J. O., Rafat, M., Ye, G. J. C., & Auguste, D. T. (2011). Nanoengineering the heart: Conductive scaffolds enhance connexin 43 expression. *Nano Letters*, *11*(9), 3643–3648. https://doi.org/10.1021/nl201514a

Yuan, S., Xiong, G., Wang, X., Zhang, S., & Choong, C. (2012). Surface modification of polycaprolactone substrates using collagen-conjugated poly(methacrylic acid) brushes for the regulation of cell proliferation and endothelialisation. *Journal of Materials Chemistry*, *22*, 13039–13049. https://doi.org/10.1039/C2JM31213A

Yue, B. (2014). NIH Public Access Author Manuscript J Glaucoma. Author manuscript; available in PMC 2015 October 01. Published in final edited form as: J Glaucoma. 2014 ; : S20–S23. doi:10.1097/IJG.0000000000000108. Biology of the Extracellular Matrix: An Overview Beatri. *J Glaucoma.*, *23*(1), 1–7. https://doi.org/10.1097/IJG.0000000000000108.Biology

Yussuf, A., Al-Saleh, M., Al-Enezi, S., & Abraham, G. (2018). Synthesis and Characterization of Conductive Polypyrrole: The Influence of the Oxidants and Monomer on the Electrical, Thermal, and Morphological Properties. *International Journal of Polymer Science*, *2018*. https://doi.org/10.1155/2018/4191747

Zaarour, B., Zhang, W., Zhu, L., Jin, X. Y., & Huang, C. (2019). Maneuvering surface structures of polyvinylidene fluoride nanofibers by controlling solvent systems and polymer concentration. *Textile Research Journal*, *89*(12), 2406–2422. https://doi.org/10.1177/0040517518792748

Zaarour, B., Zhu, L., & Jin, X. (2019). Controlling the surface structure, mechanical properties, crystallinity, and piezoelectric properties of electrospun PVDF nanofibers by maneuvering molecular weight. *Soft Materials*, *17*(2), 181–189. https://doi.org/10.1080/1539445X.2019.1582542

Zahari, A. S., Mazwir, M. H., & Misnon, I. I. (2021). Influence of molecular weight on dielectric properties and piezoelectric constant of poly(vinylidene fluoride) membranes obtained by electrospinning. *Polimery/Polymers*, *66*(10), 532–537. https://doi.org/10.14314/polimery.2021.10.4

Zaragoza, C., Gomez-guerrero, C., Martin-ventura, J. L., Blanco-colio, L., Tarin, C., Mas, S., Ortiz, A., & Egido, J. (2011). *Animal Models of Cardiovascular Diseases*. *2011*. https://doi.org/10.1155/2011/497841

Zarei, M., Samimi, A., Khorram, M., Abdi, M. M., & Golestaneh, S. I. (2021). Fabrication and characterization of conductive polypyrrole/chitosan/collagen electrospun nanofiber scaffold for tissue engineering application. *International Journal of Biological Macromolecules*, *168*, 175–186. https://doi.org/10.1016/j.ijbiomac.2020.12.031

Zargham, S., Bazgir, S., Tavakoli, A., Rashidi, A. S., & Damerchely, R. (2012). The Effect of Flow Rate on Morphology and Deposition Area of Electrospun Nylon 6 Nanofiber. *Journal of Engineered Fibers and Fabrics*, *7*(4), 155892501200700400. https://doi.org/10.1177/155892501200700414

Zhang, H., Cheng, J., & Ao, Q. (2021). Preparation of alginate-based biomaterials and their applications in biomedicine. *Marine Drugs*, *19*(5), 1–24. https://doi.org/10.3390/md19050264

Zhang, X, Peng, X., & Zhang, S. W. (2017). 7 - Synthetic biodegradable medical polymers: Polymer blends. In Xiang Zhang (Ed.), *Science and Principles of Biodegradable and Bioresorbable Medical Polymers* (pp. 217–254). Woodhead Publishing. https://doi.org/https://doi.org/10.1016/B978-0-08-100372-5.00007-6

Zhang, Xuewei, Chen, X., Hong, H., Hu, R., Liu, J., & Liu, C. (2022). Decellularized extracellular matrix scaffolds: Recent trends and emerging strategies in tissue engineering. *Bioactive Materials*, *10*, 15–31. https://doi.org/https://doi.org/10.1016/j.bioactmat.2021.09.014

Zhao, G., Qing, H., Huang, G., Genin, G. M., Lu, T. J., Luo, Z., Xu, F., & Zhang, X. (2018). Reduced graphene oxide functionalized nanofibrous silk fibroin matrices for engineering excitable tissues. *NPG Asia Materials*, *10*(10), 982–994. https://doi.org/https://doi.org/10.1038/s41427-018-0092-8

Zhao, W., Tu, H., Chen, J., Wang, J., Liu, H., Zhang, F., & Li, J. (2023). Functionalized hydrogels in neural injury repairing. *Frontiers in Neuroscience*, *17*(June), 1–9. https://doi.org/10.3389/fnins.2023.1199299

Zhou, J., Chen, J., Sun, H., Qiu, X., Mou, Y., Liu, Z., Zhao, Y., Li, X., Han, Y., Duan, C., Tang, R., Wang, C., Zhong, W., Liu, J., Luo, Y., Xing, M. M., & Wang, C. (2014). Engineering the heart: Evaluation of conductive nanomaterials for improving implant integration and cardiac function. *Scientific Reports*, *4*, 1–11. https://doi.org/10.1038/srep03733

Zhuang, R. Z., Lock, R., Liu, B., & Vunjak-Novakovic, G. (2022). Opportunities and challenges in cardiac tissue engineering from an analysis of two decades of advances. *Nature Biomedical*

Engineering, *6*(4), 327–338. https://doi.org/10.1038/s41551-022-00885-3

Zimmermann, W.-H., Schneiderbanger, K., Schubert, P., Didié, M., Münzel, F., Heubach, J. F., Kostin, S., Neuhuber, W. L., & Eschenhagen, T. (2002). Tissue engineering of a differentiated cardiac muscle construct. *Circulation Research*, *90*(2), 223–230. https://doi.org/10.1161/hh0202.103644